# Particle Engineering of Carriers for Improved Inhalation Formulations of Salbutamol Sulphate

*by*

*Carlos Molina*

Submitted in accordance with the requirements for the degree of Doctor of Philosophy

*University of Sussex*

*February 2019*

I hereby declare that this thesis has not been and will not be, submitted in whole or in part to another University for the award of any other degree.

Signature:.....

# Table of Contents

Title: *Particle Engineering of Carriers for Improved Inhalation Formulations of Salbutamol Sulphate*

**4.** Carlos Molina, Waseem Kaialy, and Ali Nokhodchi. The crucial role of leucine concentration on spray dried mannitol-leucine as a single carrier to enhance the aerosolization performance of Albuterol sulfate. Journal of Drug Delivery Science and Technology 49 (2019) 97–106. https://doi.org/10.1016/j.jddst.2018.11.007

# List of Figures

**Chapter 6: Effect of Leucine on Dry Powder Inhaler Performance of Salbutamol Sulphate containing Xylitol Crystals**



**Chapter 7: Effect Mannitol and Lactose crystals have on Aerosolized Dry Powder Inhaler Performance containing Salbutamol Sulphate**



**Chapter 8: Aerosolization performance of crystallized Mannitol-Salbutamol Sulphate with different ratios**



**Chapter 9: Physical Mixture Comparative Study**

# List of Tables

**Chapter 8: Aerosolization performance of crystallized Mannitol-Salbutamol Sulphate with different ratios**



**Chapter 9: Physical Mixture Comparative Study**



**Chapter 10: General Discussion and Future Work**

# Acknowledgements

Thank you to my friends and family for supporting me along this journey.

# Abstract

Particle engineering was used to modify particle morphology and the physicochemical/mechanical properties of carriers and active pharmaceutical ingredients. In this study, spray drying and crystallization were used as the main techniques for particle engineering; carriers included lactose, $_{D}$-mannitol, and xylitol. $_{L}$-leucine was used as an additive to modify the morphology of particles and salbutamol sulphate was used as an active pharmaceutical ingredient throughout the researched work. Engineered carriers were used, in some combination, in dry powder inhaler (DPI) formulations to determine whether or not there was an enhancement in the aerosolization performance of the engineered formulations. The prepared engineered carriers were analyzed using laser diffraction (particle size), differential scanning calorimetry (thermal behavior), scanning electron microscopy (morphology), powder X-ray diffraction (crystallinity), Fourier transform infrared spectroscopy (interaction at molecular level), powder flow characteristics (i.e. Carr's Index and angle of repose), high pressure liquid chromatography (HPLC), UV-vis spectroscopy, and *in vitro* aerosolization performance (deposition). It was determined that the efficacy, via Fine Particle Fraction (FPF), of the engineered spray dried lactose-leucine DPI formulation was improved from 25.51 ± 1.23% to 47.11 ± 9.94%. The performance of the engineered spray dried mannitol-leucine DPI formulation was also improved to 52.96 $\pm$ 5.21%. The engineered spray dried mannitol-lactose-leucine DPI formulation had an aerosolization performance of 61.42 $\pm$ 4.21%. The engineered xylitol crystals, however, had an aerosolization performance of 42.94 $\pm$ 15.21% whereas the mannitol-lactose crystals had an aerosolization performance of 68.69 $\pm$ 4.65%. Finally, the mannitol-salbutamol sulphate crystals had a fine particle fraction (FPF) of 62.53 $\pm$ 6.84%. A physical mixture comparative study showed that it was better to engineer the carriers rather than use the commercially available carriers currently in the market. In addition, the results also showed that $_{L}$-leucine acts as a lubricating agent when incorporated into the DPI formulations. Lastly, all of the engineered carriers showed some degree of agglomeration, which made coarse particles suitable for DPI formulations.

# Chapter 1

# Introduction

## *1.1 Introduction*[1]

The pulmonary tract is used in a systematic fashion to tackle chronic obstructive pulmonary disease (COPD), asthma, bronchitis, airway disease, and cystic fibrosis (CF) through the administration of therapeutic agents.[2] In addition, it is a noninvasive, rapid, and effective approach for the delivery of the therapeutic agent, both locally and systematically.[3] It comes to no surprise as the respiratory tract offers a great potential for systematic delivery because the lungs have a large surface area for absorption with an

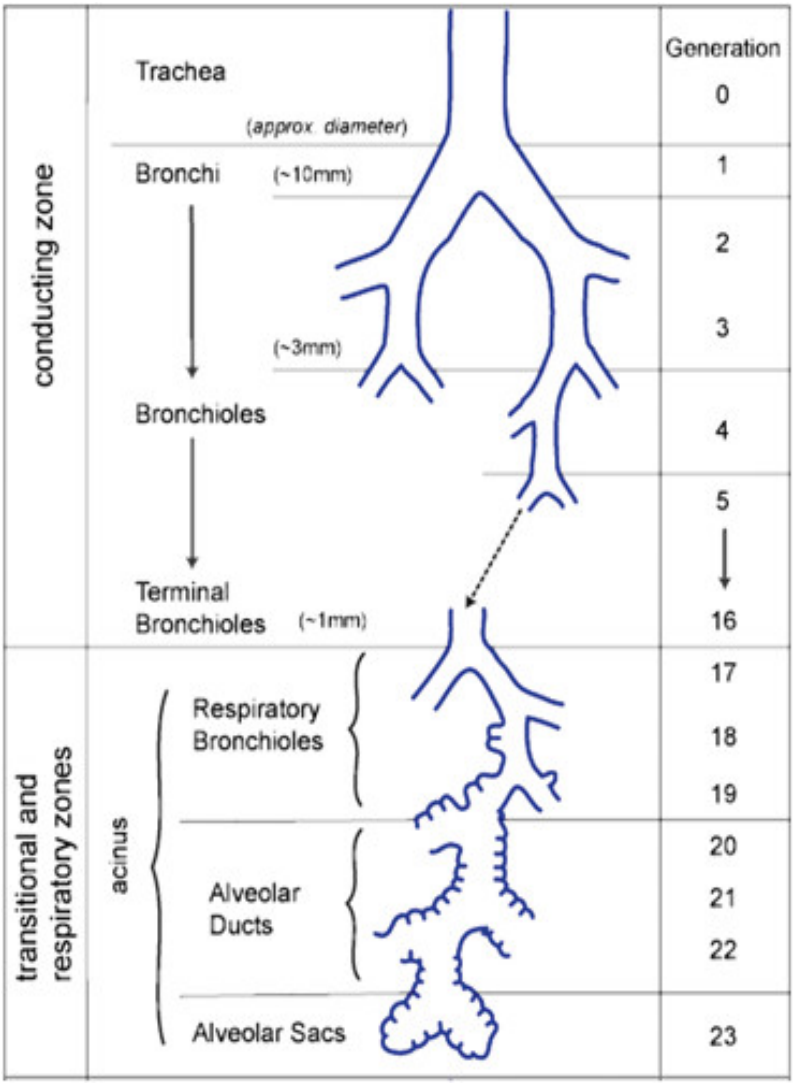


**Figure 1.1.** The Respiratory Tract. Source: Ali Nokhodchi Lecture Note; Pulmonary Drug Delivery, 2018.

abundant vasculature. There are approximately 300 million alveoli in each lung offering a surface area of about 100m$^2$ for an effective gas exchange.[4] It also contains small amounts of drug-metabolizing enzymes compared to the liver and gastrointestinal tract (GIT) providing conditions that favor drug absorption.[5] Figure 1.1 presents a respiratory tree highlighting the different sections of the reparatory tract.

The respiratory tract, however, does pose a challenge; the effectiveness of the inhalation therapy depends upon the site of deposition of the active pharmaceutical ingredient (API). Deposition of inhaled drugs is a complicated process that relies on lung anatomy and physiology, the physicochemical properties of the API, the nature and characteristics of the formulation, and the type of delivery system used for administration.[6] Only particles of a specific size (1-5μm) and shape will be able to deposit in the aveolar region, which is the main site of absorption.[5, 7] Achieving this is usually done with a carrier; the chosen carrier needs to be safe, cost-effective, and pass strict pharmacopeia guidelines. It also needs to be selected in such a manner that it adheres to chemical properties that will not interfere with the drug delivery process and that complement the API.[8–14]

Predicting the drug deposition of the drug in the respiratory tract is crucial in optimizing drug delivery and to evaluate its efficacy.[15] Pharmaceutical aerosol particles can range from $10^{-2}$ to $10^{2}$ μm and are categorized based on their size into coarse particles (≥ 5 μm), fine particles (0.1 to 5 μm), and ultra-fine particles (≤ 0.1 μm).[9] There are mathematical models available that illustrate the deposition and distribution of inhaled aerosols based on airway dimensions, flow dynamics, breathing pattern of the patient, and the shape of the particles involved.[16] Particle deposition can occur via impaction, sedimentation, interception, or diffusion and Figure 1.2[17] presents the different types of particle deposition.

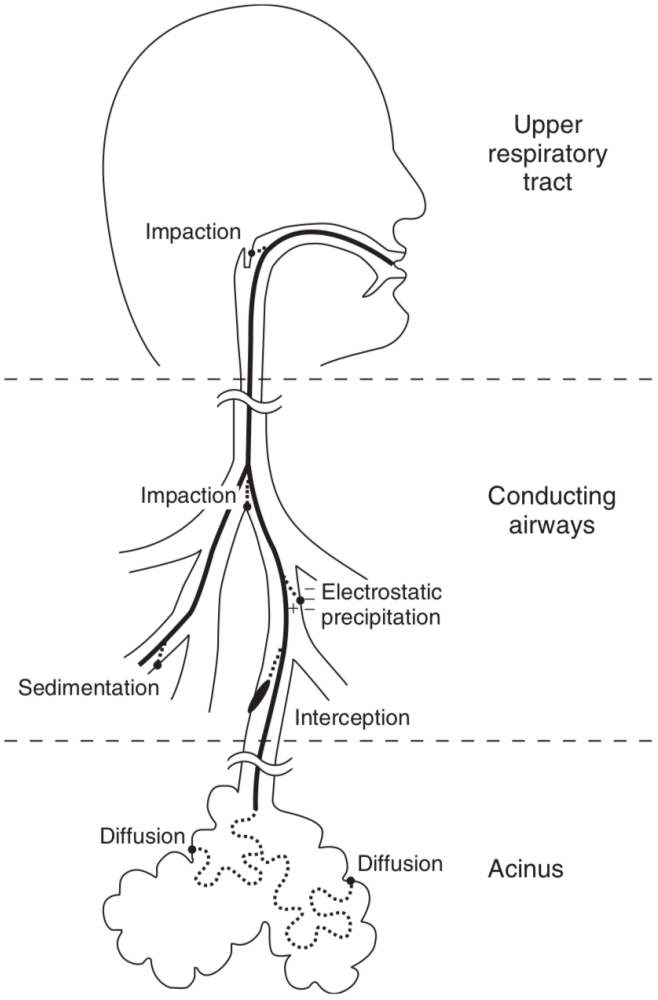


**Figure 1.2**[17]. Particle Deposition. Mechanisms of deposition of inhaled particles in the respiratory tract.

Impaction is considered a flow-dependent mechanism that is dependent on the aerodynamic diameter of the particle and is important for large particles (≥ 5 $\mu$m). Furthermore, large particles don't follow the trajectory of the airway due to inertia and are subsequently swallowed by the patient.[18-20] The deposition probability by impaction [*P(I)*] in cylindrical airways is calculated via Equation 1.1[21] and Equation 1.2

(Eq. 1.1) $$p(I) = 1 - \frac{2}{\pi}\cos^{-1}(\theta\ \mathrm{S}t) + \frac{1}{\pi}\sin[2\cos^{-1}(\theta\ \mathrm{S}t)]$$

(Eq. 1.2) $$\mathrm{S}t\ (stoke\ number) = \frac{pd^2v}{18\mu D}$$

where $\theta$ is the branching angle, $p$ is the density of the particle, $\mu$ is the viscosity of fluid, $v$ is the velocity of the particle, $D$ is the diameter of the airway, and $d$ is the particle diameter.

Sedimentation occurs in the lower bronchial airway and the alveolar region, where airflow is slower, with particles in the range of 0.5 to 5 $\mu$m. If the aerosol particle size is between 3 to 5 $\mu$m, then deposition occurs in the tracheal-bronchial region.[22] Sedimentation of particles is governed by the gravitational force acting on the particles being more dominant than the dragging force imposed by the airflow; the rate of sedimentation increases with an increase in particle size and a decrease in flow rate.[19, 22] The deposition probability by sedimentation [$P(S)$] in cylindrical airways is calculated with Equation 1.3[21]

(Eq. 1.3) $$P(\mathrm{S}) = 1 - e^{\frac{4\cdot g\cdot \mathrm{C}\cdot p\cdot d^2\cdot L\cdot\cos\theta}{9\cdot\pi\cdot\mu\cdot R\cdot v}}$$

where $g$ is the acceleration due to gravity, $\theta$ is the angle relative to gravity, $L$ is the tube length, $p$ is the density of the particle, $C$ is the Cunningham slip angle correction factor, $d$ is the radius of the particle, $R$ is the radius of the airway, and $\mu$ is viscosity of the fluid.

Particles deposited via interception do not diverge from the air stream and are elongated in their shape which causes them to be deposited as soon as they contact the airway wall. The aerodynamic diameter of these particles are smaller relative to their size causing them to be deposited in the lower airways.[22, 23]

Diffusion is the key mechanism for particles that are less than 0.5 $\mu$m due to Brownian motion, which increases with decreasing particle size and air flow rate. Particles move from an area of high concentration to an area of lower concentration across the streamline and deposit upon contact with the airway wall; this is governed by geometric rather than aerodynamic size of the particles.[21, 22, 24] The deposition probability by diffusion [*p(D)*] in cylindrical airways is calculated via Equation 1.4[21]

(Eq.1.4). $$p(D) = \sqrt{(2KTC) \cdot \frac{3\pi nd}{R}}$$

where *R* is the airy diameter, *k* is the Boltzmann constant, *T* is the absolute temperature, *n* is the gas viscosity, and *d* is the particle diameter.

The efficacy of inhaled therapy using a dry powder is dependent on at least four variables: the physicochemical properties of the formulation components, the design of the device, the mechanism of powder dispersion, and the patient inhalation maneuver.[14, 25] The principal forces involved in dry powder dispersion from a dry powder inhaler (DPI) are

frictional, drag, lift, and inertial forces.[8] Therefore, the blending technique used and the selection of the carrier properties such as size, shape, humidity, crystalline state, and surface roughness will influence the final aerosolization performance of the drug formulation.[14]

DPIs are generally grouped into three categories based on the dose metering system: single-unit dose, multi-unit dose, and multi-dose reservoir. The single dose inhaler is the most widely utilized type of DPI which requires the patient to load the devise with a hard capsule containing micronized powder formulation prior to inhalation.[26] The multi-dose devices are available with pre-metered doses stored in individually sealed protective packaging. The multi-dose reservoir contain the bulk powder formulation in a multi-dose reservoir where individual doses are metered under gravity and dispensed by a built-in mechanism.[26, 27]

Moreover, DPIs may be classified as passive or active devices. Passive devices rely solely on the energy generated by patient inspiratory flow rates to fluidize and disperse the powder. Active DPI devices possess an internal power source dispersion unit to aerosolize the powder using compressed air.[28]

These principles have been implemented with those of particle engineering in such a way as to allow for novel formulations to be constructed and tested.

## *1.2 Particle Engineering*

### § 1.2.1 Spray Drying

Methodologies for particle engineering have evolved from a traditional approach into taking on a more contemporary one, through the introduction of the spray drying technique, whose manifestation began about 140 years ago.[29] More precisely, spray drying is an analytical technique in which dry powder is produced via the evaporation of an atomized liquid when it is mixed with a drying hot gas medium.[30] Converting an aqueous solution into a solidified form in a matter of milliseconds, through the exchange of heat (ΔH), has allowed this technique to take on unique advantages while also granting it a wide spectrum of usage; both in industry and in research.[30] Capable of producing an amorphous product, where the solid state of the active pharmaceutical ingredient (API) undergoes a phase equilibria change from the crystalline, or rather solid phase, to the amorphous phase, whose transition state underlies with that of the liquid and solid phases, can be be understood via Equation 1.5, which follows the Gas Laws[30]

(Eq. 1.5). $$\Delta G = -RT\ln\left[\frac{\sigma Amorphous}{\sigma Solid}\right]$$

where $\Delta G$ represents the Gibbs free energy difference between the two phase equilibria under standard conditions, $R$ being the gas constant, $T$ being the temperature at which the measurement was taken, in Kelvin, $\sigma^{Amorphous}/\sigma^{Solid}$ as the solubility ratio of both phase equilibria, and where the moisture content and relative humidity follow US FDA guideline.

Spray drying, itself, is an energy intensive, continuous, and scalable drying process allowing for various specialized applications to be seen; from microcapsules to controlled release particles, composite micro-particles, and nanoparticles and liposomes.[31-33] Critical physical parameters that lie at the core of the process and feed variable induced changes are vapor pressure, evaporation rate, drying time, droplet size/distribution, crystallization rate, film formation rate, heat/mass transfer, and outlet temperature.[34]

Inventive and innovative methods have been developed which include the ability to prepare solid amorphous dispersions, excipients in manufacturing, pulmonary and bio-therapeutic particle engineering, encapsulation, and in drying a crystalline active API.[30] Moreover, the contemporary introduction of spray drying has allowed the, once poorly soluble API, to be more bioavailable such that there is an increase in the stability of the API in its amorphous state, an increase to the effective solubility to the API relative to the crystalline form, and in its ability to inherit crystallization of drug *in vivo* upon dosing and dissolution;[35, 36] just to name a few.

Aside from spray drying, however, other techniques are available that could be used like that of co-grinding, freeze drying, hot melt extrusion (HME), supercritical methods (SCM), or electrohydrodynamic based methods. In pharmaceutics, however, spray drying is a very well utilized unit of operation employed for drying operations to particle engineering of bulk active pharmaceutical ingredients, excipient and pulmonary formulations, granulations, etc.[30, 37] Solid dispersions are kinetically stabilized systems and the chosen

method of manufacturing has a significant impact not only on the external morphology of the particle, but also on the intricate intra- and inter-molecular arrangement of the formulation. According to Chiou and Rielman, whom define solid dispersions, they consist of a dispersion of one or more active ingredients in an inert carrier matrix at solid state prepared by melting (fusion), solvent, or melting solvent method.[38] Amorphous solid dispersions, soluble complexes, encapsulated systems, solid self-emulsifying systems, and nano-dispersion of poorly soluble drugs prepared by spray drying have become the primary solubilization strategy.[39] Due to differences in the degree of disorder of the starting material, energy input, process time, drug-carrier mixing, and behavior of the formulation components in response to the process induced stress, the chosen technique is carefully selected as the solid state of the drug, its miscibility, molecular mobility, and stability are accounted for.[40] Sugimoto *et. al* provides a comparison between the spray dried and co-grinding technique showing that the spray dried technique exhibited amorphous content while the co-grinding technique did not; highlighting an advantage to the use of the spray drying technique.[41] Dontireddy and Crean compared the spray drying technique with that of freeze drying showing the differences in amorphization between the two techniques; spray drying provided spherical particles via rapid evaporation whereas freeze drying provided irregular flake-like particles via rapid freezing.[42]

Furthermore, when comparing spray drying to that of HME, it was found that spray drying had the advantage of being able to be used for thermo-labile and high melting API while also only requiring small amounts of API during the drug development process.[34] Guns

*et. a*l, however, states that HME provided higher kinetic miscibility between miconazole and Killicoat IR when compared to spray drying;[43] opposite results were obtained by Mahmah *et. al* where a faster release rate was obtained from the spray dried formulation than with the HME formulation.[44] Conventional HME does require an additional downstream process of extrudate milling that can contribute to the destabilization of the product. Apart from differences in solid state characteristics, the formulations are also expected to differ in their powder density, surface area, morphology, and flow properties.[45]

Nevertheless, traditional methodologies implement an iterative design of experiments[46] or a statistical treatment[47] when process parameters are in the developmental stages which are time intensive and require larger quantities of API. Reasoning to its reference as a contemporary approach were derived from the notion of spray drying taking on a spectrum of fundamental models that range from steady-state and equilibrium approaches to that of rate-based and computational fluid dynamics models.[48]

Figure 1.3 presents a visual depiction of the spray drying process as an operational unit found within the laboratory; it's small scale design allows for the careful manipulation of physicochemical properties like that of particle size, morphology, and microstructure. Dependent on key process parameters, particles may attribute a hollow sphere morphology with a low bulk density (<0.2g/cm$^3$) or may have a shriveled raisin morphology having a high bulk density (0.2-0.4g/cm$^3$).[49] While other morphologies are

possible, however, large-sized spherical particles have been shown to give better flow properties and compressibility.

Nevertheless, the industrial model follows the same principle as that of Figure 1.3 with the major difference being it's intended purpose for larger scale production. Shifting from the lab scale to the production scale models requires adjustments like changing the feed system, atomization type, location, or conditions, drying gas dispensing system, chamber dimensions, exhaust gas duct, or change from single pass mode to multiple pass mode. Shifts have the capacity to alter the droplet trajectory, evaporation rate, increase the drying type, solvent mass in the drying air, and alter the wall depositions profiles, therefore it is imperative to understand the impact the parameters have on the overall system.[50] It also becomes important to consider the downstream processing of the product and its development given the numerous avenues where key properties may be affected such as residual solvent, particle size, bulk density, flowability, compressibility, compatibility, disintegration, and overall stability.[34]

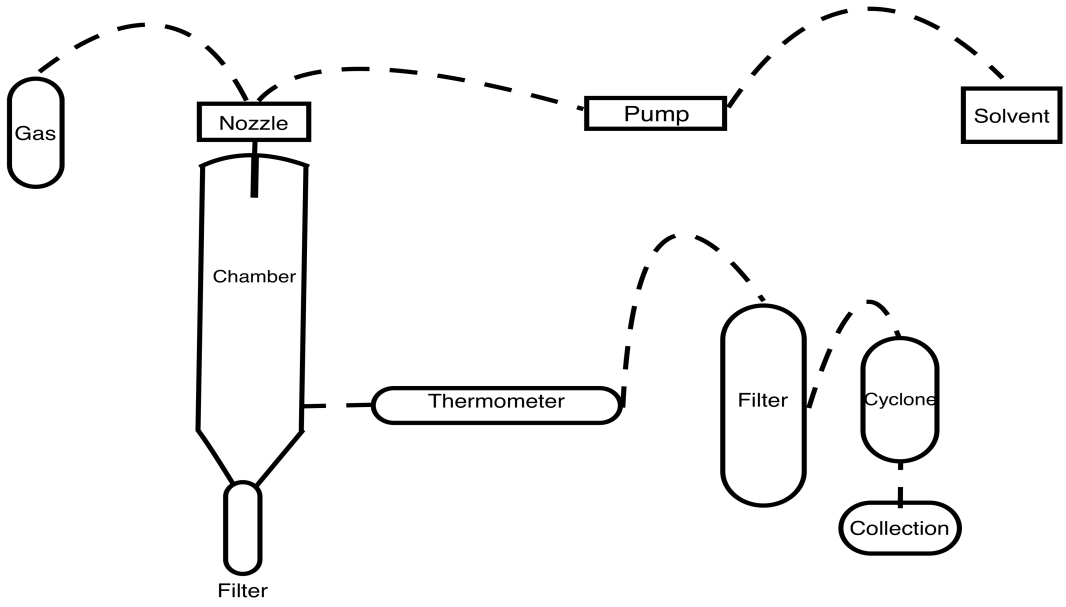


**Figure 1.3.** Spray Drying Process Configuration.

Furthermore, the spray drying process employs a series of offline experiments, an understanding of fundamental models, and a pre-disposed initial process definition that warrant a quick and efficient process. Concurrent processing of a hot gas medium, usually nitrogen, provides an inert process environment with the previously prepared organic solvent allowing spray dried solution to be atomized into droplets by the selected spray nozzle. The selected nozzles could be pneumatic, two-fluid, ultrasonic, rotary, and pressure nozzles.[50, 51] Preparation of the solvent prior to its introduction is also of importance as the addition of a solute increases the thermal efficiency of the spray dried solution given that less solvent has to be evaporated.[51] Physical properties of a solvent

such as its vapor pressure, boiling point, and freezing point are also affected upon addition of a solute.[52] Solvents are either aqueous, alcohols (methanol, ethanol, or isopropanol), or other organic solvents such as dichloromethane (DCM), acetone, methyl ethyl ketone, dioxane, tetrahydrofuran (THF), ethyl acetate, chloroform, and acetonitrile; amongst these, DCM is the most utilized despite its toxicity potential.[39] Choice of the mixture components and their ratio are critical to the process as a whole, as some combinations may result in a change in the particle's morphology, which reduces the release of the API.[53] Al-Obaidi *et. al* provides results from an investigation that explored the effect of changes in solvent ratios and their impact to the overall product.[54]

Aiding to the drying process is the cyclone; efficient in separating dispersed particles from the continuous gas phase based on density differences between the two phases. As the solid particles become subjected to the accelerating flow, there is a lag in the velocity within a rotating vortex that allows for the separation of dense particles in relation to the low density medium. Commonly used cyclones include the reverse flow type where particle air dispersions are introduced tangentially into the top part of the cyclone. At the bottom of the cyclone the gas stream reverses leaving the cyclone through the vortex finder. As the acceleration of the gas flow increases, the chance for smaller particles to be separated also increases.[39]

Droplet formation and solvent evaporation occur concurrently. This allows newly formed droplets to come into contact with the hot gas and then the encapsulated solvent

evaporates leaving behind a dried particle. The dried particle is collected in the collection chamber as shown in Figure 1.3.[55] As solvent evaporation amerces, a solute mass concentration at the surface is observed where the concentration gradient between the droplet surface and core drives solute movement inward from the surface.[56] During this movement, the droplet surface thickens the crust resisting mass transfer and any heat transfer to the droplet at this stage increases the particle temperature thereby facilitating further drying.[57] Higher solvent evaporation rate implies increased transfer of thermal energy per unit time to solute molecules present in the droplet.[58] Evaporative drying can be monitored or described using psychometric charts (Mollier diagrams) as they provide dry and wet bulb temperature, relative and absolute humidity, and enthalpy of the drying gas and relates them to one another.[39]

Selection of the drying gas is crucial as the atomization gas type influences the droplet size, number density, and velocity that ultimately affect the characteristics of the final product.[59, 60] Gases such as $N_2$, Argon, and $CO_2$ have completely varying profiles, when it comes to physical properties such as density and specific heat that are critical for the atomization process. For example, to obtain smaller droplets with high droplet velocities, lighter gases should be employed.[34] Mass flow rate, specific heat, and temperature differential of the drying gas determine the energy lost in the evaporation process where $CO_2$ provides better heat and mass transfer than that of air or $N_2$.[61, 218] Closed loop systems, while using $N_2$ or $CO_2$, have been studied and resulted in a lower yield of 40% of lactose powder as compared to 70% when air was used as the drying medium due to

lower absolute humidity in the system that used air as the drying medium.[62] In the same study, it was shown that the degree of lactose crystallization was found to be highest when $N_2$ was used when compared to $CO_2$ thereby proving that the drying gas also has an effect on particle morphology. Conditioning of the drying gas, with respect to the humidity and temperature, are recommended given that this leads to the gas exerting its heat and mass transfer properties effectively.[39]

Thermodynamic force for the solvent evaporation is the difference in the potential energy between the drying droplet and carrier gas; therefore the rate is given by Equation 1.6[63]

(Eq. 1.6) $$Rate \propto \left[\varrho^{sat}_{pure} - \varrho_{w,air}\right]$$

where $\rho^{sat}_{pure}$ refers to the vapor pressure of pure water and $\rho_{w, air}$ to the partial pressure of water in the gas phase. Nonetheless, droplet formation follows the principle of when the weight of ejected liquid overcomes the surface tension force, a newly formed droplet is observed. Such principle follows Equation 1.7[64]

(Eq. 1.7) $$W = mg = 2\pi r\gamma f\left(\frac{r}{a^2}\right)$$

where $r$ is the external radius of the opening, $\gamma$ is the surface tension of the liquid, $a^2$ is the capillary constant of the liquid which equals to $2\gamma/\rho g$, $\rho$ is the density of the liquid,

and *g* is gavity. Thereby stable performance of the nozzle becomes keen as it ensures the success of particle production[65] while also paying particular attention to the trajectories of droplets inside the drying chamber as this will avoid inter particle and particle-wall collisions.[66] Under appropriate assumptions, the critical factors of the multivariable system can be identified as taking on the Stokes-Einstein equation, which is Equation 1.8[67]

$$D = \frac{K_B T}{6\pi\eta r} \quad \text{(Eq. 1.8)}$$

where $D$ is the diffusion coefficient, $K_B$ is the Boltzmann constant [1.38 x $10^{-23}$ $m^2$ kg $s^{-2}$ $K^{-1}$], $T$ is the absolute temperature, η is the viscosity of the solution, and $r$ is the globular radius. Moreover, water activity from within the droplet relates to the ratio of partial pressure and that of relative humidity (%RH), via Equation 1.9.

$$\varrho_{water}^{vapor} = \frac{\varrho_w}{\varrho_{pure}^{sat}} = \frac{\%RH}{100} \quad \text{(Eq. 1.9)}$$

Diffusion of the drug, polymer, and the solvent becomes an important attribute from the perspective of component distribution from within the particle and for homogeneity; surface enrichment of a particle is given by Equation 1.10[30, 68]

$$\mathrm{E}_i = \frac{c_{s,i}}{c_{m,i}} = \frac{e^{0.5Pe^i}}{3\beta_i} \quad \text{(Eq. 1.10)}$$

where $E_i$ is the surface concentration of component *i* in relation to its average concentration in the droplet, $c_{S,i}$ being the surface concentration, $c_{m,\,i}$ is the average concentration of component *i,* and β is the profile function. Looking closer at the Peclet number [$Pe^i$], Equation 1.11,

$$Pe^i = \frac{K}{8D_i} \quad \text{(Eq. 1.11)}$$

which relates to *K ,* the evaporation rate, and the diffusion coefficient of component *i* in the liquid phase [$D_i$]. When $Pe^i < 1$, the solute equalizes quickly leading to a uniform component distribution and formulation, whereas when $Pe^i > 1$, leads to a quick evaporation and a heterogeneous formulation.[69]

Particle formation becomes dependent on the multivariable platform, like that of droplet formation, where the outcome of the overall system can be seen in Figure 1.4. Micro-particles collected from the collection chamber take on one of three forms: (A) Monocore, (B) Polycore, or (C) Matrix. Porous microparticles have been shown to have unique advantages over non-porous ones, as they have less inter-particulate attractive forces with better flow characteristics and exhibit smaller aerodynamic diameters than their geometric diameters, which is known to facilitate greater deposition in the lower respiratory tract.[70, 71] Dependent on the strength of the atomization, thickness of the outer

shell of the newly formed droplet, and internal pressure build up the particle can either explode, inflate, or crack.[72]

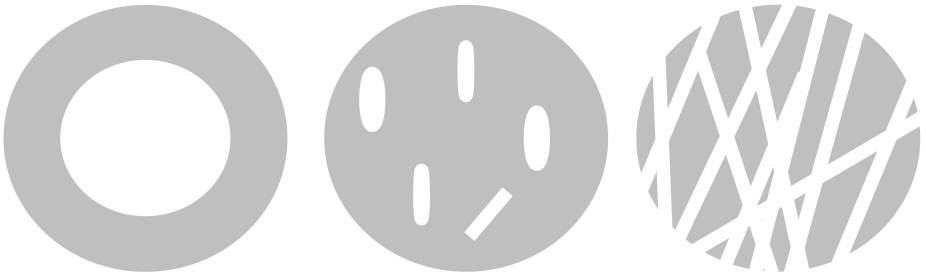


**Figure 1.4**. Spray Dried Particle Differentiation

Furthermore, large pilot-scale and production-scale spray dryers vary in that the operator may choose to operate the spray drier in an *open-loop* our *closed-loop* fashion. Differences between the two is such that in the *closed-loop* option, the drying gas is recycled and passed through a condenser, reheated, and introduced back into the system while maintaining a constant pressure and inert environment.

Two key control volumes are used in defining the physically of a spray drying unit: the *macroscopic control volume* and the *droplet-environment control volume*. *Macroscopic control volume* refers to the entire drying chamber and defines the overall thermodynamic based upon easily measured and monitored spray drying process parameters whereas

*droplet-environment control volume* comprises individual droplet formation, interaction with the hot gas and environment, and solvent evaporation.[73]

Mass-balance and energy-balance calculations can be conducted using the inputs and outputs derived from the *macroscopic control volume* [51, 74] used to predict a continuum of outlet conditions across a range of inlet parameter values that characterize the spray drying operating space and defines a process design space. Droplet kinetics is defined in the *droplet-environment control volume* which focuses on two key factors already mentioned: droplet formation via the atomization process and solvent evaporation via the atomization plume.

Choosing which mode of operation to go with is dependent on key thermodynamic process parameters and outlet conditions that relate with one another through fundamental relationships. [15] Such parameters include $M_{soln}$, drying gas flow rate ($M_{gas}$), $T_{in}$, $T_{out}$, and the relative saturation of the solvent ($\%RS_{out}$), which are related through the energy required to vaporize the solvent; as expressed in Equation 1.12

(Eq. 1.12) $$\Delta E = M_{sol} \cdot (1 - x_{solids}) \cdot \Delta H_{vap}$$

where $\Delta H_{vap}$ is the heat of vaparization and $x_{solids}$ is the mass fraction of solids in solution. Energy lost by the drying gas, however, takes on Equation 1.13

(Eq. 1.13) $$\Delta E = M_{gas} \cdot (T_{in} - T_{out}) \cdot c_p$$

where $c_p$ is the heat capacity of the drying gas. Furthermore, solving for $\%RS_{out}$ gives rise to Equation 1.14

(Eq. 1.14) $$\%RS_{out} = 100 \cdot \left(\frac{P_{chamber}}{P \cdot T_{out}}\right) \cdot \frac{M_{sol} - \frac{(1 - x_{solids})}{MW_{solids}}}{\left[M_{sol} \ln \frac{(1 - x_{solids})}{MW_{solvent}} + \frac{M_{gas}}{MW_{gas}}\right]}$$

where $MW_{solvent}$ and $MW_{gas}$ refers to the molecular weight of the respective species, $P_{chamber}$ is the absolute pressure of the spray drying chamber, and P * $T_{out}$ is the equilibrium vapor pressure of the spray solvent evaluated at $T_{out}$.

Nevertheless, it becomes important to mention that conventional methodologies use statistical design of experiment (DOE) analysis to understand the relationship of key process parameters[75, 76] and the effect those parameters have on the quality of the product.[77-84] Design space is the multidimensional combination and interaction of formulation variables and process parameters resulting in products with assured quality; therefore, the design space is crucial in post-approval manufacturing.[85] Drawbacks in such approach include it lacking to take into account the fundamental physics of the process and is limited in its translational capabilities; where the aforementioned process takes into account all five process parameters.[73] Quality by design is defined by the United State Food and Drug Administration (US FDA) as a systematic approach to development that begins with objectives and emphasizes product and process

understanding and process control, which are based on sound science and quality risk management.[86]

Efforts by FDA's process analytical technology (PAT) initiative, which coincides with those of the International Conference and Harmonization (ICH), are to assure high product quality through timely measurements of critical quality and performance attributes of raw materials, in-process materials, and final products.[87] The said initiative supports the quality by design (QbD) model in that a methodology is drafted such that the desired final product not only meets all the predefined specifications, while achieving desired quality attributes but is also more cost-effective.[88]

Needless to say, the effect that the aforementioned process parameters take on the physicochemical properties of the resulting spray dried formulation, while altering them from one another, and can be studied using the factorial design. Such design evaluates the response to surface models of the parameters while taking into account powder properties like particle size, fine particle fraction, yield, and outlet air temperature and are related to one another via Equation 1.15[89]

(Eq. 1.15).

$$y = b_0 + \sum_{i=1}^{4} b_i x_i + \sum_{i=1}^{4}\sum_{j=1}^{4} b_{ij} x_i x_j + \sum_{i=1}^{4}\sum_{j=1}^{4}\sum_{k=1}^{4} b_{ijk} x_i x_j x_k + b_{1234} x_1 x_2 x_3 x_4$$

where *y* is the response, $b_0$ - $b_{1234}$ are equation coefficients, and $x_1$ - $x_4$ are factors (*F, N, A, and* T, respectively). Equation coefficients were calculated using coded values where the various terms are able to be compared regardless of their real magnitude; a positive parameter coefficient indicates that the response value increased with increasing variable and the opposite for that of the negative coefficient.

Table 1.1[371] presents the findings of Korycka *et. al* who used the aforementioned design on D-mannitol (mannitol) powders from 17-19 °C.

**Table 1.1.** Factorial Design for Mannitol Powders

| Parameter | $T_{out}$ (°C) | *Y* (%) | VMD (*μ*m) | Span | FPF (%) |
|---|---|---|---|---|---|
| **Average** | 85 | 88.0 | 5.16 | 1.34 | 49.0 |
| **Standard Deviation** | 1.2 | 0.1 | 0.27 | 0.14 | 4.8 |
| **%CV** | 1.4 | 0.1 | 5.23 | 10.45 | 9.8 |
| **Measure of absolute error** | 2.2 | 0.1 | 0.27 | 0.14 | 2.8 |

Table 1.2[90 91] culminates the factorial design while illustrating the effect that critical process parameters have on the final product when they are altered. It is known that process parameter alterations vary the crystallinity of the spray dried material thereby affecting porosity, flowability, sorption characteristics, solubility, dissolution rate, and

bioavailability.[92] For instance, the rate at which the feed is injected influences the droplet size, its distribution, droplet velocity, and the particle's surface topography while also having an influence on the heat of fusion.[93-95] Temperature and moisture gradients generate inside the droplet due to higher temperatures influencing the particle formation process while also creating moisture gradients inside the droplet.[96] Moisture uptake is related via the relative humidity of the environment as well as, both, the chemical (i.e. hydrophilicity and hydrophobicity) and physical (i.e. powder specific surface area and particle anomeric composition) properties.[97]

**Table 1.2**. Process Parameters. Effect critical process parameters have on final product.

| Parameter | Effect on final product |
|---|---|
| **High Aspirator Rate** | Increase in outlet gas temperature |
| **High Viscosity or High Solid Content** | Decrease in residual moisture in final product |
| | Higher product uniformity |
| | Increase in outlet gas temperature |
| | Increase in particle size |
| | Increase in yield |
| | Decreased moisture content in final product |
| **High Humidity** | Increase in wall deposition |
| **High Feed Rate** | Increased moisture in final product |
| | Decrease in outlet temperature |
| | Increase in particle size and droplet size |
| | Increased moisture in final product |
| **High Gas Flow** | Decrease in outlet temperature |
| | Decrease in particle size and droplet size |

| Parameter | Effect on final product |
|---|---|
| **High Inlet Temperature** | Increase in outlet gas temperature |
| | Increased yield and a decrease in sticky nature |
| **Use of Organic Solvent** | Decrease in particle size due to a decrease in surface tension |

Moreover, selection of the correct nozzle correlates with that of the desired properties of the final product including its particle size distribution given that the droplet size, and by virtue particle size, is a function of the atomizer's geometry, spray solution attributes (i.e. viscosity and surface tension), and atomization parameters (i.e. nozzle pressure).[98] With that said, droplet size and soluble solids content directly correlate to the final size of the dried particle via Equation 1.16

(Eq. 1.16). $$D_{particle} = D_{droplet} \cdot \sqrt[3]{x_{solids} \cdot \frac{\varrho_{droplet}}{\varrho_{particle}}}$$

where $D_{particel}$ is the diameter of the dried particle, $D_{droplet}$ is the diameter of the droplet, $\rho_{particle}$ is the density of the dried particle, and $\rho_{droplet}$ is the density of the spray dried solution.

Two possible pathways arise from which nozzles are selected: continuous mode and droplet-on-demand. Operation with the continuous mode, as the name implies, introduces a continuous flowing liquid jet into the drying chamber whereas the droplet-on-demand

forms discrete droplets from a short duration of liquid jets. In practice, selection of one of the two modes becomes dependent on the required amount of droplets and the value of the liquid to be atomized.[65] From that, selection is further divided into electro-hydrodynamic generators (EHDG), mechano-hydrodynamic generators (MHDF), and thermo-hydrodynamic generators (THDG). Electro-hydrodynamic generators operate by using an external electric field to disturb the liquid jet into droplets causing there to be a surface charge in the liquid at the tip of the nozzle where the ejected liquid is transformed into a conical shape, called a Taylor cone, due to the induced electric stress.[99] Mechano-hydrodynamic generators, however, apply mechanical energy to the exiting liquid thereby disintegrating the liquid body into droplets; the applied mechanical energy may be in the form of shear force or vibrational forces via a piezoelectric transducer.[100] Thermo-hydrodynamic generators, however, employ thermal energy to the liquid causing it to heat the liquid thereby causing there to be an increase in pressure; leading to droplet formation.[101]

Common atomizers used in the pharmaceutical industry include two-fluid nozzles (pneumatic atomization), pressure nozzles (hydraulic atomization), rotary atomizers (rotating wheel atomization) and ultrasonic atomizer.[102-104] Mizoe *et. al* has introduced a methodology that uses a four-fluid atomizer system where its intent is to overcome the problem faced when needing a common solvent between two different API; here, two liquid and two gas passages are used such that it allows for the two different APIs to be dissolved in different solvents.[105] In comparison, Chen *et. al* developed an amorphous

product by using a four-fluid atomizer and passing the API and solvent from four distinct routes giving an enhanced particle distribution in the lungs while increasing its absorption.[106]

Rotary atomizers are governed by centrifugal forces and the droplet size is inversely proportional to the disk or wheel speed. Pressure nozzles, on the other hand, generate fine droplets by pressurizing a liquid feed from the pump into the nozzle orifice where the droplet size is inversely proportional to the pressure applied and directly proportional to the feed rate. Ultrasonic nozzles generate droplets based on piezoelectric driven actuators vibrating a thin perforated stainless steel membrane in a small spray cap; the membrane features an array of micron-sized holes that generates millions of droplets and a small droplet size distribution.[39]

Following the formation of the droplet and its subsequent introduction into the chamber, other important properties come into play that have a major impact on the outcome of the formulation; one of which being the glass transition temperature ($T_g$). Understanding its importance can provide insight into wall deposition, which is a key processing problem, as the deposited particles indirectly affect the quality of the product through the degradation of the deposited particles onto the wall of the drying chamber.[107] It has been shown that large drying chambers reduce wall depositions given that the walls are out of range from the particle trajectory.[108, 109] Chamber geometry plays an integral role as it directly alters the airflow patterns thereby altering the particle behavior and particle flow

pattern[110]; pure conical, lantern, hour-glass,[111] and parabolic geometries[112] have been studied along with a horizontal configuration[113].

Particle deposition occurs due to the particle's *sticky nature* as they dry, occurring above the glass transition temperature of the substance being spray dried; therefore, the outlet temperature should never be above the product's glass transition temperature.[114-116] The aforementioned *sticky nature* of the particles emerges due to the spray drying process as this produces amorphous powders that are thermoplastic due to their heating or their exposure to high humidity which results in water sorption and thermal plasticization of the particle's surface.[117] Stickiness is a significant issue with spray dried amorphous products resulting in low yields and overcoming this issue can be done by using high glass transition temperature additives.[104, 118, 119] Higher drying temperatures correlate to an increase in the product's glass transition temperature and crystalline temperature while also decreasing molecular mobility aiding in the spray drying selection process.[120] With this in mind, glass transition temperatures are a significant indicator of internal thermal stability which is why it is often regarded as a reference temperature for any given material.

At temperatures above the glass transition temperature, the amorphous structure becomes rubber-like due to the polymer molecules becoming softer and more flexible allowing the polymer particles to have a greater molecular mobility. At temperatures below the glass transition temperature, the molecules are in a glassy state where the polymer

molecules have no segmental motion but vibrate slightly.[121] Nevertheless, the introduction of additives to a formulation has been shown to increase the glass transition temperature of the droplet given that additives segregate to the surface of the droplets during spray drying.[56, 69, 123] Therefore, polymers with higher glass transition temperatures are preferred given that they increase the product's shelf-life while improving their physical stability.[124, 125]

Moreover, understanding the formulation's nucleation and saturation points may aid in the drawbacks that may be presented with the *stickiness nature* of the spray dried formulation and with attempting to preserve API and making it more cost effective. As Parimaladevi and Srinivasan presented in their work that deals with the uniformity of crystal size distribution in a solution, it was determined that when the supersaturation of the solution fell within the range of 4.51 to 5.67 (i.e. the concentration is 55-63g/100mL) nucleation of elongated needle-like crystals was observed.[126] Taking this information into account, it, then, becomes applicable to the spray dried formulation given that when spray dried, a thin-like layer develops on the drying chamber walls, thus preventing any particles from further adhering to the chamber and obtaining a higher yield along the way. It shows that maintaining higher concentrations than the thermodynamically required amount *in vivo*/*in vitro* has provided a platform for higher absorption rates to be seen thereby highlighting the supersaturation maintenance potential of the formulation.[127] Kaialy *et. al* has also presented results that affirm the success of needle-like crystals in the delivery

of salbutamol sulphate via the respiratory tract when compared to other, more uniform, spherical crystals.[128]

Nevertheless, when a compound is in its amorphous form, it is known to have a higher Gibbs free energy, therefore a glassy material recrystallizes spontaneously into a more stable crystalline form with a lower Gibbs free energy.[129] Moreover, the amorphous to crystalline transition state is a thermodynamically driven phenomenon due to the crystalline state being in a lower energy state than that of the amorphous state.[34] This phenomenon is described by the William-Landel-Ferry equation where the crystallization rate of powder (*r*) is defined by the fraction of time for crystallization ($\theta_{cr}$) at any temperature (*T*) for the time for crystallization ($\theta_g$) at $T_g$.[130, 131] Equation 1.17 summarizes the William-Landel-Ferry equation

$$\log_{10} r = \log_{10}\left(\frac{\theta_{cr}}{\theta_g}\right) = \frac{-17.44\left(T - T_g\right)}{51.6 + \left(T - T_g\right)} \quad \text{(Eq. 1,17).}$$

where it is shown that ΔT directly contributes to the rate of powder crystallization.

Given the occurrence of phase transitions in the spray drying process, it becomes important to understand the role that humidity plays in the overall schematics as the processed formulation may or may not undergo nucleation. Due to the amorphous state having a higher Gibbs free energy, thus resulting in having a higher solubility and a faster

dissolution in aqueous media,[132] the Flory-Huggins theory aids in estimating the amount of water being absorbed by the formulation which is then coupled with the kinetics of nucleation and crystallization to provide more of an understanding of the chemical processes taking place.

Another theory that becomes applicable is the Johnson-Mehl-Alvrami theory, which provides crystallization rate constants through its description of the solid-state reactions that take place and can be summarized by Equation 1.18.

$$\alpha(t) = 1 - e^{\left[-\int_0^t g\left[\int_\tau^t Y\theta d\theta\right]^m l\tau d\tau\right]} \quad \text{(Eq.1.18)}$$

where $\alpha$ is the fraction crystallized, $Y(\theta)$ represents the growth rate of all $m$ dimensions of growth. $g$ is a geometric constant, and $I(\tau)$ is the nucleation rate.[133-137] Equation 1.18 then, provides an avenue that helps understand the mechanism of nucleation that takes place during the spray drying process as the formulation begins to cool and changes its phase from liquid to solid. Continuous nucleation refers to the process where nuclei continue to form and grow throughout the transformation process. A fixed number of nucleation refers to when the growth proceeds from a fixed number of preexisting nucleation sites. Site-saturated nucleation is a hybrid of the above two cases where all nuclei are present at the beginning of the isothermal process and additional nuclei do not form during the transformation.[138]

Concentrating on the macro-level of the formulation's physical composition, carrier selection proves to be significant given the known impact it has on the downstream processibility of the overall product. Characteristics such as chemical composition, molecular weight, molecular structure, solution/melt viscosity, kinetic and thermodynamic solubility in any given solvent, solubility parameters, melting point, glass transition temperature, and hydrogen donor/acceptor counts are but a few of the properties to consider when carrier selection is thought of.[39] Determinant on composition, dispersions may be categorized into four generations with known specifications for each of them; first generation carriers utilize urea and sugars.[139] Second generational carriers utilize amorphous polymers that are either synthetic in nature or starches and sugar glass. Popular synthetic carriers include, but are not limited to, poly(vinylpyrrolidone) (PVP), polyethylene glycol (PEG), crospovidone (PVP-CL), poly(1- vinylpyrrolidone-co-vinyl acetate) (PVP-VA), or polymethacrylates. Cellulose derivatives such as hydroxypropyl methylcellulose (HPMC), hydroxypropylcellulose (HPC), hydroxypropyl methylcellulose phthalate (HPMCP), or hydroxylpropyl methylcellulose acetate succinate (HPMC-AS) have also been utilized.[34]

Third generation carriers utilize surfactants like poly(ethylene glycol)-block-poly(propylene glycol)-block-poly(ethylene glycol) (poloxamer), glyceryl dibehenate (Compritol 888 ATO), lauroyl polyoxyl-32 glycerides (Gelucire), inulin lauryl carbamate (Inutec SP1) or polyvinyl caprolactam-polyvinyl acetate-polyethylene glycol graft

copolymer (Soluplus). Meanwhile, fourth generation carriers, commonly used for controlled release purposes, are comprised of ethyl cellulose, hydroxypropyl cellulose, Eudragit RL, Eudragit RS, poly(ethylene oxide) (PEO), or poly(acrylic acid) (carbopol).[34]

### § 1.2.2 Crystallization

Crystallization is the separation of an ordered crystalline phase from a metastable solution.[140] It is generally defined as an operation in which external means are used to adjust the solubility of an un-reactive solute to produce a supersaturation.[141-143] The three major steps in the process of crystallization are the supersaturation of the solution, nucleation of the solution, and crystal growth of the target particles.

Nucleation may occur to be primary or secondary in nature; primary nucleation is independent of seed or crystal present in the solution whereas secondary nucleation occurs as a result of a crystal present in the solution. When the nucleation is primary, it may occur as homogeneous or heterogeneous. Homogeneous nucleation is considered spontaneous, dependent on the degree of supersaturation, and occurs due to the clustering of solutes whereas heterogeneous nucleation occurs due to the presence of an external substance.[144]

In essence, the main strategy in macromolecular crystallization is to gradually bring a target to solubilized in an appropriate aqueous solution to a region of supersaturation until

a crystal nucleates and grows. Crystals form under conditions that fall between those producing clear drops (conditions where macromolecular-solvent interactions are stronger than interactions between macromolecules) and those producing a precipitate.[145]

Macromolecular crystallization in itself is a phase transition; to study the coexistence of the crystal and the solution forms of a macromolecule, one needs to determine the set of conditions at which the chemical potentials of the two phases are equal. These capitulate conditions under which different phases are thermodynamically stable.[146-149] A phase, in other words, is simply a macroscopically homogeneous state of matter that does not account for any assumptions about its microscopic nature. [116]

That is to say, phase diagrams depict the state of matter under the variation of certain conditions; they help visualize different dependencies such as simple pressure-volume (P/V) isotherms or pressure-composition (P/x) diagrams. The phase diagrams that are commonly encountered in macromolecular crystallization, however, are temperature-composition (T/x) and composition-composition (x/x) phase diagrams. While these phase diagrams all serve different purposes and contain different information, they all relate to each other as they are all thermodynamic phase diagrams.[116]

In temperature-composition (T/x) phase diagrams, mixtures of the components are prepared and equilibrated at a given temperature and constant pressure and the nature

and relative amounts of phases are established point-by-point via experimental labor; from the sum of the data points, the phase fields and composition lines in the phase diagram are established. [116] In composition-composition (x/x) phase diagrams, however, the primary components of the system are (1) water, (2) protein, and (3) a third pseudo-component that contains constituents like that of buffer which is commonly known as the *reagent*. The downfall is that it is unknown where the solubility lines are, where the phase fields for stable crystals are located, or what other phases may or may not exist. [116] The area between the solubility line and the critical point is where crystallization is most likely to occur and has been coined as the nucleation zone or crystallization gap.[150, 151]

### §§ 1.2.2.1 Anti-solvent Crystallization

Anti-solvent crystallization is a technique that is favored due to it offering an extended range of solvent polarity compared to single solvents.[152] This, then, allows for the possibility to control crystal properties like that of purity[152], crystal size[153, 154], morphology[155], crystal size distribution[154], agglomeration[156, 157], and polymorphism[158-160]. With anti-solvent crystallization, it is possible to produce a supersaturation fairly simply with low energy consumption which is why it is generally conducted in either batch or semi-batch mode for industrial production.[157, 161, 162]

Supersaturation of the solution can be altered by simply adding an anti-solvent into the already supersaturated solution. Recent publications on the anti-solvent process using

various approaches are increasingly appearing in the literature.[163-166] Techniques, like that of Zarkadas and Sirkar, use a porous hollow fibre membrane to maintain and control particle size distribution while those from Chen *et. al* use a modified technique to continuously coat drug particles with a nano-sized polymer for controlled drug delivery.[167-169]

One of the main disadvantages with anti-solvent crystallization is the tendency for the solute to agglomerate uncontrollably.[170] The cause of this is that the product solution becomes surrounded by the anti-solvent which is separated into an interface of solution and anti-solvent. When the two fluids are in contact with each other, the low solubility of the anti-solvent creates a localized high supersaturation with very high supersaturation ratios in the contact area. Before molecular mixing can occur, the localized high supersaturation forces the solute out of the solution without allowing sufficient time for ordering of molecules to enable crystal growth.[171]

### *1.3 Strategic Application*

#### § 1.3.1 Manufacturing Compliance

Large-scale production and manufacturing of products used for purposes of inhalation are governed by the US FDA and the European Pharmaceutical Review in the United States and Europe, respectively. Their regulatory compliance is mandatory and failure

to comply will lead to product refusal. These governing bodies establish the standard operating procedures (SOP) for any given product while also ensuring that current good manufacturing procedures (cGMP) are followed by manufacturers.

#### §§ 1.3.1.1 United States Food and Drug Administration (US FDA)

According to the US FDA, a metered dose inhaler (MDI) consists of a drug formulation and a container closure system. A MDI drug formulation, then, contains the drug substance(s), either dissolved or suspended, in a propellant, mixture of propellants, or mixture of solvents, propellants, and/or other excipients. Concurrently, a MDI container closure system consists of the device constituent part (i.e. the canister, the actuator, the metering valve, etc.) and any additional features (i.e. integrated spacer, integrated dose counter, etc.) as well as protective secondary packaging (i.e. an overlap).[172]

A DPI, on the other hand, differs considerably from those for MDIs and contains a drug formulation (the drug constituent part) as well as a container closure system. For purposes of DPIs, however, a drug formulation contains the drug substance and excipients including a drug carrier (i.e. $_{D}$-mannitol, lactose, etc.). A DPI container closure system, then, contains the devices constituent part and any protective secondary packaging. Current designs of DPI products include pre-metered and device-metered DPIs; either of which can be driven by a patient's own inhalation (passive) or with power-assistance of some type (active) for production of drug particles intended for inhalation.[172]

Performance of MDI and DPI products depends on many key aspects of the drug formulation, container closure system, manufacturing, and patient handling. Product and process understanding is therefore critical to: (1) the development and manufacture of these products, (2) the maintenance of product quality and performance through the expiration date under patient use conditions, and (3) the maintenance of product quality and performance over the product lifecycle, including continual improvement.[172]

This is why MDIs and DPIs are considered combination products by the US FDA. A combination product is defined as a product that is composed of two or more of the three types of medical products (i.e. drug, devise, and biological product) that are physically, chemically, or otherwise combined into a single entity, co-packaged together, or, under certain circumstances, distributed separately to be used together as a cross-labeled combination product.[173] As such, they are subject to current good manufacturing practice (cGMP) requirements for drug and devises. For single-entity and co-packaged combination products, design control requirements apply to the development of the combination product as a whole. For cross-labeled combination products, design control requirements apply only to the devise constituent part but should ensure the safety and effectiveness of the device when used with the other constituent part(s) of the combination product.[174]

Thereby, design controls apply to any combination product that includes a device

constituent part that is subject to them.[175] This ensures that there are no negative interactions between the constituent parts while also ensuring that the product is safe, effective, and performs as expected. Guidance for industry on pharmaceutical development addresses product design and development procedures, which reflect quality by design principles. While quality by design and design controls share the same characteristics and goals, the device quality system regulation includes specific requirements for design development that manufacturers must satisfy.[176]

### §§ 1.3.1.2 European Pharmacopoeia Commission

The European Pharmacopoeia Commission is the decision-making body for the European Pharmacopeia and is responsible for the elaboration and maintenance of its contents. More specifically, (1) it evaluates proposals for inclusion, revision, or suppression of monographs and general chapter, (2) allocates agreed work to a group of experts or working party, (3) reviews the overall progress that is made on the work being revised on a yearly basis, and (4) approves the terms of reference of groups of experts and working parties while defining the criteria that is to be applied for the selection of experts and ad hoc specialists which it appoints.[177]

Together with the European Pharmaceutical Aerosol Group (EPAG) and the European Medicines Agency (EMEA), there exists a legal and scientific basis for quality control of medicines during their development, production, and marketing. The purpose of the

European Pharmacopeia is to promote public health through the recognized standards that promote the quality of medicines and its component; its existence allows for the free movement of medicinal products within Europe and abroad. This movement allows for the globalization and expansion of international trade to continue to develop global quality standards for medicines.[178]

### §1.3.2 Food Industry

Particle engineering via spray drying has been implemented in the food industry in a manner that allows for its innovation to continue to advance. A manner that it is used is in the conversion of fruit juices into a powder form to increase a product's shelf-life while also making it easier to handle.[179, 180] The ease by which moisture is removed from the food specimens by rapid evaporation is what makes the use of spray drying more favorable.[181] In addition, the interest of the food industry in natural flavor- and color-enriched additives has driven the demand of fruit juices powders to increase. Fruits and vegetables which have been spray dried include, but are not limited to banana, orange, bayberry, mango, apricot, blackcurrant, raspberry, ginger, guava, lime, pineapple, tomato, and watermelon.

Furthermore, the use of drying aids within the food industry is also something that is seen because they form an outer layer on the drops and alter the surface stickiness of the particles due to the transformation into a glassy state.[182, 183] The changes in surface

stickiness reduce the particle-particle cohesion resulting in less agglomeration with lower water-holding capacity of the powders.[184]

Karatas was able to develop an experimental spray dryer with a chamber wall scraper for tomato juice; a method that is useful for relatively less thermoplastic sugars like lactose and sucrose.[185] Karatas and Esin investigated the fundamental aspects involved in the drying of tomato concentrate droplets fully exposed to air of constant humidity and velocity.[186]

Masters modelled a pilot plant spray dryer with a cooling air jacket which reduced the particle stickiness on the wall while Masters introduced chambers with air brooms, which rotate slowly close to the wall, that can also cool the wall surface to prevent stickiness of powders; the air broom arm contains a row of nozzles that direct compressed air on to the wall surface.[187, 188] Furthermore, Mani *et. al* used an air broom system for spray drying of banana and mango juice.[180]

Introduction of atmospheric cool air at the lower part of the drying chamber is something that has also been seen as it results in the formation of solid particle surfaces which can also reduce the stickiness of the powder particles.[189] However, only a limited amount of air can be introduced because the cooling process raises the relative humidity which then increases the surface moisture of the particles.[190]

Tonon *et. al* spray dried acai pulp and studied the influence of inlet air temperature, feed flow rate, and maltodextrin concentration on process yield, powder moisture content, powder hygroscopicity, and anthocyanin retention, during micro-encapsulation.[191] Tonon *et. al* studied the effect of temperature, water activity, and type of carrier agent on the anthocyanin stability and antioxidant activity of spray dried acai juice.[192] Khalil and Sial studied the parameters for the production of instant mango juice powder.[193] Goula *et. a*l modeled the sorption isotherms using selected equations by spray drying tomato pulp and defining the glass transition temperature, water activity and water content relationships.[194]

Chang and Nickerson micro encapsulated omega 3-6-9 via spray drying to be able to increase their concentration in food and prevent their oxidation.[195] Papillo *et. al*, on the other hand, spray dried polyphenolic extract from Italian black rice and used it as an alternative ingredient in baked goods; they also found that the rise was a valuable source of polyphenols to produce functional foods.[196]

### §1.3.3 Pharmaceutical

Within the pharmaceutical industry, there are numerous innovative ways spray drying is used, which continue to develop the technique further. Below are some of the most recent publications that involve the use of spray drying.

Rampacci *et. al* uses spray drying in a manner that provides clues on the *in vitro* performance of azithromycin/rifampicin combinations in co-spray dried microparticles against *Rhodococcus equi*, an emerging human pathogen found responsible for worrying zoonosis.[197] Ito *et. al*, however, uses spray drying to prepare dry naked plasmid DNA (pDNA) powders which are then used to determine their effect on gene expression in the lugs of mice.[198] Katsarov *et. al*, on the other hand, used spray drying to produce muco-adhesive glutaraldehyde cross-linked chitosan micro-particles loaded with doxylamine succinate and pyridoxine hydrochloride for nasal drug delivery systems with sustained release. They found that the cross-linked particles exhibited sustained drug release at pH 6.8 over a period of 5 h with an initial burst-effect in the first 30 min.[199] Spray drying is also used by Ceschan *et. al* to formulate micro-particles carrying indomethacin (IN) for potential local (specific and non-specific bronchial inflammatory asthma responses) and systemic treatments (joint inflammation, rheumatoid arthritis and osteoarthritis pain) by optimizing micro-particle properties and characterizing their lung deposition, drug release, and evaluating cytotoxicity and also pharmacological effects *in vitro*.[200]

Looking at the component of atomization in spray drying more specifically, researchers have been focussing on innovative atomization systems which use different forms of energy than the conventional nozzles; normally based on kinetic energy, pressure energy, centrifugal force, or piezoelectrospraying for droplet formation.[34] Electrohydrodynamic spraying, also known as electrospraying, is a technique where the liquid feed is atomized via the application of electrical energy.[201 , 202]

Variations in the operating conditions, which help determine the shape of the liquid meniscus, its motion, and subsequent breakup, and introduction into the drying chamber, become tailored in such a way as to allow different jet formations and breakup patterns, or electrospraying modes, to be observed; some of which include dripping, micro-dripping, spindle, multi-spindle, cone-jet, oscillating-jet, precession, or multi-jet type.[203, 204] Such differences make electrospraying an attractive technique since it can produce particle sizes in the nanometer range.

Its sophisticated set-up along with it producing low yields does provide a few drawbacks for the technique where more development is needed to allow it to be scalable to cGMP production levels.[205, 206] However, the technique has been utilized to fabricate core-shell structures that improved the solubility of the API showing promise for the technique.[207]

Pulse combustion drying, on the other hand, does show process intensification where the atomization of the feed takes place due to sound waves that are produced by a combustor.[208, 209] Producing intermittent high temperature shock waves with a frequency of 50-100Hz makes this technique unique and promising.[210] Its hot-high pressure gases and concurrent shockwaves result in a back-to-back combustion of fuel-air mixture in the pulse combustion chamber where drying takes place via shockwaves, ultrasonic waves (>155dB), gas flow, and gas temperature (>200°C) in the drying chamber. Pulse combustion dryers have the ability to improve the drying rate by 1.2 to 3 times, reduce air

consumption, and air emissions, but fall short with the amount of noise that is produced.[211, 212] Wang *et. al* produced nitrendipine-Aerosil-Tween 80 amorphous solid dispersion particles that exhibited no agglomeration, were smaller in size and had a narrow size distribution.[213]

With respect to crystallization, however, there are researchers like that of Mazlan *et. al* who has been able to elucidate the crystal structure and characterization of GDSL esterase J15, which is a member of Family II of the lipolytic enzyme.[214] Ou *et. al*, on the other hand, used crystallization in developing a new method for the analysis of carbohydrates in matrix-assisted laser desorption/ionization (MALDI) MS.[215] Afrose *et. al* used a controlled crystallization technique to develop ibuprofen (IBP) micro-particles to be used in improved dissolution studies. Their Raman data revealed that the excipients with a large number of hydroxyl groups distributed around the IBP particle in the crystal enhanced the dissolution of the drug due to the increase in the drug-solvent interactions through hydrogen bonding.[216] Zhang *et. al* was able to use crystallization in the structural and functional characterization of a HIV-1 cell fusion inhibitor known as T20. Their crystal structure revealed the critical intra- and inter-helical interactions underlying the mechanism of action of T20 and its resistance to mutations.[217]

While these are a few of the most recent publications dealing with the application of spray drying and crystallization, there are hundreds more.

### *1.4 Aims and Objectives*

The aim of this overall study is to engineer a carrier for salbutamol sulphate that will have optimal properties for a more effective aerosolization performance. The objectives are: (1) to be able to use these findings as a referencing tool for the development of aerosols, (2) to determine whether the use of excipients made a difference to the carrier's aerosolization performance, (3) to determine optimized spray drying conditions for carriers to be used in DPI formulations, (4) to determine whether or not particle morphology and physicochemical properties played a role in the efficacy of aerosolized carriers, (5) to implement a set of practices that would be useful if any engineered formulation was to be commercialized, and (6) to find an innovative mechanism of agglomeration that resulted from the altering of physicochemical properties.

Thus, making this research important as it contributes to the current understanding of aerosolized particles by providing further conclusions. This research also proposes principles and practices that aid in the development of the current field.

Moreover, this chapter has presented the necessary background information that is needed for one to understand the intricacy of using inhalation as a means for drug delivery; it has also introduced techniques that are used in engineering a suitable formulation. Those techniques were then followed by extensively highlighting their most current application and use, both in industry and in research, while focusing on the theory

behind them. United States and European regulatory compliance agencies were also introduced as a way of illustrating the importance and magnitude that come with engineering aerosol formulations for therapeutic purposes.

Chapter 3 explored the effect that L-leucine has on the aerosolization performance of spray dried lactose while Chapter 4 looked at the effect that L-leucine has on spray dried mannitol and its use as an alternative carrier for DPI formulations. Chapter 5 invetigates the effect that spray dried mannitol and lactose, in different ratios, has on its aerosolization performance while Chapter 6 investigates the use fo xylitol crystals in DPI formulations as well as its potential use as an alternative carrier in said formulations. Chapter 7 looks at mannitol and lactose crystals and Chapter 8 looks at mannitol and salbutamol crystals to determine their aerosolization efficacy. Chapter 9, then, looks at the effect L-leucine has on the aerosolization performance of physical mixtures while comparing them to the engineered carriers from Chapters 3-8. Finally, Chapter 10 provides a summary of all the findings while proposing future investigations.

# Chapter 2

## Materials and Methodological Approach

### *2.1 Introduction*

In this chapter, a fundamental platform has been established through the creation of methodologies, which governed the original academic research presented in the chapters that follow. Here, one will find a more descriptive outline of the operating procedures that were used in the creation of the engineered carriers and drugs that were used throughout this overall study. It is important to note, however, that the standard operating procedures outlined within this chapter follow the regulatory guidelines set forth by the regulatory agencies from, both, the United States and the European Union.

### *2.2 Materials*

$_{D}$-Mannitol [Pearlitol®], Xylitol [(2S,4R)-pentane-1,2,3,4,5-pentol], and α-lactose monohydrate were supplied by *Roquette* (Lestrem, France), SS from *L.B.* (Bohle, Germany), and $_{L}$-leucine by *Acros Organics* (Geel, Belgium), a *Fisher Scientific* company. *Acros Organics* also supplied the monobasic potassium phosphate and the Trifluoroacetic acid (TFA) used for the preparation of the mobile phase for high-pressure liquid chromatography (HPLC). Methanol, Ethanol, Acetone and Hydrochloric Acid were purchased from *VWR International Ltd*. (Leighton Buzzard, United Kingdom) and were

HPLC-grade.

### *2.3 Spray Drying*

Spray drying was conducted using the *Mini Spray Dryer B-290* from *Buchi* (Flawil, Switzerland) equipped with a dehumidifier (*Dehumidifier B-296*), an inert loop (*Inert Loop B-295*), and an outlet filter at room temperature (20°C). Parameters associated with the procedure were as follows: inlet temperature of 220°C, aspirator set to 100% (~35$mm^3$/h), pump rate set to 5% (~2 mL/min), nozzle diameter of 5µm, and a flow rate of 22% designed for a closed environment with the use of nitrogen ($N_2$) gas; several rigorous optimization procedures were implemented to achieve the selected parameters and overall protocol, however.

In chapter three, each 100 mL of the solution for spray drying contained different concentrations of $_L$-leucine (0.1, 0.5, 1, 5, and 10 g) and 60 g of lactose. Meaning that the percentage of $_L$-leucine in each solution was 0.1, 0.5, 1, 5, and 10% w/v, respectively. Both leucine and lactose were dissolved in deionized (DI) water while heating the solution to 75°C with a stirring speed of 120 rpm; the final solutions were spray dried under the conditions mentioned above.

In chapter four, each 100 mL of spray dried solution contained different concentrations of $_L$-Leucine (0.0, 0.06, 0.3, 0.6, 3.0, and 6.0g) and $_D$-Mannitol (60.0, 59.94, 59.7, 59.4,

57.0, and 54.0g; respectively). Meaning that the percentage of $_{L}$-Leucine in each solution was 0.0, 0.06, 0.3, 0.6, 3.0, and 6.0% w/v, respectively. Both $_{L}$-leucine and $_{D}$-mannitol were dissolved in deionized water and were heated to 75°C with a stirring speed of 120 rpm at room temperature (20°C); the final solutions were then spray dried under the conditions mentioned above.

In chapter five, the carriers for each of the formulations were prepared by weighing a constant amount of $_{L}$-leucine (5 g) to that of $_{D}$-mannitol (1.35, 0, 47.5, 23.75, and 71.25g; respectively) and lactose (0, 1.35, 47.5, 71.25 and 23.75g; respectively) yielding the following carriers: Mannitol, Lactose, 1:1 (Mannitol:Lactose), 1:3 (Mannitol:Lactose), and 3:1 (Mannitol:Lactose) all with 5% $_{L}$-leucine (w/v). Carriers were dissolved in de-ionized (DI) water while heating the solution to 75°C while stirring at 120 rpm at room temperature (20°C); the final solutions were spray dried under the conditions mentioned above and consisted of them being w/w. Importantly, however, when preparing the $_{D}$-mannitol, lactose, and leucine solution for the carriers, it was important to add the lactose before the addition of $_{D}$-mannitol and leucine to ensure a homogeneous mixture.

### *2.4 Crystallization Methodology*

In chapter six, xylitol crystals were made with increasing concentrations of $_{L}$-leucine (0, 1, 5, and 10%; w/v) by weighing xylitol (60, 59.6, 57, and 54g, respectively) and $_{L}$-leucine (0, 0.4, 3, and 6g, respectively) and combining them in a mixture. Doing this involved weighing the material and then placing them in a beaker where the volume was adjusted

to 100 mL with deionized (DI) water. Solutions were heated to 75°C under constant stirring (120 rpm) at room temperature (20°C) and then acetone was added at a constant rate of of 5 mL/min. The solutions were allowed to cool to room temperature to facilitate crystal formation. Crystals were then filtered under vacuum, placed in a dry oven to remove any residual moisture, and saved in glass vials for future use.

In chapter seven, crystals were engineered to obtain a final stoichiometric ratio of the following carriers: [1:1 mannitol:lactose], [1:2 mannitol:lactose], [2:1 mannitol:lactose], [1:3 mannitol:lactose], and [3:1 mannitol:lactose] by weighing 25, 12.5, 25, 8.33, and 25g of $_{D}$-Mannitol, respectively, and 25, 25, 12,5, 25, and 8.33g of lactose, respectively. After which, 200 mL of DI water was added to the blended material (w/v) where heating was conducted to obtain a final temperature of 75°C accompanied by a stirring speed of 120 rpm at room temperature (20°C). Succeeding this, the solution was added to 500 mL of acetone at a constant rate of 1.5 mL/min to facilitate nucleation and, thus, crystal formation. Cooling was monitored at a close decreasing rate of 5°C/min after which the crystal formation process was allowed to ferment for 24 hrs upon nucleation. Upon completion of the incubation period, the engineered co-crystals were filtered under vacuum using 0.22 µm filters and allowed to dry completely overnight in a dry oven where the temperature was set to 50°C. The dried samples were kept in glass vials for future use.

In chapter eight, carriers were engineered to obtain the following crystals: 1:1 (salbutamol sulphate:mannitol), 1:2 (salbutamol sulphate:mannitol), 1:4 (salbutamol

sulphate:mannitol), 2:1 (salbutamol sulphate:mannitol), and 4:1 (salbutamol sulphate:mannitol). This was done by weighing salbutamol sulphate (10, 10, 6, 20, 20 g; respectively) and D-mannitol (10, 20, 24, 10, and 5 g; respectively) and mixing them with a *Turbula blender (Type T2F,* Junkermattstrasse, Switzerland) for 15 minutes at 72 rpm. After mixing, they were added to 100 mL of DI water and heated to 75°C at 200 rpm at room temperature (20°C). The heated solutions were then added to 500 mL of acetone at a rate of 1.5 mL/min and left overnight to facilitate crystallization. After crystallization had occurred the engineered co-crystals were filtered under vacuum using 0.22 µm filters and allowed to dry completely overnight in a dry oven where the temperature was set to 50°C.

### *2.5 Sieving*

Mechanincal sieving is a pharmaceutical process where particles are passed through a series of sieves with progressively smaller mesh sizes; particles are then weighed and classified into size-fractions based on which mesh they fall on.[219] In the process, coarse particles are removed from smaller particles.[220] In general, however, sieving produces lower levels of charge than other industrial processes such as micronization and pneumatic conveying.[221] In drug-carrier DPI formulations, the carrier is sieved into a range of 63-90 µm or to 70-100 µm; in this case, it was 63-90 µm to comply with US FDA guidelines and the USA Pharmacopeia.[222-226] In this study, particles that fell within the 63-90 µm range were collected using a *Retsch AS 200 Digit Analytical Sieve Shaker* (Hoan, Germany) where the collection pan was placed at the bottom, followed by the 63 µm sieving pan, and finishing with the 90 µm sieving pan. The powders were placed on

top of the 90 µm sieving pan where sieving was performed for 30 minutes with an amplitude of 100 for each of the carriers. Particles which fell within the range of 63-90 µm were collected, sealed, and stored in glass vials in an air-conditioned laboratory with a set temperature of 20°C and a relative humidity (RH) of 50% for future use within this study.

### *2.6 Particle Size Distribution Analysis*

Particle Size Distribution Analysis was conducted using a laser diffraction particle size analyzer (Sympatec Ltd.,Waterford House, United Kingdom) equipped with a *HELOS* sensor and *Windox* software. Analysis of the formulations was completed using both the Rodos dry system and Cuvette wet system; the Cuvette system required the use of absolute ethanol and a stirring speed of 1200 rpm while the Rodos system required a pressure of 3.0 bar, feed rate of 60%, and trigger conditions that used optical concentration of greater than or equal to 0.2%. Detecting the particles was done using the R3 and R5 lenses, which have a particle size detection range of 0.5-175µm and 0.5-875µm, respectively.

The span of size distribution was calculated using Equation 2.1[227]

(Eq. 2.1)

$$\boldsymbol{Span} = \left(\boldsymbol{D}_{90\%} - \boldsymbol{D}_{10\%}\right) \Big/ \boldsymbol{D}_{50\%}$$

where $D_{90\%}$, $D_{50\%}$, and $D_{10\%}$ refer to the particle size (in μm) of 90, 50, and 10% of the cumulative particle size distribution, respectively. The aerodynamic diameter was calculated using Equation 2.2[10, 11]

(Eq. 2.2) $$d_{aer} = d_g \sqrt{\frac{P}{\varkappa \cdot P_0}}$$

where $d_{aer}$ refers to the aerodynamic diameter, $d_g$ to the geometric diameter, $P$ to the density of the particle, $P_0$ to the unit density, and $\chi$ to the shape factor.

### *2.7 Preparation of Dry Powder Inhalation (DPI) formulations*

Using the stored 63-90 μm sieved carriers, salbutamol sulphate (SS) was introduced such that a final ratio (Carrier: SS) of 67.5:1 was obtained. This, then, corresponded to a theoretical dosage of 482 $\pm$ 1.5 μg of SS per single unit from 1.35 g of each carrier and 20 mg of SS. Mixing was carried out with the use of a *Turbula blender (Type T2* ,(Junkermattstrasse, Switzerland) where each of the formulations was subjected to 30 minutes of blending at a speed of 72 rpm to ensure a homogeneous formulation.

In chapter eight where salbutamol sulphate:mannitol (co-crystallised formulation) was implemented, the concentration of salbutamol sulphate was first determined. Once the salbutamol sulphate concentration was known, a final ratio of 67.5:1 was obtained for

each carrier. The carriers used were 1:1 (salbutamol sulphate:mannitol), 1:2 (salbutamol sulphate:mannitol), 1:4 (salbutamol sulphate:mannitol), 2:1 (salbutamol sulphate:mannitol), and 4:1 (salbutamol sulphate:mannitol). This meant that each carrier was weighed (30.80, 69.46, 128.43, 34.01, and 23.82 mg; respectively) and added to D-mannitol (1.289, 1.250, 1.191, 1.286, and 1.296 g;respectively) to achieve the 67.5:1 (Carrier:SS) ratio.

Each capsule (gelatin, size 3) was filled with ~33 mg of each formulation and a minimum of 10 capsules were used for one deposition test. The test was repeated three times for each formulation to obtain the mean and standard deviation. In total, 30 capsules were used in the deposition test for each formulation. Once capsule filling was completed, they were stored for 24 hours to decrease the electrostatic charge prior to them being used in the *in vitro* aerosolization study.

### *2.8 Differential Scanning Calorimetry (DSC) Analysis*

*Perkin Elmer's* (Shelton, Connecticut, United States of America) *Differential Scanning Calorimetry (DSC) 4000* equipped with a *Standard Single-Furnace* was used to perform thermodynamic analysis; viewing and analyzing the data was completed with the accompanied *Pyris Series* software. Endothermic events were displayed using the configurations shown in Figure 2.1 where an endothermic curve would point up and an exothermic curve would point down.

Nevertheless, calculating the enthalpy for each thermal event was done by using the area under each curve, given that the peak area of each thermal event is proportional to its experienced enthalpy.[228] A temperature range of 25-300 °C, 25-120 °C, 25-400 °C, or 25-150 °C was used with a heating scanning rate of 10 °C/min or 5°C/min for all of the samples; the scanning rate was decreased to 5°C/minute as such rate is known to provide a more thorough thermal analysis.[128, 228] The adopted methodology consisted of the following: (1) holding the starting temperature for one minute, followed by (2) using one of the scanning temperatures above, and (3) holding the end temperature for a minute.

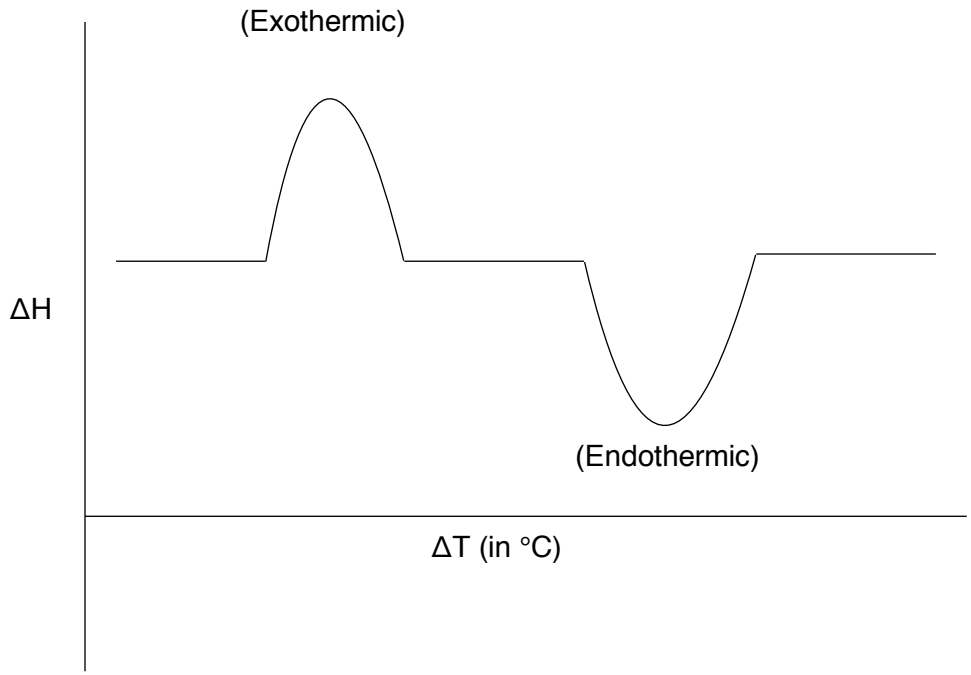


**Figure 2.1** Differential Scanning Calorimetry Curve

Determining thermal events for each carrier was completed through the analysis of the arising peak areas (enthalpy change) as it is known that such areas are proportional to thermal effects experienced by the sample. Equation 2.3[228] was used by the software to determine the peak area:

(Eq. 2.3) $$A = \Delta H \cdot m \cdot K$$

where *A* represents peak area, Δ*H* for the enthalpy associated with the sample, *m* as the mass of the sample, and *K* as the calibration constant known to be independent of temperature.

In addition, calculating the heat capacity ($C_p$) was completed by using Equation 2.4

(Eq. 2.4) $$C_p = \frac{d}{heat\ rate \cdot m}$$

where *d* is the displacement, *m* is the mass, and $C_p$ is the heat capacity; it is important to understand, however, that the rate of heat flow into the sample is proportionate to its heat capacity. [228]

### *2.9 Powder X-Ray Diffraction (PXRD)*

To investigate any changes in the solid state of the crystallized or spray dried samples

X-ray diffraction (PXRD) was used. Determination of particle crystallinity/amorphousness was completed by implementing *Siemens' Diffraktometer D5000* (Munich, Germany), where ~200 mg of each carrier was placed on a stainless steel holder such that a levelled surface was obtained when observed in comparison to the pan and diffractometer. The holder was then placed on the *Diffraktometer* in a manner where analysis was possible. At which point, the sample was exposed to X-rays (Cu $K_\alpha$ - 1.54056Å) with a voltage of 40 kV and a current of 30 mA while being scanned from 5-50° on the 2θ plane at a scanning rate of 0.1 increments per second.

### *2.10 Fourier Transform Infrared (FT-IR) Spectroscopy*

Vibrational frequencies are determined through the interactions between electromagnetic radiation and that of matter; making it possible to observe vibrations of different symmetry.[229] Therefore, vibrational spectroscopies provide definitive fingerprints of molecules through the molecule's absorption of infrared (IR) or mid-IR radiation through inelastic scattering of radiation, which produces shifts from the excitation laser wavelength.[230] These vibrational differences provide insight into the polymorphic composition of the carriers and any changes in the molecular level that are subjected to testing. Polymorphism, nonetheless, is the ability of a particle(s) to exhibit a different stereochemistry from another, thereby making them isomers; about one-third of all drugs display polymorphism.[231] Evaluation, on the basis of polymorphism and the presence or absence of functional groups was accomplished with *Perkin Elmer's*

*Spectrum One FT-IR Spectrometer* (Shelton, Connecticut, United States of America) equipped with a *Universal ATR Sampling Accessory*; the *Spectrum* software was used is unison. Preceding to analysis, methanol was used to clean the instrument, after which a few milligrams (~ 2-5 mg) of each of the carriers was used with a pressure of 100 bar. Each of the samples was scanned three times over a range of 4000-500 $cm^{-1}$ to obtain spectra with appropriate resolution.

### *2.11 Scanning Electron Microscope (SEM)*

Electron micrographs were obtained using a *JMS-820 Scanning Microscope* (Freising, Germany) with a voltage of 4 kV to evaluate the morphology, size, shape, and presence or absence of agglomerates in the samples.[232, 233] Before subjecting each formulation to electrons, they were thinly placed on double-sided carbon tape followed by them being sputter coated using *Agar Scientific's S150 Sputter Coater* (Essex, United Kingdom) with gold (Au), under vacuum in an Argon-rich environment; to view each of the carriers/formulations, different magnifications were employed.

Adjusting the brightness of the collected images was done using Equation 2.5:

(Eq. 2.5)
$$\beta = \beta_c \frac{eV}{kT}$$

where $\beta$ refers to the brightness, $\beta_c$ to the current density at the cathode surface, $e$ to the electron charge [1.59 X $10^{-19}$ C ], $V$ to the accelerating voltage, $k$ to Boltzmann's content [8.6 X $10^{-5}$ $eVK$ ], and $T$ to the absolute temperature in Kelvin.

### *2.12 Powder Flow Characterization*

#### § 2.12.1 Carr's Index (CI)

Carr's index (CI) was measured for some carriers as an indication of powder flowability using an Erweka (Heusenstamm, Germany). Each powdered carrier was filled into a 10 mL graduated cylinder and weighed. After recording the volume (bulk volume) the cylinder was tapped 100 times under standard conditions [room temperature at 20°C and relative humidity (RH) at 50%] and the new volume (tap volume) was recorded. Using mass, bulk and tapped volume, the bulk and tapped density was calculated (mass/volume). Carr's Index (CI), was calculated using Equation 2.6.

$$CI = \left( \frac{D_t - D_b}{D_b} \right) \cdot 100 \quad \text{(Eq. 2.6)}$$

where $CI$ is the Carr's index, $D_t$ is the tap density, and $D_b$ is the bulk density.

#### § 2.11.2 Angle of Repose (δ)

Angle of repose (δ) was measured using the methodology outlined in the European Pharmacopoeia[234] where the angle of repose was the constant solid angle (relative to the horizontal base) assumed naturally by a cone-shaped pile of powder. Such angle was calculated using Equation 2.8:

(Eq. 2.8) $$\tan \delta = \frac{2h}{D}$$

where *h* is the height of the powdered cone and *D* is the diameter of the base of the formed powdered pile. The angle of repose of less than 30° indicates excellent flow characteristics whereas values beyond 45° indicate poor powder flowability.

### *2.13 In vitro Deposition Study*

#### § 2.12.1 Multi-Stage Liquid Impinger (MSLI)

A *Multi-Stage Liquid Impinger* (MSLI), equipped with a *USP induction port* (Copley Scientific in Nottingham, United Kingdom), was used alongside the Critical Flow Controller (*Copley TPK*) and a High Capacity Pump (*Copley HCP5*) that allow for a 4kPa pressure drop to be observed. Because the MSLI has the capacity to filter particles, it allowed for cutoff diameters to be taken into account in each of the individual stages. Calculating the cutoff diameter for each individual stage was determined using Equation 2.9:

(Eq.2.9)
$$D_{50,Q} = D_{50,QN}\sqrt{\frac{Q_N N}{Q}}$$

where $D_{50,Q}$ refers to the cutoff diameter at the flow rate of Q, and N refers to the values obtained for each individual stage of the MSLI when the flow rate is 60 L/min. As a result, when such flow rate is used, the cutoff diameters for each of the individual stages become 13.00, 6.80, 3.10, and 1.70 μm, respectively. Furthermore, at the flow rate of 100 L/min, the cutoff diameters change and become 10.07, 5.27, 2.40, and 1.32 μm, respectively.

Moreover, the Equation 2.10 was employed to determine the test flow duration, in seconds, used within each deposition to adhere with the United States Pharmacopeia (USP) specific standard test methods for Aerosols, Nasal Sprays, Metered-dose inhalers (MDIs), and Dry Powder Inhalers.[222, 223]

(Eq.2.10)
$$T = \frac{240}{Q_{out}}$$

where $Q_{out}$ is the volume of air passing through the airflow meter. Testing the air flow through the device was done with a calibrated *Test Flow Meter DFM3* (Nottingham, United Kingdom) ensuring a 4kPa pressure drop across the whole device; the *Test Flow Meter DFM3* also conforms with USP 33 and Ph. Eur. 6.0.[235, 236]

Each *in vitro* deposition study used 10 capsules (size 3) per run where every capsule was filled with ~33 mg of the Carrier:SS being investigated which corresponded to a theoretical API dose of 482 $\pm$ 1.5 µg of salbutamol sulphate per capsule. All of the formulations were done a total of three times, equivalent to 30 capsules (each filled with ~33mg) per formulation.

In addition, specific parameters were employed for the analysis of the aerosolization of said capsules including the recovery dose (RD), emitted dose (ED), percent recovery, percent emission, impaction loss, mass median aerodynamic diameter (MMAD), geometric standard deviation (GSD), fine particle fraction (FPF), fine particle dose (FPD), drug loss (DL), dispersibility (DS), and effective inhalation index (EI).

Moreover, RD is defined as the amount of drug (in µg) recovered from the inhaler, induction port (IP), mouthpiece (M), and Stages 1-5 (S1-5), ED as the amount of drug (in µg) recovered from IP and S1-5, percent recovery as the ratio of RD to the theoretical dose (482 $\pm$ 1.5 µg), percent emission as the ratio of ED to RD, impaction loss as the mass fraction of drug in IP and S1 to RD (IP + S1: RD), MMAD as the mass median aerodynamic diameter, GSD as the geometric standard deviation, FPF as the ratio between FPD to RD (FPD:RD), FPD as the sum of drug (in µg) from S3-5, DL as the ratio of the amount of salbutamol sulphate recovered from capsules, mouthpiece, and inhaler to RD [(capsules + (I + M)): RD], and DS as the ratio of FPD to ED (FPD:ED).

Furthermore, to determine the effective inhalation index (EI) of each of the formulations, Equation 2.11 was implemented where EI refers to the effective inhalation index, EM to the percent emission, and FPF to the Fine Particle Fraction.[227, 237]

(Eq.2.11) $$EI = \sqrt{(EM + FPF)}$$

All the *in vitro* deposition studies were conducted in an air-conditioned laboratory where the temperature was 20°C and the relative humidity (RH) was 50%.

### *2.14 Homogeneity Assessment*

Assessing the uniformity of salbutamol sulphate (SS) in each of the formulations that was prepared and compare it to the theoretical dose of 482 $\pm$ 1.5µg found in each capsule [which was expressed in terms of coefficient of variation (%CV)]. To this end, ten different samples were taken from each of the formulations in an ordered fashion; eight out of the ten simulating a circle, while the ninth and tenth sample were taken directly from the middle. Carefully weighing the ten samples from each formulation, which yielded a mass range of 10-12mg, they were introduced to 100 mL of deionized (DI) water in volumetric flasks for preparation for high-pressure liquid chromatography (HPLC).

In chapter four through eight, UV-vis spectroscopy was used rather than HPLC. For those formulations, 3 or 5 samples were taken from each, which yielded a mass range of 50 mg, and were then introduced to 50 mL of deionized (DI) water in volumetric flasks;

the wavelength associated to the assay was set at 225nm. Results are based on obtaining the average of the three or five samples alongside the standard deviation for each distinct formulation.

### *2.15 High-Pressure Liquid Chromatography (HPLC)*

#### § 2.15.1 Qualitative and Quantitative Analysis of 4-[2-(tert-butylamino)-1-hydroxyethyl]-2-(hydroxymethyl)phenol;sulfuric acid

In chapters three, four, and five, qualitative and quantitative analysis of salbutamol sulphate was completed by using a mobile phase containing 95% (v/v) of 25 mM potassium phosphate (monobasic) pH 3.0 and 5% (v/v) of methanol. The flow rate of the mobile phase through the HPLC column was 1.5 mL/min with a total run time of 25 minutes per injection set at a wavelength of 225 nm yielding a retention time of 12min. To adjust the pH to 3.0, a 1 M HCl solution was used while stirring at 180rpm, after which the mobile phase was filtered and degassed using a *Fisher Scientific* (Leicestershire, England) 0.22-µm filter before its use.

In chapters six, seven, and eight, however, a mobile phase containing 80% 0.1% Trifluoroacetic acid (TFA) and 20% methanol was used at a flow rate of 1.5mL/min with a total run time of 10 minutes per injection and a wavelength of 225 nm, which yielded a retention time of 6 min. Samples in chapter nine used both methods. The methodology was adjusted due to the residual matter that accumulated in the crevices of the system.

Nonetheless, HPLC was executed via the *Agilent 1100 series HPLC system* (Santa Clara, California, USA) where a degasser (G1322A), binary pump (G1312A), variable wavelength detector (VWD G1314A), column thermostat (G1316A), and thermostatic autosampler (ALS G1329A) coupled with the *Waters Spherisorb 5 µm ODS2 4.6 × 150 mm* analytical column (Milford, Massachusetts, USA). Likewise, internal standards of varying salbutamol sulphate concentrations (0.00. 0.50, 2.50, and 5.00 µg/mL, respectively) were used to calibrate and normalize the results.

### § 2.15.2 Qualitative and Quantitative Analysis of L-Leucine

Qualitative and quantitative analysis of L-Leucine was completed by using a mobile phase containing 50% (v/v) of 0.1% Trifluoroacetic acid (TFA) in water and 50% (v/v) of methanol. The flow rate of the mobile phase through the HPLC column was 0.8 mL/min with a total run time of 15 minutes per injection set at a wavelength of 260 nm which yielded a retention time of 3 minutes. Standard solutions of varying L-Leucine concentrations (0.00, 0.50, 1.00, 5.00, and 10.00mg/mL, respectively) were used to calibrate and normalize the results.

## *2.16 Statistical Analysis (ANOVA)*

One-way analysis of variance (*ANOVA*) was used to evaluate the results in this study where statistical probability (*P*) values less than 0.05 were considered a significant

difference. The test was followed by the Tukey's Honestly Significant Difference (*HSD*) test. All data is expressed as the mean ± standard deviation.

### *2.17 Air Jet Mill*

Air jet milling was conducted using an MC Jet Mill MC One from DEC Group with the following settings: Venturi set to 5 and the Ring set to 4.

# Chapter 3

## Agglomerated novel spray dried lactose-leucine tailored as a carrier to enhance the aerosolization performance of salbutamol sulphate from DPI formulations

### *3.1 Introduction*

In this chapter, the focus was to engineer a spray dried carrier composed of lactose and leucine and investigate the effect that leucine has on the overall aerosolized dry powder inhaler (DPI) performance for salbutamol sulphate. To date, lactose is the most commonly documented carrier in the pharmaceutical industry due to it being highly stable, adhering to good flow properties, and being widely accepted as a safe excipient.[14] Although other carriers such as mannitol[128] and sorbitol[238] have been suggested in DPI formulations, lactose is still the only excipient approved by the US FDA in DPI formulations of APIs.

The use of leucine, however, has previously been shown to improve the aerosolization performance of several drugs from DPIs because it reduces the inter-particulate adhesive forces and API aerodynamic particle size due to its surfactant behavior.[239-242] Coupling both lactose and leucine together in a spray dried solution allowed for the manufacture of an agglomerate

spray dried lactose-leucine system to be created which was aimed to enhance the performance of salbutamol sulphate in DPI formulations.

### *3.2 Materials and Methodology*

**§ 3.2.1- 3.2.12**

Refer to Chapter 2 sections *2.2, 2,3, 2.5-2.11, 2.14, and 2.15.*

### *3.3 Results and Discussion*

#### § 3.3.1 Particle Size Analysis

Figure 3.1 shows two cumulative particle size distribution (PSD) diagrams that illustrate each of the carrier's PSD when using the (A) dry system and when using the (B) wet system. Because of the use of the *Mini Spray Dryer B-290*, it was expected to obtain particle sizes below the approved range of 63–90-µm (Figure 3.1A), given that the spray drying process produces particles below 10µm.[68]

Likewise, Figure 3.1B shows that the particle sizes of each of the carriers, when using the wet system, fell within the 63– 90 µm range. The known occurrence of agglomeration was exploited in such a manner that allowed for it to be used as a carrier within this study. Such focus offered the opportunity to investigate the agglomerates on the basis of parameters that are used in the characterization and analysis of single particles. The particle size measurement in the dry system was able to break the aggregates of spray dried particles (due to applying a pressure of 3 bar during the measurement) whereas in the wet system the spray dried particles stayed as aggregates, although the ultrasound was applied during the measurement.

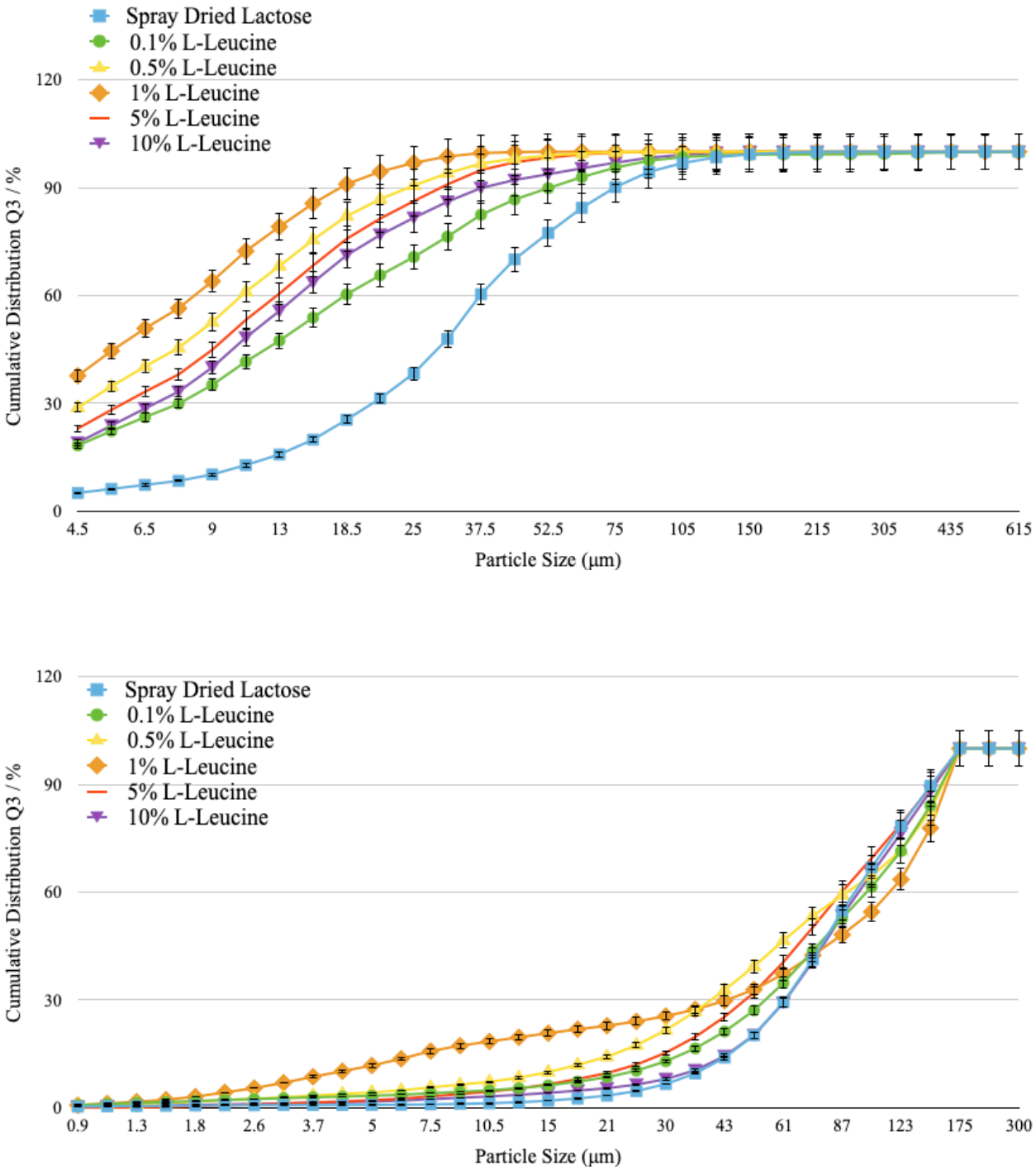


**Figure 3.1** Particle Size Distribution. Particle size distribution (PSD) diagrams of each carrier when using the (A) RODOS dry system and when using the (B) CUVETTE wet system; the carriers used were spray dried lactose monohydrate containing 0, 0.1, 0.5, 1, 5, and 10% $_{L}$-leucine

Table 3.1 highlights each of the carrier's distinct characteristics such as volume mean diameter (VMD) and span of the RODOS dry system and the CUVETTE wet system comparing each characteristic side by side. Table 3.1 shows that all of the carriers experienced a significant difference in their VMDs when comparing each system to one another. For the dry system, the VMD ranged from 8.39 ± 0.40 to 37.97 ± 0.08 µm whereas the range for the wet system was 79.31 ± 2.19 to 87.95 ± 1.91 µm due to the presence of aggregated particles. The dry system experienced a particle diameter range of 1.56 ± 0.05 µm ($D_{10\%}$) to 75.46 ± 7.22 µm ($D_{90\%}$) whereas the particle diameter range for the wet system fell between 20.77 ± 11.02 µm ($D_{10\%}$) and 147.87 ± 170.11 µm ($D_{90\%}$). Due to the aggregation of particles, samples that were measured through the wet system showed smaller span values (narrower distribution) compared to that of the dry system, coinciding with the possibility of the dry system containing mixtures of aggregated and de-aggregated spray dried particles during the measurement (Table 3.1).

**Table 3.1** Particle Analysis. Particle analysis of spray-dried lactose monohydrate and spray-dried lactose monohydrate-leucine where the concentration of leucine was 0.1, 0.5, 1, 5, and 10%

| Formulation | VMD (µm) Dry System | VMD (µm) Wet System | Span Dry System | Span Wet System |
|---|---|---|---|---|
| **Spray Dried Lactose** | 37.97 ± 0.08 | 87.14 ± 0.35 | 2.12 ± 0.09 | 1.36 ± 0.01 |
| **0.1% L-Leucine** | 23.95 ± 5.35 | 87.47 ± 4.94 | 3.61 ± 0.11 | 1.61 ± 0.14 |
| **0.5% L-Leucine** | 11.50 ± 0.28 | 79.68 ± 1.78 | 2.67 ± 0.13 | 2.14 ± 0.10 |
| **1% L-Leucine** | 8.39 ± 0.40 | 86.88 ± 0.84 | 2.57 ± 0.06 | 1.73 ± 0.03 |
| **5% L-Leucine** | 13.58 ± 0.20 | 79.31 ± 2.19 | 2.62 ± 0.12 | 1.74 ± 0.08 |
| **10% L-Leucine** | 17.47 ± 0.63 | 87.95 ± 1.91 | 3.10 ± 0.23 | 1.40 ± 0.02 |

showing the volume mean diameter (VMD) and span when using the RODOS dry system *vs* the CUVETTE wet system (mean + standard deviation)

Such outcomes, then, allowed for the carriers to be implemented and further studied to determine their physicochemical properties and particle morphology given that they underwent spray drying, known to alter such characteristics, while also introducing $_{L}$-leucine as an excipient. VMD (obtained via wet method) of the formulation after mixing for 30 min with salbutamol sulphate showed that the mixing process was unable to break down the agglomerates as the VMD was similar to the VMD of particles before mixing. For example, the VMD of formulations containing 0.1 and 10% $_{L}$-Leucine after 30 min of mixing with SS was 88.0 ± 9.62 and 71.97 ± 0.16 µm, respectively.

Figure 3.2 highlights the electron micrographs of each of the carriers making it evident that all of the formulations, with respect to their carrier, experienced some agglomeration giving way to their larger particle size; thereby supporting the results presented in Figure 3.1 and Table 3.1. Moreover, the SEM micrographs also indicate each of the carrier's morphology contains spherical particles with some agglomerates, particularly in the cases of 0.5% leucine (some of these agglomerated particles for each formulation are shown by red arrows). Such irregularity has previously been shown to be more effective in the delivery of salbutamol sulphate when compared to particles that are classified as being more spherical and regular in shape.[243] The morphology of the spray dried lactose, with increasing concentrations of leucine, is supported by data published by Aquino *et al.* where they showed that more irregular and corrugated particles were obtained in the presence of high concentrations of leucine.[244] Generally, corrugated particles disperse better than spherical ones as this kind of particle reduces contact areas and decreases inter-particulate cohesion.

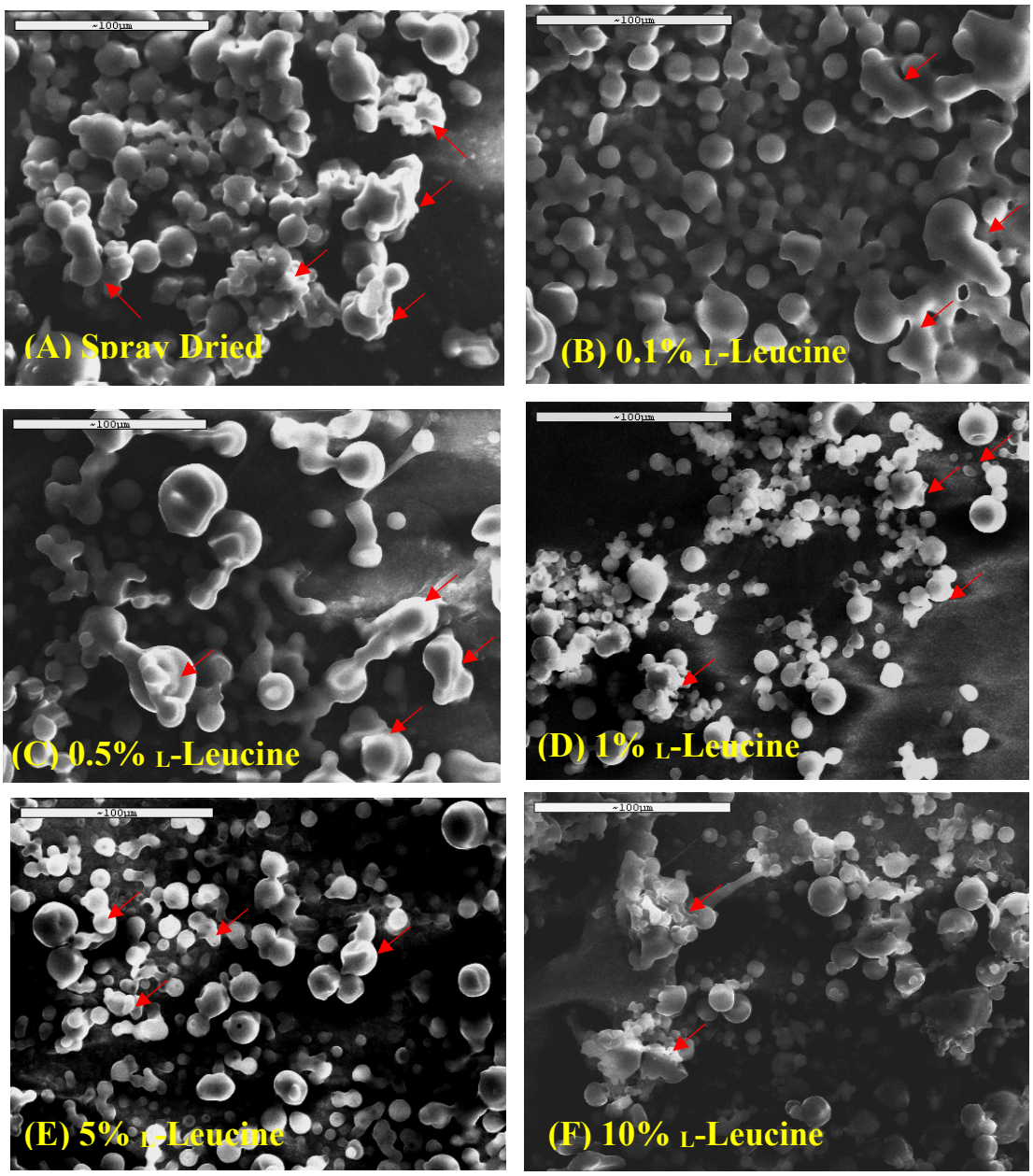


**Figure 3.2** Scanning Electron Microscopy. SEM images of (A) spray dried lactose monohydrate, spray dried lactose containing leucine where leucine concentrations were (B) 0.1%, (C) 0.5%, (D) 1%, (E) 5%, and (F) 10% L-leucine.

Therefore, it was expected that the formulation composition of the leucine carrier would result with an enhanced aerosolization performance when compared to the carrier without leucine, which, in essence, would deliver salbutamol sulphate more poorly.

### § 3.3.2 Solid-state characterization of spray dried samples

Figure 3.3 shows DSC traces of L-leucine, original lactose monohydrate, and spray dried lactose containing 0, 0.1, 0.5, 1, 5, and 10% L-leucine indicating where water evaporation, amorphous lactose recrystallization ($H_c$), α- lactose melting ($H_\alpha$), and β-lactose melting ($H_\beta$) took place. It is obvious from the figure that commercial lactose monohydrate shows an endothermic peak around 149°C, which corresponds to the evaporation of water, followed by an exothermic peak around 171°C, indicating the amorphous state in the sample; moreover, the endothermic peak around 220°C corresponds to the melting of α-lactose whereas any peak around 238°C is an indication of the presence of β-lactose in the sample.[224]

Pure L-leucine was also tested to determine whether or not any thermal events arose between the 25–300°C range, which would rule out whether such events were due to the presence of L-leucine or not. No thermal events were seen within the range where lactose thermal events occurred and the endothermic peak around 300°C corresponds to the melting of L-leucine or its decomposition. Spray dried lactose showed three main thermal events with the first being an exothermic peak around 170°C, attributed to the recrystallization of amorphous lactose to both α-lactose and β-lactose, which was then followed by the melting of α-lactose at around 220°C; furthermore, the third endothermic peak around 238°C was an indication of β-lactose in the sample. Moreover, spray dried lactose did not show any thermal traces for the water evaporation which was a similar pattern that was observed for spray dried lactose containing 0.1, 0.5, and 1%

leucine but with different intensities when compared to the spray dried carrier with no leucine. Spray dried formulations containing 5 and 10% L-leucine did not show any sharp or obvious peaks for water evaporation, the transition of amorphous lactose to crystalline lactose, and melting of lactose.

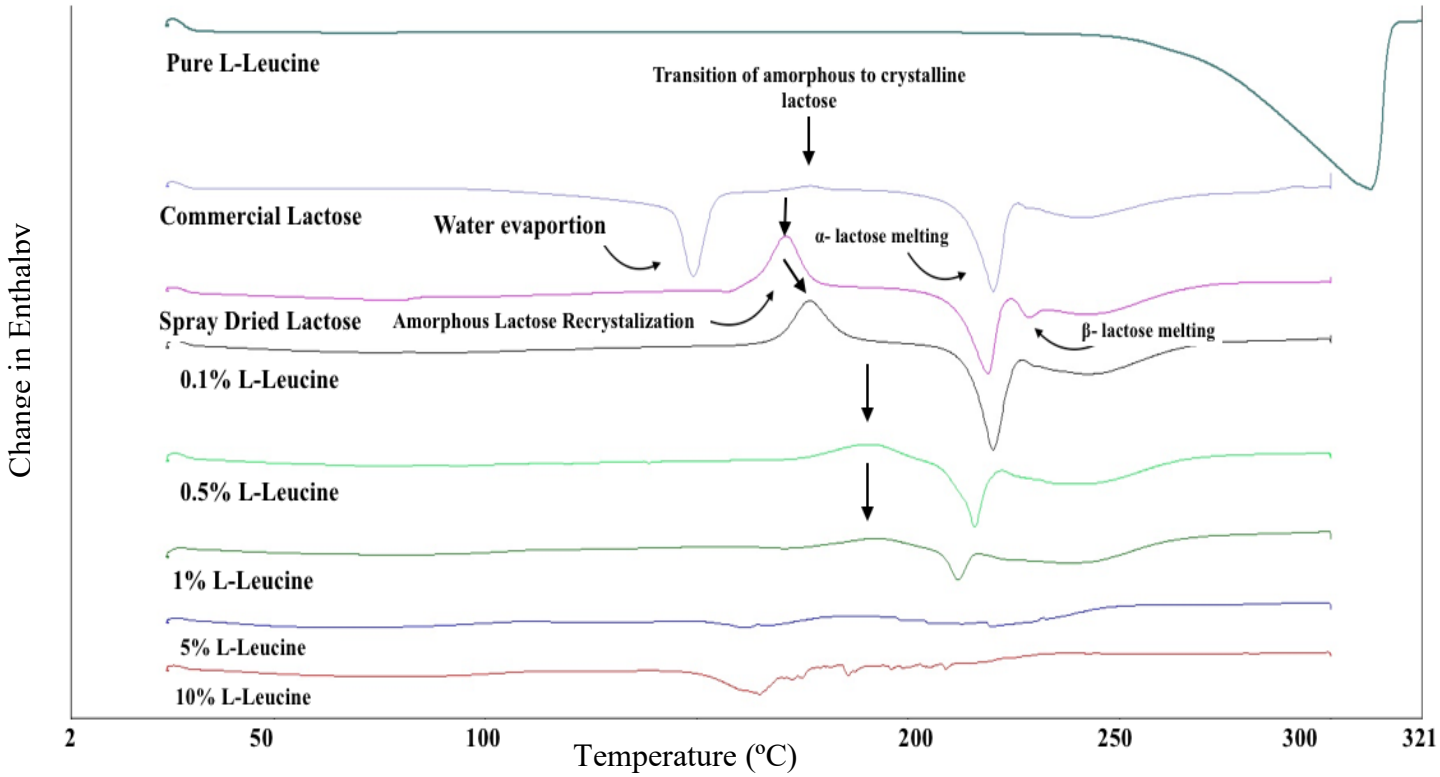


**Figure 3.3** Differential Scanning Calorimetry. DSC thermal peaks of L-leucine, commercial lactose monohydrate, spray-dried lactose monohydrate-leucine where the concentration of leucine were 0, 0.1, 0.5, 1, 5, and 10% w/v (where an exothermic peak would point up and an endothermic peak would point down).

On the basis of this information, all spray dried carriers were considered to be in their amorphous state as the data that was collected indicates given that a definite crystalline structure was not

present prior to their analysis which would have been depicted through the emergence of the amorphous lactose recrystallization enthalpy. Neither a recrystallization nor a melting peak was observed in the 5 and 10% $_{L}$-leucine carrier which serves as an indicator of their higher stability against recrystallization. Such results follow similar patterns that have been presented elsewhere where amorphous drug carriers were formulated in such a way as to increase amorphous stability.[245-248] To make sure spray dried lactose was in the amorphous state, a more reliable technique (PXRD) was used.

Figure 3.4 contains the X-ray diffraction peaks for spray dried lactose monohydrate containing 0, 0.1, 0.5, 1, 5, and 10% $_{L}$-leucine which provides an insight into the polymorphic state of each of the carriers. A carrier's morphology plays an integral role in the drug delivery process that dictates whether a formulation is deemed effective in the delivery of the API of interest.[224]

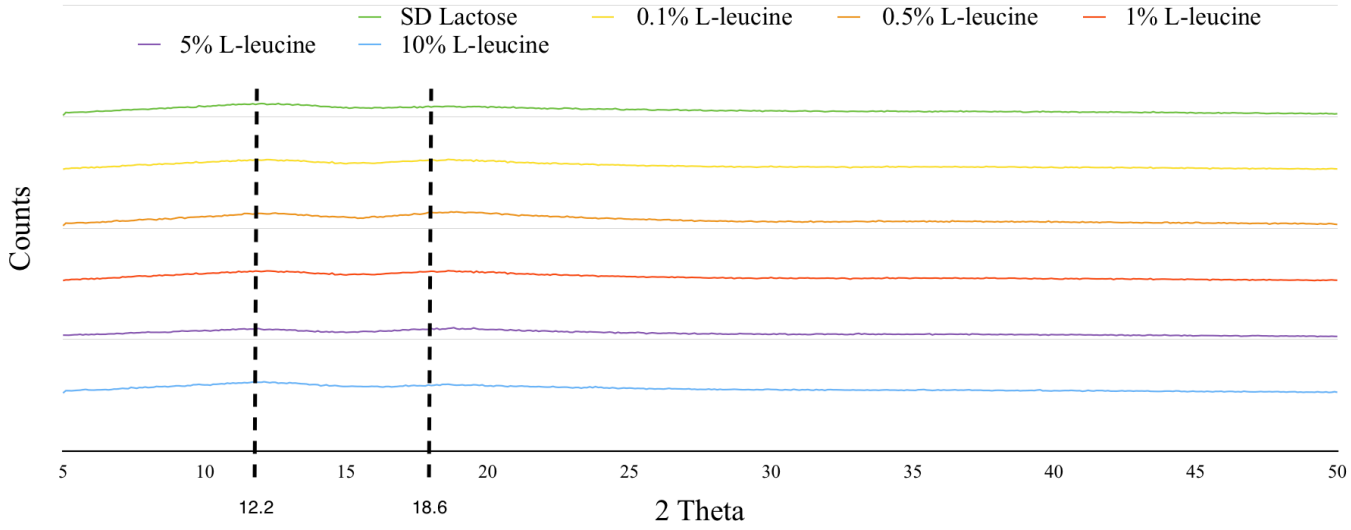


**Figure 3.4.** X-Ray Diffraction. X-Ray diffraction patterns of spray dried lactose monohydrate, spray dried lactose monohydrate-leucine where the concentration of leucine was: 0.1%, 0.5%, 1%, 5% and 10%.

Looking at Figure 3.4 more closely, it becomes evident that all of the carriers, from each of the formulations, were classified as being in their amorphous state given the absence of peaks (halo structure). In addition, all of the carriers showed two distinct peaks each (2θ = 12.2° and 18.6°) that were broad and distributed over a wide range of degrees on the 2θ plane, which also characterizes them as being of amorphous state. Likewise, given that all of the carriers exhibited irregular diffraction of electromagnetic radiation when compared to pure L-leucine (XRD not shown), it correspondingly catalogues them as amorphous as well.[249]

To further assess the solid-state of each carrier within this study and identify any interaction between lactose and leucine at the molecular level, FT-IR spectroscopy was implemented with the understanding that amorphous lactose displays a distinct frequency at 1260 and at 900 $cm^{-1}$, α-lactose monohydrate at 920 $cm^{-1}$, and β-lactose at 950 $cm^{-1}$.[224] Figure 3.5 presents the results for the FT-IR spectra of L-leucine, spray-dried lactose monohydrate with its different concentrations of L-leucine (0, 0.1, 1, 5, and 10%), and further supports the fact that the carriers are in their amorphous state as the aforementioned peaks were present. In addition, Figure 3.5 also reveals that, with the increasing concentration of L-leucine, each formulation underwent a phenomenon known as Fermi resonance where a shift in the vibrational energy causes the spectra to have a change in its intensity and resolution.[250 251]

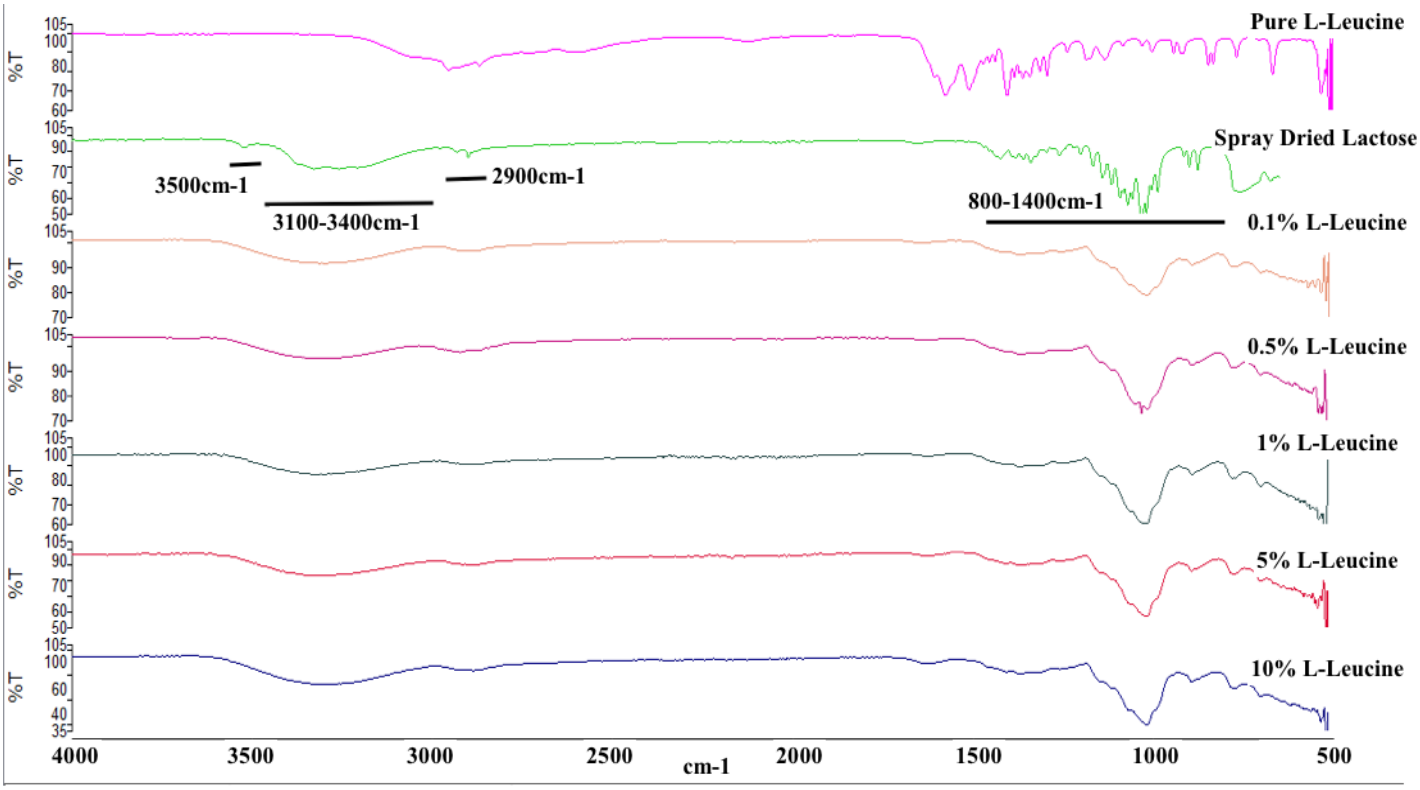


**Figure 3.5.** FT-IR**.** FT-IR spectra of pure L-leucine, spray dried lactose monohydrate, spray dried lactose monohydrate-leucine where the concentration of leucine was: 0.1%, 0.5%, 1%, 5% and 10% highlighting the areas that are eliminated or broadened as the concentration of L-leucine increases while also showing where the amorphous, α-lactose, and β-lactose peaks are to be found.

Such variation within the spectra explains why the frequencies that are associated to key functional groups like aromatic C-H, alkanes, aldehydes, hydroxyl, carbonyl, ethers, and primary amines (which have frequencies at 2900, 3100–3400, 800–1400, and 3500 $cm^{-1}$) become broadened or eliminated completely.

### § 3.3.3 *In vitro* analysis of DPI formulations

#### §§ 3.3.3.1 Salbutamol sulphate assessment

Performance of the drug delivery profile of salbutamol sulphate, with respect to each of the formulations within this overall study, is defined in Figure 3.6 where the amount of salbutamol sulphate recovered from each individual section within the MSLI is looked with a narrower focus: capsules (C), inhaler (I), mouthpiece (M), induction port (IP), stage 1, stage 2, stage 3, stage 4, and filter (stage 5). All of the formulations experienced minimal salbutamol sulphate deposits in the capsules with 5 and 10% $_{L}$-leucine having the least amount after their actuation due to the lubrication effect of leucine, which makes particles flow more easily from the capsule to the inhaler device (Cyclohaler). The lubrication effect of the spray dried leucine has been reported where increasing amounts of $_{L}$-leucine show good lubricating properties.[252] As particles manoeuvre through the respiratory tract, spray dried lactose monohydrate along with 0.1% $_{L}$-leucine experienced the highest amounts of salbutamol sulphate (43.63 ± 23.48 and 49.89 ± 27.80µg, respectively) in the inhaler device when compared to the concentrations above 0.5% $_{L}$-leucine which experienced the least amount at 13.79 ± 11.47µg; the lubrication effect of leucine can also be observed here, as described previously. Furthermore, all of the formulations showed about the same amount of salbutamol sulphate in the mouthpiece (Figure 3.6) but begin to differ at the IP as spray dried lactose monohydrate had the highest amount (65.24 ± 4.26µg) when compared to the other formulations, which had a range of 12.66 ± 5.66 to 29.02 ± 18.56µg.

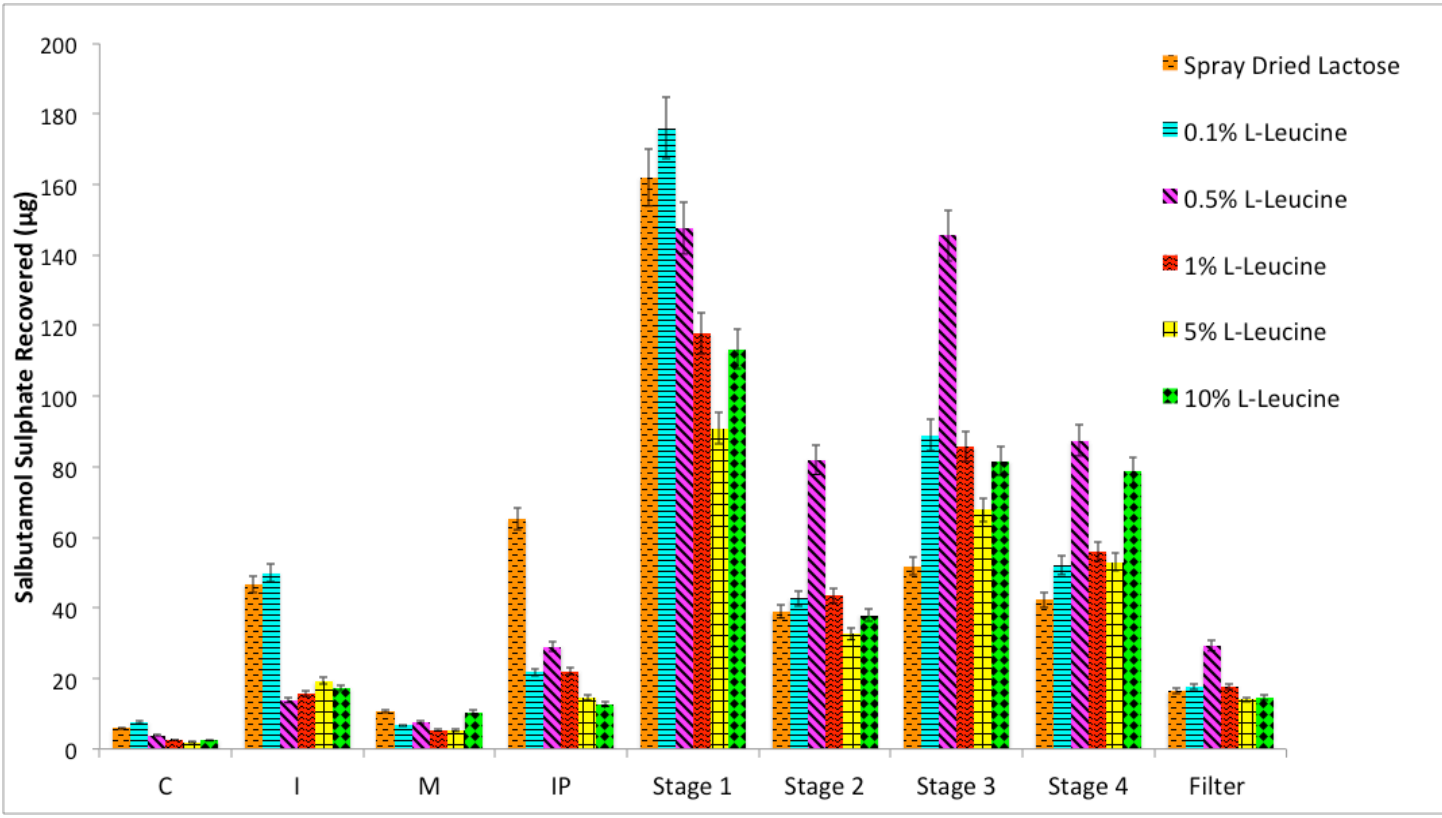


**Figure 3.6**. Aerosolization Profile. Aerosolization performance of each of the formulations (spray dried lactose monohydrate, spray dried lactose monohydrate-leucine where the concentration of leucine was: 0.1%, 0.5%, 1%, 5% and 10% highlighting the amount of SS recovered (percent recovered).

Moreover, 0.1% L-leucine had the highest salbutamol sulphate recovered from within stage 1 (176.06 ± 50.94µg), but where it began to change was with stage 2 onward as 0.5% L-leucine experienced the highest salbutamol sulphate amounts in stage 2, stage 3, stage 4, and filter (81.89 ± 50.20, 145.58 ± 88.08, 87.45 ± 48.49, and 29.25 ± 20.16µg, respectively) indicative of it

being the most successful at delivering salbutamol sulphate to the targeted area that correlates to the alveoli, found in the lower respiratory tract. In other words, the formulations ranked in the following order 0.5% $_{L}$-leucine > 0.1% $_{L}$-leucine > 1% $_{L}$-leucine > spray dried lactose monohydrate > 5% $_{L}$-leucine > 10% $_{L}$-leucine.

Table 3.2 shows the aerosolization performance and deposition data for all formulations studied. All of the formulations differed remarkably ($p < 0.05$) from one another with respect to DL and percentage emission (Table 3.2) given that they all undertook a high number of actuations (n = 10) per run, with each being filled with a consistent weight of around 33 ± 1 mg. The table shows that the performance of DPI formulations containing spray dried leucine is much better than when leucine was excluded from the formulation (the lowest drug loss belonged to spray dried lactose containing 0.5% $_{L}$-leucine).

Impaction loss (IL) within the formulations varied from 34.61 ± 12.38%, attributed to 0.5% $_{L}$-leucine, to 52.49 ± 2.81%, belonging to spray dried lactose monohydrate. Such variation between the formulations could be attributed to their aerodynamic diameter given that impaction is a flow-dependent mechanism governed by particle size.[18]

Effective inhalation index (EI) ranged from 10.87 ± 0.22 (spray dried lactose monohydrate) to 11.98 ± 0.37 (0.5% $_{L}$-leucine) aligning with other data suggesting that 0.5% $_{L}$-leucine has a high-drug aerosolization efficiency.

DS and FPD also showed a variation among the formulations with ranges of 29.31 ± 0.36 to 48.94 ± 10.78% and 262.28 ± 156.60 to 110.41 ± 4.77 µg, respectively. Such variation was attributed to the formulation's particle size given that the phenomenon of inertial impaction becomes prevalent for large particles.[18]

When it came to MMAD and GSD, however, all of the formulations gave similar results with MMAD being 3.12 ± 0.10 µm and GSD being 2.12 ± 0.03 µm. Because particles greater than or equal to 10 µm are removed by the mucociliary escalator and subsequently swallowed in the upper respiratory tract, it was determined that SS had the ability to enter the respiratory tract without facing any problems.[20, 21]

The results showed that spray dried lactose-leucine (containing 0.5% L-leucine) exhibited the highest FPF of 47.11 ± 9.94% suggesting that such formulation was the most efficient at delivering the most SS to the lower respiratory tract. This is because of the correlation that is seen between FPF and amount of SS delivered; that is to say, when FPF increases, the expected amount of SS that is delivered to the lower respiratory tract also increases.[253] Such values, when compared to those obtained by Kaialy *et. al*[254] (FPF of 44.85 ± 1.76%) and Kaialy and Nokhodchi[255] (FPF of 46.9 ± 3.6%), prove to be an increase in the efficacy of salbutamol sulphate's aerosolization performance. This formulation also had the highest percentage emission of 96.41 ± 1.23%, when compared to the other formulations (Table 3.2), suggesting that SS was able to detach itself from the carrier easier when compared to the other formulations. This means that optimal physicochemical properties were attained such that a complementary system emerged between SS and the 0.5% L-leucine carrier. On the other hand, spray dried lactose monohydrate showed the lowest percentage emission (87.02 ± 3.79%) and consequently the lowest FPF (25.51 ±

1.23%). Such results infer that SS had a more difficult time detaching itself from the spray dried lactose monohydrate carrier during inhalation when compared to 0.5% $_{L}$-leucine.

**Table 3.2** Aerosolization Parameters. Recovered dose (RD), emitted dose (ED), percent recovery, percent emission, percent impact loss, mass median aerodynamic diameter (MMAD), geometric standard deviation (GSD), fine particle dose (FPD), fine particle fraction (FPF), drug loss (DL), dispersibility (DS), and effective inhalation index (EI) of salbutamol sulphate obtained from each of the different formulations (spray dried lactose monohydrate, spray dried lactose-leucine where the concentration of leucine was 0.1%, 0.5%, 1%, 5% and 10% )

| Formulation | RD (µg) | ED (µg) | Recovery (%) | Emission (%) | Impact Loss (%) | MMAD (µm) | GSD (µm) | FPD (µg) | FPF (%) | DL (%) | DS (%) | EI |
|---|---|---|---|---|---|---|---|---|---|---|---|---|
| **SD Lactose** | 434.09 ± 40.27 | 376.79 ± 19.65 | 90.25 ± 8.37 | 87.02 ± 3.79 | 52.49 ± 2.81 | 3.13 ± 0.15 | 2.18 ± 0.07 | 110.41 ± 4.77 | 25.51 ± 1.23 | 14.31 ± 4.12 | 29.31 ± 0.36 | 10.87 ± 0.22 |
| **0.1% L-Leucine** | 455.47 ± 53.13 | 398.95 ± 29.95 | 94.69 ± 11.05 | 87.92 ± 4.89 | 43.46 ± 10.14 | 3.19 ± 0.09 | 2.09 ± 0.03 | 158.53 ± 39.73 | 34.99 ± 8.89 | 13.72 ± 5.34 | 39.62 ± 8.79 | 10.93 ± 0.39 |
| **0.5% L-Leucine** | 542.26 ± 297.51 | 520.92 ±281.30 | 112.74 ± 61.85 | 96.41 ± 1.23 | 34.61 ± 12.38 | 3.26 ± 0.05 | 2.09 ± 0.01 | 262.28 ± 156.60 | 47.11 ± 9.94 | 4.14 ± 1.52 | 48.94 ± 10.78 | 11.98 ± 0.37 |
| **1% L-Leucine** | 363.63 ± 49.05 | 342.77 ± 51.17 | 75.60 ± 10.20 | 94.15 ± 1.54 | 37.60 ± 10.86 | 3.16 ± 0.13 | 2.10 ± 0.03 | 159.45 ± 14.31 | 44.33 ± 6.53 | 6.55 ± 1.53 | 47.12 ± 7.23 | 11.77 ± 0.26 |
| **5% L-Leucine** | 297.32 ±175.08 | 272.87 ±179.66 | 61.81 ± 36.40 | 88.91 ± 7.43 | 35.95 ± 4.00 | 3.00 ± 0.18 | 2.13 ± 0.08 | 134.81 ± 91.41 | 43.08 ± 7.38 | 12.00 ± 8.18 | 48.26 ± 5.35 | 11.48 ± 0.63 |
| **10% L-Leucine** | 366.52 ±166.33 | 338.81 ±149.50 | 76.20 ± 34.58 | 92.82 ± 2.34 | 38.74 ± 22.45 | 2.99 ± 0.23 | 2.12 ± 0.08 | 174.83 ± 121.38 | 44.50 ± 17.40 | 7.82 ± 2.26 | 48.27 ± 19.67 | 11.71 ± 0.66 |

### §§ 3.3.3.2 Homogeneity assessment

Assessing the homogeneity of each of the formulations was an essential phase of this study given that a uniform formulation will give rise to a more effective drug delivery profile with a consistent dose to the patient. Table 3.3 eludes the homogeneity profile of each of the formulations (spray dried lactose monohydrate, samples spray dried with 0.1, 0.5, 1, 5, and 10% L-leucine) under investigation showing the potency of each and also presents the percent content homogeneity, which is expressed as the percent coefficient of variation (%CV), of each of the aforementioned formulations. The drug content of all formulations was within 75–125%, and the smallest %CV of 5.48% belonged to 0.5% L-leucine, which was the formulation that showed the best aerosolization performance. Such results indicate that 0.5% L-leucine had the best salbutamol sulphate content homogeneity among all of the formulations followed by 0.1% L-leucine with a %CV of 7.15%. In addition, the results showed that it is a bit difficult to obtain a very low CV% for DPI formulation containing salbutamol sulphate in the DPI formulation studied in the current research. This should be investigated more in the future ongoing research.

**Table 3.3.** Content Homogeneity. Content homogeneity of Spray Dried Lactose Monohydrate, 0.1% L-Leucine, 0.5% L-Leucine, 1% L-Leucine, 5% L-Leucine, and 10% L-Leucine expressed as the percentage coefficient of variation (%CV).

| Formulation | Potency | %CV |
|---|---|---|
| **Spray Dried Lactose** | 91.36 ± 9.40 | 10.29 |
| **0.1% L-Leucine** | 83.62 ± 5.98 | 7.15 |
| **0.5% L-Leucine** | 102.66 ± 5.62 | 5.48 |
| **1% L-Leucine** | 94.72 ± 16.97 | 17.92 |
| **5% L-Leucine** | 89.71 ± 11.87 | 13.23 |
| **10% L-Leucine** | 89.98 ± 7.78 | 8.65 |

*However, has not been taken into account for *in vivo* inhalation studies.

### *3.4 Conclusion*

The results presented in this chapter have proven that the addition of $_{L}$-leucine into the spray dried solutions altered the physicochemical properties of lactose. This alteration allowed for a more effective aerosolization performance of salbutamol sulphate to be observed; there was a two-fold increase in the fine particle fraction (FPF) of the 0.5% $_{L}$-leucine formulation. Furthermore, the addition of $_{L}$-leucine also proved to improve the stability of amorphous spray dried lactose, as was evident in the DSC data. $_{L}$-leucine also provided a lubrication effect for the formulations, which the *in vitro* deposition study showed. All these benefits provide a foundational platform from which to build on in the chapters that follow. Never the less, this chapter has also proven that a more effective formulation can be achieved than the one that is currently in use in the market.

# Chapter 4

## The Crucial Role of Leucine Concentration on Spray Dried Mannitol-Leucine as a Single Carrier to Enhance the Aerosolization Performance of Albuterol Sulphate

### *4.1 Introduction*

The main aim of this chapter is to explore D-mannitol (mannitol) as an alternative carrier to lactose for lactose intolerant patients. To this end, in this chapter, the focus was to engineer a spray dried carrier composed of D-mannitol and leucine and investigate the effect of leucine concentration on the overall aerosolized DPI performance for albuterol sulphate; DPIs are a common tool for use in patients facing COPD and asthma. It has previously been documented that pulmonary delivery of a therapeutic dose has tremendous advantages over any other form of administrative route.[256] In recent years, the respiratory tract has been used as a diagnostic tool for patients suffering from intermittent allergic asthma or allergic rhinitis through the use of D-mannitol as a means to increase the water content in the respiratory tract.[257] It has also been postulated that D-mannitol could be an alternative carrier in DPI formulations to lactose,[258] which is a carrier that is widely used in the pharmaceutical industry.[14]

Efforts to use D-mannitol have shown to have an altering effect on the viscoelastic properties associated to the phlegm, which is located in the airway, while also increasing the water content by creating an osmotic gradient, which facilitates an efflux of water into the airway lumen.[259-265] In addition, D-mannitol is not classified as being a reducing sugar, given the absence of the aldehyde

functional group, and it is less hygroscopic than lactose. $_D$-Mannitol also provides a sweet aftertaste which can be used as a benefit for the patient by confirming that an adequate dose has been delivered.[266, 267]

In Chapter 3, it was determined that the addition of $_L$-leucine improved the aerosolization performance of the 0.5% $_L$-leucine carrier by altering its physicochemical properties causing an increase in the FPF to 47.11 ± 9.94%. In this chapter, an investigation was carried out to see if the same concentration will have the same effect on $_D$-mannitol. In addition, this chapter explores the modified $_D$-mannitol as an alternative to lactose to be used in dry powder inhalation formulations. Moreover, $_D$-mannitol on the market usually shows poor aerosolization performance, therefore, the commercial $_D$-mannitol has to be modified to enhance its performance in DPI formulations..

### *4.2 Materials and Methodology*

**§ 4.2.1- § 4.2.13**

Refer to Chapter 2 sections *2.2, 2,3, 2.5-2.11,* and *2.13-2.16.*

### *4.3 Results and Discussion*

**§ 4.3.1 Particle size analysis**

Figure 4.1 shows the cumulative size distribution obtained by two distinct systems: Rodos (dry system; Figure 4.1A) and Cuvette (wet system; Figure 4.1B). Based on the information from the figure, it was deduced that the carriers all underwent a degree of agglomeration. The pressure applied to the carriers in the dry system was able to de-agglomerate particles and reduce their size range. This explains why there was such a remarkable difference in the size of the particles

between the two systems. The difference was expected because the spray drying technique produces single particles between 1-10µm.[268, 269]

The agglomeration, however, was explored further in a manner that helped in the understanding of the carrier's adhesive and cohesive forces. It was these forces that helped in the characterization of whether or not a formulation was effective in its aerosolization performance. The emergence of agglomerates arising after spray drying is not something new as it has been found before (see Chapter 3) where lactose agglomerated into more coarse particles and were then implemented into the engineered DPI formulations being investigated.[227]

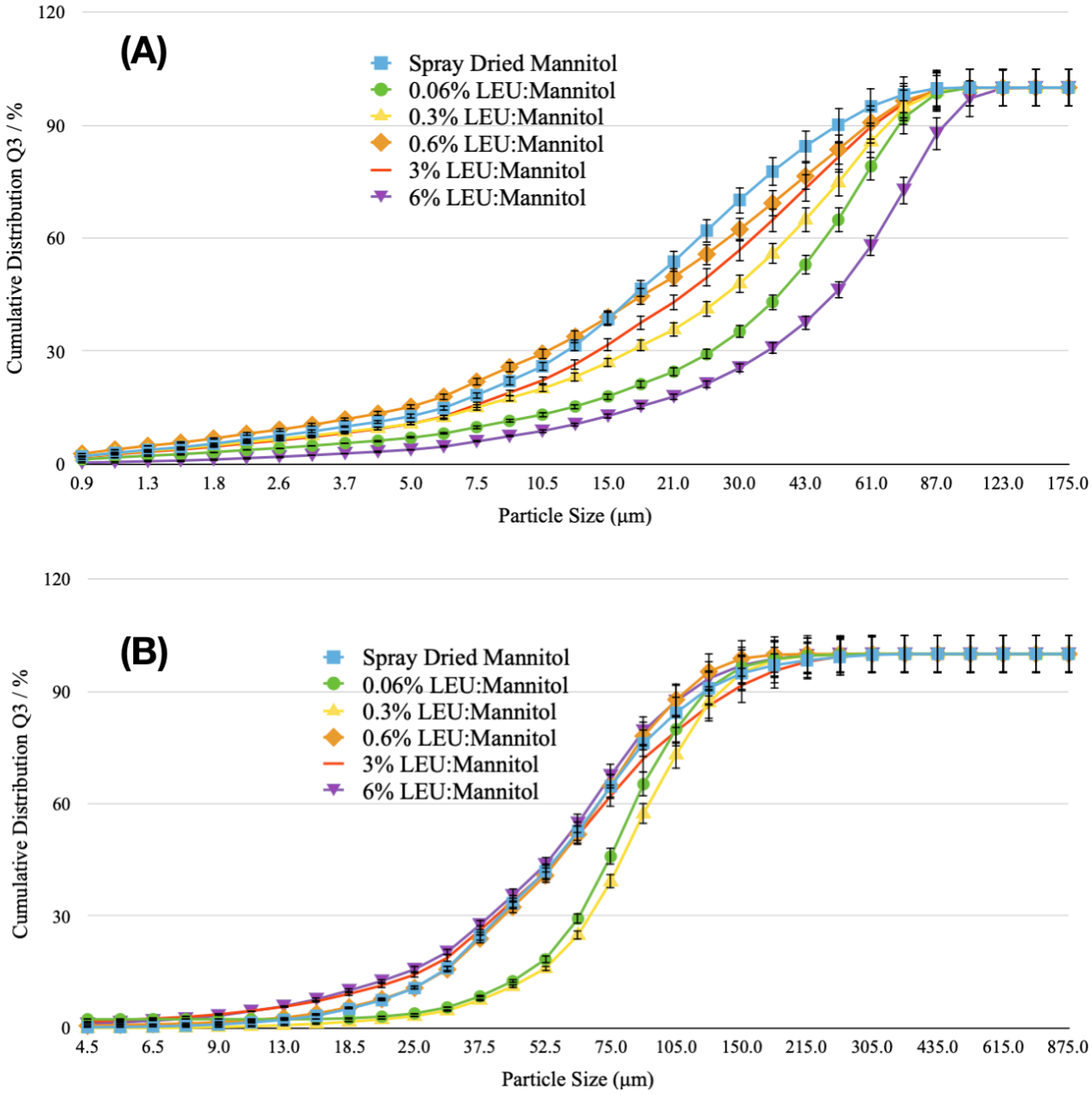


**Figure 4.1**. Particle Size Distribution. Particle Size Distribution (PSD) diagrams of each formulation's carriers when using the (A) Rodos dry system and when using the (B) Cuvette wet system; Spray Dried Mannitol, 0.06% L-leucine:Mannitol, 0.3% L-leucine:Mannitol, 0.6% L-leucine:Mannitol, 3% L-leucine:Mannitol, and 6% L-leucine:Mannitol.

Table 4.1 elucidates the volume mean diameter (VMD) along with the span of each of the distinct carriers comparing the Rodos and Cuvette systems side-by-side. All of the carriers experienced a significant difference in their VMDs ($p < 0.05$) with ranges from 23.98 ± 0.26µm (Spray Dried Mannitol) to 52.99 ± 4.05µm (6% $_{L}$-Leucine) when the dry system was used; in the case of using the wet system, these values increased (Table 4.1). In all the cases, the results showed that the VMDs for the spray dried samples were smaller when measured with the dry system than when the wet system was used. Furthermore, it was concluded that all of the carriers from each of the formulations underwent a degree of agglomeration, which supports the data already presented. The values for the dry system are smaller than the wet system because a pressure of 3 bar was used during the measurement, which allowed the aggregated particles to de-agglomerate, as previously stated. The wet system's aggregated particle sizes, however, were close to the size of carriers used in DPI formulations. Moreover, it was concluded that the performance of the DPI system was not compromised due to the size of the particles.

**Table 4.1**. Particle Analysis. Particle Analysis of Spray Dried Mannitol, 0.06% $_{L}$-leucine, 0.3% $_{L}$-leucine, 0.6% $_{L}$-leucine, 3% $_{L}$-leucine, and 6% $_{L}$-leucine showing the volume mean diameter (VMD) and span when using the Rodos dry system or the Cuvette wet system.

| Carrier | VMD (µm) Dry System | VMD (µm) Wet System | Span Dry System | Span Wet System |
|---|---|---|---|---|
| **Spray Dried Mannitol** | 23.98 ± 0.26 | 69.55 ± 3.85 | 2.43 ± 0.09 | 1.65 ± 3.50 |
| **0.06% $_{L}$-Leucine** | 40.50 ± 0.73 | 81.10 ± 2.34 | 1.55 ± 0.83 | 1.08 ± 2.77 |
| **0.3% $_{L}$-Leucine** | 33.91 ± 1.34 | 87.03 ± 2.54 | 1.97 ± 0.63 | 1.09 ± 2.60 |
| **0.6% $_{L}$-Leucine** | 27.05 ± 0.95 | 64.74 ± 1.69 | 2.69 ± 0.44 | 1.42 ± 2.02 |
| **3% $_{L}$-Leucine** | 29.86 ± 0.19 | 72.82 ± 0.07 | 2.25 ± 1.95 | 2.02 ± 0.20 |
| **6% $_{L}$-Leucine** | 52.99 ± 4.05 | 63.46 ± 0.18 | 1.45 ± 0.15 | 1.63 ± 6.71 |

With respect to the Span, all of the carriers experienced similar values ($p > 0.05$) having ranges from 1.45 $\pm$ 0.15 (belonging to 6% L-Leucine) to 2.69 $\pm$ 0.44 (belonging to 0.6% L-Leucine) and 1.08 $\pm$ 2.77 (from 0.06% L-Leucine) to 2.02 $\pm$ 0.20 (from 3% L-Leucine); for both the dry and wet systems, respectively. Moreover, the dry system experienced a particle diameter range of 5.98 $\pm$ 0.76 µm ($D_{10\%}$) to 66.76 $\pm$ 1.66 µm ($D_{90\%}$) where the particle diameter range for the wet system fell between 28.77 $\pm$ 0.62 µm ($D_{10\%}$) and 124.72$\pm$3.62 µm ($D_{90\%}$).

Figure 4.2, nonetheless, presents the electron micrographs of each of the carriers in each formulation (0, 0.06, 0.3, 0.6, 3, and 6% L-Leucine; respectively). All of the carriers were characterized as spheroidal with confirmation of there being some degree of agglomeration, which correlates to the results already presented in Figure 4.1 and Table 4.1.

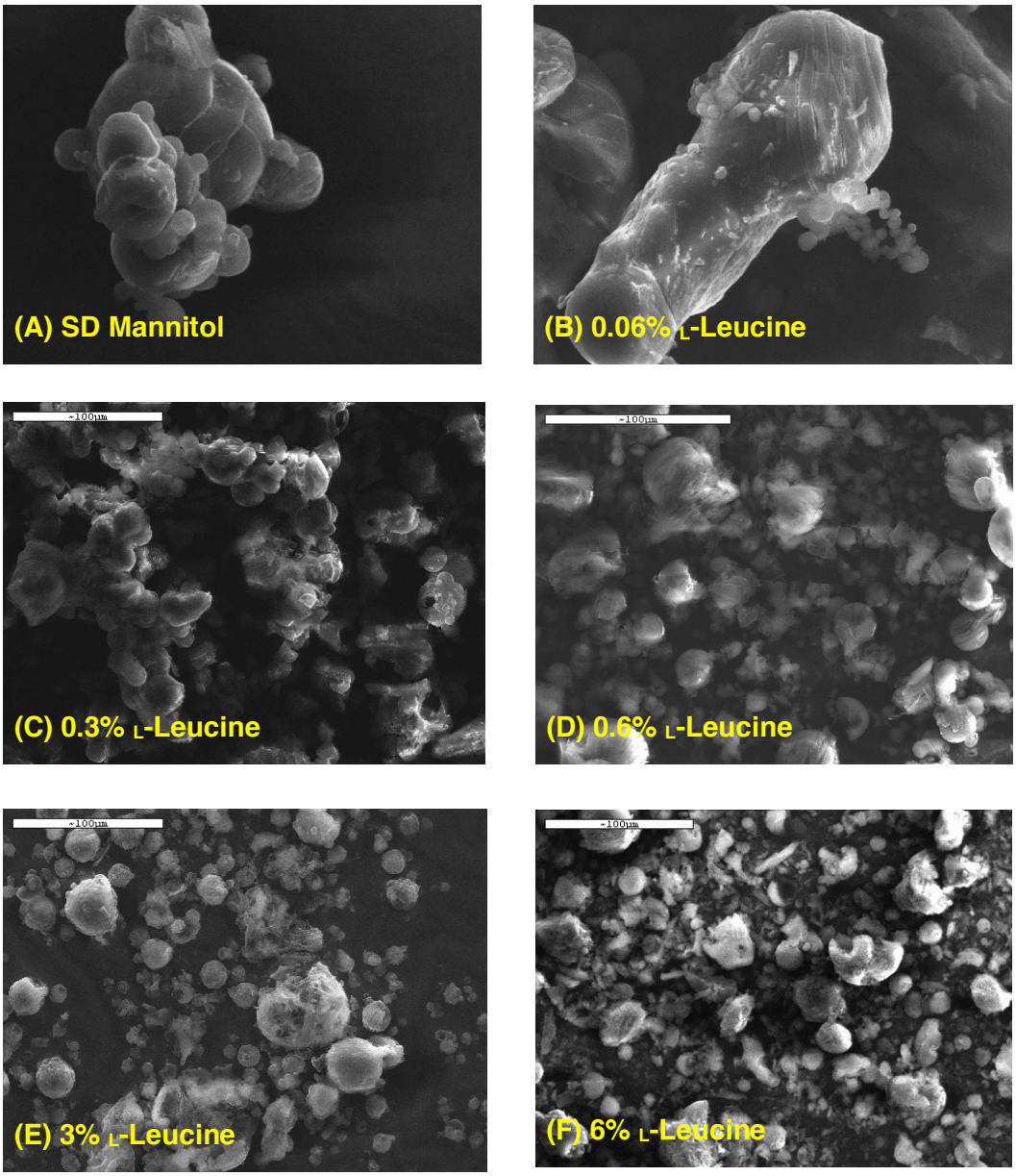


**Figure 4.2**. Scanning Electron Microscopy. SEM electron micrograms of (A) Spray Dried Mannitol, (B) 0.06% $_{L}$-leucine, (C) 0.3% $_{L}$-leucine, (D) 0.6% $_{L}$-leucine, (E) 3% $_{L}$-leucine, and (F) 6% $_{L}$-leucine.

### § 4.3.2 Solid-state characterization of spray dried samples

Figure 4.3 presents the DSC traces of L-leucine, Spray Dried Mannitol, 0.06% L-leucine, 0.3 L-leucine, 0.6% L-leucine, 3% L-leucine, and 6% L-leucine; the endothermic peak is associated to the melting of mannitol. Moreover, Table 4.2 summarizes the enthalpy and melting peak of each formulation.

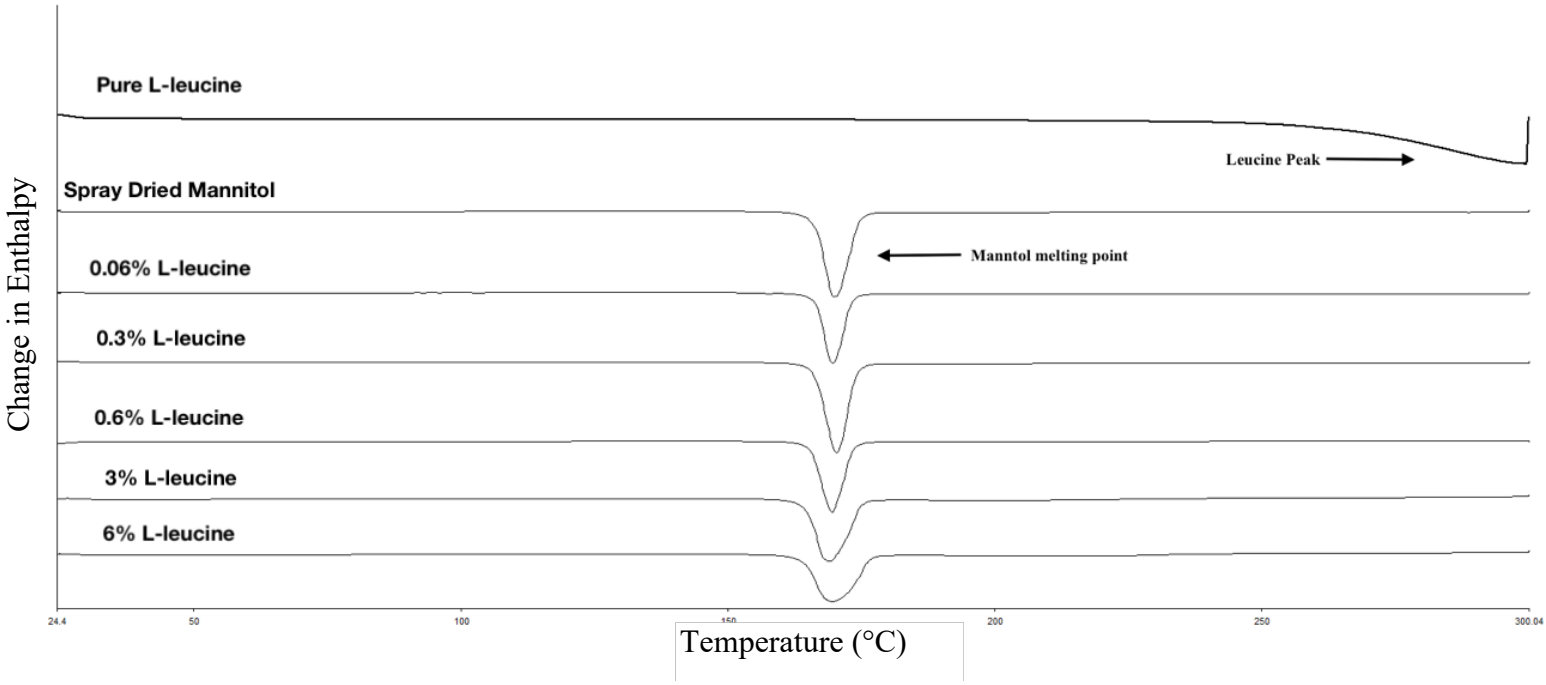


**Figure 4.3.** Differential Scanning Calorimetry. DSC thermal peaks of L-Leucine, Spray Dried Mannitol, 0.06% L-leucine, 0.3% L-leucine, 0.6% L-leucine, 3% L-leucine, and 6% L-leucine, where an exothermic peak would point up and an endothermic peak would point down.

Table 4.2 authenticates the results presented in Figure 4.3, where it illustrates an endothermic event at 169.79 ± 0.45°C which is known to be the melting of mannitol.[237, 270] An important observation to highlight, nonetheless, is the broadening of the endothermic peak as the leucine concentration increases. The increase in enthalpy can be associated to the ability for leucine to provide a stabilization effect for the carriers. This stabilization effect is supported by the fact that more energy is needed to melt the mannitol crystals as the concentration of leucine increases.

Additionally, pure leucine was tested to determine whether or not any thermal event would take place between the 25-300°C range, and, as can be seen in Figure 4.3, it was well above 300°C. Furthermore, Table 4.3 shows the actual amount of leucine presents in each of the carriers via HPLC analysis.

In a study conducted by Kaialy *et. al*, it was found that freeze-dried mannitol containing the three polymorphic forms (α-, β-, and Δ-) produced a larger endotherm peak than mannitol with two polymorphic forms (α- and β-).[271] Conventionally, the melting enthalpy (ΔH) represents the degree of crystallinity of a substance. By mixing two substances, the purity is reduced and lower melting points appear in the DSC thermographs. Any shift in melting point is indicative of a strong solid-solid interaction, which explains why the 6% Leucine carrier had the broadest thermal peak.[272 273]

**Table 4.2**. DSC Thermal Traces. DSC thermal traces of Spray Dried Mannitol, 0.06% $_{L}$-leucine, 0.3% $_{L}$-leucine, 0.6% $_{L}$-leucine, 3% $_{L}$-leucine, 6% $_{L}$-leucine, and $_{L}$-leucine that indicate the enthalpy, in J/g, of mannitol melting (ΔH) along with the Temperature (°C) of where such melting took place.

| Carrier | Temperature (°C) | ΔH (J/g) |
|---|---|---|
| **Spray Dried Mannitol** | $170.01 \pm 0.16$ | $198.38 \pm 8.97$ |
| **0.06% $_{L}$-Leucine** | $170.07 \pm 0.77$ | $175.52 \pm 55.68$ |
| **0.3% $_{L}$-Leucine** | $170.45 \pm 0.11$ | $213.10 \pm 6.17$ |
| **0.6% $_{L}$-Leucine** | $169.49 \pm 0.06$ | $182.87 \pm 19.44$ |
| **3% $_{L}$-Leucine** | $169.32 \pm 0.33$ | $201.98 \pm 16.61$ |
| **6% $_{L}$-Leucine** | $169.41 \pm 0.15$ | $213.79 \pm 3.21$ |
| **$_{L}$-Leucine** | — | — |

**Table 4.3**. L-Leucine Content. Actual amount of L-leucine found in each of the carriers (Spray Dried Mannitol, 0.06% L-leucine, 0.3% L-leucine, 0.6% L-leucine, 3% L-leucine, 6% L-leucine).

| Formulation | % L-Leucine |
|---|---|
| **Spray Dried Mannitol** | 0.00 ± 0.00 |
| **0.06% L-Leucine** | 0.02 ± 0.02 |
| **0.3% L-Leucine** | 0.82 ± 1.84 |
| **0.6% L-Leucine** | 2.86 ± 1.22 |
| **3% L-Leucine** | 7.24 ± 2.01 |
| **6% L-Leucine** | 12.93 ± 1.19 |

Figure 4.4 demonstrates the powder X-ray diffraction (PXRD) patterns obtained from each of the formulation's carriers highlighting the presence and location of the distinctive polymorphic characterization. It is understood that mannitol possesses three distinctive polymorphs (α-, β-, and Δ-) that are characterized by where they present themselves on the diffraction patterns; with α-mannitol exhibiting peaks at 9.57° and 13.79°, β-mannitol at 10.56° and at 14.71°, and Δ-mannitol with a peak at 9.74° and 22.2°.[271, 274-276]

PXRD of commercial mannitol showed the main diagnostic peaks for β-mannitol at 10.56°, 14.71°, 23.40°, 29.50° and 38.80°. This indicates that the commercial mannitol contains only β form of mannitol. Spray Dried Mannitol showed extra peaks at 2θ of 13.79° and around 17° which is an indication of α-mannitol; this shows that the spray dried mannitol contains both α- and β- mannitol.

It is obvious from PXRD of spray dried mannitol containing various concentrations of L-Leucine that these samples contained both α- and β-mannitol. Although all spray died samples showed the presence of α- and β-mannitol, the intensities of diagnostic peaks are not the same, which could be an indication of different ratios of these two polymorphic forms in the sample. The lack of any diagnostic peak at 9.74° and 22.2 indicates there is no Δ-mannitol in the samples. Table 4.4 summarizes all the polymorphic forms of mannitol associated with each carrier. In conclusion, XRD results showed that all formulations are in a crystalline state regardless of the type of polymorphic form they contain.

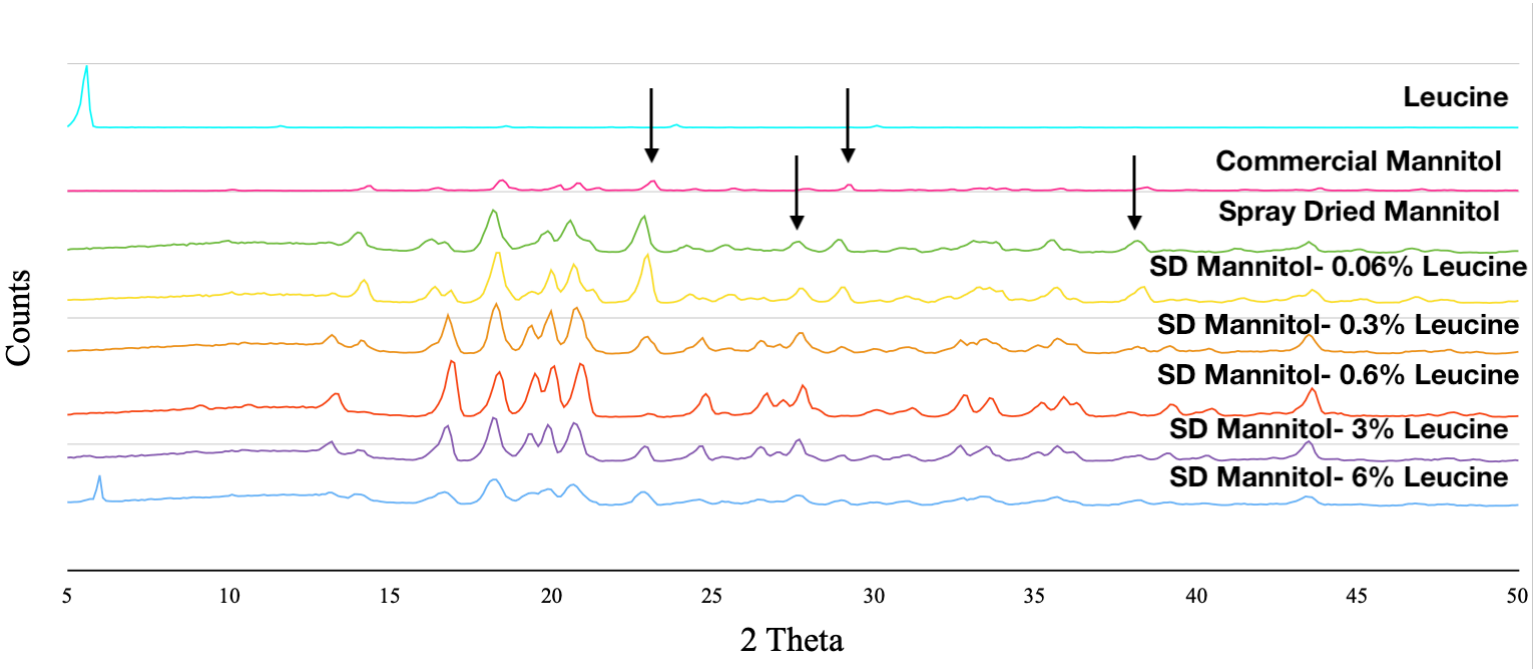


**Figure 4.4.** X-Ray Diffraction. Powder X-Ray diffraction patterns of Leucine, Spray Dried Mannitol (SDM), SDM- 0.06% L-leucine, SDM-0.3% L-leucine, SDM-0.6% L-leucine, SDM-3% L-leucine, and SDM-6% L-leucine.

**Table 4.4.** Mannitol Polymorphs. Characterization of mannitol polymorphs found within each formulation's carriers.

| Carrier | α-mannitol | β-mannitol | Δ-mannitol |
|---|---|---|---|
| **Commercial Mannitol** | — | ✓ | — |
| **Spray Dried Mannitol** | ✓ | ✓ | — |
| **0.06% L-Leucine** | ✓ | ✓ | — |
| **0.3% L-Leucine** | ✓ | ✓ | — |
| **0.6% L-Leucine** | ✓ | ✓ | — |
| **3% L-Leucine** | ✓ | ✓ | — |
| **6% L-Leucine** | ✓ | ✓ | — |

Solid-state characterization was further assessed with the implementation of FT-IR (Figure 4.5). It was understood that α-mannitol exhibits a peak at 1195cm$^{-1}$, β-mannitol at 929cm$^{-1}$, 959cm$^{-1}$, and 1209cm$^{-1}$, and Δ-mannitol at 967cm$^{-1}$.[258] Looking at Figure 4.5, it is clear that the commercial mannitol showed the main peaks for β-mannitol. Spray Dried Mannitol exhibited the peaks associated to the β-polymorph (α-mannitol was not detectable due to a very low concentration, it was more clear in the XRD figure) whereas all other spray dried samples containing leucine showed peaks associated to the α-mannitol and β-mannitol polymorphs.

The apparent broadening and widening in the peaks within 2500-3700cm$^{-1}$ is due to the presence of L-leucine in the samples. L-Leucine, being a branched-chain amino acid (BCAA), belongs to a group of proteins that are known for having an aliphatic side-chain and that are non-polar; the

aliphatic side-chain explains the results obtained in the spectra. In essence, the presence of L-leucine allowed for there to be an increase in the vibrational stretching that is observed by the hydroxyl group.[277]

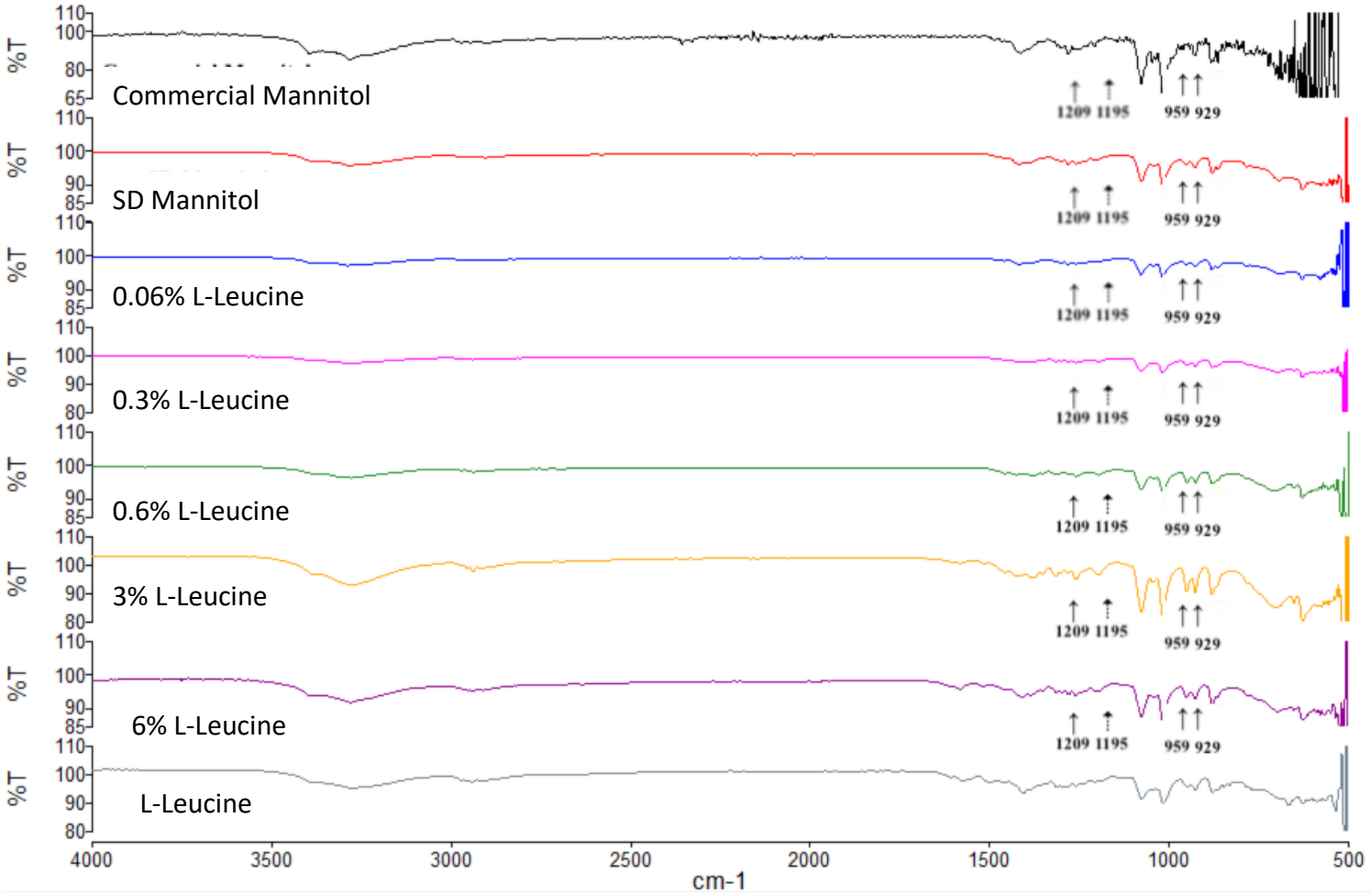


**Figure 4.5.** FT-IR. FT-IR spectra of commercial mannitol, Spray Dried Mannitol, spray dried mannitol containing 0.06% L-leucine, 0.3% L-leucine, 0.6% L-leucine, 3% L-leucine, 6% L-leucine, and L-leucine where ↟ represents α-mannitol, ↑ represents β-mannitol, and ↡ represents Δ-mannitol.

### § 4.3.3 *In vitro* analysis of DPI formulations

#### §§ Albuterol sulphate assessment

Aerosolization performance of all of the formulations is summarized in Figure 4.6 where the amount of Albuterol sulphate deposited in each of the stages of the deposition is shown [capsules (C), inhaler (I), mouthpiece (M), induction port (IP), Stage 1, Stage 2, Stage 3, Stage 4, and Stage 5]. All of the formulations experienced minimal Albuterol sulphate deposits ($p > 0.05$) in the capsules with 3% $_{L}$-leucine having the highest amount (6.62 + 4.59µg) and 0.06% $_{L}$-leucine having the lowest amount (2.98 + 0.42 µg). As particles maneuvered through the simulated respiratory tract (MSLI), 3% $_{L}$-leucine experienced the highest amount of Albuterol sulphate (51.35 + 49.66µg) in the inhaler when compared to 6% $_{L}$-leucine, which experienced the least amount at 13.26+6.34µg. Furthermore, all of the formulations showed similar amounts of Albuterol sulphate in the mouthpiece and induction port (see Figure 4.6), but began to differ at Stage 1 where aerodynamic particle size becomes more significant.

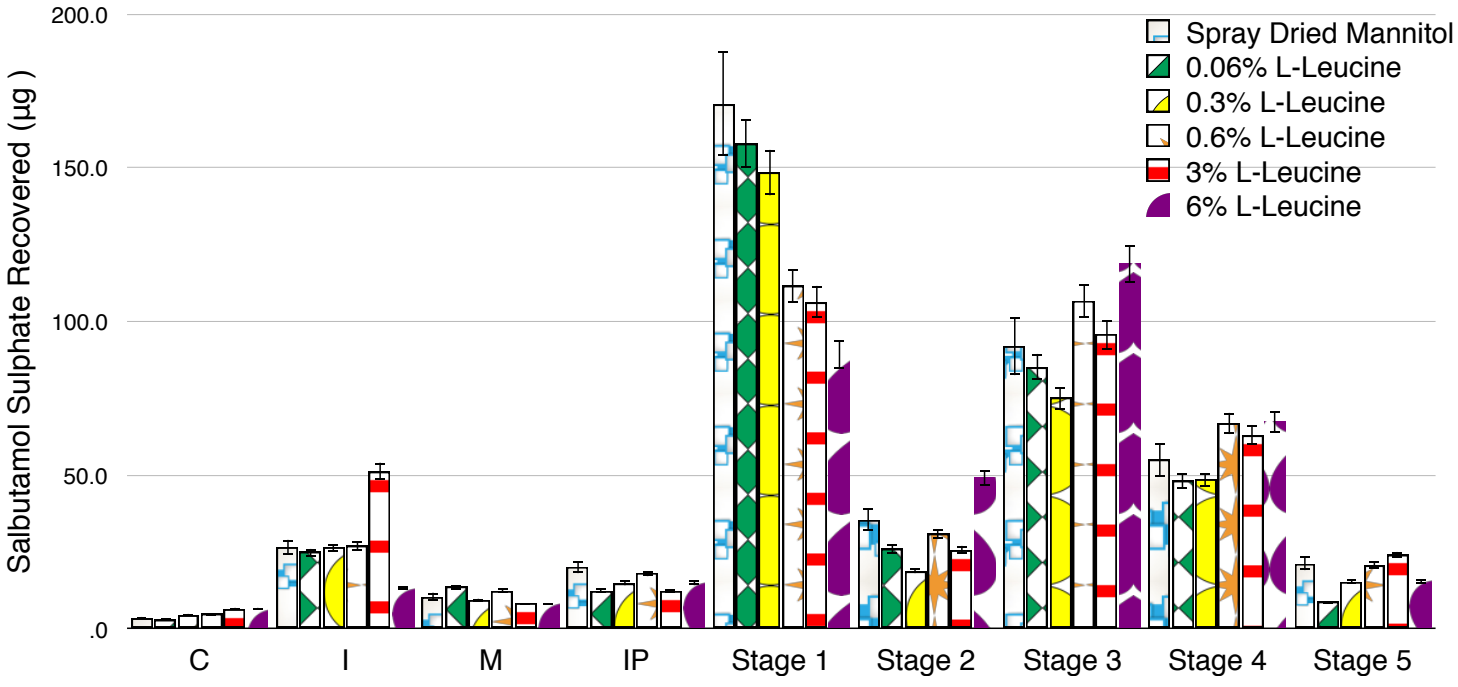


**Figure 4.6**. Aerosolization Profile. Aerosolization performance of each formulation (Spray Dried Mannitol, spray dried mannitol containing 0.06% $_{L}$-leucine, 0.3% $_{L}$-leucine, 0.6% $_{L}$-leucine, 3% $_{L}$-leucine, and 6% $_{L}$-leucine) highlighting the amount of Albuterol sulphate (AS) recovered (percent recovered).

Moreover, Spray Dried Mannitol had the highest Albuterol sulphate recovered from within Stage 1 (170.70 + 37.06µg), but 0.06% $_{L}$-leucine and 0.3% $_{L}$-leucine were not far behind with 157.75 + 9.04µg and 148.30 + 32.12µg, respectively. This shows that as the concentration of $_{L}$-leucine increases the amount of Albuterol sulphate deposits in Stage 1 decreases. This could be due to the lubrication effect that is seen when $_{L}$-leucine is added as an excipient (Chapter 3). The results showed that 6% $_{L}$-leucine experienced the highest Albuterol sulphate amounts from within Stage 3, and Stage 4 (118.74 + 44.84µg, and 67.40 + 15.75µg; respectively) indicative of it being the most successful at delivering Albuterol sulphate to the lower part of the lungs. In other words, the formulations, with respect to MMAD, ranked in the following order: 6% $_{L}$-leucine = 0.06% $_{L}$-leucine > Spray Dried Mannitol > 0.6% $_{L}$-leucine > 0.3% $_{L}$-leucine > 3% $_{L}$-leucine.

Likewise, looking at the RD, ED, and percentage recovery of each formulation, which is presented in Table 4.5, it was concluded that all of the formulations, with the exception of Spray Dried Mannitol, experienced similar values ($p < 0.05$). Such results are indicative of $_{L}$-leucine's powder dispersion effect,[244, 278, 279] its ability to act as a lubricant (see Chapter 3), and its ability to aid in storage and stability[280] as Spray Dried Mannitol showed significantly different results and contained no $_{L}$-leucine.

Additionally, all of the formulations differed remarkably from one another ($p < 0.05$) with respect to drug loss (DL), see Table 4.5, given that they all undertook a high number of actuations (n= 10) per run with each being filled with a consistent weight of 33.13 + 0.46 mg. Nevertheless, 6% $_{L}$-leucine experienced the least amount of drug loss with 9.64 + 1.01% indicative of optimized properties allowing for the best attachment and detachment of Albuterol sulphate when compared to all other formulations.

**Table 4.5.** Aerosolization Parameters. Recovered Dose (RD), Emitted Dose (ED), Percent Recovery, Percent Emission, Percent Impact Loss, Mass Median Aerodynamic Diameter (MMAD), Geometric Standard Deviation (GSD), Fine Particle Dose (FPD), Fine Particle Fraction (FPF), Drug Loss (DL), Dispersibility (DS), and Effective Inhalation Index (EI) of Albuterol sulphate obtained from each of the different formulations (Spray Dried Mannitol, 0.06% L-leucine, 0.3% L-leucine, 0.6% L-leucine, 3% L-leucine, and 6% L-leucine)

| Formulation | RD (µg) | ED (µg) | Recovery (%) | Emission (%) | Impact Loss (%) | MMAD (µm) | GSD (µm) | FPD | FPF (%) | DL (%) | DS (%) | EI |
|---|---|---|---|---|---|---|---|---|---|---|---|---|
| **Spray Dried Mannitol** | 431 ± 143.68 | 394.56 ± 147.19 | 89.74 ± 29.87 | 90.34 ± 5.20 | 45.59 ± 6.29 | 3.06 ± 0.10 | 2.10 ± 0.08 | 168.20 ± 85.39 | 37.06 ± 8.66 | 10.54 ± 5.35 | 40.75 ± 7.55 | 11.28 ± 0.62 |
| **0.06% L-Leucine** | 376.84 ± 41.04 | 338.39 ± 41.00 | 78.034 ± 8.53 | 89.72 ± 1.16 | 45.34 ± 2.08 | 3.20 ± 0.05 | 2.01 ± 0.03 | 142.08 ± 24.68 | 37.54 ± 2.46 | 11.08 ± 1.25 | 41.83 ± 2.19 | 11.28 ± 0.16 |
| **0.3% L-Leucine** | 356.54 ± 7.83 | 320.93 ± 15.09 | 74.13 ± 1.63 | 89.98 ± 2.43 | 45.84 ± 9.97 | 2.92 ± 0.07 | 2.09 ± 0.01 | 138.80 ± 32.62 | 38.86 ± 8.54 | 11.29 ± 2.76 | 43.19 ± 9.34 | 11.35 ± 0.40 |
| **0.6% L-Leucine** | 394.58 ± 61.56 | 355.06 ± 58.83 | 82.03 ± 12.80 | 89.88 ± 1.58 | 33.68 ± 9.98 | 3.01 ± 0.11 | 2.07 ± 0.06 | 194.60 ± 61.90 | 48.45 ± 9.44 | 11.30 ± 1.67 | 53.80 ± 9.69 | 11.76 ± 0.47 |
| **3% L-Leucine** | 386.66 ± 97.37 | 327.19 ± 109.64 | 80.39 ± 20.24 | 84.25 ± 13.76 | 30.01 ± 4.96 | 2.91 ± 0.17 | 2.11 ± 0.06 | 182.85 ± 73.96 | 47.19 ± 13.76 | 17.42 ± 13.92 | 55.15 ± 8.13 | 11.42 ± 1.24 |
| **6% L-Leucine** | 376.34 ± 73.37 | 354.95 ± 68.08 | 78.24 ± 15.25 | 94.35 ± 0.64 | 28.74 ± 9.13 | 3.20 ± 0.21 | 2.05 ± 0.05 | 201.78 ± 58.77 | 52.96 ± 5.21 | 9.64 ± 1.01 | 56.14 ± 5.61 | 12.14 ± 0.21 |

It is interesting to note that when the concentration of L-leucine increased from 0 to 0.3% no significant changes were observed in impaction loss (IL), whereas beyond 0.3% a significant reduction was observed for the IL value so that samples containing 6% L-leucine showed the least IL (28.74 + 9.13%). Such variation between the formulations could be attributed to their aerodynamic diameter given that impaction is a flow-dependent mechanism governed by particle size.[18] In addition, 6% L-leucine showed the smallest VMD of its coarse particulate matter (VMD of 63.46 + 0.18µm; results from Table 4.1) when compared to the other formulations; all of which had higher VMDs for their agglomerated coarse particles (see Table 4.1 and Figure 4.2).

Effective inhalation index (EI) ranged from 11.28 + 0.16 (0.06% L-leucine) to 12.14 + 0.21 (6% L-leucine) showing a linear relationship with FPF ($r^2 = 0.81$), data not shown. This indicates that the presence of L-leucine is necessary to enhance the EI value.

DS (dispersibility) and FPD also confirmed that samples with a higher concentration of L-leucine showed better dispersibility and high fine particle dose where both are an indication of a good aerosolization performance of Albuterol sulphate. There was a linear relationship ($r^2 = 0.89$) between the carriers of the wet system's VMDs and that of FPD (data not shown) which brings in the notion of inertial impaction and its prevalence, as previously discussed; such relationship also builds upon the variations observed between the formulations.

When it came to MMAD and GSD, however, all of the formulations gave similar results with MMAD and GSD ($p > 0.05$). In addition, a linear correlation ($r^2 = 0.69$) between the L-leucine concentration and FPF was established (data not shown) suggesting that L-leucine played a significant role ($p$

$< 0.05$) in decreasing the particle's density and size,[279] while providing an anti-hygroscopic effect,[280] as it has been shown for L-leucine to precipitate on the surface of drying droplets when spray drying.[30, 278, 279, 281, 282] These precipitated L-leucine patches were accounted for when engineering the carriers as the end product shows; knowing this aids in the developmental process for physicochemical property selection and with the invention/creation of methodological processes.

Furthermore, 6% L-leucine witnessed the highest FPF of 52.96 + 5.21% indicative of it being the most efficient at delivering the highest amount of Albuterol sulphate to the lower respiratory tract. In addition, this formulation also showed the best drug-carrier cohesive-adhesive balance ratio as this ratio is directly related to the FPF of any given API.[283] Such results also support those of Labiris and Dolovich which experienced a similar outcome.[284] Moreover, this formulation also had the highest percentage emission of 94.35 + 0.64%, when compared to the other formulations (see Table 4.5) inferring that it released the most Albuterol sulphate into the simulated system providing sufficient evidence to classify it as the best formulation.

All in all, optimal properties were attained such that a complementary system emerged between Albuterol sulphate and the 6% L-leucine carrier and one that was effective when implemented. Arriving to this conclusion was done through numerous factors and checkpoints (i.e physicochemical properties, particle size, particle density, etc.) along the way that catalyzed a cascade of favorable conditions for the 6% L-leucine carrier-to-Albuterol sulphate system. On the other hand, Spray Dried Mannitol showed the lowest FPF (37.06 + 8.66%) inferring that Albuterol sulphate had a more difficult time detaching itself from the Spray Dried Mannitol carrier during the

inhalation process when compared to 6% L-leucine, which performed with the highest efficacy profile for aerosolization purposes.

#### §§ 4.3.3.2 Homogeneity assessment

Assessing the homogeneity of each formulation was an essential phase of this overall study given that a uniform formulation will give rise to a more effective drug delivery profile with a consistent dose to the patient; it also adheres to USP guidelines. Figure 4.7 eludes the homogeneity profile of each of the formulations (0, 0.06, 0.3, 0.6, 3, and 6% L-leucine) under investigation showing the potency of each while Table 4.6 presents the percentage content homogeneity, which is expressed as the percentage coefficient of variation (%CV), of each of the aforementioned formulations.

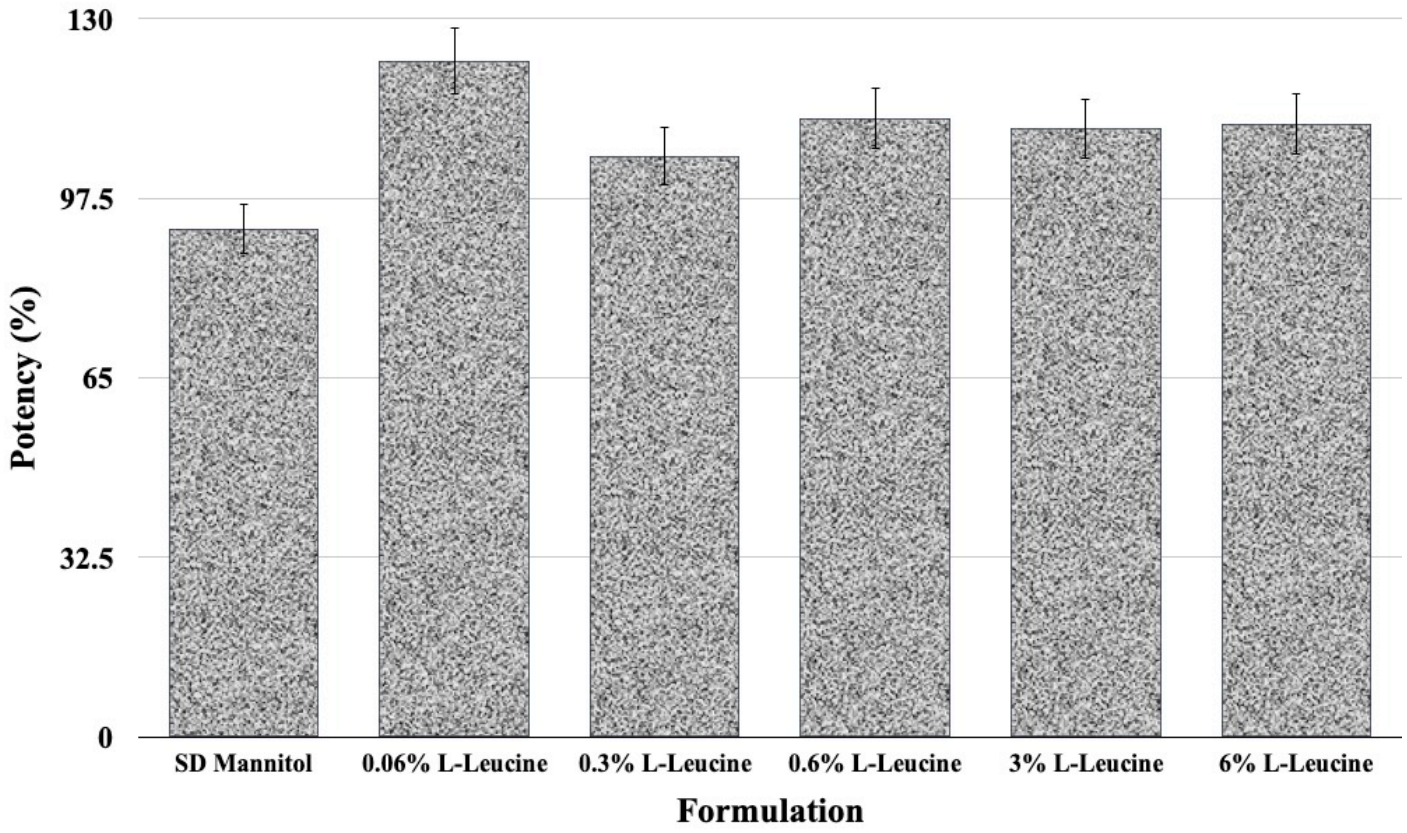


**Figure 4.7.** Potency**.** Percent potency of each formulation (Spray Dried Mannitol, spray dried mannitol containing 0.06% $_{L}$-leucine, 0.3% $_{L}$-leucine, 0.6% $_{L}$-leucine, 3% $_{L}$-leucine, and 6% $_{L}$-leucine) with respect to Albuterol sulphate.

**Table 4.6.** Content Homogeneity. Content homogeneity of Spray Dried Mannitol, 0.06% L-leucine, 0.3% L-leucine, 0.6% L-leucine, 3% L-leucine, and 6% L-leucine expressed as the percent coefficient of variation (%CV)

| Formulation | Assay % | % CV |
|---|---|---|
| **Spray Dried Mannitol** | 91.95 ± 19.22 | 20.90 |
| **0.06% L-Leucine** | 122.37 ± 4.75 | 3.88 |
| **0.3% L-Leucine** | 105.18 ± 14.81 | 14.08 |
| **0.6% L-Leucine** | 112.02 ± 13.38 | 11.94 |
| **3% L-Leucine** | 110.07 ± 13.11 | 11.90 |
| **6% L-Leucine** | 110.96 ± 14.84 | 13.38 |

*However, has not been taken into account for *in vivo* inhalation studies.

All of the formulations varied considerably from one another with regard to potency with a range of 122.37 + 4.75% (sample containing 0.06% L-leucine) to 91.95 + 19.22% (Spray Dried Mannitol without L-leucine). Regarding %CV, the smallest %CV of 3.88% belonged to 0.06% L-leucine and the highest %CV of 20.90 belonged to Spray Dried Mannitol without L-leucine (see Table 4.6). Such results indicate that 0.06% L-leucine had the best Albuterol sulphate content homogeneity amongst all of the formulations. Table 4.6 also showed that the presence of L-leucine improved the homogeneity of the samples compared to the sample without L-leucine. The table also shows that all formulations adhered to the acceptable range of 75-125% set by the USP and its European counterpart.

### *4.4 Conclusion*

The results presented in this chapter have proven that mannitol solutions containing different concentrations of L-leucine were successfully spray dried. In addition, it was also shown that the

presence of L-leucine changed the properties of the resultant spray dried particles. This modified mannitol showed an improvement in the aerosolization performance of Albuterol sulphate (FPF = 52.96 + 5.21%), which was measured through the FPF. The results also confirmed that mannitol can serve as a suitable alternative carrier over lactose in DPI formulations and could be suitable for lactose intolerant patients suffering from asthma or COPD. In the future, it would be beneficial to explore the use of both spray dried lactose and mannitol, together, to determine their effect when used in DPI formulations.

# Chapter 5

## Effect Different Mixtures of the Spray Dried Mannitol and Lactose with Leucine have on Dry Powder Inhaler Performance of Salbutamol Sulphate (Albuterol)

### *5.1 Introduction*

In this chapter, the focus was to engineer a spray dried carrier composed of mannitol, lactose, and 5% $_{L}$-leucine (w/w) and investigate the effect that different mannitol:lactose ratios have on the overall aerosolized dry powder inhaler (DPI) performance for salbutamol sulphate. $\beta_2$-Andrenergic receptor agonists, like that of to salbutamol sulphate, acts on the $\beta_2$-andrenergic receptor facilitating smooth muscle relaxation and dilation of bronchial passages.[285] This enables patients suffering from asthma, a chronic inflammatory disease characterized by the obstruction of airflow due to bronchial airway constriction in response to a stimulus,[286] the ability to breathe. Such process, however, is achieved via delivery of a successful therapeutic dosage of salbutamol sulphate to be deposited more peripherally; that is to say, in the middle and small airway.[287, 288] Therefore, aerosolization performance becomes a significant factor in the development and implementation of any given dry powder inhaler (DPI) formulation given that inter-particulate forces are directly influenced by particle density, morphology, surface roughness, particle-size distribution, presence of fine particle excipients, surface energy, carrier flow, and carrier material.[289, 290]

In Chapter 4, it was determined that the aerosolization performance of albuterol sulphate containing spray dried 6% L-leucine with mannitol was affected in such a way that the FPF was increased to 52.96% from 47.11% (Chapter 3). This increase suggested that mannitol can serve as an alternative carrier to lactose. In this investigation, the goal is to determine whether a spray dried formulation containing binary mixtures of mannitol:lactose with different ratios (with 5% L-leucine; w/w) can improve the aerosolization performance further or not.

## *5.2 Materials and Methodology*

**§ 5.2.1- § 5.2.13**

Refer to Chapter 2 sections *2.2, 2,3, 2.5-2.11,* and *2.14-2.16.*

## *5.3 Results and Discussion*

### § 5.3.1 Particle Size Analysis and Morphology

Particle interactions are of great importance in DPI formulations where the dispersion of the active pharmaceutical ingredient particles from carrier particles is critical for lung deposition.[220] It holds true that particles with a diameter between 5-10 µm deposit primarily in the extrathoracic airways and particles between 1-5 µm mostly deposit in the tracheo-bronchiol region; particles with a diameter below 1 µm deposit in the alveolar region.[291, 292]

Nonetheless, particle analysis was carried out for each of the carriers within this study to determine whether their volume mean diameter (VMD) fell within the pre-requisite range of 63-90 µm.[222, 293] Figure 5.1 presents the particle size distribution (PSD) diagrams of the carriers illustrating their particle size and their cumulative distribution when using the (A) Rodos dry

system (Figure 5.1A) and (B) Cuvette wet system (Figure 5.1B). As is clear by Figure 5.1B, the carrier's VMDs are greater than those in Figure 5.1A due to particle agglomeration. Small particles carry a greater net charge-to-surface ratio (net-CSR) than larger particles as particle charge is inversely related to particle mean diameter.[128, 294, 295]

Furthermore, the aggregated particles comply with pharmacopoeia guidelines as they all fall between 63-90 µm; Table 5.1 provides the true numerical VMD values along with the span for each of the carriers for both the dry and wet systems. When the carriers were subjected to the Rodos system, their VMDs ranged from 13.58 $\pm$ 0.20 µm (Lactose) to 37.52 $\pm$ 0.52µm (3:1 [Mannitol:Lactose]), however, with the Cuvette system, this range became 69.59 $\pm$ 0.99µm (1:3 [Mannitol:Lactose]) to 86.38 $\pm$ 1.62µm (3:1 [Mannitol:Lactose]). The span for the carriers was determined to be 1.62 $\pm$ 0.05 (3:1 [Mannitol:Lactose]) to 2.62 $\pm$ 0.12 (Lactose) and 1.15 $\pm$ 0.02 (1:1 [Mannitol:Lactose]) to 2.03 $\pm$ 0.02 (1:3 [Mannitol:Lactose]) for the dry and wet systems, respectively. The dry system experienced a particle diameter range of 6.48 $\pm$ 2.22 µm ($D_{10\%}$) to 64.94 $\pm$ 9.70 µm ($D_{90\%}$) whereas the wet system showed a range of 52.88 $\pm$ 6.36 µm ($D_{10\%}$) to 142.66 $\pm$ 19.14 µm ($D_{90\%}$).

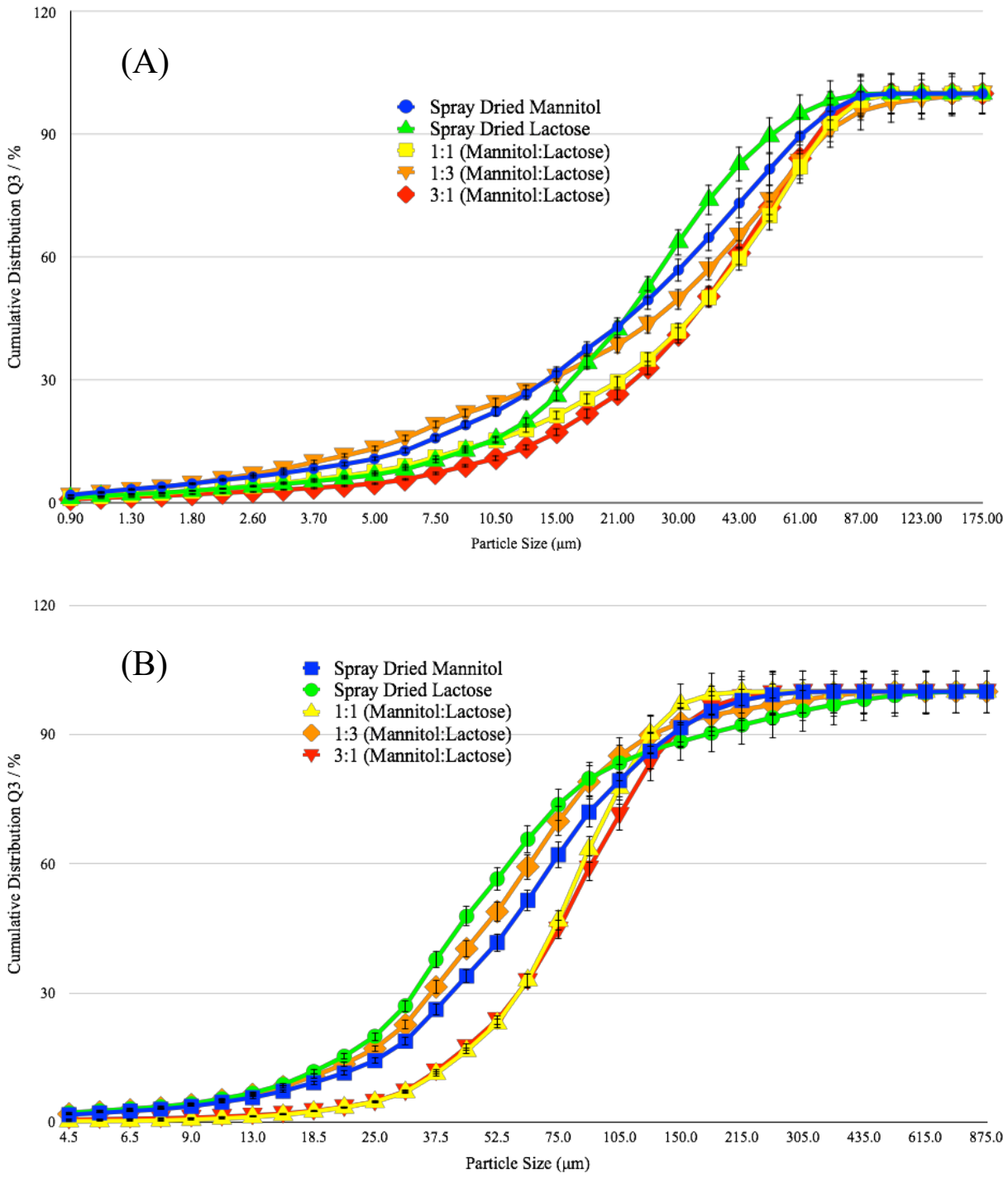


**Figure 5.1.** Particle Size Distribution. Particle Size Distribution (PSD) diagrams of carriers (Spray Dried Mannitol, Spray Dried Lactose, 1:1 [Mannitol:Lactose], 1:3 [Mannitol:Lactose], and 3:1 [Mannitol:Lactose]) when using the (A) Rodos dry system and when using the (B) Cuvette wet system.

**Table 5.1**. Particle Analysis. Particle size Analysis of Spray Dried Mannitol, Spray Dried Lactose, mixtures of mannitol:lactose (1:1, 1:3, and 3:1) showing the volume mean diameter (VMD) and span when using the Rodos dry system or the Cuvette wet system.

| Carrier | VMD (µm) Dry System | VMD (µm) Wet System | Span Dry System | Span Wet System |
|---|---|---|---|---|
| **Spray Dried Mannitol** | 29.86 ± 0.19 | 72.82 ± 0.07 | 2.25 ± 1.95 | 2.02 ± 0.20 |
| **Spray Dried Lactose** | 13.58 ± 0.20 | 79.31 ± 2.19 | 2.62 ± 0.12 | 1.74 ± 0.08 |
| **1:1 [Mannitol:Lactose]** | 37.51 ± 0.48 | 79.95 ± 1.16 | 1.75 ± 0.04 | 1.15 ± 0.02 |
| **1:3 [Mannitol:Lactose]** | 35.06 ± 6.21 | 69.59 ± 0.99 | 2.28 ± 0.19 | 2.03 ± 0.02 |
| **3:1 [Mannitol:Lactose]** | 37.52 ± 0.52 | 86.38 ± 1.62 | 1.62 ± 0.05 | 1.36 ± 0.01 |

Figure 5.2 presents the electron micrograms of all the carriers (SD Mannitol, SD Lactose, different ratios of Mannitol:Lactose (1:1,1:3 and 3:1). Both the SD Mannitol and SD Lactose carriers were characterized as resembling the structure of a tomahawk while the other ratios of Mannitol:Lactose] (1:1, 1:3 and 3:1) were characterized as spherical. Based on the electron micrograms, nonetheless, it was deduced that some degree of agglomeration took place which coincides with the data presented in Figure 5.1 and Table 5.1.

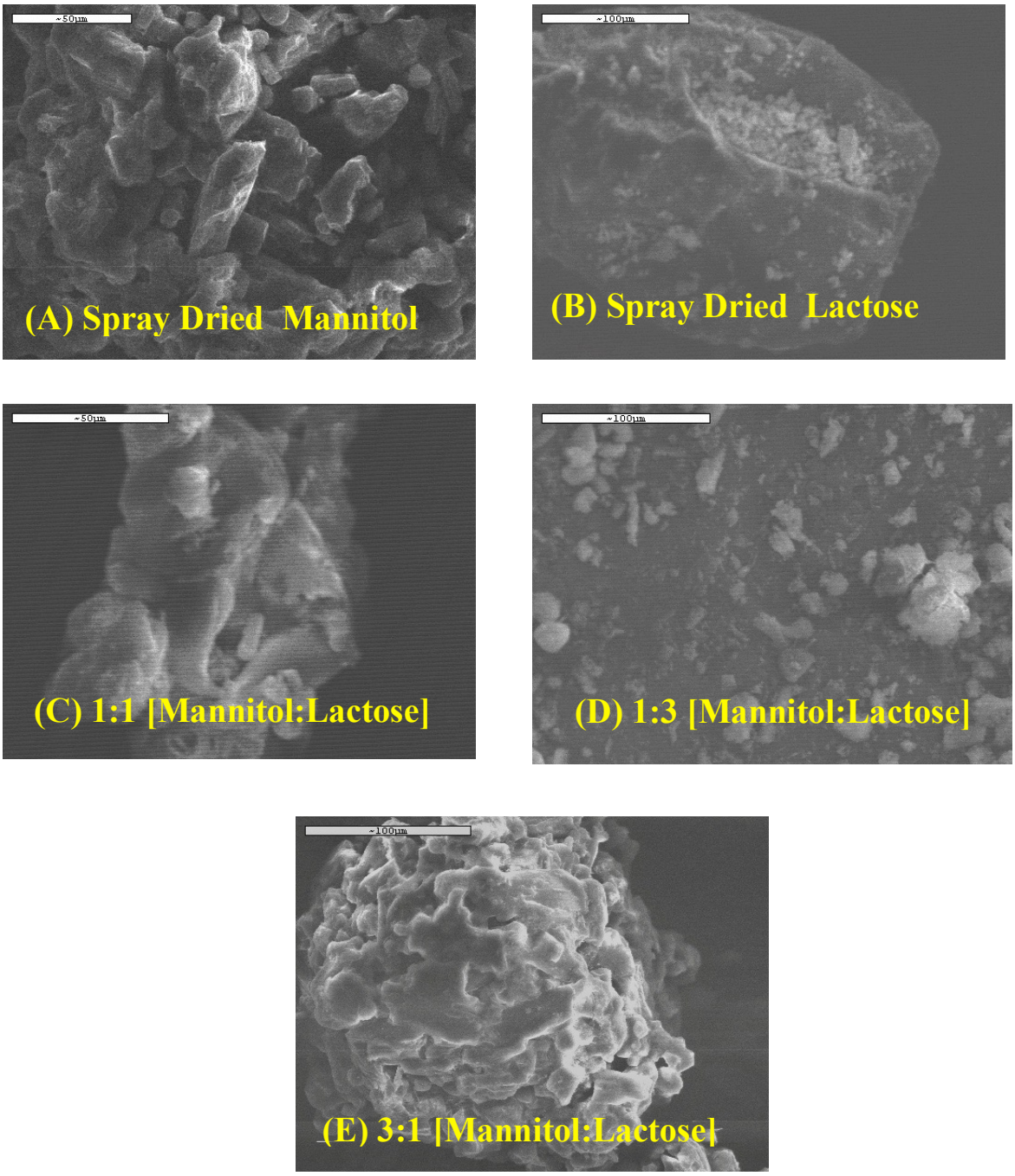


**Figure 5.2**. Scanning Electron Microscopy. SEM electron micrograms of (A) Spray Dried Mannitol, (B) Spray Dried Lactose, (C) SD 1:1 [Mannitol:Lactose], (D) SD 1:3 [Mannitol:Lactose], and (E) SD 3:1 [Mannitol:Lactose] all with 5% $_{L}$-leucine (w/w).

### § 5.3.2 Solid-state characterization of spray dried samples

Figure 5.3 presents the thermal traces associated to each of the carriers while highlighting the endotherm or exotherm found within each sample. To rule out the possibility of L-leucine having any thermal events within the 25-300°C range, a pure sample of L-leucine was analyzed; as can be seen from Figure 5.3, L-leucine had no thermal event within the aforementioned range.

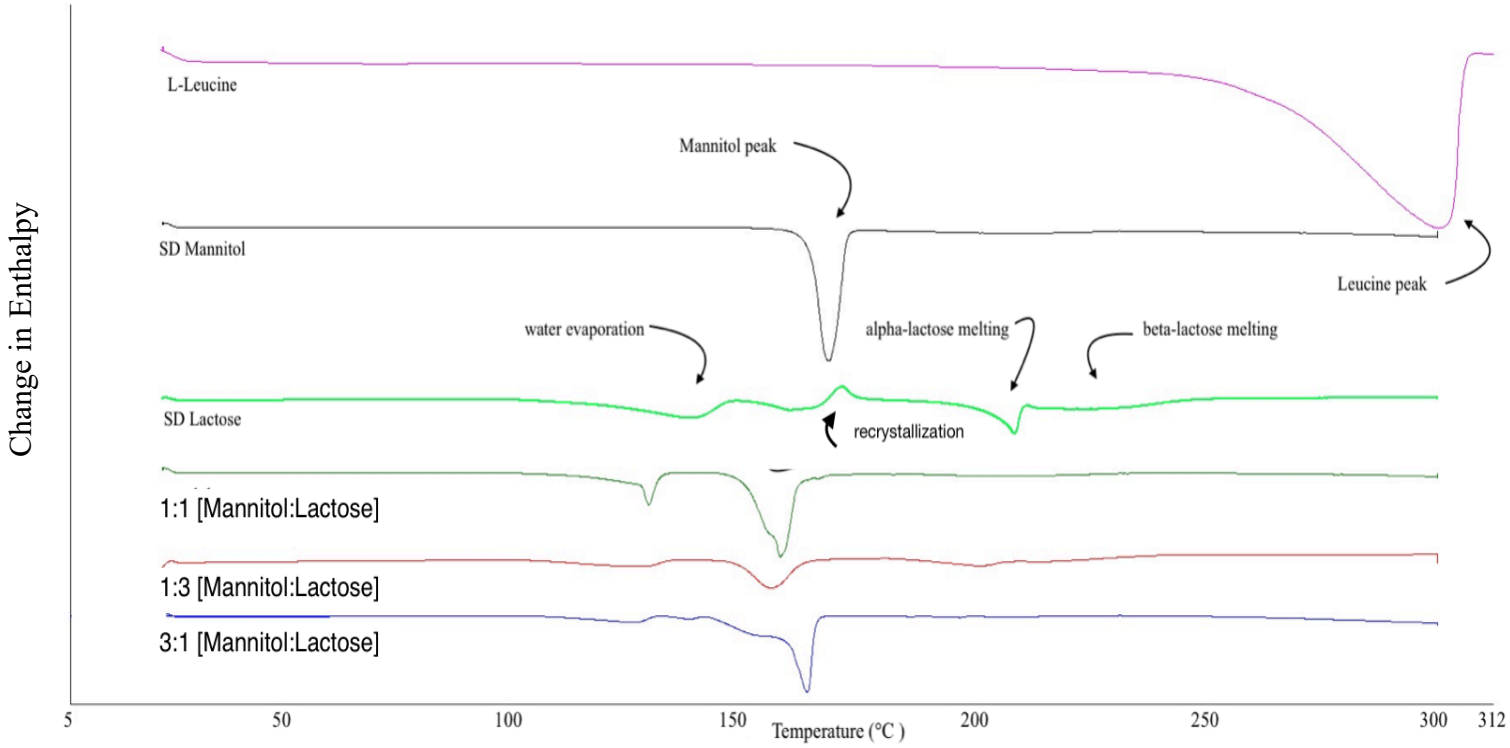


Spray Dried Mannitol with 5% L-leucine (w/w) presented an endothermic peak at 169.79 ± 0.35 °C, known to be attributed to the melting of mannitol,[224, 270] with a resulting enthalpy of 208.66 ± 6.87J/g (Table 5.2). Spray Dried Lactose with 5% L-leucine (w/w), however, showed four endothermic peaks (138.88 ± 1.06, 160.16 ± 0.13, 208.48 ± 0.30, and 227.45 ± 1.82°C) and one exothermic peak (171.13± 0.23°C). The first and second endothermic peaks (138.88 ± 1.06°C and 160.16 ± 0.13°C), which are associated to the evaporation of water,[297] resulted with an

enthalpy of 84.15 ± 9.29 and 33.04 ± 10.72 J/g (Table 5.2) whereas the third endothermic peak (208.48 ± 0.30°C), associated to the melting of α-lactose,[297] gave an enthalpy of 53.96 ± 5.98 J/g (Table 5.2). The last endothermic peak at 227.45 ± 1.82°C associated to the melting of β-lactose,[297] resulted with an enthalpy of 29.87 ± 4.65J/g (Table 5.2). The exothermic peak at 171.13± 0.23°C is due to the crystallization of amorphous lactose[297] which had an enthalpy of -16.35 ± 2.09J/g (Table 5.2).

**Table 5.2**. DSC Thermal Traces. DSC thermal traces of Spray Dried Mannitol, Spray Dried Lactose, 1:1 [Mannitol:Lactose], 1:3 [Mannitol:Lactose], and 3:1 [Mannitol:Lactose] (all with 5% $_{L}$-leucine [w/w]) that indicate the enthalpy (ΔH), in J/g, of each thermal event along with the Temperature (°C) of where such thermal event took place.

| | Water Evaporation | | | | Mannitol Melting | | Amorphous Lactose | | α-lactose melting | | β-lactose melting | |
|---|---|---|---|---|---|---|---|---|---|---|---|---|
| **Formulation** | **Temperature (°C)** | **ΔH (J/g)** | **Temperature (°C)** | **ΔH (J/g)** | **Temperature (°C)** | **ΔH (J/g)** | **Temperature (°C)** | **ΔH (J/g)** | **Temperature (°C)** | **ΔH (J/g)** | **Temperature (°C)** | **ΔH (J/g)** |
| **Spray Dried Mannitol** | — | — | — | — | 168.79 ± 0.35 | 208.66± 6.87 | — | — | — | — | — | — |
| **Spray Dried Lactose** | 138.88 ± 1.06 | 84.15 ± 9.29 | 160.07 ± 0.13 | 33.04 ± 10.72 | — | — | 171.13 ± 0.23 | -16.3± 2.09 | 208.48 ± 0.30 | 53.9± 5.98 | 227.45 ± 1.82 | 29.87 ± 4.65 |
| **1:1** | 129.77 ± 0.00 | 49.07 ± 11.40 | – | – | 158.19 ± 0.05 | 166.39± 19.04 | — | — | — | — | — | — |
| **1:3** | 127.22 ± 2.98 | 36.88 ± 3.03 | – | – | 156.11 ± 0.16 | 91.36 ± 9.80 | – | – | 201.34 ± 0.08 | 33.71 ± 23.48 | 219.55 ± 5.09 | 9.54 ± 5.12 |
| **3:1** | 126.33 ± 0.25 | 21.54 ± 0.53 | – | – | 163.94 ± 0.01 | 178.22± 25.63 | 138.46 ± 0.05 | 3.00 ± 0.12 | — | — | — | — |
| **L-Leucine** | — | — | — | — | — | — | — | — | — | — | — | — |

Furthermore, when looking at the carriers containing mixtures of Mannitol:Lactose with 5% L-leucine (w/w) and their respective thermal events, it appears that they all experienced temperature shifts from those observed from the Spray Dried Mannitol and Spray Dried Lactose both with 5% L-leucine (w/w) (see Figure 5.3 and Table 5.2). This shift is associated to the introduction of L-leucine in the samples prior to undergoing spray drying.

Nevertheless, the 1:1 [Mannitol:Lactose] carrier exhibited two endothermic peaks at 129.77 ± 0.00 and 158.19 ± 0.05 °C) corresponding to the evaporation of water and the melting of mannitol with enthalpies of 49.07 ± 11.40 J/g and 166.39 ± 19.04 J/g, respectively. The 1:3 [Mannitol:Lactose] carrier, however, experienced four endothermic peaks (127.22 ± 2.98, 156.11 ± 0.16, 201.34 ± 0.08, and 219.55 ± 5.09°C) where the enthalpies for the endothermic peaks were 36.88 ± 3.03, 91.36 ± 9.80, 33.71 ± 23.48, and 9.54 ± 5.12J/g (respectively) [see Table 5.2]. These thermal events indicate the occurrence of water evaporation (127.22 ± 2.98°C), amorphous lactose recrystallization (175.23 ± 7.87°C), the melting of mannitol (156.11 ± 0.16°C), α-lactose melting (201.34 ± 0.08°C), and β-lactose melting (219.55 ± 5.09°C); see Figure 5.3 and Table 5.2.

Moreover, the 3:1 [Mannitol:Lactose] carrier resulted in having three endothermic peaks (126.33 ± 0.25, 138.46 ± 0.05, and 163.94 ± 0.01°C) where the enthalpy for the evaporation of water (126.33 ± 0.25°C) was 21.54 ± 0.53J/g, amorphous lactose recrystallization (138.46 ± 0.05°C) was 3.00 ± 0.12J/g, and the enthalpy for the melting of mannitol (163.94 ± 0.01°C) was 178.22 ± 25.63J/g. Interestingly, the 1:1 [Mannitol:Lactose] and 3:1 [Mannitol:Lactose] carriers failed to show any traces of α-lactose or β-lactose melting suggesting their absence in the sample. Moreover the 3:1 [Mannitol:Lactose] carrier showed signs of its amorphicity through the presence

of the amorphous lactose recrystallization enthalpy, which was absent in the 1:1 [Mannitol:Lactose] carrier.

Figure 5.4 shows the powder X-Ray diffraction (PXRD) peaks associated to each carrier, aiding in the characterization of the carrier's polymorphic form. Powder X-Ray Diffraction (XRPD) can identify if the sample is crystalline or amorphous.

Mannitol's polymorphic forms ( α-, β-, and Δ-) are known to exhibit distinguishable diffraction peaks with α-mannitol having such peaks at 9.57° and 13.79°, β-mannitol at 10.56° and 14.71°, and Δ-mannitol at 9.74° (see Chapter 3).[296] With the results presented in the Figure, it was determined that spray dried mannitol, 1:1 [Mannitol:Lactose], 1:3 [Mannitol:Lactose], and 3:1 [Mannitol:Lactose] were composed of the α- and β-polymorph as indicated in the Figure. Spray Dried Lactose, on the other hand, differed remarkably from all the other carriers due to its amorphous nature; the broadened and shallow peaks at 12.5° and 18.3° have been reported elsewhere as being attributed to lactose's amorphicity (see Chapter 3). Moreover, such results support those presented in Figure 5.3 via a more reliable and accepted technique of solid-state characterization of newly developed formulations.

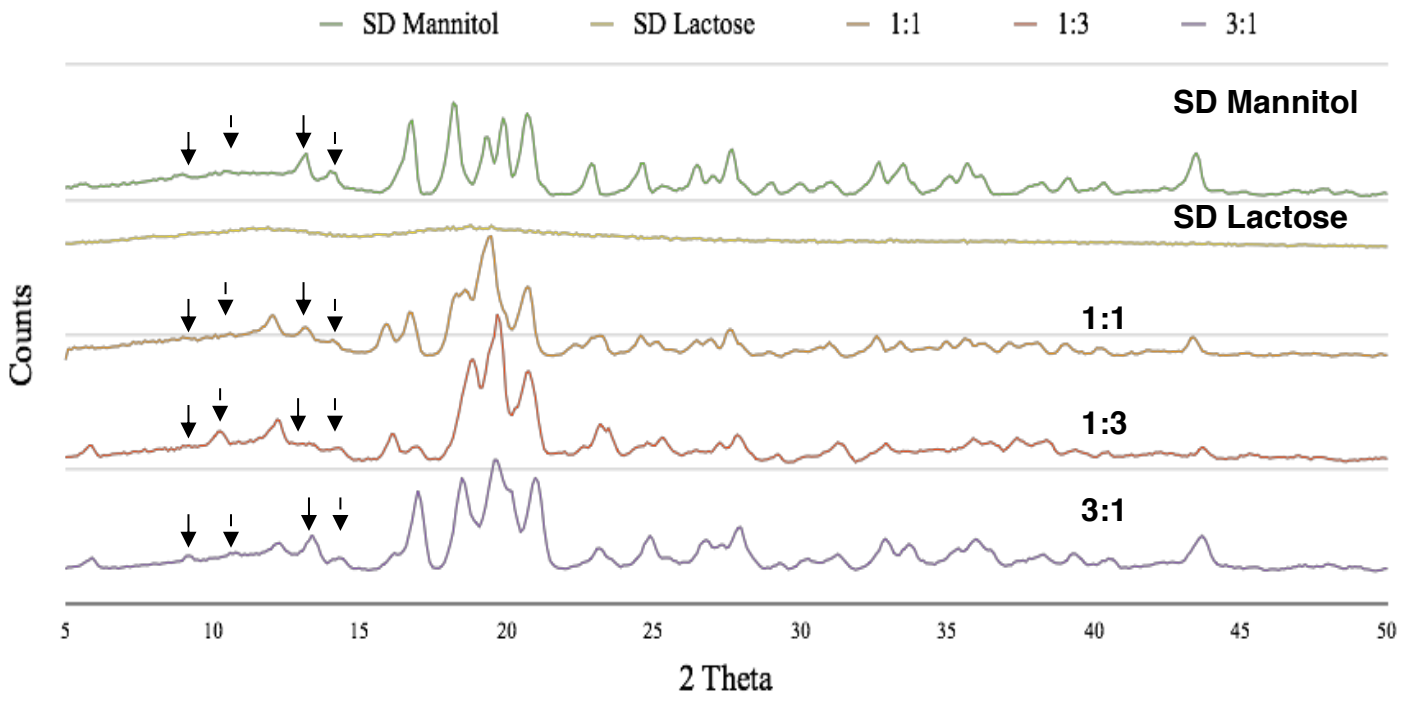


α-mannitol

β-mannitol

**Figure 5.4**. X-Ray Diffraction. Powder X-Ray diffraction patterns of Spray Dried Mannitol, Spray Dried Lactose, 1:1 [Mannitol:Lactose], 1:3 [Mannitol:Lactose], and 3:1 [Mannitol:Lactose].

Figure 5.5 presents the infrared spectrum of all the carriers, and that of L-leucine, indicating the solid-state characterization of each carrier within this overall study. It has been documented elsewhere that lactose possesses four peaks within the spectra that elucidates its polymorphic form; amorphous lactose presenting peaks at 1260cm$^{-1}$ and 900cm$^{-1}$, α-lactose at 920cm$^{-1}$, and β-lactose at 950cm$^{-1}$. Mannitol, on the other hand, is distinguishable via five peaks: α-mannitol at 1195cm$^{-1}$, β-mannitol at 929cm$^{-1}$, 959cm$^{-1}$, and 1209cm$^{-1}$, and Δ -mannitol at 967cm$^{-1}$.[296]

By looking at Figure 5.5, Spray Dried Mannitol is composed of the α- and β-polymorph, Spray Dried Lactose with amorphous content, α-lactose and β-lactose, 1:1 [Mannitol:Lactose] with α- and β-mannitol, 1:3 [Mannitol:Lactose] with amorphous lactose, α-lactose, β-lactose, α-mannitol, and β-mannitol, and 3:1 [Mannitol:Lactose] with amorphous lactose, α-mannitol, and β-mannitol. Furthermore, these results, and those presented in Figure 5.3, complement one another and were, therefore, used in the solid-state characterization of the carriers.

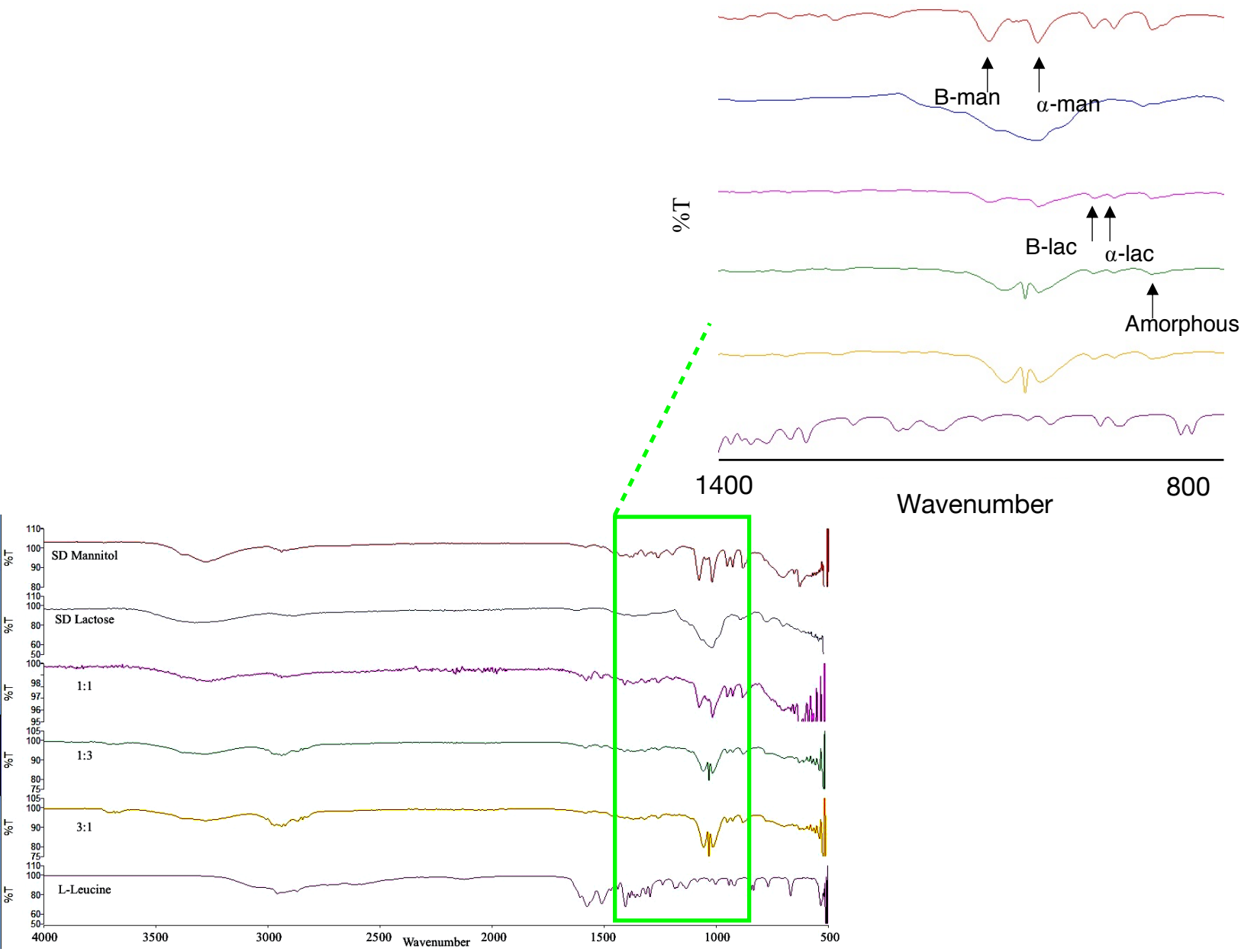


**Figure 5.5**. FT-IR. FT-IR spectra of Spray Dried Mannitol, Spray Dried Lactose, 1:1 [Mannitol:Lactose], 1:3 [Mannitol:Lactose], 3:1 [Mannitol:Lactose], and L-leucine where ↟ represents α-mannitol, ↑ represents β-mannitol, and ↡ represents Δ-mannitol.

### § 5.3.3 *In vitro* analysis of DPI formulations

#### §§ 5.3.3.1 Salbutamol sulphate assessment

Aerosolization performance of all of the formulations is summarized in Figure 5.6 where the amount of salbutamol sulphate deposited into each of the stages of the Multi-Stage Liquid Impinger (MSLI) is shown [capsules (C), inhaler (I), mouthpiece (M), induction port (IP), Stage 1, Stage 2, Stage 3, Stage 4, and Stage 5]. As can be seen in the figure, spray dried lactose obtained the lowest amount of salbutamol sulphate in the capsules with 1.90 ± 0.58 µg while the 1:1 [Mannitol:Lactose] carrier obtained the highest with 9.52 ± 7.32 µg. When it came to the inhaler device, however, the 1:3 [Mannitol:Lactose] carrier exhibited the least with 8.82 ± 2.47 µg whereas the 1:1 [Mannitol:Lactose] carrier exhibited the highest amount with 42.11 ± 41.74 µg.

When it came to the mouthpiece, spray dried mannitol obtained the least amount of salbutamol sulphate with 8.11 ± 0.91 µg while the 1:1 [Mannitol:Lactose] carrier obtained the highest amount with 12.21 ± 4.93 µg. In the induction port, the 1:3 [Mannitol:Lactose] carrier obtained the least mount of salbutamol sulphate with 7.84 ± 3.42 µg while spray dried lactose obtained the highest amount with 14.58 ± 6.15µg. The 1:3 [Mannitol:Lactose] carrier also had the least amount of salbutamol sulphate in Stage 1 with 73.30 ± 14.22 µg while the 3:1 [Mannitol:Lactose] carrier had the most with 130.33 ± 23.93µg. In Stage 2-5, the 1:3 [Mannitol:Lactose] carrier obtained the highest amount of salbutamol sulphate with 41.30 ± 23.89, 128.10 ± 56.12, 79.01 ± 33.48, and 24.51 ± 15.16µg (respectively) categorizing it as the optimal carrier. As far as the lowest amounts are concerned, the 3:1 [Mannitol:Lactose] carrier obtained 19.68 ± 8.86µg for Stage 2, Spray Dried Lactose obtained 67.78 ± 48.36µg for Stage

3, the 3:1 [Mannitol:Lactose] carrier obtained 49.90 ± 12.55µg for Stage 4, and the 1:1 [Mannitol:Lactose] carrier obtained 9.56 ± 2.35µg for Stage 5.

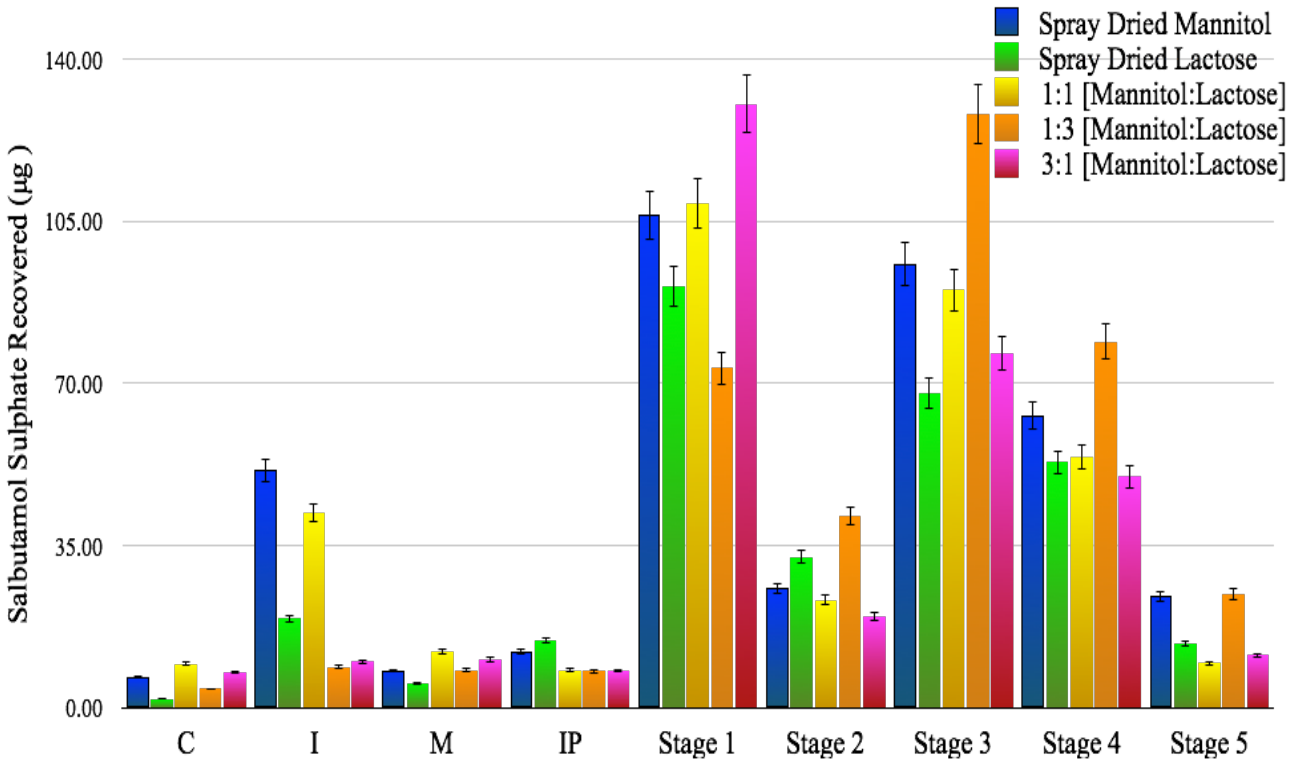


**Figure 5.6**. Aerosolization Profile. Aerosolization performance of each formulation (Spray Dried Mannitol, Spray Dried Lactose, 1:1 [Mannitol:Lactose], 1:3 [Mannitol:Lactose], and 3:1 [Mannitol:Lactose]) highlighting the amount of salbutamol sulphate recovered (percent recovered).

Table 5.3 presents the recovered dose (RD), emitted dose (ED), percent recovery, percent emission, percent impact loss, mass median aerodynamic diameter (MMAD), geometric standard deviation (GSD), fine particle dose (FPD), fine particle fraction (FPF), drug loss (DL), dispersibility (DS), and effective inhalation index (EI) for salbutamol sulphate obtained from each of the different formulations (Spray Dried Mannitol, Spray Dried Lactose, 1:1 [Mannitol:Lactose], 1:3 [Mannitol:Lactose], and 3:1 [Mannitol:Lactose]) and correlates with the data already presented in

Figure 5.6. With that being said, Spray Dried Mannitol accounted for receiving the least amount of salbutamol sulphate for RD, ED, percent recovery, and percent emission with 213.23 ± 59.44µg, 147.97 ± 53.44µg, 44.33 ± 12.36%, and 73.03 ± 28.66% (respectively); the 1:3 [Mannitol:Lactose] carrier, however, received the highest amount of salbutamol sulphate for RD, ED, percent recovery, and percent emission with 371.01 ± 144.43µg, 354.07 ± 140.71µg, 77.13 ± 30.03%, and 95.21 ± 0.95% (respectively).

The 1:3 [Mannitol:Lactose] carrier received the lowest impact loss with 23.29 ± 5.83% whereas the highest was the 3:1 [Mannitol:Lactose] carrier with 44.65 ± 11.75%. These results suggest that the 1:3 [Mannitol:Lactose] carrier obtained the best aerosolized performance amongst the carriers. With respect to MMAD, the 1:1 [Mannitol:Lactose] carrier obtained the largest diameter with 3.10 ± 0.06µm, whereas Spray Dried Lactose obtained the lowest diameter with 3.00 ± 0.18µm. In addition, the 1:1 [Mannitol:Lactose] carrier also received the lowest GSD with 2.03 ± 0.04µm whereas the highest GSD came from Spray Dried Lactose with 2.13 ± 0.08µm.

With respect to FPD, the 1:3 [Mannitol:Lactose] carrier obtained the highest amount with 231.63 ± 103.21 and the lowest amount was from Spray Dried Mannitol with 75.82 ± 43.07. The 1:3 [Mannitol:Lactose] carrier received the highest FPF with 61.42 ± 4.21% whereas the lowest was from Spray Dried Mannitol with 38.10 ± 21.84%. These results prove that the 1:3 [Mannitol:Lactose] carrier was the best engineered carrier amongst all the carriers. The 1:3 [Mannitol:Lactose] carrier also received the lowest drug loss with 5.93 ± 1.04% whereas the highest drug loss was from Spray Dried Mannitol with 29.10 ± 30.22%. The 1:3 [Mannitol:Lactose] carrier had the highest dispersibility with 64.49 ± 3.77% and effective inhalation index with 12.51 ± 0.21 whereas the lowest dispersibility came from the 3:1 [Mannitol:Lactose] carrier with 45.82 ± 10.19% and the lowest effective inhalation index came from Spray Dried Mannitol with 10.32 ±

2.63. All in all, taking all of the measurements as a whole and not individually, the 1:3 [Mannitol:Lactose] carrier navigated itself as having the best aerosolization performance when compared to the other carriers. That being said, this carrier is the most effective at delivering salbutamol sulphate to the lower respiratory tract via a dry powder inhaler.

**Table 5.3.** Aerosolization Parameters. Recovered Dose (RD), Emitted Dose (ED), Percent Recovery, Percent Emission, Percent Impact Loss, Mass Median Aerodynamic Diameter (MMAD), Geometric Standard Deviation (GSD), Fine Particle Dose (FPD), Fine Particle Fraction (FPF), Drug Loss (DL), Dispersibility (DS), and Effective Inhalation Index (EI) of salbutamol sulphate obtained from each of the different formulations (Spray Dried Mannitol, Spray Dried Lactose, 1:1 [Mannitol:Lactose], 1:3 [Mannitol:Lactose], and 3:1 [Mannitol:Lactose]).

| Formulation | RD (µg) | ED (µg) | Recovery (%) | Emission (%) | Impact Loss (%) | MMAD (µm) | GSD (µm) | FPD | FPF (%) | DL (%) | DS (%) | EI |
|---|---|---|---|---|---|---|---|---|---|---|---|---|
| **Spray Dried Mannitol** | 213.23 ± 59.44 | 147.97 ± 53.44 | 44.33 ± 12.36 | 73.03 ± 28.66 | 28.89 ± 3.20 | 3.05 ± 0.14 | 2.05 ± 0.01 | 75.82 ± 43.07 | 38.10 ± 21.84 | 29.10 ± 30.22 | 48.53 ± 14.22 | 10.32 ± 2.63 |
| **Spray Dried Lactose** | 297.32 ± 175.08 | 272.87 ± 179.66 | 61.83 ± 36.40 | 88.91 ± 7.43 | 35.95 ± 4.00 | 3.00 ± 0.18 | 2.13 ± 0.08 | 134.81 ± 91.41 | 43.08 ± 7.38 | 12.00 ± 8.18 | 48.26 ± 5.35 | 11.48 ± 0.63 |
| **1:1** | 348.55 ± 68.13 | 294.22 ± 87.42 | 72.46 ± 14.16 | 83.63 ± 14.25 | 34.42 ± 7.71 | 3.10 ± 0.06 | 2.03 ± 0.04 | 153.89 ± 83.95 | 42.58 ± 18.43 | 18.96 ± 14.88 | 49.30 ± 15.65 | 11.17 ± 1.51 |
| **1:3** | 371.01 ± 144.43 | 354.07 ± 140.71 | 77.13 ± 30.03 | 95.21 ± 0.95 | 23.29 ± 5.83 | 3.02 ± 0.17 | 2.08 ± 0.03 | 231.63 ± 103.21 | 61.42 ± 4.21 | 5.93 ± 1.04 | 64.49 ± 3.77 | 12.51 ± 0.21 |
| **3:1** | 316.06 ± 38.22 | 295.68 ± 34.92 | 65.71 ± 7.95 | 93.57 ± 0.49 | 44.65 ± 11.75 | 3.02 ± 0.06 | 2.04 ± 0.03 | 137.69 ± 47.09 | 42.85 ± 9.36 | 8.91 ± 1.57 | 45.82 ± 10.19 | 11.68 ± 0.38 |

#### §§ 5.3.3.2 Homogeneity assessment

To assess the formulations for their homogeneity they underwent a uniformity assessment. Figure 5.7 presents the homogeneity profiles for all of the formulations (Spray Dried Mannitol, Spray Dried Lactose, 1:1 [Mannitol:Lactose], 1:3 [Mannitol:Lactose], and 3:1 [Mannitol:Lactose]) through percent potency; Table 5.4 shows the percent content homogeneity, which is expressed as the percent coefficient of variation (%CV).

With respect to their potency, all of the formulations adhered to the required specification set by the US Food and Drug Administration by falling within the 75-125% range. When it came to %CV, 3:1 [Mannitol:Lactose] obtained the smallest %CV with 0.76% whereas the largest %CV was obtained by the 1:3 [Mannitol:Lactose] carrier with 23.47%. These results indicate that the 3:1 [Mannitol:Lactose] carrier had the best content homogeneity amongst all of the carriers and the 1:3 [Mannitol:Lactose] carrier had the worst content homogeneity. The 1:3 [Mannitol:Lactose] carrier, which was the best engineered carrier, obtained a %CV of 23.47%.

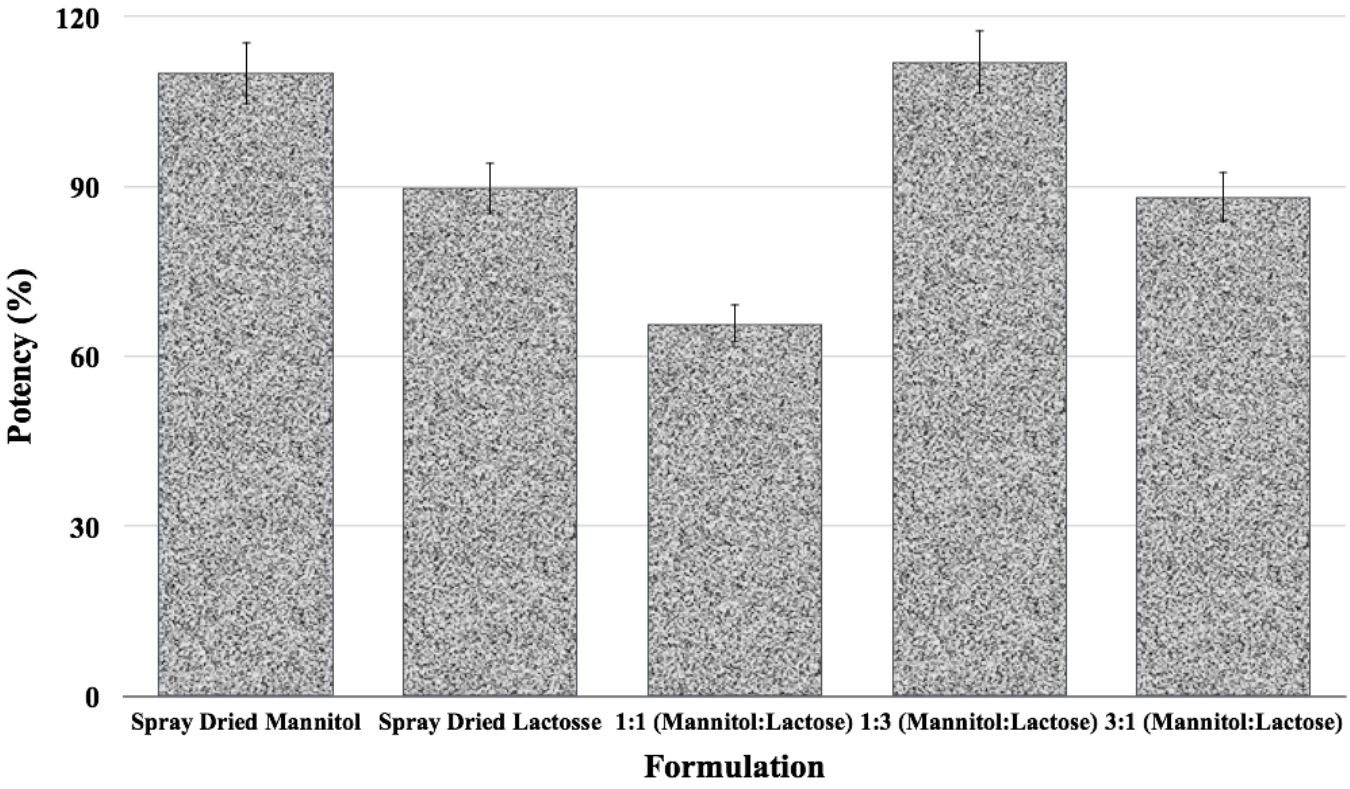


**Figure 5.7.** Potency. Percent potency of each formulation (Spray Dried Mannitol, Spray Dried Lactose, 1:1 [Mannitol:Lactose], 1:3 [Mannitol:Lactose], and 3:1 [Mannitol:Lactose]) with respect to salbutamol sulphate.

**Table 5.6.** Content Homogeneity. Content homogeneity of Spray Dried Mannitol, Spray Dried Lactose, 1:1 [Mannitol:Lactose], 1:3 [Mannitol:Lactose], and 3:1 [Mannitol:Lactose] expressed as the percent coefficient of variation (%CV).

| Formulation | % CV |
|---|---|
| **Spray Dried Mannitol** | 11.90 |
| **Spray Dried Lactose** | 13.23 |
| **1:1 (Mannitol:Lactose)** | 13.22 |
| **1:3 (Mannitol:Lactose)** | 23.47 |
| **3:1 (Mannitol:Lactose)** | 0.76 |

*However, has not been taken into account for *in vivo* inhalation studies.

### *5.4 Conclusion*

The results presented in this chapter have proven that different concentrations of mannitol:lactose solutions were successfully spray dried. They also show that the aerosolization performance of the 1:3 [Mannitol:Lactose] carrier was successfully achieved; this achievement was measured in the carrier's FPF, which was 61.42 ± 4.21%. The use of 5% $_{L}$-leucine (w/w) modified the physicochemical properties of the spray dried particles along with their morphology. The results also showcase the lubrication effect that $_{L}$-leucine provides to the carriers upon aerosolization. They also show that by combining mannitol and lactose in a spray dried solution, with 5% $_{L}$-leucine, an improved DPI formulation can be achieved; one more effective than the current marketed brand.

# Chapter 6

## Effect of Leucine on Dry Powder Inhaler Performance of Salbutamol Sulphate containing Xylitol Crystals

### *6.1 Introduction*

In this chapter, the focus was to engineer a crystal composed of xylitol and different concentrations of $_{L}$-leucine and investigate the effect it has on the overall aerosolized DPI performance of salbutamol sulphate. In addition, the current chapter investigates whether xylitol could be a good alternative to lactose in DPI formulations containing salbutamol sulphate. (2S,4R)-pentane-1,2,3,4,5-pentol, commonly known as xylitol, is a five carbon sugar found in berries, mushrooms, cauliflower, lettuce, corn, and birch tree bark and it is most commonly used as a diabetic sweetner. Xylitol is not metabolized by cariogenic bacteria, which are cavity-causing bacteria found in the human mouth, allowing for its popular use as an ingredient in chewing gum. Studies have shown that xylitol chewing gum prevents acute otitis media (ear aches or infections) because the continuous act of chewing and swallowing assist with the disposal and removal of earwax while also clearing the middle ear.[298] Having a low glycemic index and it being insulin independent has allowed xylitol to be used by non-insulin dependent diabetics as well as by the obese.[299]

Orally administered xylitol is known to prevent colds and facilitate calcium absorption, which is known to give way to stronger bones; it's cooling effect serves as an effective means of masking unpleasant flavors associated to medications.[300] Furthermore, its use in tableting has been known to significantly improve a tablet's mechanical strength and dissolution behavior.[301] Its use as a carrier in DPI formulations, however, has never been studied, and is the focal point of this overall study.

Among metered-dose inhalers (MDI), nebulizers, and DPIs, which are the three aerosol devices used to deliver therapeutic agents to the lungs, the DPI is the most promising due to them being propellant-free, portable, easy to use, cost-effective, and the formulations used with said device experience enhanced stability when stored.[302] Crystals, as a whole, provide a unique opportunity by allowing one to modulate their physicochemical properties and limit polymorphs.[303] Moreover, crystal engineering also improves solubility[304-306], physical stability[307, 308], mechanical properties[309, 310] such as flowability and compressibility, increases bioavailability[311], improves pharmacokinetic properties[312], and improves permeability[301]. Use of an additive (i.e. $_{L}$-leucine) has already been reported to alter the micrometric properties (i.e. size and shape) of engineered crystals.[301]

In addition, an attempt was made in this chapter to investigate whether or not $_{L}$-leucine can enhance the aerosolization behavior of salbutamol sulphate in DPI formulations used with a cyclohaler device. Furthermore, an attempt was made to explore whether or not xylitol can act as another carrier to replace lactose DPI formulations for lactose intolerant patients.

## *6.2 Materials and Methodology*

### § 6.2.1- § 6.2.13

Refer to Chapter 2 sections *2.2, 2.4-2.11,* and *2.13-2.16.*

## *6.3 Results and Discussion*

### § 6.3.1 Particle size analysis

Figure 6.1 provides the particle size distribution (PSD) diagrams of the unseived engineered carriers from each formulation for both the RODOS and Cuvette systems. In Figure 6.1A, all of the carriers, with the exception of Xylitol with 0% $_{L}$-leucine (LEU), experienced similar particle size distribution curves; therefore, it was determined that the presence of $_{L}$-leucine affected the kinetics and nucleation behavior of xylitol. Xylitol with 0% LEU experienced a fixed number of nucleations, thereby given larger crystals, whereas all the other carriers experienced a continuous nucleation process, henceforth the smaller crystals. Figure 6.1B, however, shows all of the carriers adhering to, and satisfying, the requirement of being between 63-90µm when used for inhalation. The results also show that the engineered carriers underwent some degree of agglomeration given the difference in particle size between the Rodos and Cuvette systems.

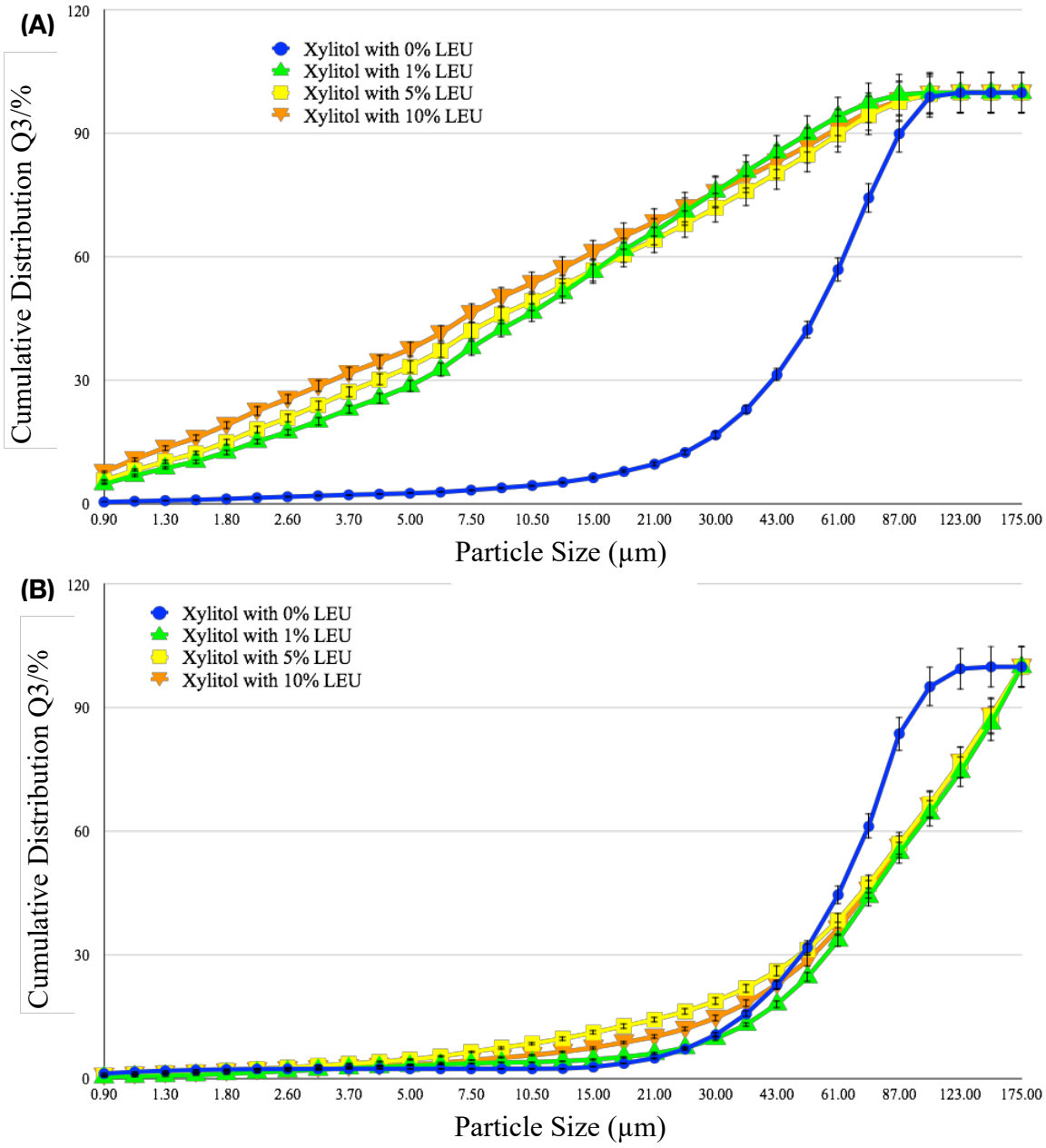


**Figure 6.1.** Particle Size Distribution. Particle Size Distribution (PSD) diagrams of the engineered carriers (Xylitol with 0% LEU, Xylitol with 1% LEU, Xylitol with 5% LEU, and Xylitol with 10% LEU) when using the (A) Rodos dry system and when using the (B) Cuvette wet system.

Table 6.1 presents the volume mean diameter (VMD) alongside the span for each of the engineered carriers under Rodos and Cuvette conditions. All of the carriers experienced a difference in their VMDs with ranges from 19.68 ± 2.66 µm from Xylitol with 1% LEU to 55.49 ± 4.06 µm from Xylitol with 0% LEU and 63.40 ± 1.21 µm from Xylitol with 0% LEU to 86.75 ± 12.92 µm from Xylitol with 1% LEU for the dry and wet systems, respectively.

With respect to the carrier's span, the dry system experienced a range of 1.17 ± 0.13 from Xylitol with 0% LEU to 6.37 ± 0.56 from Xylitol with 10% LEU while the wet system experienced a range from 1.02 ± 0.07 from Xylitol with 0% LEU to 1.81 ± 0.12 from Xylitol with 5% LEU. Furthermore, the dry system experienced a particle diameter range of 6.44 ± 9.60 µm ($D_{10\%}$) to 64.34 ± 14.78 µm ($D_{90\%}$) where the particle diameter range for the wet system fell between 23.75 ± 8.53 µm ($D_{10\%}$) and 137.73 ± 25.84 µm ($D_{90\%}$).

**Table 6.1**. Particle Analysis. Particle Analysis of Xylitol with 0% LEU, Xylitol with 1% LEU, Xylitol with 5% LEU, and Xylitol with 10% LEU showing the volume mean diameter (VMD) and span when using the Rodos dry system and the Cuvette wet system.

| Carrier | VMD (µm) Dry System | VMD (µm) Wet System | Span Dry System | Span Wet System |
|---|---|---|---|---|
| **Xylitol with 0% LEU** | 55.49 ± 4.06 | 63.40 ± 1.21 | 1.17 ± 0.13 | 1.02 ± 0.07 |
| **Xylitol with 1% LEU** | 19.68 ± 2.66 | 86.75 ± 12.92 | 4.14 ± 0.50 | 1.52 ± 0.34 |
| **Xylitol with 5% LEU** | 22.03 ± 0.62 | 80.34 ± 3.25 | 5.53 ± 0.10 | 1.81 ± 0.12 |
| **Xylitol with 10% LEU** | 19.93 ± 1.69 | 82.80 ± 1.16 | 6.37 ± 0.56 | 1.66 ± 0.04 |

Figure 6.2 presents the electron micrograms of all the carriers where it was determined that both commercial Xylitol and Xylitol with 1% LEU presented needle-like shapes, Xylitol with 0% LEU showed a spherical shape, and Xylitol with 5% LEU along with Xylitol with 10% LEU showed a tomahawk shape. Based on these results and those reported by Kaialy *et. al* [313] where it was argued that a needle-like shape serves as a better carrier than that of a spherical one or tomahawk one; thus, it was determined that either Commercial Xylitol or Xylitol with 1% LEU would perform the best in the aerosolization study.

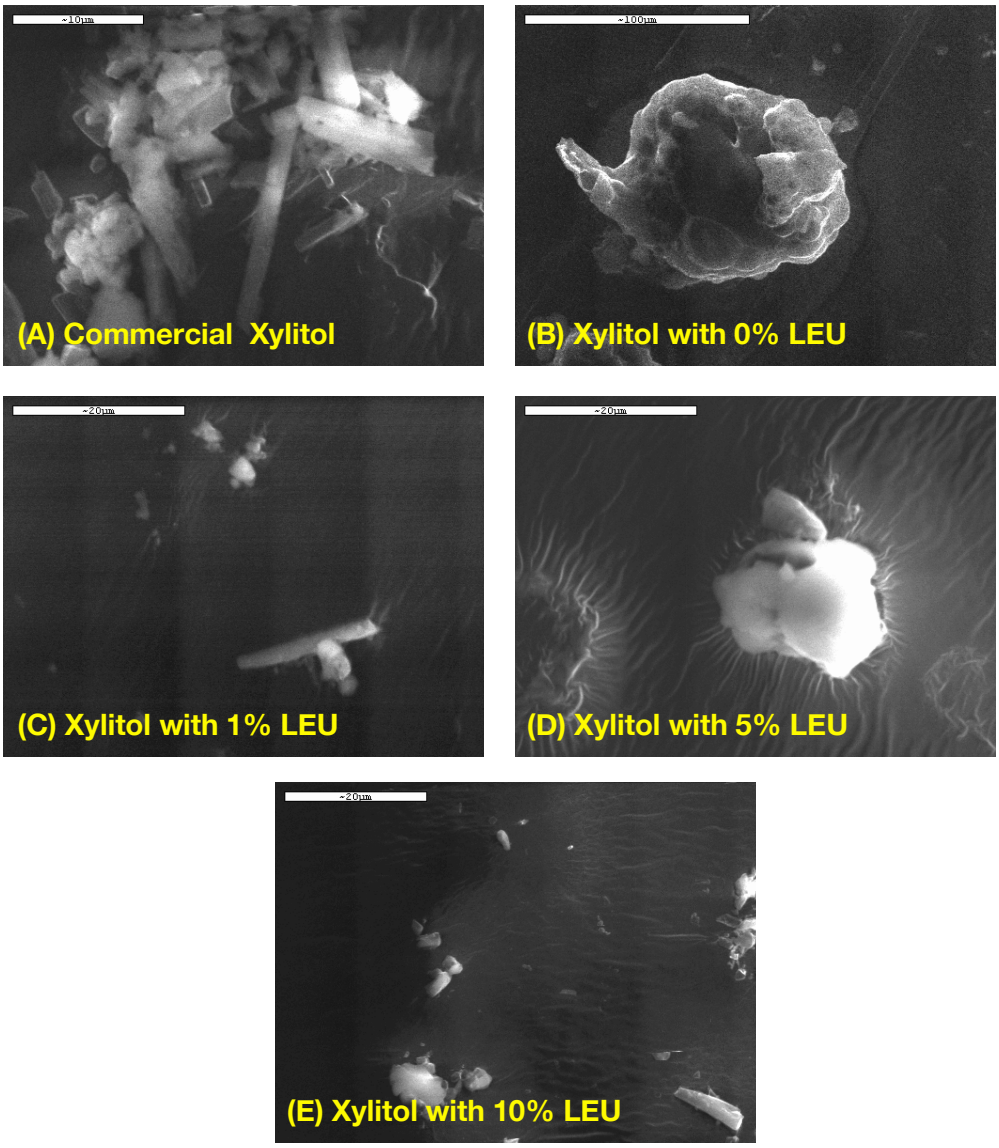


**Figure 6.2.** Scanning Electron Microscopy. SEM micrograms of (A) Commercial Xylitol, (B) Xylitol with 0% LEU, (C) Xylitol with 1% LEU, (D) Xylitol with 5% LEU, and (E) Xylitol with 10% LEU.

### § 6.3.2 Solid-state characterization of engineered carriers

Figure 6.3 presents the chromatographs of Commercial Xylitol and the engineered carriers (Xylitol with 0% LEU, Xylitol with 1% LEU, Xylitol with 5% LEU, and Xylitol with 10% LEU) indicating the location of any thermal event taking place; whereas Table 6.2 summarizes the enthalpy of the

reaction ($\Delta H_{rxn}$) for each individual carrier's thermal event with the corresponding temperature, in °C.

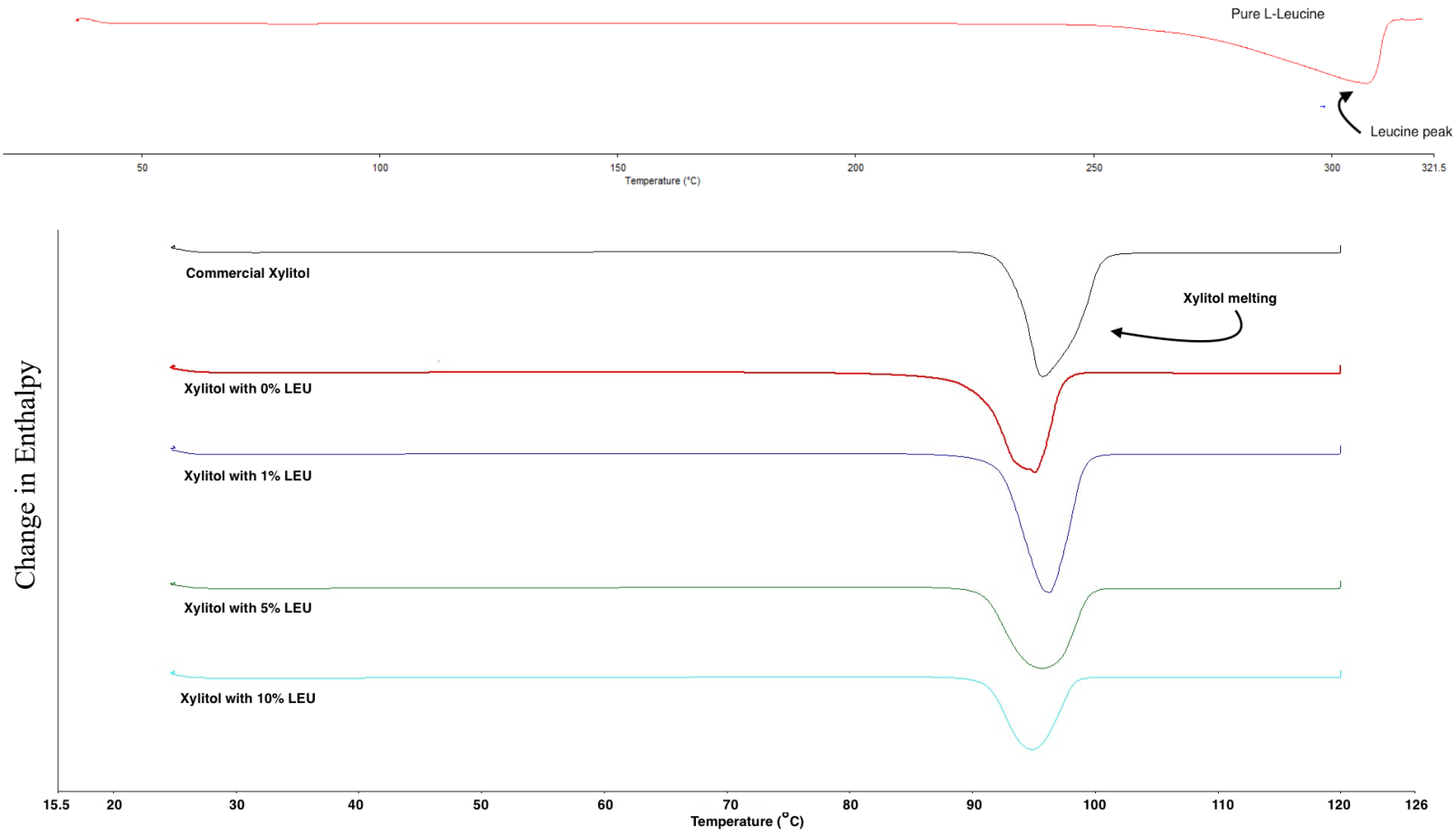


**Figure 6.3.** Differential Scanning Calorimetry. DSC thermal peaks of $_{L}$-Leucine, Commercial Xylitol, Xylitol with 0% LEU, Xylitol with 1% LEU, Xylitol with 5% LEU, and Xylitol with 10% LEU, where an exothermic peak points up and an endothermic peak points down.

**Table 6.2**. DSC Thermal Traces. DSC thermal traces of Commercial Xylitol, Xylitol with 0% LEU, Xylitol with 1% LEU, Xylitol with 5% LEU, and Xylitol with 10% LEU, and $_{L}$-Leucine indicating the enthalpy, in J/g, of xylitol melting ($\Delta H_{rxn}$) along with the Temperature (°C) of where such melting took place.

| Carrier | Temperature (°C) | $\Delta H_{rxn}$ (J/g) |
|---|---|---|
| **Commercial Xylitol** | 95.87 ± 0.14 | 194.09 ± 2.67 |
| **Xylitol with 0% LEU** | 95.36 ± 0.40 | 146.37 ± 3.92 |
| **Xylitol with 1% LEU** | 95.78 ± 0.66 | 196.44 ± 8.97 |
| **Xylitol with 5% LEU** | 95.74 ± 0.03 | 116.34 ± 5.03 |
| **Xylitol with 10% LEU** | 95.01 ± 0.26 | 96.25 ± 6.75 |
| **Pure Leucine** | — | — |

Data presented in Table 6.2 authenticates the illustrated data presented in Figure 6.3 where it shows a xylitol exothermic event at 95.53 ± 0.57°C, which is known to being associated to the melting of the orthorhombic stable form of xylitol.[314] Due to the lack of any thermal events below 100°C, it was determined that there were no detectable amounts of free water in the samples. Absence of said peaks can also be attributed to the presence of $_{L}$-leucine as it is known to facilitate moisture protection while providing stability for the formulation. Furthermore, the lack of any thermal event at 61°C in all xylitol samples indicates the absence of the monoclinic hygroscopic metastable form of xylitol in the carriers.[315]

$_{L}$-Leucine's introduction into the engineered formulations had an effect on the enthalpies of the reactions of all the samples by manifesting a reduction in the sample's overall enthalpy as the concentration of $_{L}$-leucine increases; this linear correlation (data not shown) is attributed to the inter- and intra-molecular interactions (i.e. Van dar Waals, hydrogen bonding, etc.) that have been

altered, in the micro level, from the original. Using the crystallization methodology of this study proved to have no significant impact on xylitol's polymorphous form or its molecular structure given that FT-IR spectroscopy showed no significant changes from sample to sample (data not shown).

Figure 6.4 depicts the powder X-ray diffraction (PXRD) patterns for Commercial Xylitol, $_{L}$-leucine, and all of the engineered carriers (Xylitol with 0% LEU, Xylitol with 1% LEU, Xylitol with 5% LEU, and Xylitol with 10% LEU) providing insight into their crystallinity. Demonstrating sharp diffraction angles with no halo background or widening allowed for them to be classified as crystalline. Moreover, a linear correlation ($r^2 = 0.99$) existed between the increase in $_{L}$-leucine concentration and the sharpening of the peaks, as seen in the figure. It is also worth noting that the desired polymorph was obtained by all of the carriers which presented improved pharmaceutical performance.

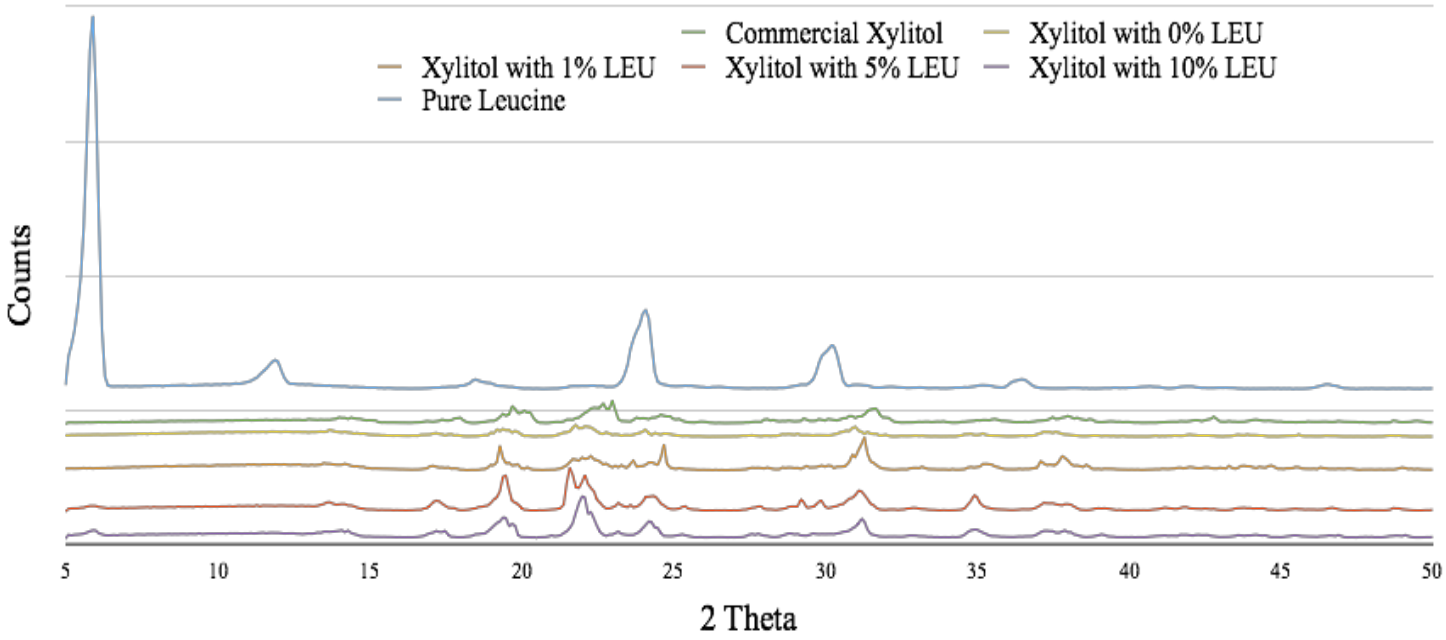


**Figure 6.4.** X-Ray Diffraction. Powder X-Ray diffraction patterns of Pure Leucine, Commercial Xylitol, Xylitol with 0% LEU, Xylitol with 1% LEU, Xylitol with 5% LEU, and Xylitol with 10% LEU.

### § 6.3.3 *In vitro* analysis of DPI formulations

#### §§ 6.3.3.1 Salbutamol sulphate assessment

Aerosolization performance of all of the formulations is summarized in Figure 6.5 where the amount of salbutamol sulphate deposited into each of the stages of the Multi-Stage Liquid Impinger (MSLI) is shown [capsules (C), inhaler (I), mouthpiece (M), induction port (IP), Stage 1, Stage 2, Stage 3, Stage 4, and Stage 5 (filter)]. As can be seen in the figure, Commercial Xylitol obtained the lowest amount of salbutamol sulphate in the capsules with 1.16 ± 0.32 µg while

Xylitol with 10% LEU obtained the highest amount with 6.09 ± 4.98 µg. When it came to the inhaler device, however, Commercial Xylitol exhibited the highest amount with 14.26 ± 4.26 µg and Xylitol with 10% LEU with the least amount with 5.27 ± 2.49 µg.

Additionally, Commercial Xylitol obtained the lowest amount of salbutamol sulphate in both the mouthpiece, with 3.87 ± 2.18 µg, and induction port, with 4.89 ± 2.74 µg; whereas Xylitol with 5% LEU received the highest amount, with 11.93 ± 2.31 µg, in the mouthpiece and Xylitol with 10% LEU received the highest amount with 12.71 ± 3.27 µg in the induction port. For Stages 1-5, Xylitol with 5% LEU accounted for obtaining the highest amount in all five stages: 141.73 ± 5.97, 32.34 ± 20.46, 88.37 ± 62.34, 56.33 ± 32.09, and 38.78 ± 43.23 µg, respectively. For the lowest amounts, however, Xylitol with 0% LEU obtained 75.87 ± 21.63 µg in Stage 1, Xylitol with 1% LEU obtained 19.06 ± 4.71 µg for Stage 2, 23.28 ± 15.21 µg for Stage 3, 16.02 ± 8.12 µg for Stage 4, and Xylitol with 0% LEU obtained 6.11 ± 4.95 µg for Stage 5. These preliminary results suggested that Xylitol with 5% LEU would prove to be the most effective at delivering the salbutamol sulphate into the alveoli rather than the Commercial Xylitol and Xylitol with 1% LEU, which were both previously categorized as needle-like in shape.

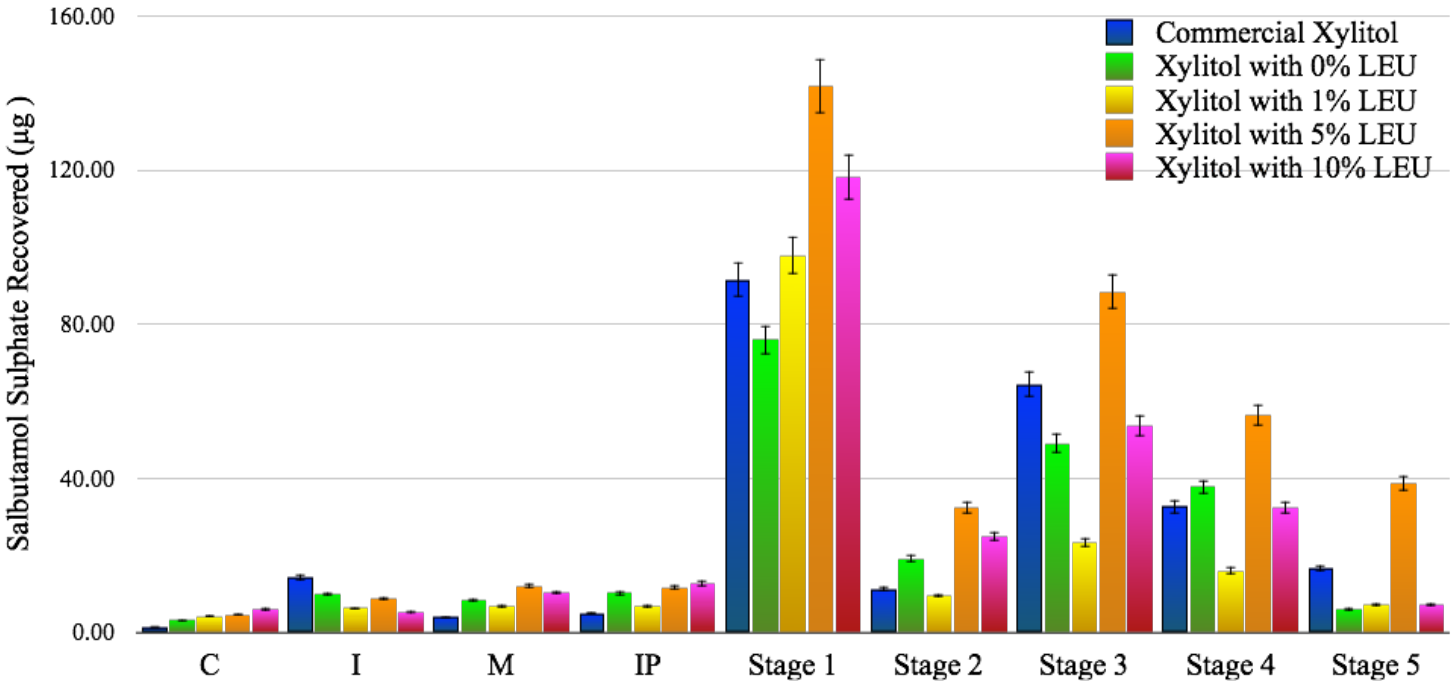


**Figure 6.5**. Aerosolization Profile. Aerosolization performance of Commercial Xylitol and each engineered formulation (Xylitol with 0% LEU, Xylitol with 1% LEU, Xylitol with 5% LEU, and Xylitol with 10% LEU) highlighting the amount of SS recovered (percent recovered) for each and comparing them side-by-side.

Table 6.3 presents the recovered dose (RD), emitted dose (ED), percent recovery, percent emission, percent impact loss, mass median aerodynamic diameter (MMAD), geometric standard deviation (GSD), fine particle dose (FPD), fine particle fraction (FPF), drug loss (DL), dispersibility (DS), and effective inhalation index (EI) for salbutamol sulphate obtained from each of the different formulations (Commercial Xylitol, Xylitol with 0% LEU, Xylitol with 1% LEU, Xylitol with 5% LEU, and Xylitol with 10% LEU) and correlates with the data already presented in Figure 6.5. Xylitol with 1% LEU accounted for receiving the least amount of salbutamol sulphate for RD, ED, and percent recovery with 173.67 ± 44.85 µg, 160.49 ± 38.62 µg, and 36.11 ± 9.32%, respectively; Xylitol with 5% LEU, however, received the highest amount of salbutamol sulphate

for RD, ED, and percent recovery with 390.01 ± 163.29 µg, 369.23 ± 154.57 µg, and 81.08 ± 33.95%, respectively.

Moreover, Xylitol with 5% LEU also received the highest percent emission with 94.67 ± 0.01% whereas Xylitol with 0% LEU received the lowest with 91.91 ± 3.46% suggesting that Xylitol with 5% LEU was capable of injecting more of the engineered formulation into the system than any other formulations.

Xylitol with 1% LEU received the highest impaction loss with 61.38 ± 13.21% whereas Commercial Xylitol received the lowest amount with 43.72 ± 12.20%. With respect to MMAD, Xylitol with 10% LEU obtained the largest diameter with 3.29 ± 0.10 µm, which further supports its performance fallacy, whereas Commercial Xylitol received the lowest with 2.77 ± 0.45µm indicating a positive correlation between the smaller particle diameter to that of its efficacy. In addition, Xylitol with 5% LEU obtained the largest GSD with 2.21 ± 0.13µm and Xylitol with 10% LEU received the smallest with 2.05 ± 0.01 µm.

With respect to FPD, Xylitol with 5% LEU received the highest with 183.48 ± 137.26 $\mu$g and the lowest was Xylitol with 1% LEU with 46.41 ± 26.06 $\mu$g. Commercial Xylitol proved to obtain the highest FPF amongst all of the formulations with a FPF of 44.13 ± 11.27%, whereas Xylitol with 5% LEU came at a close second with 42.94 ± 15.21%. A linear correlation ($r^2 = 0.97$) between FPF and effective inhalation index was established correlating to the formulation's effeciency. Xylitol with 5% LEU, however, was managed to obtain the lowest drug loss with 6.57 ± 0.39%, but the highest with 10.28 ± 1.95% was from Xylitol with 1% LEU; thereby placing Commercial Xylitol as the more effective formulation as a whole. Commercial Xylitol did receive the highest dispersibility with 47.90 ± 11.69%, but the lowest went to Xylitol with 1% LEU with 27.88 ± 11.96%.

Lastly, Xylitol with 5% LEU received the highest effective inhalation index with 11.72 $\pm$ 0.65 whereas Xylitol with 1% LEU obtained the lowest with 10.88 $\pm$ 0.50.

**Table 6.3.** Aerosolization Parameters. Recovered Dose (RD), Emitted Dose (ED), Percent Recovery, Percent Emission, Percent Impact Loss, Mass Median Aerodynamic Diameter (MMAD), Geometric Standard Deviation (GSD), Fine Particle Dose (FPD), Fine Particle Fraction (FPF), Drug Loss (DL), Dispersibility (DS), and Effective Inhalation Index (EI) of salbutamol sulphate obtained from each of the different formulations (Commercial Xylitol, Xylitol with 0% LEU, Xylitol with 1% LEU, Xylitol with 5% LEU, and Xylitol with 10% LEU).

| Formulation | RD (µg) | ED (µg) | Recovery (%) | Emission (%) | Impact Loss (%) | MMAD (µm) | GSD (µm) | FPD | FPF (%) | DL (%) | DS (%) | EI |
|---|---|---|---|---|---|---|---|---|---|---|---|---|
| **Commercial Xylitol** | 239.29 ± 111.70 | 221.16 ± 106.22 | 49.75 ± 23.22 | 92.01 ± 1.75 | 43.72 ± 12.20 | 2.77 ± 0.45 | 2.18 ± 0.31 | 113.57 ± 82.45 | 44.13 ± 11.27 | 8.56 ± 2.11 | 47.90 ± 11.69 | 11.66 ± 0.53 |
| **Xylitol with 0% LEU** | 216.19 ± 170.69 | 197.97 ± 154.33 | 44.95 ± 35.49 | 91.91 ± 3.46 | 50.01 ± 19.40 | 3.10 ± 0.10 | 2.09 ± 0.06 | 92.87 ± 109.59 | 34.25 ± 16.98 | 10.12 ± 3.94 | 37.27 ± 18.73 | 11.21 ± 0.78 |
| **Xylitol with 1% LEU** | 173.67 ± 44.85 | 160.49 ± 38.62 | 36.11 ± 9.32 | 92.75 ± 2.08 | 61.38 ± 13.21 | 2.92 ± 0.24 | 2.19 ± 0.10 | 46.41 ± 26.06 | 25.84 ± 11.05 | 10.28 ± 1.95 | 27.88 ± 11.96 | 10.88 ± 0.50 |
| **Xylitol with 5% LEU** | 390.01 ± 163.29 | 369.23 ± 154.57 | 81.08 ± 33.95 | 94.67 ± 0.01 | 43.87 ± 16.61 | 2.83 ± 0.26 | 2.21 ± 0.13 | 183.48 ± 137.26 | 42.94 ± 15.21 | 6.57 ± 0.39 | 45.36 ± 16.07 | 11.72 ± 0.65 |
| **Xylitol with 10% LEU** | 264.91 ± 76.86 | 249.25 ± 69.90 | 55.07 ± 15.98 | 94.25 ± 0.88 | 49.13 ± 13.56 | 3.29 ± 0.10 | 2.05 ± 0.01 | 93.27 ± 33.93 | 35.61 ± 12.58 | 7.88 ± 2.12 | 37.75 ± 13.10 | 11.39 ± 0.57 |

All in all, taking all of the measurements as a whole and not individually, Xylitol with 5% Leu was the formulation with the best aerosolization performance given its FPD over that of Commercial Xylitol which had the best FPF. That is to say, Xylitol with 5% Leu delivered more salbutamol to the lower stages of the MSLI compared to Commercial Xylitol making Xylitol with 5% Leu the better formulation.

#### §§ 6.3.3.2 Homogeneity Assessment

All of the formulations underwent a homogeneity assessment to determine their uniformity which allows each formulation to be referenced with the specification guidelines set by the pharmaceutical governing bodies. Figure 6.6 presents the homogeneity profiles for all of the formulations (Commercial Xylitol, Xylitol with 0% LEU, Xylitol with 1% LEU, Xylitol with 5% LEU, and Xylitol with 10% LEU) through percent potency; Table 6.4 shows the percent content homogeneity, which is expressed as the percent coefficient of variation (%CV).

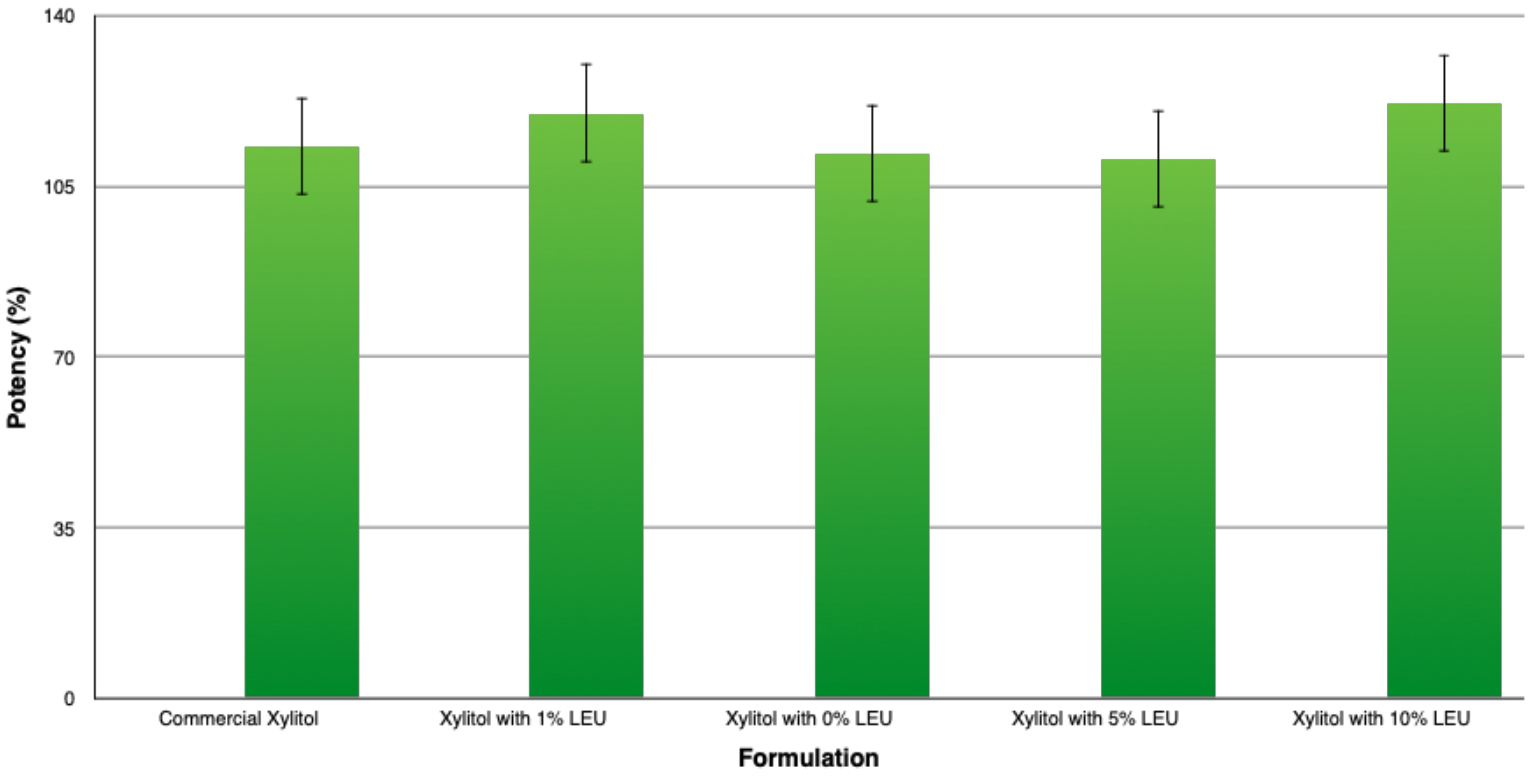


**Figure 6.6.** Potency. Percent potency of each formulation (Commercial Xylitol, Xylitol with 0% LEU, Xylitol with 1% LEU, Xylitol with 5% LEU, and Xylitol with 10% LEU) with respect to salbutamol sulphate.

With respect to percent potency, all of the formulations adhered to the required specification set by the US Food and Drug Administration by falling within the 75-125% potency range. Xylitol with 5% Leu had the smallest potency with a potency of 110.60 + 15.30% while Xylitol with 10% Leu had the highest potency with 121.06 + 3.07%. Moreover, Xylitol with 10% LEU obtained the smallest %CV with 2.53% whereas Xylitol with 1% LEU obtained the highest %CV with 19.68% (see Table 6.4). These results indicate that Xylitol with 10% LEU had the best content uniformity amongst all of the formulations highlighting the significant role that $_{L}$-leucine plays as an excipient. $_{L}$-Leucine improves the inter- and intra- molecular interactions of the particles by altering the

physicochemical properties of the formulation, yielding a favorable uniformity profile.

**Table 6.4.** Content Homogeneity. Content homogeneity of Commercial Xylitol, Xylitol with 0% LEU, Xylitol with 1% LEU, Xylitol with 5% LEU, and Xylitol with 10% LEU expressed as the percent coefficient of variation (%CV).

| Formulation | Potency (%) | % CV |
|---|---|---|
| **Commercial Xylitol** | 113.03 ± 15.09 | 13.35 |
| **Xylitol with 0% LEU** | 119.07 ± 14.05 | 11.72 |
| **Xylitol with 1% LEU** | 111.76 + 22.00 | 19.68 |
| **Xylitol with 5% LEU** | 110.60 + 15.30 | 13.83 |
| **Xylitol with 10% LEU** | 121.06 + 3.07 | 2.52 |

*However, has not been taken into account for *in vivo* inhalation studies.

### *6.4 Conclusion*

The results presented in this chapter have proven that xylitol crystals with different concentrations of $_{L}$-leucine can be successfully crystalized. They also showed that $_{L}$-leucine altered the physicochemical properties of the carriers affecting their inter- and intra-molecular interactions. This caused the uniformity of the carriers to improve with increasing $_{L}$-leucine concentration. Xylitol with 5% LEU (FPF = 42.94 ± 15.21) was the best DPI formulation within this study. This formulation had particles classified as tomahawk, which is known to show better aerosolized efficacy over particles with spherical morphology. The Xylitol with 5% LEU, however, does not compare to the 1:3 [Mannitol:Lactose] carrier from Chapter 5 whose FPF was 61.42 ± 4.21%.

# Chapter 7

## Effect Mannitol and Lactose crystals have on Aerosolized Dry Powder Inhaler Performance containing Salbutamol Sulphate

### *7.1 Introduction*

In this chapter, the focus was to engineer a crystal composed of mannitol:lactose in different concentrations and investigate the effect it has on the overall aerosolized DPI performance of salbutamol sulphate. Crystal engineering is viewed as a form of supramolecular synthesis, often referred to as *the chemistry beyond the molecule,* and contributes to the continued development of pharmaceuticals and functional materials.[316-318] For instance, Roy *et. al* engineered a crystal in such a way as to provide supramolecular hybrids where they were synthesized by a hydrothermal route under different pH using a hydrolyzable naphthalene diimide ligand.[319]

Moreover, crystal engineering offers an opportunity to optimize physicochemical properties, such as solubility, stability, hydration, and melting point, mechanical properties, such as flowability and compressibility, pharmacokinetic properties, bioavailability, and permeability.[320-323] Because amorphous powders have a higher surface free energy over crystalline material, it makes crystalline material a more favorable choice for drug formulation.[324]

Conventional DPI methods include milling, spray drying, and freeze drying[9] whereas those associated to crystal formation include slurry solutions[325-327], ultrasonic crystallization[328], evaporation[329], or supercritical fluids[330]; supercritical fluids being the chosen method here. During the process, supersaturation is generated by adding a second liquid to a solution of the crystals to be crystallized, which is miscible with the solvent and in which the crystals are insoluble or sparingly soluble.[331]

DPIs as a dosage form consist of a powder formulation designed to deliver an API to the respiratory tract. Formulations are filled into hard-gelatin capsules that are subsequently pierced by the inhaler devise directly before its application.[332] Recent studies have shown mannitol's and lactose's aerosolization performance in a DPI formulation showing mannitol's more favorable performance over that of lactose; fine particle fraction (FPF) of 52.96 $\pm$ 5.21% [Chapter 4] and 47.11 $\pm$ 9.94% [Chapter 3], respectively. Another study showed the aerosolization performance of spray dried mannitol and lactose combined in different ratios where the FPF was found to be 61.42 $\pm$ 4.21% [Chapter 5]. Additionally, xylitol crystals have also been used as a carrier in a DPI formulation where the resulting FPF was 42.94 $\pm$ 15.21% [Chapter 6].

Mannitol and lactose are popular carriers to be used in DPI formulation. In many cases, researchers have made attempts to engineer these carriers individually. The author of this thesis believes that crystallization of these two carriers with different ratios simultaneously might create a carrier with optimum properties suitable for DPI formulations as a carrier. With this in mind, the aim of this study was to engineer a crystal using different mannitol-lactose ratios and observe the impact it had on aersolization performance and the efficacy of the physicochemical properties of the DPI formulation for the delivery of salbutamol sulphate.

### *7.2 Materials and Methodology*

**§ 7.2.1- § 7.2.14**

Refer to Chapter 2 sections *2.2 and 2.4-2.16.*

### *7.3 Results and Discussion*

**§7.3.1 Particle size analysis**

Dispersion of inhaled particles is dependent on the aerodynamic stress and particle aggregate strength associated to the particulates. In addition, other interdependent factors such as particle morphology, size, density are also at play.[333-337] Figure 7.1 presents the particle size distribution (PSD) diagrams of the engineered carriers (1:1 [Mannitol:Lactose], 1:2 [Mannitol:Lactose]. 1:3 [Mannitol:Lactose], 2:1 [Mannitol:Lactose], and 3:1 [Mannitol:Lactose]) when using the Rodos and Cuvette systems of analysis. Figure 7.1A focusses on the Rodos system which shows the carriers' true particle size, and Figure 7.1B focusses on the Cuvette system which shows the carrier's size in a liquid. Comparing these two figures, it can be concluded that some degree of agglomeration occurred between the particles in the wet system. This occurrence has to do with the fact that for mixtures containing fine and coarse particles, fine particles tend to charge negatively, whereas large particles tend to charge positively regardless of whether the net-charge is positive or negative;[338-341] in other words, it has to do with electrostatic charge. This accounts for the discrepancies in size between the two systems. In addition, the wet system might have not generated enough force to de-aggregate the particles, whereas in dry system a pressure of 3 bars wa sufficient enough to de-aggregate the particles to their original size.

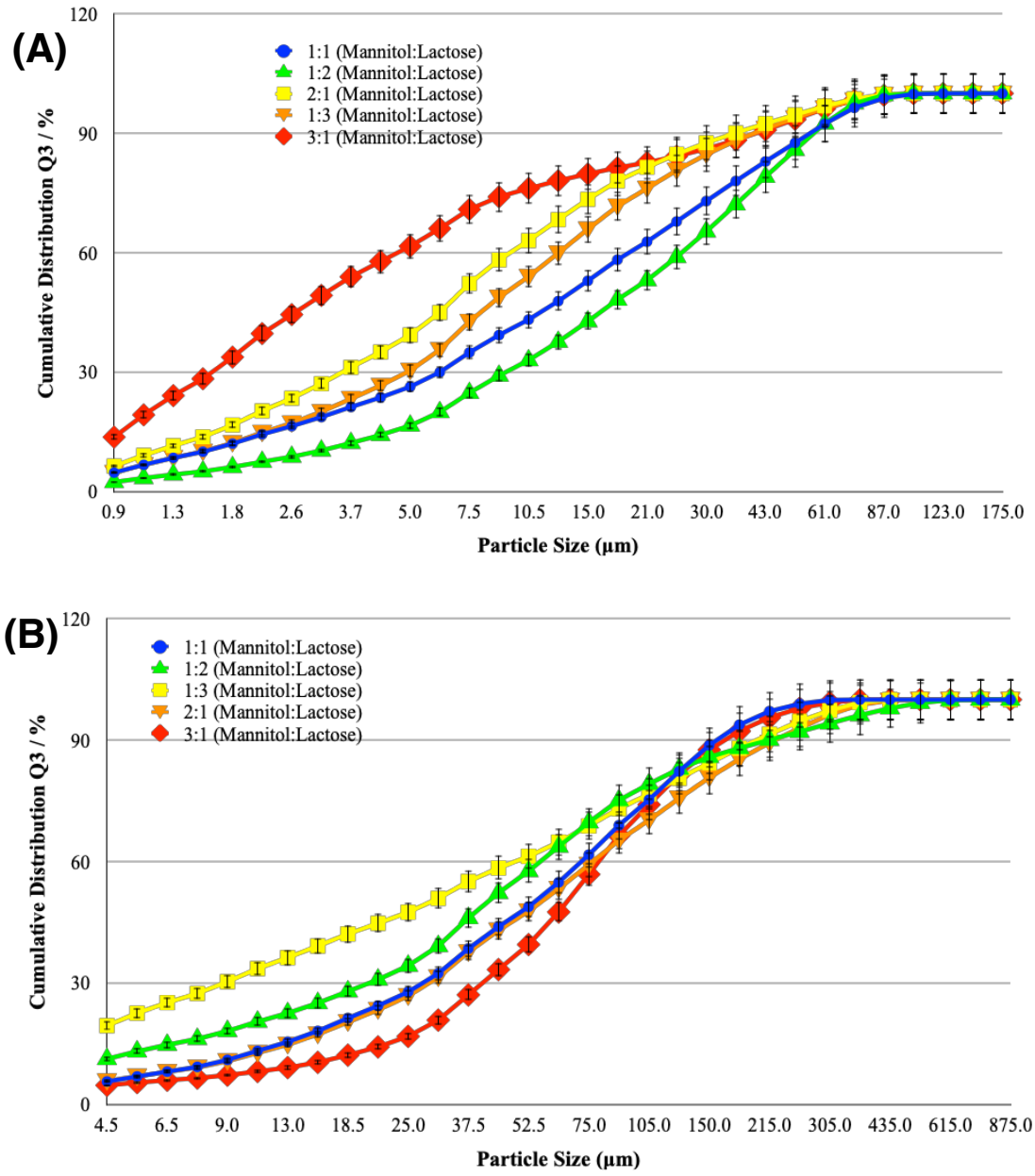


**Figure 7.1**. Particle Size Distribution. Particle Size Distribution (PSD) diagrams of carriers (1:1 [Mannitol:Lactose], 1:2 [Mannitol:Lactose]. 1:3 [Mannitol:Lactose], 2:1 [Mannitol:Lactose], and 3:1 [Mannitol:Lactose]) when using the (A) Rodos dry system and when using the (B) Cuvette wet system.

Taking a closer look at the particle size for each system, Table 7.1 provides the volume mean diameter (VMD) and the particle span for the carriers. Carriers experienced differences in their VMDs ranging from 11.45 ± 1.57µm for the 3:1 (Mannitol:Lactose) carrier to 25.20 ± 0.38µm for the 1:2 (Mannitol:Lactose) carrier and 67.82 ± 3.76µm for the 1:3 (Mannitol:Lactose) carrier to 88.21 ± 1.28µm for the 2:1 (Mannitol:Lactose) carrier, in the Rodos and Cuvette systems respectively. It becomes important to mention that large particles have been shown to manifest higher surface roughness[225, 342, 343], more likely to exhibit surface impurities[344], greater shape irregularities (i.e. cracks and dislocations)[345], decreased disorder in crystal lattice[225, 342, 346], and lower moisture uptake[347], when compared to smaller particles. Moreover, particle span also showed differences between the two systems with particles falling between 2.85 ± 0.07 for the 1:2 (Mannitol:Lactose) carrier to 11.87 ± 0.22 for the 3:1 (Mannitol:Lactose) carrier to 2.28 ± 0.03 for the 3:1 (Mannitol:Lactose) carrier to 7.22 ± 0.48 for the 1:3 (Mannitol:Lactose) carrier in the Rodos and Cuvette systems, respectively. Furthermore, the Rodos system experienced a particle diameter range of 1.51 ± 0.79µm ($D_{10\%}$) to 42.95 ± 10.17µm ($D_{90\%}$) where the particle diameter range for the Cuvette system fell between 7.14 ± 4.42µm ($D_{10\%}$) and 180.01 ± 33.46µm ($D_{90\%}$).

It becomes important to note that electrostatic forces become more significant and may even dominate over other particulate forces, including van der Waals forces, when the particle size is decreased in low environmental humidities; therefore, powder charge is inversely related to particle mean diameter.[128, 294, 295] In addition, it has been suggested that the energy required to transfer an electron between two insulating solid particles is highly dependent on particle size.[348, 349] It has been reported that the amount of net-charge accumulated on mannitol increases with the fine particle fraction of small mannitol while it has also been shown that the net-charge of

lactose increases with decreasing particle size.[350-354] Moreover, during the mixing of a cohesive powder, it is the coarser particles which act like a nuclei where they are subsequently coated with a thin layer of fine particles which could be the case in our study (see Figure 7.1 and Table 7.1).[355] In the event that fine particles are in excess, it becomes true that one of the finer particulates will act as the nuclei thereby facilitating the catalysis of agglomeration.

**Table 7.1**. Particle Analysis. Particle Analysis of 1:1 [Mannitol:Lactose], 1:2 [Mannitol:Lactose], 1:3 [Mannitol:Lactose], 2:1 [Mannitol:Lactose], and 3:1 [Mannitol:Lactose] showing the volume mean diameter (VMD) and span when using the Rodos dry system and the Cuvette wet system.

| Carrier | VMD (µm) Dry System | VMD (µm) Wet System | Span Dry System | Span Wet System |
|---|---|---|---|---|
| **1:1 (Mannitol:Lactose)** | 21.72 ± 0.80 | 70.76 ± 1.14 | 4.00 ± 0.10 | 2.76 ± 0.04 |
| **1:2 (Mannitol:Lactose)** | 25.20 ± 0.38 | 79.76 ± 4.25 | 2.85 ± 0.07 | 5.01 ± 0.50 |
| **1:3 (Mannitol:Lactose)** | 15.72 ± 0.42 | 67.82 ± 3.76 | 4.15 ± 0.18 | 7.22 ± 0.48 |
| **2:1 (Mannitol:Lactose)** | 13.32 ± 0.76 | 88.21 ± 1.28 | 4.84 ± 0.23 | 3.77 ± 0.02 |
| **3:1 (Mannitol:Lactose)** | 11.45 ± 1.57 | 80.21 ± 1.54 | 11.87 ± 0.22 | 2.28 ± 0.03 |

Figure 7.2 presents the electron micrograms of all the carriers where it was determined that the 1:1 [Mannitol:Lactose] carrier and the 3:1 [Mannitol:Lactose] carrier exhibited needle-like crystal structures whereas the 1:2 [Mannitol:Lactose], 1:3 [Mannitol:Lactose], and 2:1 [Mannitol:Lactose] carriers exhibited rhombic crystal structures. These results indicate that the 1:1 [Mannitol:Lactose] carrier and the 3:1 [Mannitol:Lactose] carrier would perform better than the 1:2 [Mannitol:Lactose], 1:3 [Mannitol:Lactose], and 2:1 [Mannitol:Lactose] carriers due to the results found by Kaialy *et. al* [313] where it was argued that needle-like crystal structures aerosolize more

effectively over rhombic and spherical crystal structures. In addition, it is important to nderstand that most pharmaceutical solid particles are diverged from the spherical shape and that a particle's shape has a significant effect on that particle's net charge.[356 357]

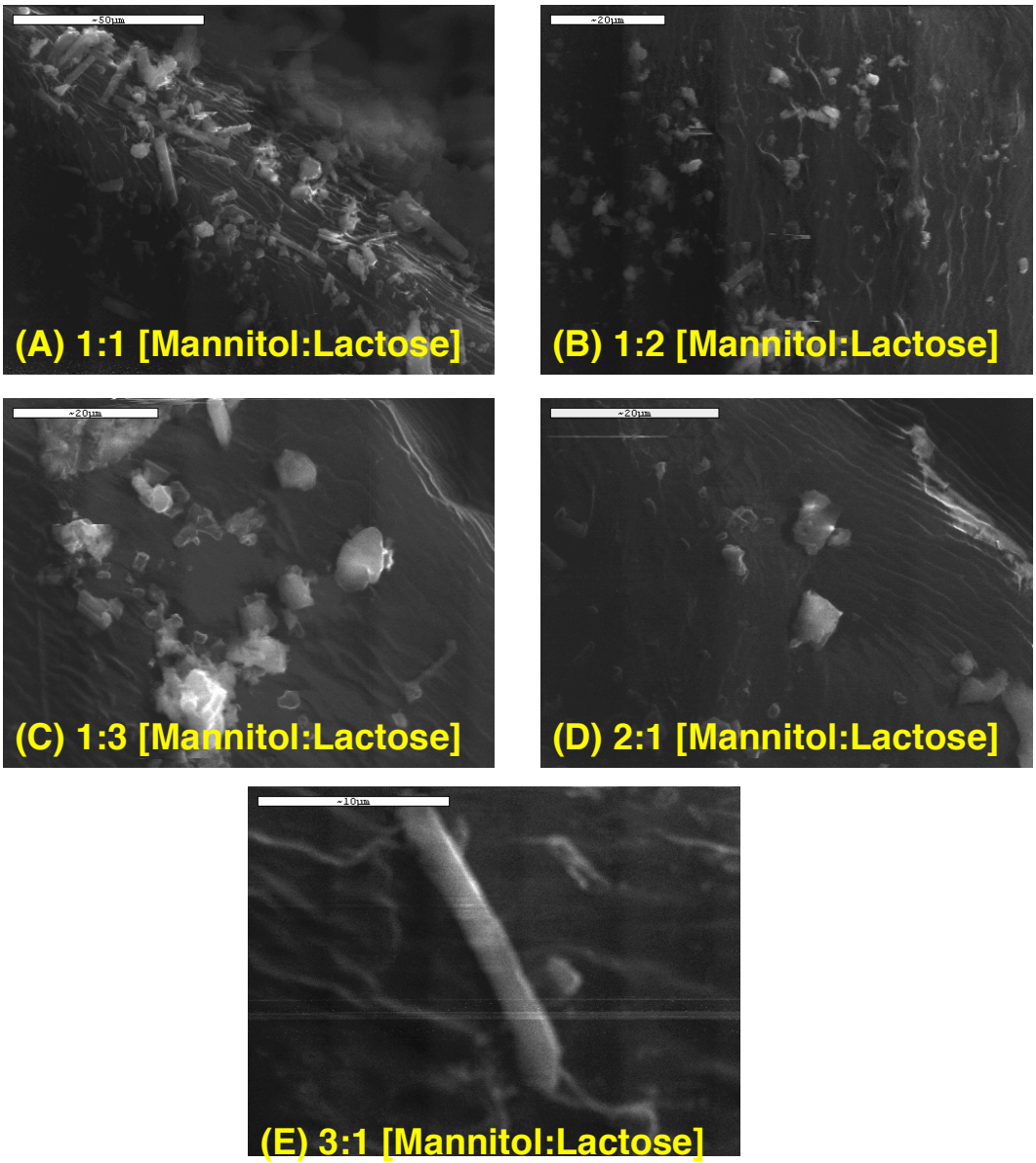


**Figure 7.2**. Scanning Electron Microscopy. SEM micrograms of (A) 1:1 [Mannitol:Lactose], (B) 1:2 [Mannitol:Lactose], (C) 1:3 [Mannitol:Lactose], (D) 2:1 [Mannitol:Lactose], and (E) 3:1 [Mannitol:Lactose] carrier.

### § 7.3.2 Solid-state Characterization of Engineered Carriers

Polymorphism provides the ability of a particle to exist in more than one isomer; about one-third of all drugs exhibit some form of polymorphism.[231] Polymorphism is an obstacle in the pharmaceutical industry because different polymorphs display different physical properties making it important to isolate different polymorphs in a batch.[331] Crystal formation has been shown to improve physicochemical properties (i.e. solubility, dissolution, and stability) as well as the mechanical properties and bioavailability of the crystal.[358-360] With this in mind, Figure 7.3 presents the chromatographs of the engineered crystal carriers (1:1 [Mannitol:Lactose], 1:2 [Mannitol:Lactose]. 1:3 [Mannitol:Lactose], 2:1 [Mannitol:Lactose], and 3:1 [Mannitol:Lactose]) indicating the location of any thermal event taking place; whereas Table 7.2 summarizes the enthalpy of the reaction ($\Delta H_{rxn}$) for each individual carrier's thermal event with the corresponding temperature, in °C, where such event took place.

Moreover, a particle's surface area is considered a measure of surface geometry whereas surface free energy represents the amount of energy needed to separate particles from surfaces.[361] In general, particles that exhibit smaller size distributions and more surface irregularities have higher surface areas[362] whereas powders with higher specific surface areas tend to show higher moisture uptake[347] and higher surface free energies[363]. Consequently, particle surface roughness affects the overall charge-transfer because it affects the inter-particulate and particle-surface contact areas.[364] Looking at the results obtained from SEM and particle size analysis, it was determined that the above is true for this study.

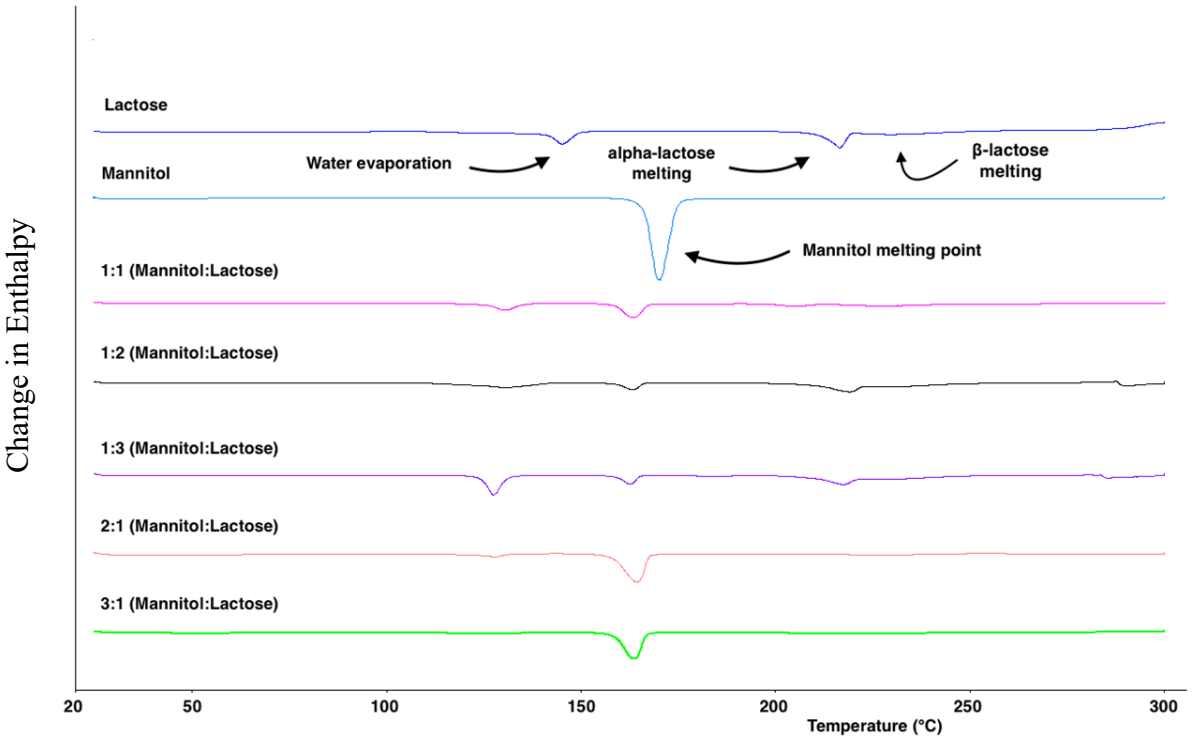


**Figure 7.3.** Differential Scanning Calorimetry. DSC thermal peaks of 1:1 [Mannitol:Lactose], 1:2 [Mannitol:Lactose]. 1:3 [Mannitol:Lactose], 2:1 [Mannitol:Lactose], and 3:1 [Mannitol:Lactose]; where an exothermic peak points up and an endothermic peak points down.

Data presented in Table 7.2 authenticates the illustrated data presented in Figure 7.3 where it shows lactose having an endothermic event at 145.16 ± 0.00°C, which corresponds to the evaporation of water, and another endothermic event at both 216.56 ± 0.11°C and 231.41 ± 0.94°C, which are indicative of $\alpha$-lactose and β-lactose, respectively. Moisture uptake is directly related to relative humidity (an external factor) as well as the chemical (i.e. hydrophilicity and hydrophobicity) and physical (i.e. powder specific surface area and particle anomeric composition) properties.[347] In the context of aerosolization performance, it has been suggested

that in an optimal relative humidity there is a balance between electrostatic and capillary forces leading to minimal cohesive forces and, thus, an improved DPI dispersion behavior.[365]

**Table 7.2**. DSC Thermal Traces. DSC thermal traces of Commercial Lactose, Commercial Mannitol, 1:1 [Mannitol:Lactose], 1:2 [Mannitol:Lactose], 1:3 [Mannitol:Lactose], 2:1 [Mannitol:Lactose], and 3:1 [Mannitol:Lactose] indicating the enthalpy ($\Delta H_{rxn}$), in J/g, along with the Temperature (°C) of where such event took place.

| Formulation | Temperature (°C) | $\Delta H_{rxn}$ (J/g) | Temperature (°C) | $\Delta H_{rxn}$ (J/g) | Temperature (°C) | $\Delta H_{rxn}$ (J/g) | Temperature (°C) | $\Delta H_{rxn}$ (J/g) |
|---|---|---|---|---|---|---|---|---|
| **Commercial Lactose** | 145.16 ± 0.00 | 102.52 ± 3.96 | — | — | 216.56 ± 0.11 | 85.17 ± 1.29 | 231.41 ± 0.94 | 39.72 ± 2.63 |
| **Commercial Mannitol** | — | — | 168.91 ± 0.66 | 186.64 ± 19.55 | — | — | — | — |
| **1:1 (Mannitol:Lactose)** | 130.46 ± 0.12 | 49.48 ± 9.32 | 163.29 ± 0.16 | 73.77 ± 17.04 | 204.66 ± 0.25 | 14.02 ± 4.35 | 228.20 ± 0.06 | 22.49 ± 6.39 |
| **1:2 (Mannitol:Lactose)** | 131.13 ± 0.71 | 77.79 ± 21.67 | 163.42 ± 0.29 | 29.70 ± 7.86 | 219.60 ± 0.69 | 40.62 ± 11.64 | 232.65 ± 0.12 | 11.04 ± 1.89 |
| **1:3 (Mannitol:Lactose)** | 127.66 ± 0.19 | 82.07 ± 13.15 | 162.61 ± 0.11 | 33.68 ± 4.17 | 217.07 ± 0.40 | 39.36 ± 5.42 | 230.36 ± 0.06 | 11.18 ± 1.58 |
| **2:1 (Mannitol:Lactose)** | 128.33 ± 0.60 | 13.42 ± 2.14 | 164.37 ± 0.00 | 171.51 ± 7.67 | — | — | 228.84 ± 1.31 | 11.65 ± 0.77 |
| **3:1 (Mannitol:Lactose)** | 129.99 ± 0.58 | 19.83 ± 4.95 | 163.96 ± 0.00 | 142.98 ± 2.54 | — | — | 229.12 ± 0.42 | 11.38 ± 1.97 |

Furthermore, because of the absence of any thermal event taking place at 177°C, it was concluded that none of the carriers were in the amorphous state as this is the corresponding place it is found in.[237] On the other hand, mannitol experienced one endothermic event at 168.91 ± 0.66°C which corresponds to the melting of mannitol.[237, 283] Determining mannitol's polymorphic state, however, required further analysis (i.e. the implementation of PXRD) given that DSC, alone, cannot distinguish mannitol's polymorphs.

Nevertheless, 1:1 [Mannitol:Lactose], 1:2 [Mannitol:Lactose], and 1:3 [Mannitol:Lactose] where characterized as having both α- and β-lactose polymorphs along with the exhibition of the mannitol thermal event and 2:1 [Mannitol:Lactose] and 3:1 [Mannitol:Lactose] were characterized as having the mannitol thermal event along with being composed of only the β-lactose polymorph, as the α-lactose polymorph peak was found to be missing (see Figure 7.3 and Table 7.2).

Figure 7.4 depicts the powder X-ray diffraction (PXRD) patterns for all of the engineered carriers providing insight into their crystalline state as well as differentiating between their polymorphic forms. It is known that lactose has two polymorphs (α- and β-), which are distinguishable via thermodynamic analysis, and mannitol is known to have three possible polymorphic forms (α-, β-, and Δ-), which are known to have specific diffraction patterns when using PXRD; α-mannitol is known to have peaks at 9.57° and 13.79° on the 2θ plane, β-mannitol is known to exhibit peaks at 10.56° and 14.71° on the 2θ plane, and Δ-mannitol is known to possess peaks at 9.74° on the 2θ plane. [274, 275, 334] With that said, 1:1 [Mannitol:Lactose] was composed of the α- and β-mannitol, 1:2 [Mannitol:Lactose] was composed of all three mannitol polymorphs (α-, β-, and Δ-), 1:3

[Mannitol:Lactose] was composed of α- and Δ-mannitol, 2:1 [Mannitol:Lactose] was composed of α- and β-mannitol, and 3:1 [Mannitol:Lactose] was composed of α- and β-mannitol. In addition, the peaks demonstrated sharp diffraction angles with no halo background, therefore they were classified as crystalline.

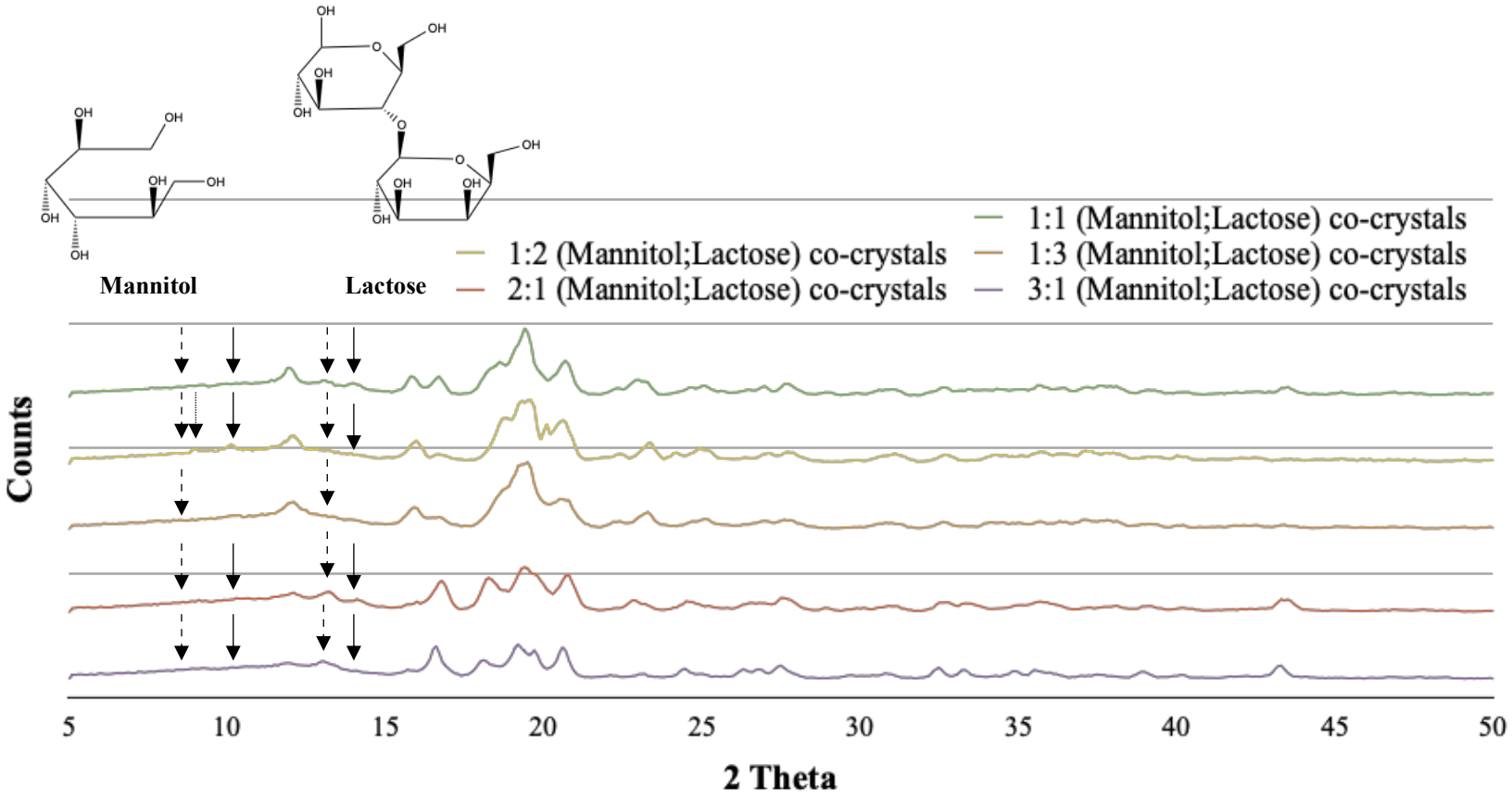


**Figure 7.4.** X-Ray Diffraction. Powder X-Ray diffraction patterns of the 1:1 [Mannitol:Lactose], 1:2 [Mannitol:Lactose]. 1:3 [Mannitol:Lactose], 2:1 [Mannitol:Lactose], and 3:1 [Mannitol:Lactose] carriers.

To further assess and characterize the engineered carriers, FT-IR spectra can be seen in Figure 7.5 where α-Lactose exhibits a distinct peak at 920 $cm^{-1}$ and β-lactose at 950 $cm^{-1}$ whereas

α-mannitol exhibits a distinct peak at 1195 $cm^{-1}$, β-mannitol at 929 $cm^{-1}$, 959 $cm^{-1}$, and 1209 $cm^{-1}$, and Δ-mannitol at 967 $cm^{-1}$.[227, 237, 296] FT-IR spectra confirmed the classifications already mentioned (see Figure 7.4) for the carriers; furthermore, Table 7.3 summarizes the results of the different polymorphic forms for each carrier contained.

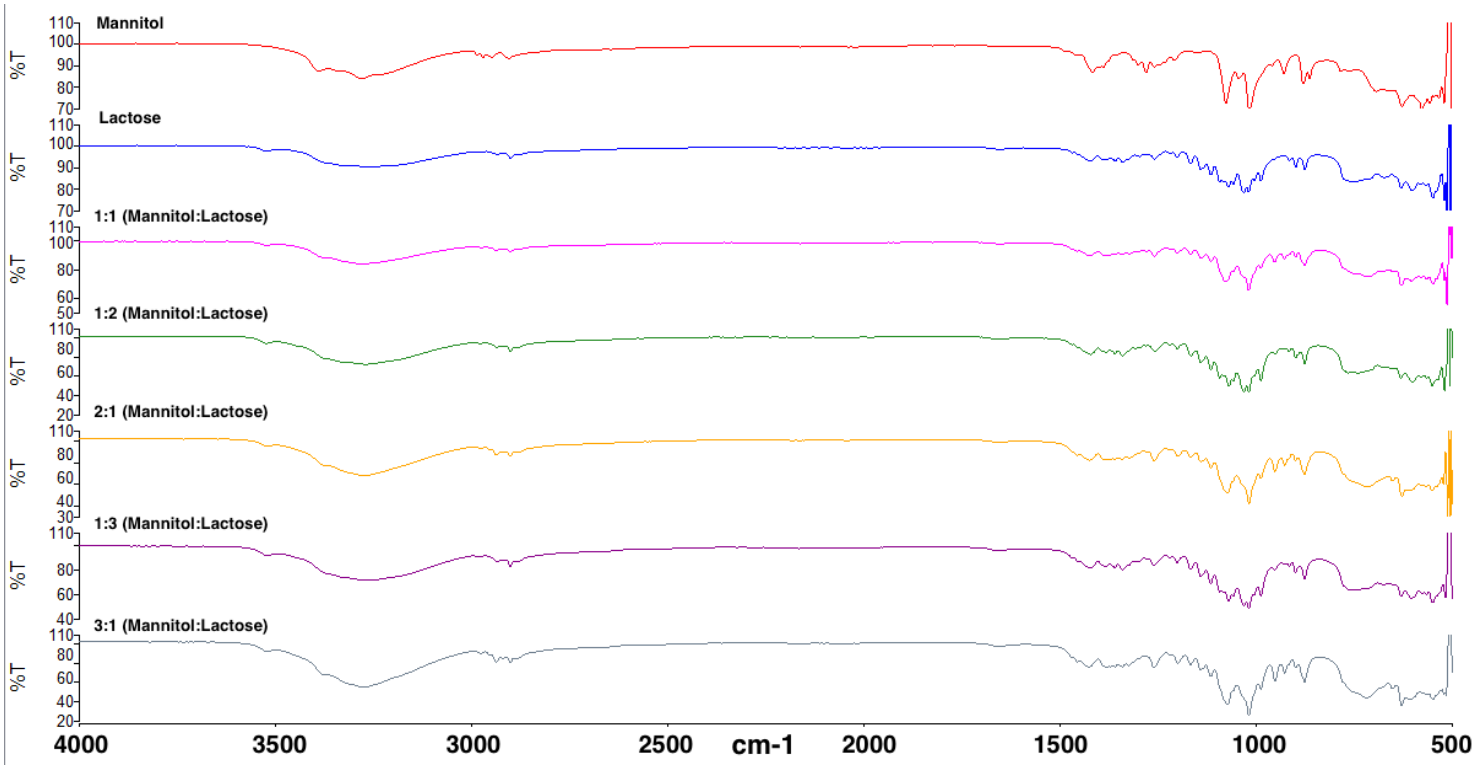


**Figure 7.5.** FT-IR. FT-IR spectra of commercial mannitol, commercial lactose, and the 1:1 [Mannitol:Lactose], 1:2 [Mannitol:Lactose]. 1:3 [Mannitol:Lactose], 2:1 [Mannitol:Lactose], and 3:1 [Mannitol:Lactose] carriers.

**Table 7.3**. Summary of Polymorphic Form. Summary of the different polymorphic forms each carrier contains.

| Carrier | α-lactose | β-lactose | α-manntol | β-mannitol | Δ-mannitol |
|---|---|---|---|---|---|
| 1:1 (Mannitol:Lactose) | ✓ | ✓ | ✓ | ✓ | — |
| 1:2 (Mannitol:Lactose) | ✓ | ✓ | ✓ | ✓ | ✓ |
| 1:3 (Mannitol:Lactose) | ✓ | ✓ | ✓ | — | ✓ |
| 2:1 (Mannitol:Lactose) | — | ✓ | ✓ | ✓ | — |
| 3:1 (Mannitol:Lactose) | — | ✓ | ✓ | ✓ | — |

### § 7.3.3 Powder Flow Characterization

Bulk density ($D_b$), tap density ($D_t$), Carr's Index (CI), and angle of repose ($\delta$) for each of the carriers is listed in Table 7.4. Comparing the different carriers, the 1:3 (Mannitol:Lactose) and 3:1 (Mannitol:Lactose) carrier had the lowest $D_b$ (0.28 ± 0.00 g/cm$^3$) and the 1:1 (Mannitol:Lactose) carrier had the highest $D_b$ (0.36 ± 0.00 g/cm$^3$) whereas, for $D_t$, the 3:1 (Mannitol:Lactose) carrier had the lowest (0.29 ± 0.01 g/cm$^3$) and the 1:1 (Mannitol:Lactose) carrier had the highest (0.49 ± 0.02 g/cm$^3$). Such results are attributed the solid state characteristics already discussed in the previous section. Regarding the CI and angle of repose, the 2:1 (Mannitol:Lactose) and 3:1 (Mannitol:Lactose) carriers showed the best flow characteristics, which is needed to achieve satisfactory DPI formulation metering, fluidization, and dispersion.[366]

**Table 7.4**. Powder Flow Characteristics. Bulk density ($D_b$), tap density ($D_t$), Carr's Index (CI), and angle of repose ($\delta$) for each of the carriers: 1:1 [Mannitol:Lactose], 1:2 [Mannitol:Lactose]. 1:3 [Mannitol:Lactose], 2:1 [Mannitol:Lactose], and 3:1 [Mannitol:Lactose].

| Carrier | $D_b$ (g/cm$^3$) | $D_t$ (g/cm$^3$) | CI (%) | Angle of repose (°) |
|---|---|---|---|---|
| **1:1 (Mannitol:Lactose)** | 0.36 ± 0.00 | 0.49 ± 0.02 | 48.67 ± 5.77 | 46.21 ± 0.00 |
| **1:2 (Mannitol:Lactose)** | 0.32 ± 0.00 | 0.43 ± 0.01 | 33.33 ± 4.04 | 29.13 ± 0.00 |
| **1:3 (Mannitol:Lactose)** | 0.28 ± 0.02 | 0.38 ± 0.00 | 41.00 ± 8.66 | 35.83 ± 0.00 |
| **2:1 (Mannitol:Lactose)** | 0.30 ± 0.01 | 0.32 ± 0.01 | 6.33 ± 3.51 | 29.13 ± 0.00 |
| **3:1 (Mannitol:Lactose)** | 0.28 ± 0.00 | 0.29 ± 0.01 | 5.00 ± 1.73 | 30.14 ± 0.00 |

### § 7.3.4 *In vitro* analysis of DPI formulations

#### §§ 7.3.4.1 Salbutamol sulphate assessment

Aerosolization performance of all of the formulations is summarized in Figure 7.6 where the amount of salbutamol sulphate deposited into each of the stages of the Multi-Stage Liquid Impinger (MSLI) is shown [capsules (C), inhaler (I), mouthpiece (M), induction port (IP), Stage 1, Stage 2, Stage 3, Stage 4, and Stage 5]. As can be seen in the figure, 1:2 (Mannitol:Lactose) obtained the lowest amount of salbutamol sulphate in the capsules with 2.03 ± 1.02 µg while 3:1 (Mannitol:Lactose) obtained the highest amount with 7.69 ± 7.23 µg. When it came to the inhaler device, however, 3:1 (Mannitol:Lactose) exhibited the highest amount with 28.54 ± 6.71µg and 1:3 (Mannitol:Lactose) with the least amount with 3.95 ± 1.50 µg.

In addition, the 1:2 (Mannitol:Lactose) carrier obtained the lowest amount of salbutamol sulphate (SS), in both, the mouthpiece (M) and induction port (IP) with 10.58 ± 6.42µg and 16.92 ± 6.30µg, respectively. In contrast, the 2:1 (Mannitol:Lactose) carrier obtained the highest amount of SS, in both, the M and IP with 18.05 ± 9.83µg and 35.42 ± 13.83µg, respectively. When it came to stages 1-5, the following occurred: the highest amount of SS for Stage 1 went to the 3:1 (Mannitol:Lactose) carrier with 116.79 ± 18.30µg, for Stage 2 the 1:3 (Mannitol:Lactose) carrier obtained the highest amount with 109.55 ± 18.62µg, for Stage 3 the 2:1 (Mannitol:Lactose) carrier obtained the highest amount with 233.62 ± 54.94µg, for Stage 4 and Stage 5 the 1:3 (Mannitol:Lactose) carrier obtained the highest amount with 200.22 ± 41.53µg and 80.52 ± 22.39µg, respectively. Therefore, it was determined that the 1:3 (Mannitol:Lactose) carrier was better at delivering salbutamol sulphate to the lower regions of the lung suggesting a high fine particle fraction (FPF) from this carrier.

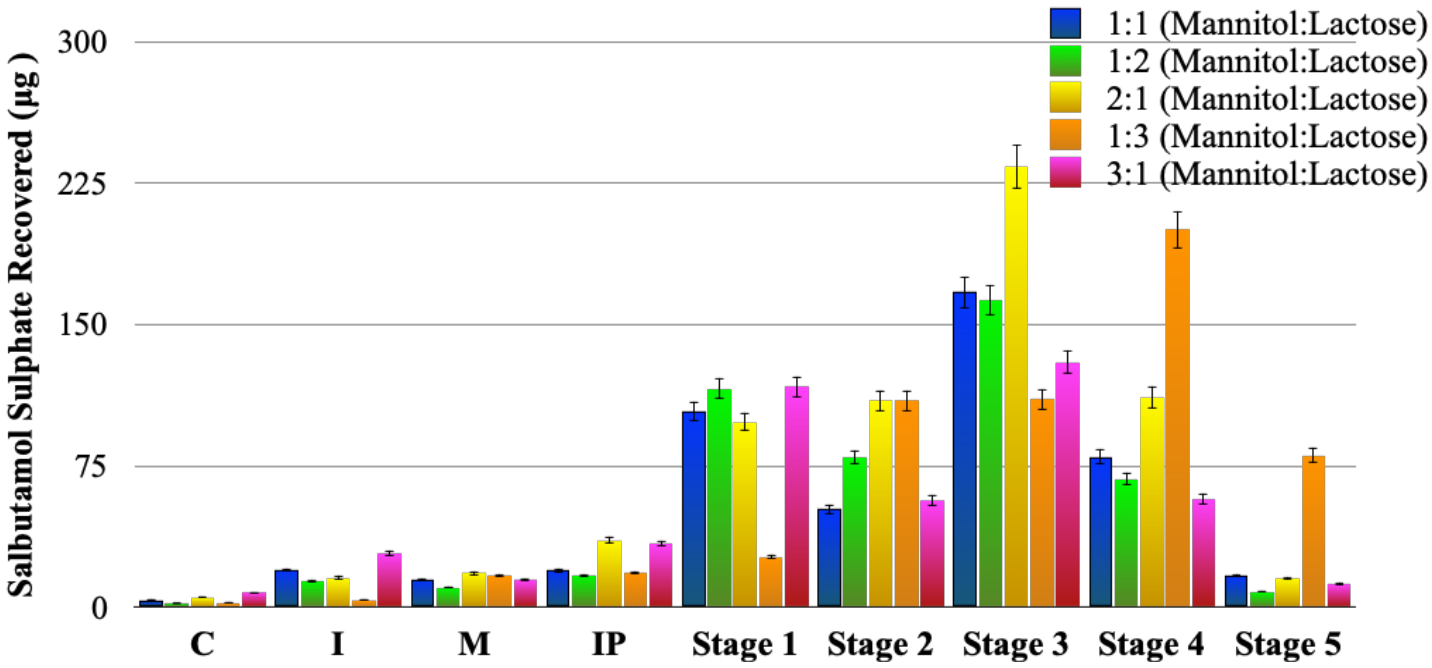


**Figure 7.6**. Aerosolization Profile. Aerosolization performance of each engineered formulation (1:1 [Mannitol:Lactose], 1:2 [Mannitol:Lactose]. 1:3 [Mannitol:Lactose], 2:1 [Mannitol:Lactose], and 3:1 [Mannitol:Lactose]) highlighting the amount of SS recovered (percent recovered) for each and comparing them side-by-side.

Table 7.5 presents the recovered dose (RD), emitted dose (ED), percent recovery, percent emission, percent impact loss, mass median aerodynamic diameter (MMAD), geometric standard deviation (GSD), fine particle dose (FPD), fine particle fraction (FPF), drug loss (DL), dispersibility (DS), and effective inhalation index (EI) for salbutamol sulphate obtained from each of the different engineered formulations (1:1 [Mannitol:Lactose], 1:2 [Mannitol:Lactose], 1:3 [Mannitol:Lactose], 2:1 [Mannitol:Lactose], and 3:1 [Mannitol:Lactose]). With that being said, the 1:1 [Mannitol:Lactose] carrier accounted for having the lowest RD with 474.28 $\pm$ 194.53 µg while the 3:1 [Mannitol:Lactose] carrier obtained the lowest ED, percent recovery, and percent emission with 407.26 $\pm$ 190.92 µg, 93.70 $\pm$ 40.56 %, 89,53 $\pm$ 3.26% respectively; the 2:1 [Mannitol:Lactose]

carrier, however, received the highest RD, ED, and percent recovery with 637.30 $\pm$ 149.78 µg, 603.51 $\pm$ 129.20 µg, and 132.49 $\pm$ 31.14% respectively.

**Table 7.5.** Aerosolization Parameters. Recovered Dose (RD), Emitted Dose (ED), Percent Recovery, Percent Emission, Percent Impact Loss, Mass Median Aerodynamic Diameter (MMAD), Geometric Standard Deviation (GSD), Fine Particle Dose (FPD), Fine Particle Fraction (FPF), Drug Loss (DL), Dispersibility (DS), and Effective Inhalation Index (EI) of salbutamol sulphate obtained from each of the different engineered formulations (1:1 [Mannitol:Lactose], 1:2 [Mannitol:Lactose]. 1:3 [Mannitol:Lactose], 2:1 [Mannitol:Lactose], and 3:1 [Mannitol:Lactose]).

| Formulation | RD (µg) | ED (µg) | Recovery (%) | Emission (%) | Impact Loss (%) | MMAD (µm) | GSD (µm) | FPD | FPF (%) | DL (%) | DS (%) | EI |
|---|---|---|---|---|---|---|---|---|---|---|---|---|
| **1:1 (Mannitol:Lactose)** | 474.28 ± 194.53 | 439.55± 188.18 | 98.60 ± 40.44 | 92.30 ± 2.58 | 30.23 ± 16.13 | 3.22 ± 0.31 | 2.01± 0.03 | 263.61± 147.77 | 52.34± 15.08 | 8.59± 2.80 | 56.74± 16.79 | 12.02± 0.63 |
| **1:2 (Mannitol:Lactose)** | 475.48 ± 134.09 | 451.24± 117.27 | 98.85 ± 27.88 | 95.31 ± 2.62 | 29.30 ± 7.29 | 3.60 ± 0.13 | 1.97± 0.02 | 238.91 ± 89.82 | 49.13± 5.94 | 5.02± 2.69 | 51.64± 7.53 | 12.02± 0.14 |
| **2:1 (Mannitol:Lactose)** | 637.30 ± 149.78 | 603.51± 129.20 | 132.49 ± 31.14 | 94.98 ± 1.82 | 21.33 ± 2.38 | 3.47 ± 0.04 | 1.99± 0.01 | 360.50 ± 88.20 | 56.49± 1.54 | 5.89± 1.63 | 59.50± 2.30 | 12.31± 0.08 |
| **1:3 (Mannitol:Lactose)** | 566.51 ± 100.14 | 545.53± 93.29 | 117.78 ± 20.82 | 96.36 ± 0.59 | 7.82 ± 1.09 | 2.64 ± 0.19 | 2.37± 0.04 | 391.00 ± 89.41 | 68.69± 4.65 | 4.08± 0.57 | 71.29± 4.95 | 12.85± 0.18 |
| **3:1 (Mannitol:Lactose)** | 450.70 ± 195.11 | 407.26± 190.92 | 93.70 ± 40.56 | 89.53 ± 3.26 | 37.39 ± 13.75 | 3.38 ± 0.10 | 2.0± 0.02 | 200.05± 138.32 | 41.18± 11.17 | 12.82± 5.14 | 45.76± 10.75 | 11.42± 0.61 |

In addition, the 1:3 [Mannitol:Lactose] carrier obtained the highest percent emission and lowest impact loss with 96.36 ± 0.59% and 7.82 ± 1.09% meaning that this carrier was the most effective at introducing the most API into the system while also preventing its loss during the process; the 3:1 [Mannitol:Lactose] carrier obtained the highest impact loss with 37.39 ± 13.75% thereby having poor physicochemical properties as the salbutamol sulphate couldn't detach itself from the carrier.

With respect to MMAD and GSD, the 1:2 [Mannitol:Lactose] carrier obtained the highest MMAD with 3.60 ± 0.13 µm while the 1:3 [Mannitol:Lactose] carrier obtained the lowest with 2.64 ± 0.19µm; the highest GSD was attributed to the 1:3 [Mannitol:Lactose] carrier with 2.37 ± 0.04 while the lowest GSD was attributed to the 1:2 [Mannitol:Lactose] carrier with 1.97 ± 0.02. A linear correlation ($r^2$ = 0.87) between EI and GSD was established between all of the carriers. Therefore, given these correlations and those between performance efficacy, particle size (i.e. lower MMAD), and FPF, it was concluded that the 1:3 [Mannitol:Lactose] carrier was the most effective at its delivery of salbutamol sulphate.

Furthermore, the highest FPD received was from the 1:3 [Mannitol:Lactose] carrier with 391.00 ± 89.41µg while the lowest was attained by the 3:1 [Mannitol:Lactose] carrier with 200.05 ± 138.32µg. The 1:3 [Mannitol:Lactose] carrier proved to obtain the highest FPF from all of the engineered carriers with a FPF of 68.69 ± 4.65% with the second highest being the 2:1 [Mannitol:Lactose] carrier with a FPF of 56.49 ± 1.54%. These results justify the results already discussed in Figure 7.6 where the 1:3 [Mannitol:Lactose] carrier deposited the most salbutamol sulphate in Stages 4 and 5. A linear correlation ($r^2$ = 0.98) between FPF and effective inhalation index (EI) was established supporting the notion of the carrier's aerosolized efficacy. With regard to the drug loss, the 1:3 [Mannitol:Lactose] carrier had the lowest percentage with 4.08 ± 0.57%

while the highest drug loss was from the 3:1 [Mannitol:Lactose] carrier with 12.82 ± 5.14%; as the results show, the most effective carrier from this overall study was the 1:3 [Mannitol:Lactose] carrier. In addition, the 1:3 [Mannitol:Lactose] carrier also obtained the highest dispersibility with 71.29 ± 4.95% while the lowest was from the 3:1 [Mannitol:Lactose] carrier with 45.76 ± 10.75%; a linear correlation ($r^2$ = 0.95) was established between EI and the dispersibility of the carriers. Lastly, as was expected, the 1:3 [Mannitol:Lactose] carrier obtained the highest EI with 12.85 ± 0.18 whereas the 3:1 [Mannitol:Lactose] carrier obtained the lowest with 11.42 ± 0.61.

In summary, taking all of the results that have been presented into account, the carrier that showed the best aerosolized performance profile was the 1:3 [Mannitol:Lactose] carrier; a carrier containing optimal physical, chemical, and mechanical properties.

#### §§ 7.3.4.2 Homogeneity Assessment

Because the manufacturing process is considered to be an important specification looked at for regulatory bodies, it comes to no surprise that the blending of API with its carrier provides a critical checkpoint in determining blend homogeneity for a quality product. Therefore, all of the formulations underwent a homogeneity assessment to determine their uniformity and to determine whether they abided to the tightly regulated specifications from the US FDA and the European counterpart. Figure 7.7 presents the homogeneity profiles for all of the formulations within this study showcasing their percent potency; all of the engineered carriers adhered and passed the potency specification, which is set to the range of 75-125%. Table 7.6 shows the percent content homogeneity, which is expressed as the percent coefficient of variation (%CV) for each of the carriers. The 3:1 (Mannitol:Lactose) carrier obtained the smallest %CV with 1.60% whereas the 2:1 (Mannitol:Lactose) carrier received the highest %CV with 12.51% (see Table 7.6) indicting

that the 3:1 (Mannitol:Lactose) carrier had the best content uniformity amongst all the formulations and the 2:1 (Mannitol:Lactose) carrier had the worst.

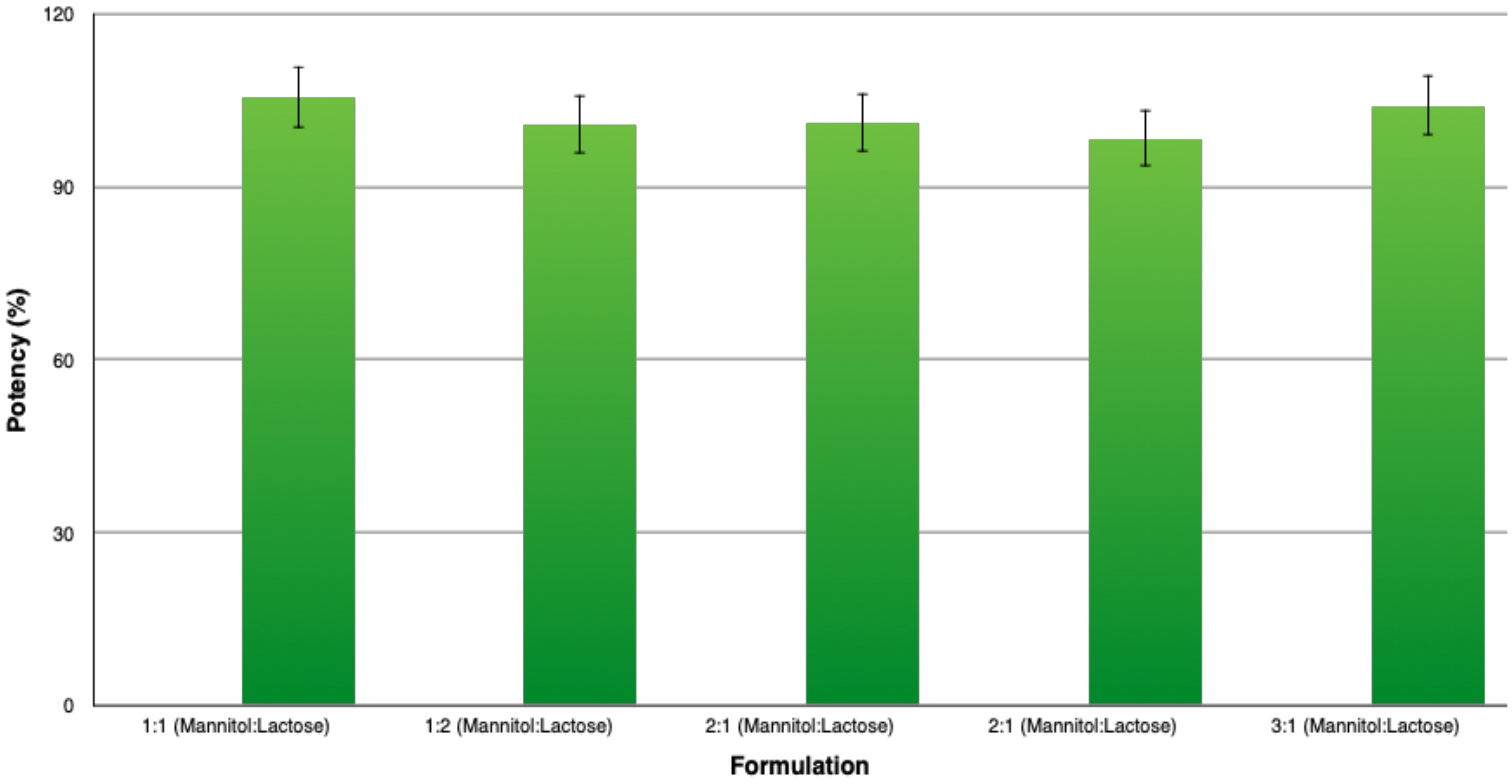


**Figure 7.7.** Potency**.** Percent potency of each engineered formulation (1:1 [Mannitol:Lactose], 1:2 [Mannitol:Lactose]. 1:3 [Mannitol:Lactose], 2:1 [Mannitol:Lactose], and 3:1 [Mannitol:Lactose]) with respect to salbutamol sulphate.

**Table 7.6.** Content Homogeneity. Content homogeneity of 1:1 [Mannitol:Lactose], 1:2 [Mannitol:Lactose]. 1:3 [Mannitol:Lactose], 2:1 [Mannitol:Lactose], and 3:1 [Mannitol:Lactose] expressed as the percent coefficient of variation (%CV).

| Formulation | % CV |
|---|---|
| **1:1 (Mannitol:Lactose)** | 7.39 |
| **1:2 (Mannitol:Lactose)** | 6.27 |
| **2:1 (Mannitol:Lactose)** | 12.51 |
| **1:3 (Mannitol:Lactose)** | 5.88 |
| **3:1 (Mannitol:Lactose)** | 1.60 |

*However, has not been taken into account for *in vivo* inhalation studies.

### *7.4 Conclusion*

The results presented in this chapter have proven that mannitol:lactose crystals with different weight per weight ratios can be successfully crystalized. They have also shown a positive correlation between particle size and concentration of mannitol with regard to the dry system; when the concentration of mannitol increases the particle size decreases. The opposite holds true for the wet system, however; when the concentration of mannitol increases, the particle size of the carriers also increases. The results have also shown that the 1:3 (Mannitol:Lactose) carrier [FPF= 68.69 $\pm$ 4.65%] was the most effective at delivering salbutamol sulphate to the deep regions of the lung. This formulation had crystals classified as rhombic in structure and out-performed the 1:3 [Mannitol:Lactose] carrier from Chapter 5 whose FPF was 61.42 $\pm$ 4.21%.

# Chapter 8

## Aerosolization performance of crystallized Mannitol-Salbutamol Sulphate with different ratios

### *8.1 Introduction*

In this chapter, the focus was to engineer a crystal composed of salbutamol:mannitol in different concentrations and investigate the effect it had on the overall aerosolized DPI performance of salbutamol sulphate. As already discussed in Chapter 7, pulmonary drug delivery has transformed from being a platform for local pulmonary disease treatment to being a means of systematic drug delivery. Particle properties are critical as they affect inhalation efficacy, pulmonary deposition, drug delivery, and overall performance. Moreover, crystal engineering provides an opportunity to optimize particles at the morphological, physicochemical, and molecular levels.[367]

With that said, the aim of this study was to engineer a crystal using different salbutamol-mannitol ratios and observe the impact it had on aersolization performance and the efficacy of the physicochemical properties of the DPI formulation for the delivery of salbutamol sulphate.

## *8.2 Materials and Methodology*

### § 8.2.1- § 8.2.14

Refer to Chapter 2 sections *2.2, 2.4-2.11,* and *2.13-2.17.*

## *8.3 Results and Discussion*

### § 8.3.1 Particle size analysis

The salbutamol-mannitol crystals were originally above the approved 1-5 $\mu$m range (see Table 8.1), therefore they were all subjected to air jet milling to decrease their particle size. Figure 8.1 presents the particle size distribution (PSD) diagram of the engineered air jet milled carriers in this study (1:1 [Salbutamol:Mannitol], 1:2 [Salbutamol:Mannitol]. 1:4 [Salbutamol:Mannitol], 2:1 [Salbutamol:Mannitol], and 4:1 [Salbutamol:Mannitol]) when using the Rodos system of analysis.

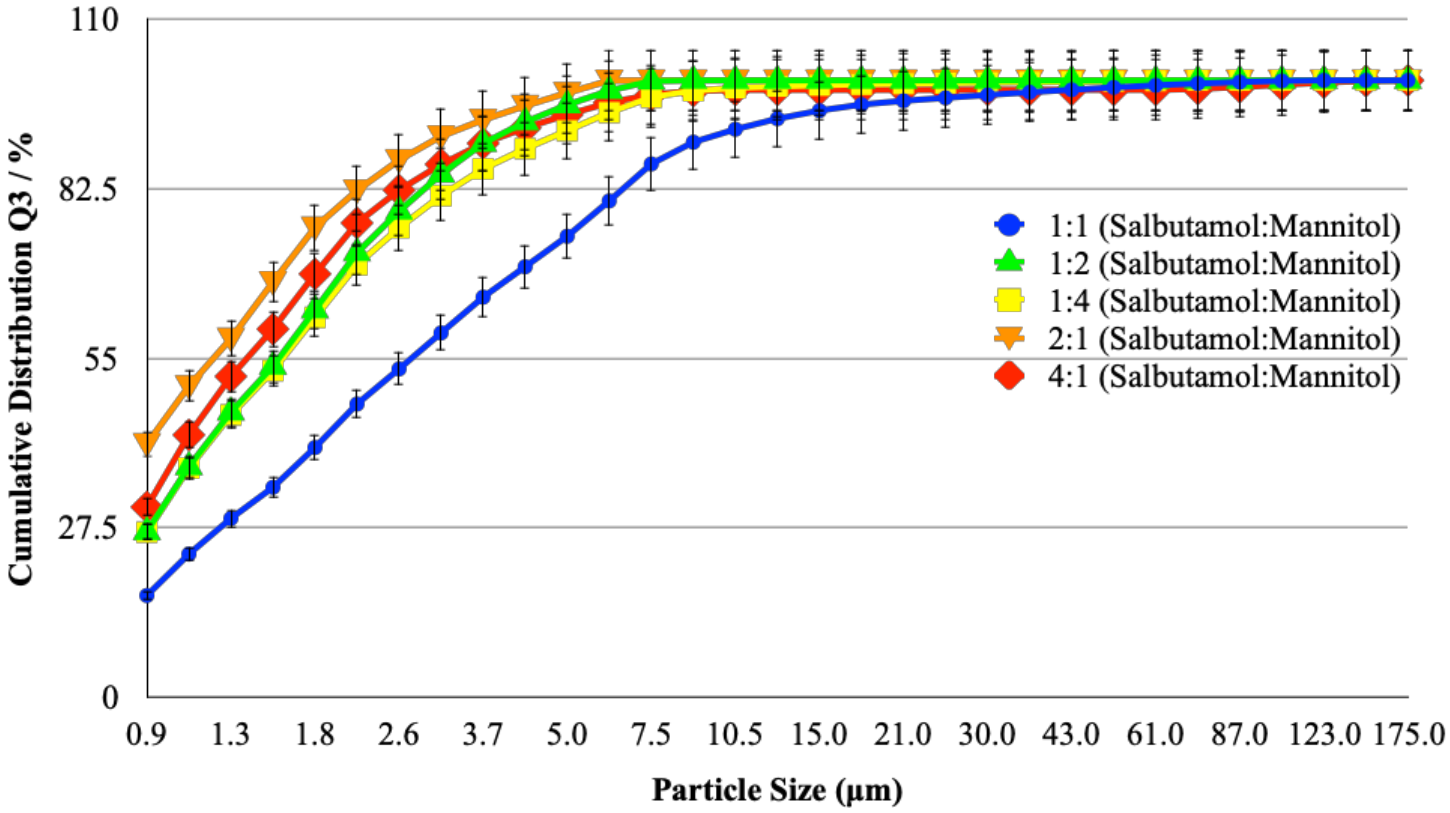


**Figure 8.1**. Particle Size Distribution. Particle Size Distribution (PSD) diagram of engineered air jet milled carriers (1:1 [Salbutamol:Mannitol], 1:2 [Salbutamol:Mannitol]. 1:4 [Salbutamol:Mannitol], 2:1 [Salbutamol:Mannitol], and 4:1 [Salbutamol:Mannitol]) when using the Rodos dry system.

Taking a closer look at the particle size, Table 8.1 provides the volume mean diameter (VMD) before and after air jet milling and the particle span for the engineered air jet milled carriers. Carriers experienced differences in their original VMDs ranging between 9.79 µm for the 4:1 [Salbutamol:Mannitol] carrier to 26.52 µm for the 1:1 [Salbutamol:Mannitol] carrier. After being subjected to air jet milling, the carrier's VMDs ranged between 1.74 $\pm$ 0.12 µm for the 2:1 [Salbutamol:Mannitol] carrier to 4.94 $\pm$ 2.09 µm for the 1:1 [Salbutamol:Mannitol] carrier. These results indicate that there was a successful reduction in particle size coming from the carriers.

Moreover, the particle span of the air jet milled carriers fell between 2.21 ± 0.09 for the 1:2 [Salbutamol:Mannitol] carrier to 3.55 ± 0.68 $\mu$m for the 1:1 [Salbutamol:Mannitol] carrier. Furthermore, the Rodos system experienced a particle diameter range of 0.66 ± 0.05µm ($D_{10\%}$) to 5.11 ± 2.86µm ($D_{90\%}$).

**Table 8.1**. Particle Analysis. Particle Analysis of the 1:1 [Salbutamol:Mannitol], 1:2 [Salbutamol:Mannitol]. 1:4 [Salbutamol:Mannitol], 2:1 [Salbutamol:Mannitol], and 4:1 [Salbutamol:Mannitol] carriers showing the original and air jet milled volume mean diameter (VMD) and span of the air jet milled carriers.

| Carrier | VMD (µm) Original | VMD (µm) Air Jet Milled | Span of Air Jet Milled |
|---|---|---|---|
| **1:1 [Salbutamol:Mannitol]** | 26.52 | 4.94 ± 2.09 | 3.55 ± 0.68 |
| **1:2 [Salbutamol:Mannitol]** | 19.14 | 1.85 ± 0.13 | 2.21 ± 0.09 |
| **1:4 [Salbutamol:Mannitol]** | 16.53 | 2.29 ± 0.61 | 2.81 ± 0.60 |
| **2:1 [Salbutamol:Mannitol]** | 16.39 | 1.74 ± 0.12 | 2.26 ± 0.14 |
| **4:1 [Salbutamol:Mannitol]** | 9.79 | 3.29 ± 2.77 | 2.47 ± 0.32 |

Figure 8.2 presents the electron micrograms of all the carriers after air jet milling where it was determined that all of the engineered carriers (1:1 [Salbutamol:Mannitol], 1:2 [Salbutamol:Mannitol]. 1:4 [Salbutamol:Mannitol], 2:1 [Salbutamol:Mannitol], and 4:1 [Salbutamol:Mannitol]) were rhombic in their crystal structure.

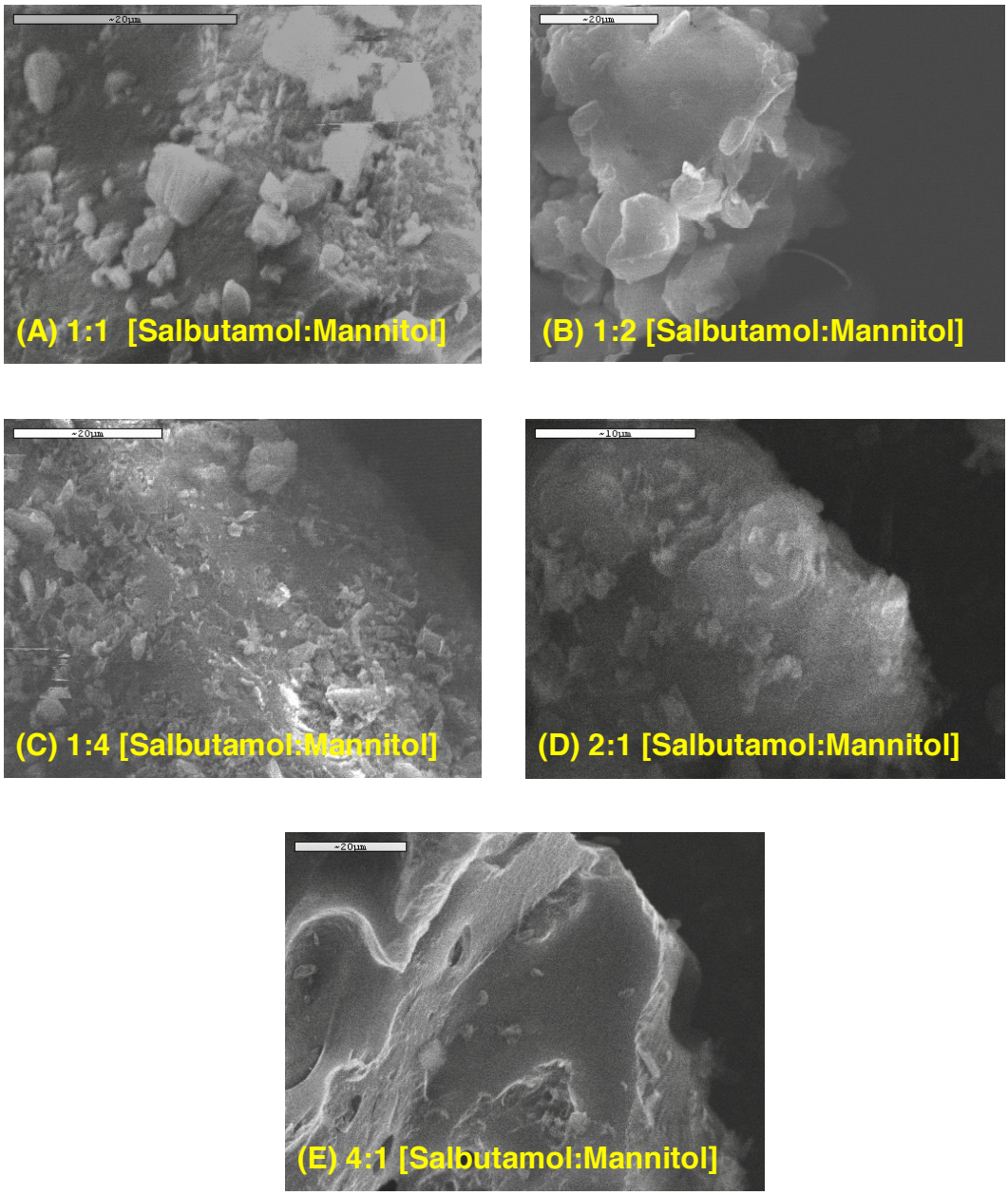


**Figure 8.2**. Scanning Electron Microscopy. SEM micrograms of (A) 1:1 [Salbutamol:Mannitol], (B) 1:2 [Salbutamol:Mannitol], (C) 1:4 [Salbutamol:Mannitol], (D) 2:1 [Salbutamol:Mannitol], and (E) 4:1 [Salbutamol:Mannitol] carrier.

### § 8.3.2 Solid-state Characterization of Engineered Carriers

Figure 8.3 presents the DSC traces of the engineered crystal carriers (1:1 [Salbutamol:Mannitol], 1:2 [Salbutamol:Mannitol]. 1:4 [Salbutamol:Mannitol], 2:1 [Salbutamol:Mannitol], and 4:1 [Salbutamol:Mannitol]) indicating the location of any thermal event taking place; whereas Table 8.2 summarizes the enthalpy (ΔH) for each individual carrier's thermal event with the corresponding temperature, in °C, where such event took place.

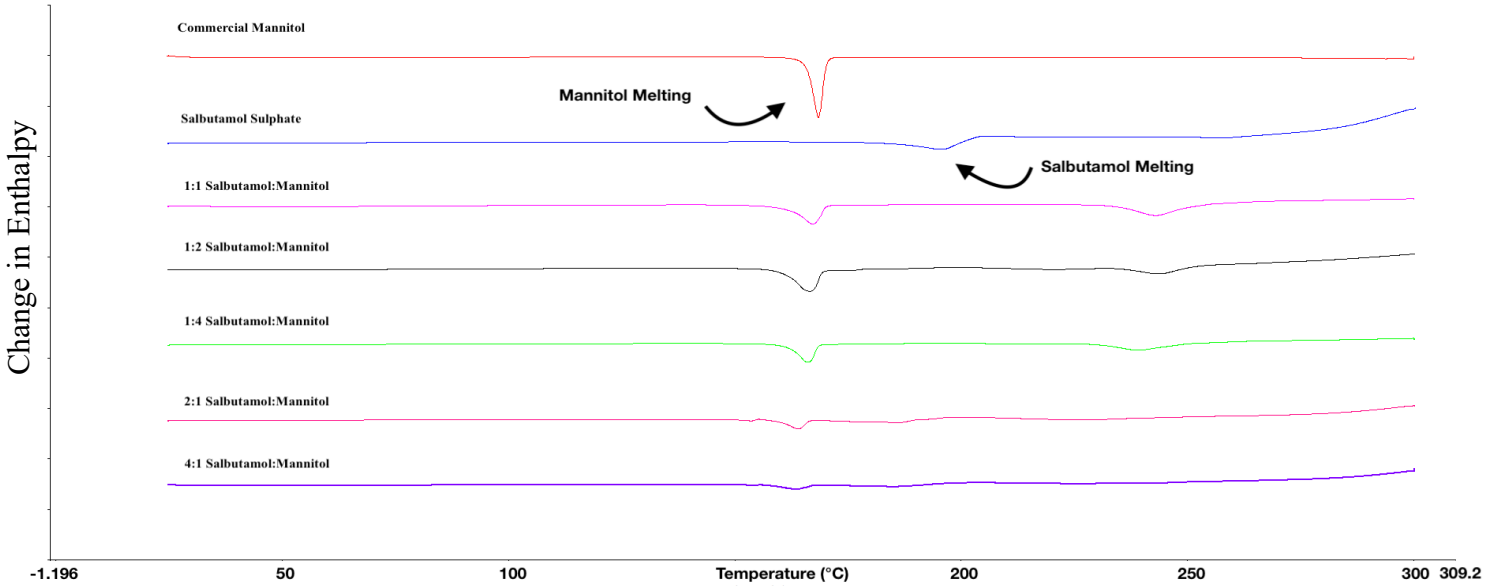


**Figure 8.3.** Differential Scanning Calorimetry. DSC thermal peaks of 1:1 [Salbutamol:Mannitol], 1:2 [Salbutamol:Mannitol]. 1:4 [Salbutamol:Mannitol], 2:1 [Salbutamol:Mannitol], and 4:1 [Salbutamol:Mannitol]; where an exothermic peak points up and an endothermic peak points down.

Data presented in Table 8.2 authenticates the illustrated data presented in Figure 8.3 where it shows all of the carriers, with the exemption of commercial salbutamol, having an endothermic

event at 166.02 ± 2.10°C which corresponds to the melting of mannitol. It also shows that all of the carriers, with the exemption of commercial mannitol, having an endothermic event at 229.79 ± 17.94°C, which corresponds to the melting of salbutamol sulphate. The carriers (1:1 [Salbutamol:Mannitol], 1:2 [Salbutamol:Mannitol]. 1:4 [Salbutamol:Mannitol], 2:1 [Salbutamol:Mannitol], and 4:1 [Salbutamol:Mannitol]) exhibited a dramatic shift ($p < 0.05$) in their salbutamol endothermic temperature going from 196.31 ± 0.71°C to 236.49 ± 8.12°C. The mannitol endothermic shift, however, was not as significant going from 169.27 ± 0.30°C to 165.37 ± 1.53°C ($p > 0.05$).

**Table 8.2**. DSC Thermal Traces. DSC thermal traces of Commercial Mannitol, Commercial Salbutamol, 1:1 [Salbutamol:Mannitol], 1:2 [Salbutamol:Mannitol]. 1:4 [Salbutamol:Mannitol], 2:1 [Salbutamol:Mannitol], and 4:1 [Salbutamol:Mannitol] indicating the enthalpy (ΔH), in J/g, along with the Temperature (°C) of where such event took place.

| Formulation | Temperature (°C) | ΔH (J/g) | Temperature (°C) | ΔH (J/g) |
|---|---|---|---|---|
| **Commercial Mannitol** | 169.27 ± 0.30 | 193.34 ± 16.39 | — | — |
| **Commercial Salbutamol** | — | — | 196.31 ± 0.71 | 141.97 ± 36.15 |
| **1:1 [salb.:mannitol]** | 167.31 ± 0.14 | 120.03 ± 11.53 | 244.54 ± 1.91 | 124.06 ± 19.35 |
| **1:2 [salb.:mannitol]** | 166.16 ± 0.62 | 98.61 ± 30.60 | 241.82 ± 2.83 | 58.57 ± 13.12 |
| **1:4 [salb.:mannitol]** | 165.70 ± 0.48 | 71.30 ± 31.13 | 240.02 ± 1.24 | 86.13 ± 11.55 |
| **2:1 [salb.:mannitol]** | 164.19 ± 0.21 | 45.47 ± 5.14 | 225.28 ± 0.23 | 44.21 ± 3.78 |
| **4:1 [salb.:mannitol]** | 163.51 ± 0.07 | 36.59 ± 14.56 | 230.77 ± 7.06 | 36.01 ± 8.06 |

Figure 8.4 depicts the powder X-ray diffraction (PXRD) patterns for all of the engineered carriers providing insight into their crystalline state as well as differentiating between their polymorphic form. Mannitol is known to have three possible polymorphic forms (α-, β-, and Δ-), which are known to have specific diffraction patterns when using PXRD. α-mannitol is known to have peaks at 9.57° and 13.79° on the 2θ plane, β-mannitol is known to exhibit peaks at 10.56° and 14.71° on the 2θ plane, and Δ-mannitol is known to possess peaks at 9.74° on the 2θ plane.[274, 275] With that said, the 1:1 [Salbutamol:Mannitol] carrier was composed of α- and β-mannitol, the 1:2 [Salbutamol:Mannitol] carrier was composed of all three mannitol polymorphs (α-, β-, and Δ-), the 1:4 [Salbutamol:Mannitol] carrier was composed of α- and β-mannitol, the 2:1 [Salbutamol:Mannitol] carrier was composed of β- and Δ-mannitol, and the 4:1 [Salbutamol:Mannitol] carrier was composed of α- and β-mannitol. In addition, the peaks demonstrated sharp diffraction angles with no halo background, therefore they were classified as crystalline.

To further assess and characterize the engineered carriers, FT-IR spectra can be seen in Figure 8.5 where α-mannitol exhibits a distinct peak at 1195 $cm^{-1}$, β-mannitol at 929 $cm^{-1}$, 959 $cm^{-1}$, and 1209 $cm^{-1}$, and Δ-mannitol at 967 $cm^{-1}$.[237, 296] FT-IR spectra confirmed the classifications already mentioned (see Figure 8.4) for the carriers; furthermore, Table 8.3 summarizes the results of the different polymorphic forms each carrier contained. The broadening in the 3,000-3,500 $cm^{-1}$ region is due to the increase in mannitol concentration.

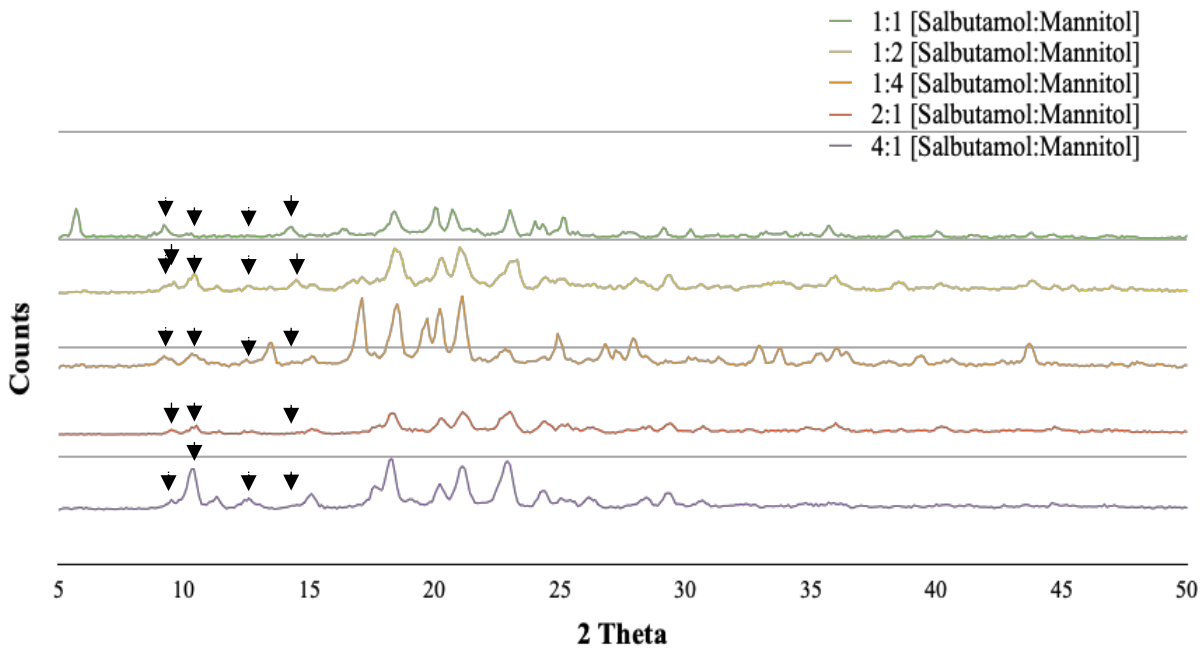


**Figure 8.4.** X-Ray Diffraction. Powder X-Ray diffraction patterns of the 1:1 [Salbutamol:Mannitol], 1:2 [Salbutamol:Mannitol]. 1:4 [Salbutamol:Mannitol], 2:1 [Salbutamol:Mannitol], and 4:1 [Salbutamol:Mannitol] carriers.

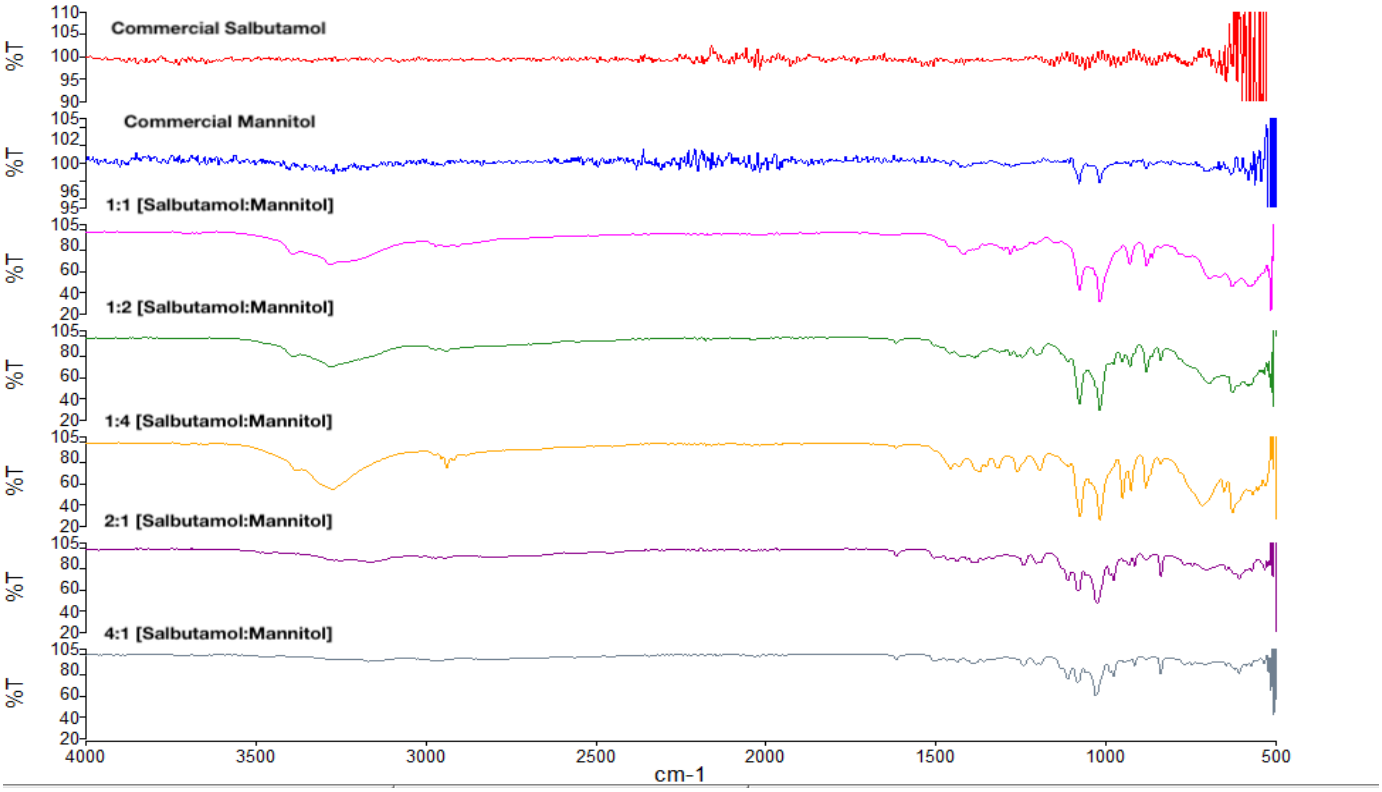


**Figure 8.5**. FT-IR. FT-IR spectra of commercial mannitol, commercial salbutamol, and the 1:1 [Salbutamol:Mannitol], 1:2 [Salbutamol:Mannitol]. 1:4 [Salbutamol:Mannitol], 2:1 [Salbutamol:Mannitol], and 4:1 [Salbutamol:Mannitol] carriers.

**Table 8.3**. Summary of Polymorphic Form. Summary of the different polymorphic forms each carrier contains.

| Carrier | α-manntol | β-mannitol | Δ-mannitol |
|---|---|---|---|
| 1:1 (Salbutamol:Mannitol) | ✓ | ✓ | — |
| 1:2 (Salbutamol:Mannitol) | ✓ | ✓ | ✓ |
| 1:4 (Salbutamol:Mannitol) | ✓ | ✓ | — |
| 2:1 (Salbutamol:Mannitol) | — | ✓ | ✓ |
| 4:1 (Salbutamol:Mannitol) | ✓ | ✓ | — |

### § 8.3.3 *In vitro* analysis of DPI formulations

#### §§ 8.3.3.1 Salbutamol Sulphate Assessment

Aerosolization performance of all of the engineered formulations is summarized in Figure 8.6 where the amount of salbutamol sulphate deposited into each of the stages of the Multi-Stage Liquid Impinger (MSLI) is shown [capsules (C), inhaler (I), mouthpiece (M), induction port (IP), Stage 1, Stage 2, Stage 3, Stage 4, and Stage 5]. As can be seen in the figure, the 1:1 [Salbutamol:Mannitol] carrier obtained the lowest amount of salbutamol sulphate in the capsules with 2.12 $\pm$ 0.11 µg while the 4:1 [Salbutamol:Mannitol] carrier obtained the highest amount with 5.80 $\pm$ 0.72 µg. When it came to the inhaler device, however, the 2:1 [Salbutamol:Mannitol] carrier obtained the highest amount of salbutamol sulphate with 18.89 $\pm$ 3.23 µg while the lowest went to the 1:1 [Salbutamol:Mannitol] carrier with 6.36 $\pm$ 4.09 µg.

Furthermore, the 1:2 [Salbutamol:Mannitol] carrier obtained the lowest amount of salbutamol sulphate (SS), in both, the mouthpiece (M) and induction port (IP) with 6.92 ± 2.56 µg and 20.03

± 8.23 µg, respectively. In contrast, the 2:1 [Salbutamol:Mannitol] carrier obtained the highest amount of SS for the mouthpiece with 13.58 ± 1.46 µg while the 1:4 [Salbutamol:Mannitol] carrier obtained the highest amount in the IP with 27.70 ± 7.61 µg. With regard to Stages 1-5, the 1:4 [Salbutamol:Mannitol] carrier obtained the highest amount for Stage 1 (157.03 ± 19.27µg), the 2:1 [Salbutamol:Mannitol] carrier obtained the highest amount for Stages 2-4 (82.61 ± 45.27, 211.95 ± 49.51, and 109.23 ± 26.55µg; respectively), and the 4:1 [Salbutamol:Mannitol] carrier obtained the highest amount in Stage 5 (24.28 ± 9.28µg). Moreover, the 4:1 [Salbutamol:Mannitol] carrier obtained the lowest amount in Stage 1 (76.82 ± 20.49µg), and the 1:1 [Salbutamol:Mannitol] carrier obtained the lowest amount in Stage 2-5 (35.08 ± 3.84, 34.02 ± 8.30, 9.54 ± 3.33, and 2.12 ± 0.81 µg; respectively). It was, therefore, determined that the 2:1 [Salbutamol:Mannitol] carrier was better at delivering salbutamol sulphate to the lower regions of the lung suggesting a high fine particle fraction (FPF) from this carrier.

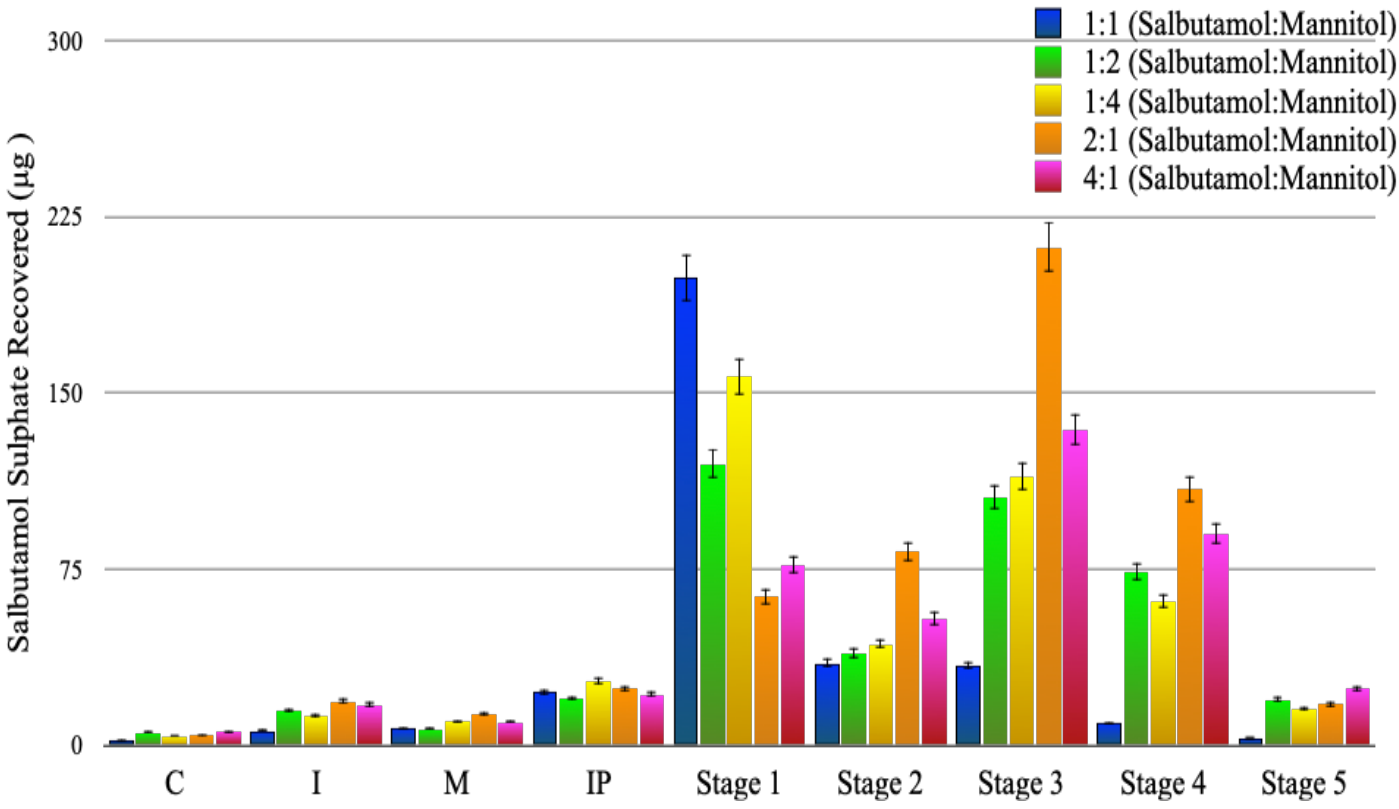


**Figure 8.6**. Aerosolization Profile. Aerosolization performance of each engineered formulation (1:1 [Salbutamol:Mannitol], 1:2 [Salbutamol:Mannitol]. 1:4 [Salbutamol:Mannitol], 2:1 [Salbutamol:Mannitol], and 4:1 [Salbutamol:Mannitol]) highlighting the amount of SS recovered (percent recovered) for each and comparing them side-by-side.

Table 8.4 presents the different parameters that were taken into account in determining the formulation's aerosolization performance. The 1:1 [Salbutamol:Mannitol] carrier obtained the lowest RD, ED, and percent recovery with 317.30 ± 34.31 µg, 303.66 ± 30.33 µg, and 65.97 ± 7.13% respectively while the 2:1 [Salbutamol:Mannitol] carrier obtained the highest RD, ED, and percent recovery with 541.42 ± 83.72 µg, 508.95 ± 85.45 µg, and 112.56 ± 17.41% respectively.

With respect to percent emission, the 1:1 [Salbutamol:Mannitol] carrier obtained the highest percentage with 95.76 ± 1.11% while the 4:1 [Salbutamol:Mannitol] carrier obtained the lowest

percentage with 93.35 ± 3.85%. This suggests that the 1:1 [Salbutamol:Mannitol] carrier emitted the most API than any other formulation. The 1:1 [Salbutamol:Mannitol] carrier, however, did have the highest impact loss with 70.16 ± 2.52% while the 2:1 [Salbutamol:Mannitol] carrier obtained the lowest with 16.41 ± 2.35%.

**Table 8.4.** Aerosolization Parameters. Recovered Dose (RD), Emitted Dose (ED), Percent Recovery, Percent Emission, Percent Impact Loss, Mass Median Aerodynamic Diameter (MMAD), Geometric Standard Deviation (GSD), Fine Particle Dose (FPD), Fine Particle Fraction (FPF), Drug Loss (DL), Dispersibility (DS), and Effective Inhalation Index (EI) of salbutamol sulphate obtained from each of the different engineered formulations (1:1 [Salbutamol:Mannitol], 1:2 [Salbutamol:Mannitol]. 1:4 [Salbutamol:Mannitol], 2:1 [Salbutamol:Mannitol], and 4:1 [Salbutamol:Mannitol]).

| Formulation | RD (µg) | ED (µg) | Recovery (%) | Emission (%) | Impact Loss (%) | MMAD (µm) | GSD (µm) | FPD | FPF (%) | DL (%) | DS (%) | EI |
|---|---|---|---|---|---|---|---|---|---|---|---|---|
| **1:1 (Salbutamol:Mannitol)** | 317.30 ± 34.31 | 303.66 ± 30.33 | 65.97 ± 7.13 | 95.76 ± 1.11 | 70.16 ± 2.52 | 4.09 ± 0.11 | 2.03 ± 0.03 | 46.50 ± 10.63 | 14.52 ± 1.94 | 4.93 ± 0.80 | 15.18 ± 2.11 | 10.50 ± 0.08 |
| **1:2 (Salbutamol:Mannitol)** | 399.70 ± 30.89 | 378.12 ± 32.81 | 83.10 ± 6.42 | 94.55 ± 1.34 | 35.34 ± 6.52 | 3.04 ± 0.16 | 2.08 ± 0.02 | 198.79 ± 35.35 | 49.47 ± 5.23 | 6.86 ± 0.71 | 52.29 ± 5.08 | 12.00 ± 0.26 |
| **1:4 (Salbutamol:Mannitol)** | 442.96 ± 7.24 | 419.72 ± 8.63 | 92.09 ± 1.51 | 94.76 ± 1.49 | 41.72 ± 5.13 | 3.22 ± 0.19 | 2.03 ± 0.03 | 191.70 ± 25.21 | 43.23 ± 5.04 | 6.14 ± 1.64 | 45.61 ± 5.11 | 11.75 ± 0.25 |
| **2:1 (Salbutamol:Mannitol)** | 541.42 ± 83.72 | 508.95 ± 85.45 | 112.56 ± 17.41 | 93.86 ± 1.39 | 16.41 ± 2.35 | 3.33 ± 0.17 | 2.00 ± 0.06 | 338.73 ± 68.45 | 62.53 ± 6.84 | 6.99 ± 1.65 | 66.63 ± 7.33 | 12.50 ± 0.28 |
| **4:1 (Salbutamol:Mannitol)** | 428.86 ± 93.95 | 401.47 ± 94.81 | 89.16 ± 19.39 | 93.35 ± 3.85 | 23.96 ± 8.77 | 3.04 ± 0.22 | 2.09 ± 0.07 | 249.06 ± 76.31 | 57.39 ± 4.93 | 8.06 ± 4.03 | 61.52 ± 5.35 | 12.28 ± 0.28 |

With respect to MMAD and GSD, however, the 1:1 [Salbutamol:Mannitol] carrier obtained the highest MMAD with 4.09 ± 0.11 µm while the 1:2 [Salbutamol:Mannitol] carrier and the 4:1 [Salbutamol:Mannitol] carrier obtained 3.04 ± 0.16 µm and 3.04 ± 0.22 µm, respectively; the highest GSD was attributed to the 4:1 [Salbutamol:Mannitol] carrier with 2.09 ± 0.07 while the lowest GSD was from the 2:1 [Salbutamol:Mannitol] carrier with 2.00 ± 0.06. A linear relationship ($r^2$ = 0.73) was established between MMAD and FPF for all of the carriers.

Furthermore, the highest FPD has been obtained for the 1:2 [Salbutamol:Mannitol] carrier with 338.73 ± 68.45 while the lowest was for the 1:1 [Salbutamol:Mannitol] carrier with 46.50 ± 10.63. The 1:2 [Salbutamol:Mannitol] carrier showed the highest FPF with 62.53 ± 6.84% while the second highest was obtained for the 4:1 [Salbutamol:Mannitol] carrier with 57.39 ± 4.93%. These results proved that the 1:2 [Salbutamol:Mannitol] carrier was the most effective at aerosolizing salbutamol sulphate and support the results presented in Figure 8.6. A linear correlation ($r^2$ = 0.99) between FPF and effective inhalation index (EI) was established supporting the carrier's aerosolized efficacy. Regarding drug loss, however, the 4:1 [Salbutamol:Mannitol] carrier had the highest percentage with 8.06 ± 4.03% while the 1:1 [Salbutamol:Mannitol] carrier had the lowest with 4.93 ± 0.80%. To no surprise, the 2:1 [Salbutamol:Mannitol] carrier obtained the highest dispersibility and effective inhalation index (EI) with 66.63 ± 7.33% and 12.50 ± 0.28 respectively. The results showed that the lowest dispersibility and EI was obtained for the 1:1 [Salbutamol:Mannitol] carrier; a linear relationship ($r^2$ = 0.99) was established between EI and the dispersibility of the carriers..

**§§ 8.3.3.2 Homogeneity Assessment**

The 1:1 [Salbutamol:Mannitol] carrier was the only carrier to abide by the tightly regulated

specifications from the US Food and Drug Administration (US FDA) and the European counterpart.[368] All the other carriers (1:2 [Salbutamol:Mannitol], 1:4 [Salbutamol:Mannitol], 2:1 [Salbutamol:Mannitol], and 4:1 [Salbutamol:Mannitol]) went above the 75-125% range. Figure 8.7 presents the homogeneity profiles for all of the formulations within this study. Table 8.5 presents the percent content homogeneity, expressed as the percent coefficient of variation (%CV), for each of the carriers. The 2:1 (Salbutamol:Mannitol) carrier obtained the smallest %CV with 1.66% whereas the 1:2 (Salbutamol:Mannitol) carrier received the highest %CV with 7.15% (see Table 8.5) which indicate that the 2:1 (Salbutamol:Mannitol) carrier had the best content uniformity amongst all the formulations and the 1:2 (Salbutamol:Mannitol) carrier had the worst.

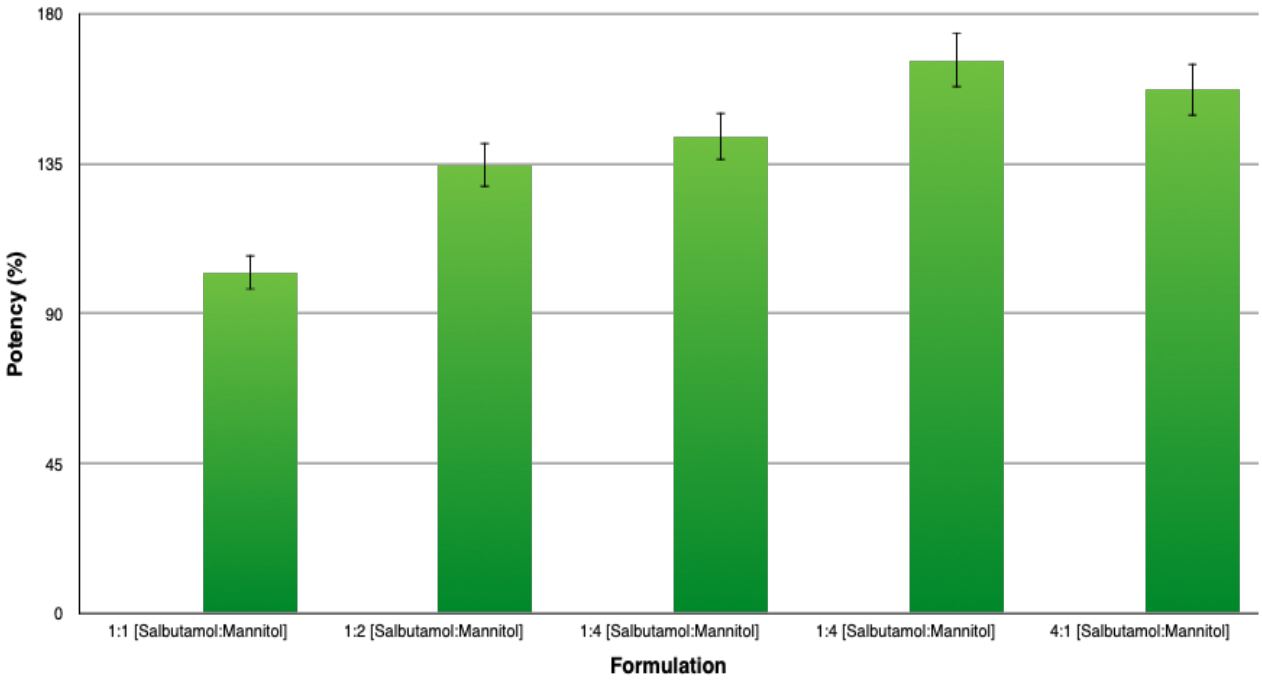


**Figure 8.7.** Potency. Percent potency of each engineered formulation (1:1 [Salbutamol:Mannitol], 1:2 [Salbutamol:Mannitol]. 1:4 [Salbutamol:Mannitol], 2:1 [Salbutamol:Mannitol], and 4:1 [Salbutamol:Mannitol]) with respect to salbutamol sulphate.

**Table 8.5.** Content Homogeneity. Content homogeneity of the 1:1 [Salbutamol:Mannitol], 1:2 [Salbutamol:Mannitol]. 1:4 [Salbutamol:Mannitol], 2:1 [Salbutamol:Mannitol], and 4:1 [Salbutamol:Mannitol] carrier expressed as the percent coefficient of variation (%CV).

| Formulation | % CV |
|---|---|
| **1:1 (Salbutamol:Mannitol)** | 2.30 |
| **1:2 (Salbutamol:Mannitol)** | 7.15 |
| **1:4 (Salbutamol:Mannitol)** | 2.16 |
| **2:1 (Salbutamol:Mannitol)** | 1.66 |
| **4:1 (Salbutamol:Mannitol)** | 2.86 |

*However, has not been taken into account for *in vivo* inhalation studies.

### *8.4 Conclusion*

The results presented in this chapter have proven that salbutamol:mannitol crystals can be successfully crystalized to enhanced its aerosolization performance. They have also shown that when the concentration of salbutamol increases the particle size of the resultant crystal decreases. It was also proven that salbutamol:mannitol crystals can be successfully air jet milled. The results have also shown that the 2:1 (Salbutamol:Mannitol) carrier [FPF = 62.53 $\pm$ 6.84%] was the most effective at delivering salbutamol sulphate to the deep regions of the lung. This carrier had crystals classified as rhombic in structure and was unable to out-perform the 1:3 (Mannitol:Lactose) carrier from Chapter 7 whose FPF was 68.69 $\pm$ 4.65%.

# Chapter 9

## Physical Mixture Comparative Study

### *9.1 Introduction*

In this chapter, the focus was to compare each of the individual studies (Chapters 3-8) to its respective physical mixture counterpart. This allowed for the opportunity to determine whether it is most cost-effective to engineer each carrier separately or to simply use physical mixtures of the commercially available product. Furthermore, this chapter continued to investigate the effect $_{L}$-leucine concentration on each physical mixture formulation had on the overall aerosolized dry powder inhaler (DPI) performance of salbutamol sulphate.

### *9.2 Materials and Methodology*

**§ 9.2.1- § 9.2.6**

Refer to Chapter 2 sections *2.2, 2.7,* and *2.13-2.16.*

### *9.3 Results and Discussion*

**§ 9.3.1 *In vitro* analysis of DPI formulations**

**§§ 9.3.1.1 Spray Dried Lactose-Leucine**

Evaluating each of the formulations on their aerosolization performance, with increasing $_{L}$-Leucine concentration, with that of its spray dried counterpart was done through a physical mixture comparative study. Figure 9.1 presents the data collected from the study where the amount of salbutamol sulphate (in $\mu$g) is reported for each of the MSLI compartments [capsules (C), inhaler (I), mouthpiece (M), induction port (IP), Stage 1, Stage 2, Stage 3, Stage 4, and Stage 5]. Comparing the spray dried formulations with that of the physical mixture formulations, which consisted of mixing spray dried lactose monohydrate, salbutamol sulphate, and the respective $_{L}$-Leucine concentration, it became evident that all of the physical mixture formulations had similar aerosolization performance from one another with all of them delivering the most salbutamol sulphate to Stage 1 (Figure 9.1) whereas the spray dried formulations experienced more of an array of salbutamol sulphate delivery (see Chapter 3) with 0.5% $_{L}$leucine acquiring the most effective aerosolization performance amongst all of the formulations.

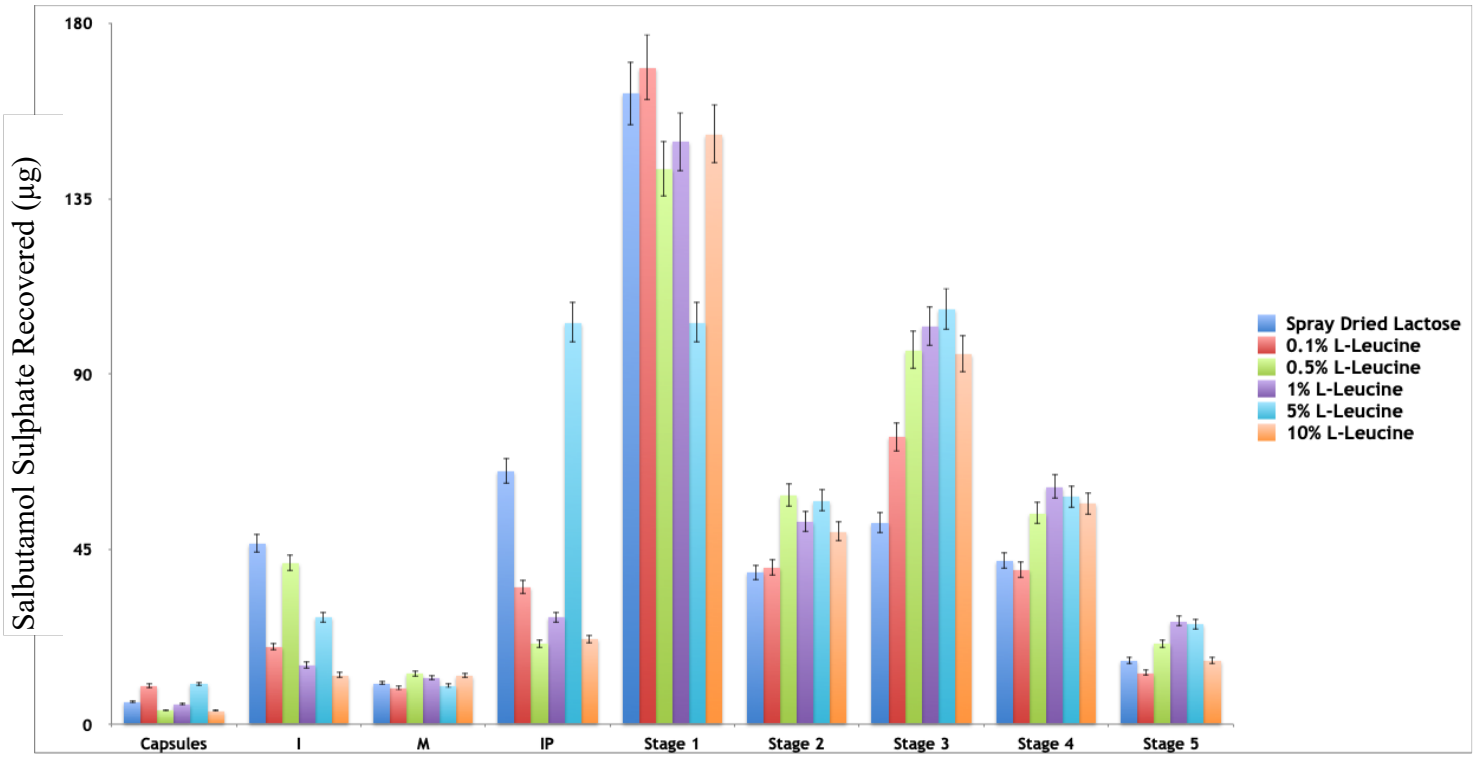


**Figure 9.1**. Aerosolization Profile of Spray Dried Lactose-Leucine. Aerosolization performance of each of the physical mixture formulations (Spray Dried Lactose Monohydrate, 0.1% $_{L}$-leucine, 0.5% $_{L}$-leucine, 1% $_{L}$-leucine, 5% $_{L}$-leucine, and 10% $_{L}$-leucine) highlighting the amount of SS recovered (percent recovered).

Furthermore, taking a closer look at the data that is presented in Table 9.1 it becomes apparent that the physical mixture formulations on an overall case, with the exception of 0.5% $_{L}$-leucine, attained higher RD, ED, percent recovery, and percent emission when compared to the spray dried formulations. On the other hand, the spray dried formulations had less impaction loss than the physical mixture formulations which explains their higher FPF, DS, and EI. That is to say, while the physical mixture formulations were able to deliver more salbutamol sulphate into the respiratory tract than the spray dried formulations, the spray dried formulations were able to deliver more salbutamol sulphate further into the lower respiratory tract than the physical mixture formulations. Therefore, it was deduced that the spray dried formulations were more effective in their

aerosolization performance than the physical mixture formulations. The spray dried 0.5% L-leucine formulation was the most effective with an FPF of 47.11 ± 9.94% (see Chapter 3).

**Table 9.1.** Aerosolization Parameters of Physical Mixtures of Lactose-Leucine. Recovered Dose (RD), Emitted Dose (ED), Percent Recovery, Percent Emission, Percent Impact Loss, Mass Median Aerodynamic Diameter (MMAD), Geometric Standard Deviation (GSD), Fine Particle Dose (FPD), Fine Particle Fraction (FPF), Drug Loss (DL), Dispersibility (DS), and Effective Inhalation Index (EI) of salbutamol sulphate obtained from each of the different physical mixture formulations (Spray Dried Lactose Monohydrate, 0.1% L-leucine, 0.5% L-leucine, 1% L-leucine, 5% L-leucine, and 10% L-leucine).

| Formulation | RD (µg) | ED (µg) | Recovery (%) | Emission (%) | Impact Loss (%) | MMAD (µm) | GSD (µm) | FPD (µg) | FPF (%) | DL (%) | DS (%) | EI |
|---|---|---|---|---|---|---|---|---|---|---|---|---|
| **SD Lactose** | 434.09 ± 40.27 | 376.79 ± 19.65 | 90.25 ± 8.37 | 87.02 ± 3.79 | 52.49 ± 2.81 | 3.13 ± 0.15 | 2.18 ± 0.07 | 110.41 ± 4.77 | 25.51 ± 1.23 | 14.31 ± 4.12 | 29.31 ± 0.36 | 10.87 ± 0.22 |
| **0.1% L-Leucine** | 400.75 ± 74.78 | 371.34 ± 81.01 | 83.32 ± 15.55 | 92.32 ± 3.29 | 50.43 ± 7.27 | 3.29 ± 0.20 | 2.08 ± 0.06 | 126.89 ± 22.45 | 31.90 ± 4.98 | 10.33 ± 5.06 | 34.55 ± 5.22 | 11.23 ± 0.33 |
| **0.5% L-Leucine** | 448.39 ± 90.97 | 393.77 ± 49.03 | 93.22 ± 18.91 | 88.69 ± 6.66 | 37.14 ± 5.19 | 3.31 ± 0.09 | 2.10 ± 0.02 | 171.29± 35.23 | 38.21 ± 1.79 | 12.08 ± 7.00 | 43.22 ± 3.41 | 11.14 ± 0.38 |
| **1% L-Leucine** | 446.87 ± 101.35 | 419.43 ± 96.19 | 92.90 ± 21.07 | 93.84 ± 0.73 | 40.55 ± 5.95 | 3.14 ± 0.11 | 2.13 ± 0.04 | 190.00 ± 66.58 | 41.68 ± 5.55 | 7.32 ± 0.81 | 44.41 ± 5.79 | 11.89 ± 0.67 |
| **5% L-Leucine** | 413.69 ± 59.04 | 376.05 ± 71.15 | 86.01 ± 12.27 | 90.49 ± 4.42 | 31.27 ± 4.73 | 3.22 ± 0.11 | 2.11 ± 0.05 | 190.99 ± 54.83 | 45.53 ± 6.71 | 11.86 ± 2.84 | 50.16 ± 5.04 | 11.48 ± 0.77 |
| **10% L-Leucine** | 416.86 ± 204.87 | 391.55 ± 203.14 | 86.67 ± 42.59 | 93.07 ± 2.71 | 38.46± 12.38 | 3.27 ± 0.08 | 2.07 ± 0.02 | 168.36 ± 61.70 | 42.38 ± 8.87 | 7.84 ± 2.98 | 45.71 ± 10.53 | 11.51 ± 0.14 |

### §§ 9.3.1.2 Spray Dried Mannitol-Leucine

Figure 9.2 presents the data collected from the study where the amount of salbutamol sulphate (in □g) is reported for each of the MSLI compartments. Comparing the spray dried formulations with that of their physical mixture counterpart, which consisted of mixing spray dried mannitol, salbutamol sulphate, and the respective L-leucine concentration, it became evident that 0.5% L-leucine, 5% L-leucine, and 10% L-leucine delivered the most salbutamol sulphate to Stage 1, while 0.1% L-leucine and 1% L-leucine to Stage 3. Nevertheless, their delivered amounts were significantly less ($p < 0.05$) than that of the spray dried formulations, where 6% L-leucine (see Chapter 4) had the most effective aerosolization performance.

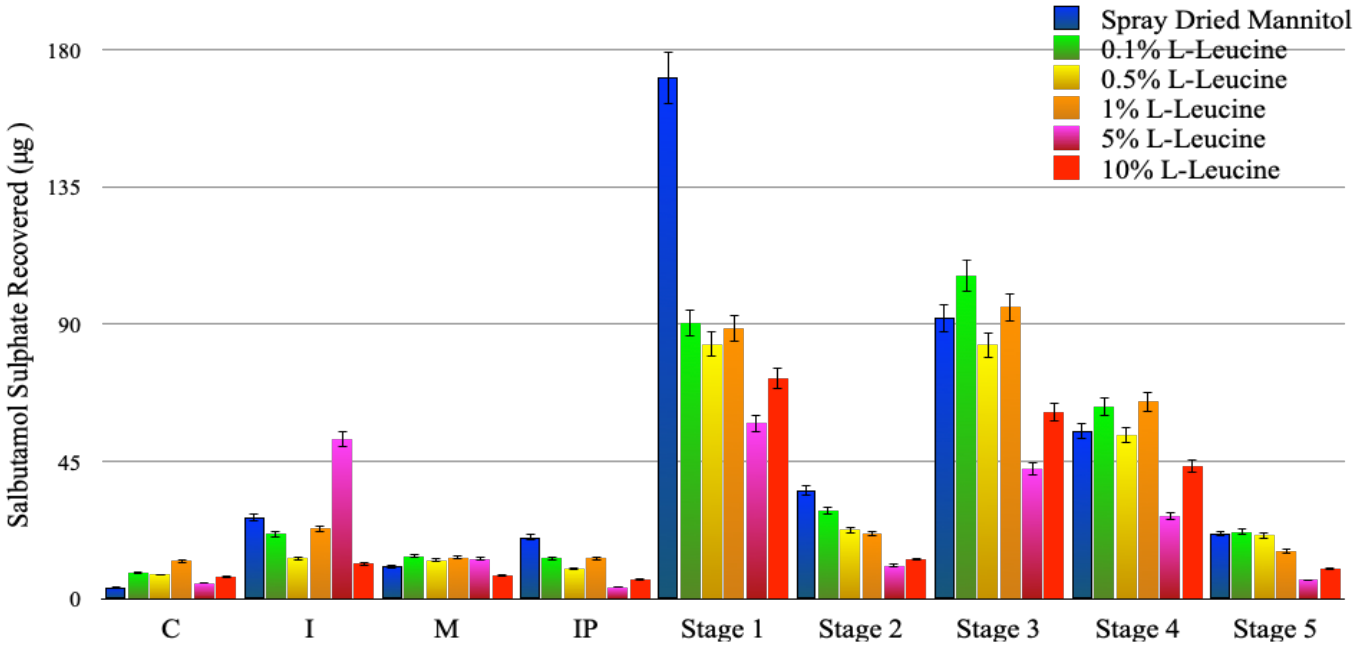


**Figure 9.2**. Aerosolization Profile of Spray Dried Mannitol-Leucine. Aerosolization performance of each physical mixture formulation (Spray Dried Mannitol, 0.1% L-leucine, 0.5% L-leucine, 1 L-leucine, 5% L-leucine, and 10% L-leucine) highlighting the amount of SS recovered (percent recovered) for each and comparing them side-by-side.

Furthermore, taking a closer look at the data that is presented in Table 9.2 it becomes apparent that the physical mixture formulations, on an overall case, attained lower RD, ED, and percent recovery when compared to the engineered spray dried formulations. In addition, the spray dried formulations, for the most part, also witnessed higher impact loss than the physical mixture formulations, but the physical mixture formulations, on an overall case, showed higher percent emission values than the spray dried formulations. That is to say, while the physical mixture formulations were able to deliver more salbutamol sulphate into the system than the spray dried formulations, the spray dried formulations were able to deliver more salbutamol sulphate further into the lower respiratory tract than the physical mixture formulations. In addition, the RD of the spray dried formulations surpasses that of the physical mixture formulations suggesting that attachment/detachment of SS from the physical mixture formulations was compromised. Therefore, based on such comparison, it was deduced that the spray dried formulations were more effective in their aerosolization performance than the physical mixture formulations. The spray dried 6% $_{L}$-leucine formulation was the most effective with an FPF of 52.96 $\pm$ 5.21% (see Chapter 4).

**Table 9.2.** Aerosolization Parameters of Physical Mixtures of Mannitol-Leucine. Recovered Dose (RD), Emitted Dose (ED), Percent Recovery, Percent Emission, Percent Impact Loss, Mass Median Aerodynamic Diameter (MMAD), Geometric Standard Deviation (GSD), Fine Particle Dose (FPD), Fine Particle Fraction (FPF), Drug Loss (DL), Dispersibility (DS), and Effective Inhalation Index (EI) of salbutamol sulphate obtained from each of the different physical mixture formulations (Spray Dried Mannitol, 0.1% $_{L}$-leucine, 0.5% $_{L}$-leucine, 1% $_{L}$-leucine, 5% $_{L}$-leucine, and 10% $_{L}$-leucine).

| Formulation | RD (µg) | ED (µg) | Recovery (%) | Emission (%) | Impact Loss (%) | MMAD (µm) | GSD (µm) | FPD | FPF (%) | DL (%) | DS (%) | EI |
|---|---|---|---|---|---|---|---|---|---|---|---|---|
| **Spray Dried Mannitol** | 431 ± 143.68 | 394.56 ± 147.19 | 89.74 ± 29.87 | 90.34 ± 5.20 | 45.59 ± 6.29 | 3.06 ± 0.10 | 2.10 ± 0.08 | 168.20 ± 85.39 | 37.06 ± 8.66 | 10.54 ± 5.35 | 40.75 ± 7.55 | 11.28 ± 0.62 |
| **0.1% L-Leucine** | 358.27 ± 56.95 | 323.00 ± 55.85 | 74.48 ± 11.84 | 90.01 ± 1.59 | 29.73 ± 7.94 | 2.96 ± 0.08 | 2.09 ± 0.02 | 190.60 ± 53.42 | 52.45 ± 7.23 | 12.44 ± 2.03 | 58.19 ± 7.12 | 11.93 ± 0.37 |
| **0.5% L-Leucine** | 299.25 ± 95.92 | 273.32 ± 91.84 | 62.21 ± 19.94 | 91.07 ± 1.43 | 33.21 ± 9.83 | 2.83 ± 0.22 | 2.14 ± 0.08 | 157.59 ± 77.77 | 50.91 ± 8.23 | 11.81 ± 2.37 | 55.83 ± 8.18 | 11.91 ± 0.40 |
| **1% L-Leucine** | 335.68 ± 68.56 | 299.12 ± 58.47 | 69.79 ± 14.25 | 89.22 ± 1.22 | 30.12 ± 2.73 | 2.95 ± 0.06 | 2.06 ± 0.01 | 175.69 ± 32.76 | 52.48 ± 1.59 | 14.19 ± 3.26 | 58.81 ± 0.98 | 11.90 ± 0.12 |
| **5% L-Leucine** | 204.82 ± 54.55 | 147.97 ± 53.44 | 42.58 ± 11.34 | 76.29 ± 31.09 | 30.10 ± 4.93 | 3.05 ± 0.14 | 2.05 ± 0.01 | 75.82 ± 43.07 | 39.97 ± 23.39 | 25.91 ± 32.54 | 48.53 ± 14.22 | 10.54 ± 2.80 |
| **10% L-Leucine** | 225.30 ± 41.38 | 206.25 ± 43.17 | 46.84 ± 8.60 | 91.26 ± 2.70 | 35.04 ± 1.93 | 2.93 ± 0.10 | 2.06 ± 0.05 | 114.56 ± 29.01 | 50.49 ± 3.38 | 11.97 ± 2.67 | 55.30 ± 2.56 | 11.90 ± 0.24 |

#### §§ 9.3.1.3 Spray Dried Mannitol-Lactose-Leucine

Figure 9.3 presents the data collected from the study where the amount of salbutamol sulphate (in μg) is reported for each of the MSLI compartments. Comparing the spray dried formulations with that of their physical mixture counterpart, which consisted of mixing spray dried mannitol, spray dried lactose, salbutamol sulphate, and the respective L-leucine concentration, it became evident that the spray dried mannitol, 1:1 [Mannitol:Lactose], 1:3 [Mannitol:Lactose], and the 3:1 [Mannitol:Lactose] physical mixture formulations delivered the most salbutamol sulphate to Stage 1 while the spray dried lactose delivered the most salbutamol sulphate to Stage 3. The 1:3 [mannitol:lactose] physical mixture formulation was the most effective in its aerosolization performance delivering the most salbutamol to Stages 3-5 when comparing them to the rest of the physical mixture formulations. When comparing the physical mixture formulations to their spray dried counterpart, however, the spray dried 1:3 [mannitol:lactose] carrier was the most effective in its aerosolization performance.

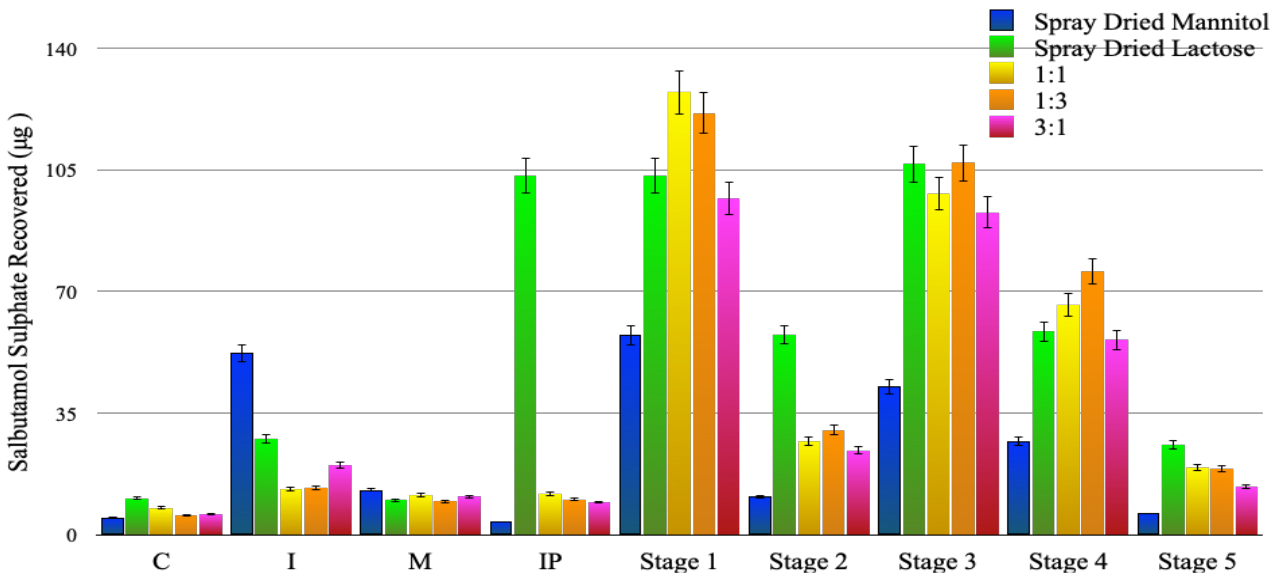


**Figure 9.3**. Aerosolization Profile of Spray Dried Mannitol-Lactose-Leucine. Aerosolization performance of each physical mixture formulation (Spray Dried Mannitol, Spray Dried Lactose, 1:1 [Mannitol:Lactose], 1:3 [Mannitol:Lactose], and 3:1 [Mannitol:Lactose]) highlighting the amount of SS recovered (percent recovered) for each and comparing them side-by-side.

Furthermore, taking a closer look at the data that is presented in Table 9.3 it becomes apparent that the physical mixture formulations, on an overall case, attained similar results to the spray dried formulations. The 1:3 [mannitol:lactose] physical mixture carrier obtained the best aerosolization profile amongst all the physical mixture formulations, but, when compared to the spray dried formulations, the 1:3 [mannitol:lactose] spray dried carrier obtained the best aerosolization profile amongst all the carriers with an FPF of 61.42 ± 4.21% (see Chapter 5).

**Table 9.3.** Aerosolization Parameters of Physical Mixtures of Mannitol-Lactose-Leu. Recovered Dose (RD), Emitted Dose (ED), Percent Recovery, Percent Emission, Percent Impact Loss, Mass Median Aerodynamic Diameter (MMAD), Geometric Standard Deviation (GSD), Fine Particle Dose (FPD), Fine Particle Fraction (FPF), Drug Loss (DL), Dispersibility (DS), and Effective Inhalation Index (EI) of salbutamol sulphate obtained from each of the different physical mixture formulations (Spray Dried Mannitol, Spray Dried Lactose, 1:1 [Mannitol:Lactose], 1:3 [Mannitol:Lactose], and 3:1 [Mannitol:Lactose]).

| Formulation | RD (µg) | ED (µg) | Recovery (%) | Emission (%) | Impact Loss (%) | MMAD (µm) | GSD (µm) | FPD | FPF (%) | DL (%) | DS (%) | EI |
|---|---|---|---|---|---|---|---|---|---|---|---|---|
| **Spray Dried Mannitol** | 204.82 ± 54.55 | 147.97 ± 53.44 | 42.58 ± 11.34 | 76.29 ± 31.09 | 30.10 ± 4.93 | 3.05 ± 0.14 | 2.05 ± 0.01 | 75.82 ± 43.07 | 39.97 ± 23.39 | 25.91 ± 32.54 | 48.53 ± 14.22 | 10.54 ± 2.80 |
| **Spray Dried Lactose** | 413.69 ± 59.04 | 376.05 ± 71.15 | 86.01 ± 12.27 | 90.49 ± 4.42 | 31.27 ± 4.73 | 3.22 ± 0.11 | 2.11 ± 0.05 | 190.99 ± 54.83 | 45.53 ± 6.71 | 11.86 ± 2.84 | 50.16 ± 5.04 | 11.48 ± 0.77 |
| **1:1** | 374.64 ± 49.47 | 350.00 ± 48.71 | 77.89 ± 10.28 | 93.36 ± 1.40 | 36.98 ± 8.97 | 3.28 ± 0.59 | 2.09 ± 0.01 | 183.82 ± 36.17 | 49.11 ± 8.34 | 8.83 ± 3.22 | 52.53 ± 8.23 | 11.93 ± 0.40 |
| **1:3** | 386.73 ± 53.24 | 363.49 ± 54.58 | 80.40 ± 11.07 | 93.88 ± 1.42 | 34.69 ± 8.80 | 3.30 ± 0.58 | 2.06 ± 0.06 | 201.78 ± 51.52 | 51.63 ± 6.43 | 7.62 ± 2.13 | 54.96 ± 6.33 | 12.06 ± 0.31 |
| **3:1** | 324.10 ± 73.47 | 293.03 ± 75.19 | 67.38 ± 15.27 | 90.03 ± 3.16 | 33.94 ± 11.28 | 3.04 ± 0.01 | 2.04 ± 0.01 | 162.59 ± 69.68 | 48.88 ± 10.11 | 11.94 ± 3.63 | 54.25 ± 10.55 | 11.78 ± 0.49 |

### §§ 9.3.1.4 Xylitol-Leucine Crystals

Figure 9.4 presents the data collected from the physical mixture comparative study where the amount of salbutamol sulphate (in µg) is reported for each of the MSLI compartments. When comparing the data, it became evident that the physical mixture formulations carried significantly more ($p > 0.05$) salbutamol sulphate to Stage 1 than the crystallized formulations. Furthermore, when it came to the inhaler (I), mouthpiece (M), and induction port (IP), the physical mixture formulations also exhibited more salbutamol sulphate, but in this case, more salbutamol sulphate suggests more API being delivered to the non-targeted area.

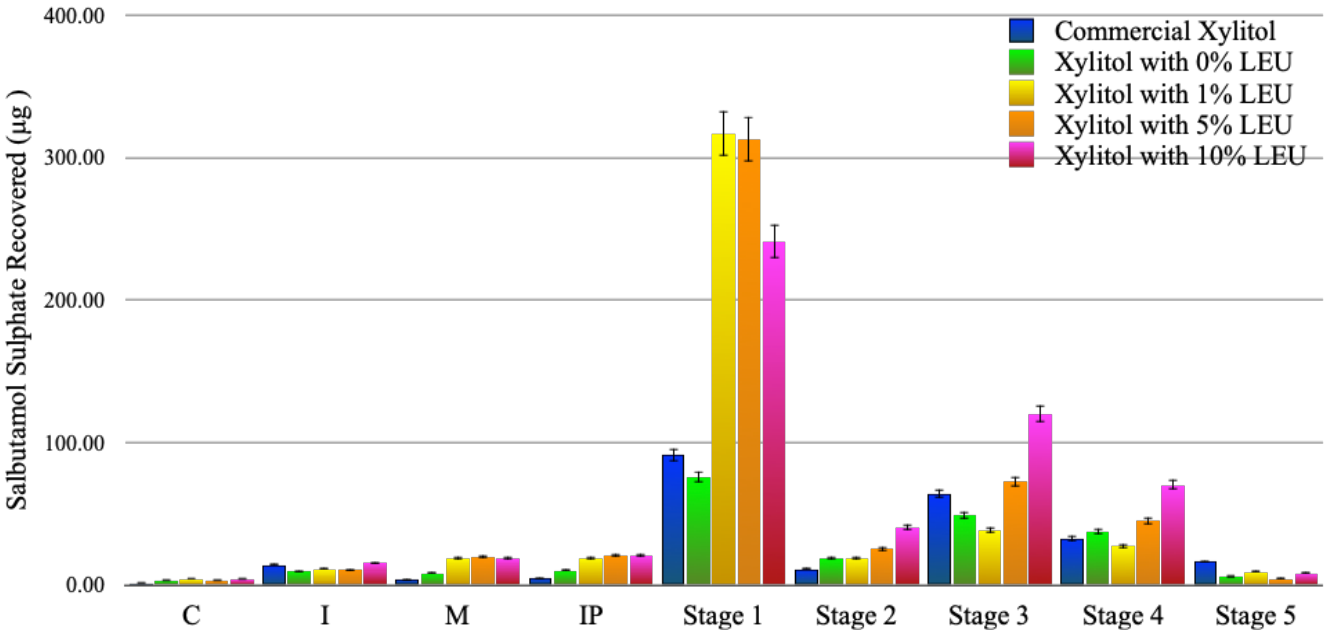


**Figure 9.4**. Aerosolization Profile of Xylitol-Leucine Crystals. Aerosolization performance of each physical mixture formulation (Commercial Xylitol, Xylitol with 0% LEU, Xylitol with 1% LEU, Xylitol with 5% LEU, and Xylitol with 10% LEU) highlighting the amount of SS recovered (percent recovered) for each and comparing them side-by-side.

Moreover, Table 9.4 presents the data from the aerosolization of the physical mixtures; comparing this data, it becomes evident that the physical mixture formulations observed higher RD, ED, and percent recovery when compared to their crystallized counterpart. Both the crystallized and the physical mixture formulations experienced similar percent emission values suggesting salbutamol sulphate being introduced into the system at a consistent rate. When it comes to impaction loss, however, the physical mixture formulations experienced higher values meaning more salbutamol sulphate was lost as a result of poor adhesive and cohesive forces; such results also correspond to their bigger size as indicated by their higher MMAD values. GSD for the crystallized formations was higher than the physical mixture formulations, but their FPD was higher. In addition, as a result of their bigger size and despite their higher dosage, the physical mixture formulations resulted in obtaining higher FPF with commercial xylitol having the highest FPF with 44.13 $\pm$ 11.27% when compared to the crystallized formulations where xylitol with 5% LEU obtained 42.94 $\pm$ 15.21% (see Chapter 6). While commercial xylitol obtained the highest FPF from all of the formulations, it failed to adhere to the potency specification, like previously mentioned. Drug loss was higher with the crystallized formulations along with the effective inhalation index, but lower in dispersibility.

**Table 9.4.** Aerosolization Parameters of Physical Mixtures of Xylitol-Leucine Crystals. Recovered Dose (RD), Emitted Dose (ED), Percent Recovery, Percent Emission, Percent Impact Loss, Mass Median Aerodynamic Diameter (MMAD), Geometric Standard Deviation (GSD), Fine Particle Dose (FPD), Fine Particle Fraction (FPF), Drug Loss (DL), Dispersibility (DS), and Effective Inhalation Index (EI) of salbutamol sulphate obtained from each of the different physical mixture formulations (Commercial Xylitol, Xylitol with 0% LEU, Xylitol with 1% LEU, Xylitol with 5% LEU, and Xylitol with 10% LEU).

| Formulation | RD (µg) | ED (µg) | Recovery (%) | Emission (%) | Impact Loss (%) | MMAD (µm) | GSD (µm) | FPD | FPF (%) | DL (%) | DS (%) | EI |
|---|---|---|---|---|---|---|---|---|---|---|---|---|
| **Commercial Xylitol** | 239.29 ± 111.70 | 221.16 ± 106.22 | 49.75 ± 23.22 | 92.01 ± 1.75 | 43.72 ± 12.20 | 2.77 ± 0.45 | 2.18 ± 0.31 | 113.57 ± 82.45 | 44.13 ± 11.27 | 8.56 ± 2.11 | 47.90 ± 11.69 | 11.66 ± 0.53 |
| **Xylitol with 0% LEU** | 216.19 ± 170.69 | 197.97 ± 154.33 | 44.95 ± 35.49 | 91.91 ± 3.46 | 50.01 ± 19.40 | 3.10 ± 0.10 | 2.09 ± 0.06 | 92.87 ± 109.59 | 34.25 ± 16.98 | 10.12 ± 3.94 | 37.27 ± 18.73 | 11.21 ± 0.78 |
| **Xylitol with 1% LEU** | 461.51 ± 55.77 | 431.00 ± 53.37 | 95.95 ± 11.59 | 93.37 ± 1.29 | 73.20 ± 7.64 | 3.08 ± 0.02 | 2.14 ± 0.05 | 75.48 ± 39.98 | 16.02 ± 7.76 | 7.56 ± 1.31 | 17.09 ± 8.03 | 10.45 ± 0.43 |
| **Xylitol with 5% LEU** | 511.81 ± 135.10 | 481.56 ± 131.94 | 106.40 ± 28.09 | 93.89 ± 1.18 | 65.43 ± 4.82 | 3.26 ± 0.04 | 2.00 ± 0.02 | 122.23 ± 44.08 | 23.57 ± 3.98 | 6.77 ± 1.52 | 25.10 ± 4.15 | 10.84 ± 0.20 |
| **Xylitol with 10% LEU** | 535.92 ± 73.24 | 501.43 ± 66.79 | 111.42 ± 15.23 | 93.59 ± 1.08 | 48.89 ± 5.33 | 3.27 ± 0.06 | 1.99 ± 0.01 | 198.78 ± 34.95 | 37.05 ± 3.05 | 7.16 ± 1.13 | 39.61 ± 3.70 | 11.43 ± 0.09 |

### §§ 9.3.1.5 Mannitol-Lactose Crystals

Figure 9.5 presents the data collected from the study where the amount of salbutamol sulphate (in µg) is reported for each of the MSLI compartments. Comparing the crystallized formulations with that of their physical mixture counterpart, which consisted of mixing mannitol, lactose, and salbutamol sulphate, it became evident that the 1:1 [mannitol:lactose], 1:2 [mannitol:lactose], and 1:3 [mannitol:lactose] carriers delivered the most salbutamol sulphate to Stage 1. The 2:1 [mannitol:lactose] carrier delivered the most salbutamol sulphate to Stage 3 while the 3:1 [mannitol:lactose] carrier delivered the most salbutamol sulphate to Stage 2.

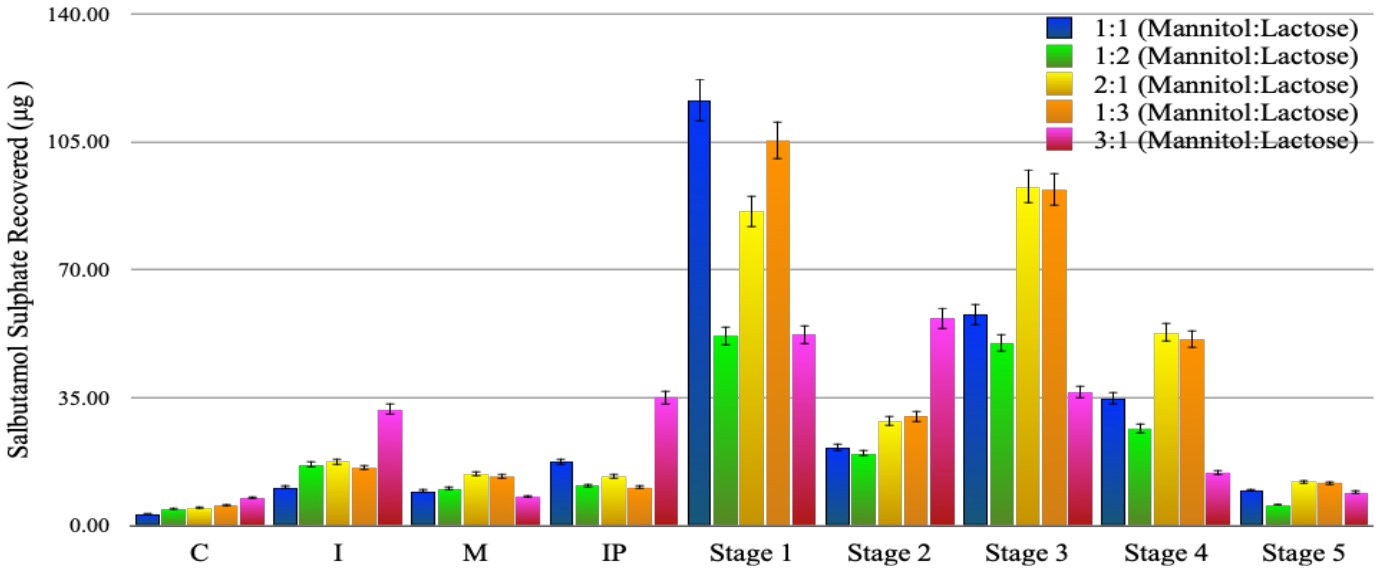


**Figure 9.5**. Aerosolization Profile of Mannitol-Lactose Crystals. Aerosolization performance of each physical mixture formulation (1:1 [Mannitol:Lactose], 1:2 [Mannitol:Lactose], 2:1 [Mannitol:Lactose], 1:3 [Mannitol:Lactose], and 3:1 [Mannitol:Lactose]) highlighting the amount of SS recovered (percent recovered) for each and comparing them side-by-side.

Furthermore, taking a closer look at the data that is presented in Table 9.5 it becomes apparent that the physical mixture formulations, on an overall case, attained lower RD, ED, percent recovery, and percent emission than the crystallized formulations. The physical mixture formulations, however, obtained higher impact loss but lower MMAD and GSD when compared to the crystallized formulations. The crystallized formulations attained higher FPD and FPF when compared to the physical mixture formulations, but the physical mixture formulations attained higher drug loss. The crystallized formulations also obtained higher dispersibility and effective inhalation index. As a whole, the crystallized formulations outperformed the physical mixture formulations in their aersolization profile. The highest FPF for the crystallized formulations was from the 1:3 [mannitol:lactose] carrier with 68.69 $\pm$ 4.65% (see Chapter 7) whereas for the physical mixture formulations the 2:1 [mannitol:lactose] carrier obtained an FPF of 46.00 $\pm$ 15.03%.

#### §§ 9.3.1.6 Mannitol-Salbutamol Crystals

A physical mixture comparative study was not conducted for the mannitol:salbutamol sulphate crystals since it would have consisted of mixing mannitol with salbutamol sulphate, which has already been done in this overall study. Therefore, the values obtained from the spray dried mannitol-leucine carriers were used, specifically the Spray Dried Mannitol sample, and it was determined that it was better to crystallize the carriers than to physically mix them. The highest FPF from the crystallized carriers was from the 2:1 [salbutamol:mannitol] carrier with an FPF of 62.53 $\pm$ 6.84% (see Chapter 8) whereas the Spray Dried Mannitol physical mixture carrier had an FPF of 37.06 $\pm$ 8.66%.

**Table 9.5.** Aerosolization Parameters of Physical Mixtures of Mann.-Lac. Crystals. Recovered Dose (RD), Emitted Dose (ED), Percent Recovery, Percent Emission, Percent Impact Loss, Mass Median Aerodynamic Diameter (MMAD), Geometric Standard Deviation (GSD), Fine Particle Dose (FPD), Fine Particle Fraction (FPF), Drug Loss (DL), Dispersibility (DS), and Effective Inhalation Index (EI) of salbutamol sulphate obtained from each of the different physical mixture formulations (1:1 [Mannitol:Lactose], 1:2 [Mannitol:Lactose], 1:3 [Mannitol:Lactose], 2:1 [Mannitol:Lactose], and 3:1 [Mannitol:Lactose]).

| Formulation | RD (µg) | ED (µg) | Recovery (%) | Emission (%) | Impact Loss (%) | MMAD (µm) | GSD (µm) | FPD | FPF (%) | DL (%) | DS (%) | EI |
|---|---|---|---|---|---|---|---|---|---|---|---|---|
| **1:1 (Mannitol:Lactose)** | 277.95 ± 52.19 | 257.85 ± 49.66 | 57.79 ± 10.85 | 92.72 ± 0.42 | 48.22 ± 0.94 | 3.15 ± 0.30 | 2.07 ± 0.10 | 102.58 ± 25.68 | 36.64 ± 2.19 | 8.47 ± 0.72 | 39.52 ± 2.20 | 11.37 ± 0.11 |
| **1:2 (Mannitol:Lactose)** | 192.03 ± 37.55 | 165.10 ± 46.66 | 39.92 ± 7.81 | 84.96 ± 8.59 | 34.03 ± 9.26 | 3.21 ± 0.21 | 2.05 ± 0.07 | 82.17 ± 39.90 | 41.14 ± 12.86 | 17.54 ± 9.16 | 47.73 ± 10.82 | 11.20 ± 0.96 |
| **2:1 (Mannitol:Lactose)** | 317.19 ± 123.10 | 285.55 ± 115.17 | 65.94 ± 25.59 | 89.64 ± 1.50 | 35.05 ± 14.79 | 3.17 ± 0.07 | 2.03 ± 0.05 | 157.54 ± 100.74 | 46.00 ± 15.03 | 12.12 ± 2.42 | 51.14 ± 16.02 | 11.63 ± 0.72 |
| **1:3 (Mannitol:Lactose)** | 329.80 ± 120.01 | 300.45 ± 111.88 | 68.57 ± 24.95 | 90.94 ± 1.23 | 39.42 ± 17.88 | 3.05 ± 0.26 | 2.09 ± 0.12 | 154.65 ± 111.62 | 43.27 ± 14.99 | 10.90 ± 2.21 | 47.51 ± 16.08 | 11.57 ± 0.66 |
| **3:1 (Mannitol:Lactose)** | 244.24 ± 188.34 | 204.43 ± 194.57 | 50.78 ± 39.16 | 73.41 ± 21.63 | 38.02 ± 6.86 | 3.44 ± 0.80 | 2.16 ± 0.07 | 60.32 ± 56.56 | 21.16 ± 9.34 | 31.07 ± 23.49 | 27.88 ± 6.78 | 9.63 ± 1.65 |

### § 9.3.2 Homogeneity Assessment

#### §§ 9.3.2.1 Spray Dried Lactose-Leucine

A homogeneity assessment was completed to assess the uniformity of each of the physical mixture formulations. Table 9.6 presents the results where it shows the percent potency and the coefficient of variation (%CV), which was the indicator used to assess the homogeneity of the formulations. SD lactose was the only formulation that passed the specification requirement that is set by the US Food and Drug Administration and its European counterpart with a potency of 91.36%; the range being 75-125%. The formulation that was the most homogeneous was the 1% Leu with a %CV of 5.27%.

**Table 9.6.** Potency and Homogeneity of Physical Mixtures of Lactose-Leucine. Percent potency and content homogeneity of the Spray Dried Lactose-Leucine physical mixture formulations (SD Lactose, 0.1% Leu, 0.5% Leu, 1% Leu, 5% Leu, and 10% Leu), expressed as the percent coefficient of variation (%CV).

| Formulation | Potency (%) | % CV |
|---|---|---|
| **SD Lactose** | 91.36 | 10.29 |
| **0.1% Leu** | 49.54 | 10.31 |
| **0.5% Leu** | 48.50 | 13.54 |
| **1% Leu** | 44.39 | 5.27 |
| **5% Leu** | 58.90 | 28.71 |
| **10% Leu** | 33.32 | 35.31 |

*However, has not been taken into account for *in vivo* inhalation studies.

### §§ 9.3.2.2 Spray Dried Mannitol-Leucine

Table 9.7 presents the percent potency and the coefficient of variation (%CV), which was the indicator used to assess the homogeneity of the formulations, for the spray dried mannitol-leucine physical mixture formulations. The results show that all of the physical mixture formulations adhered to the potency specifications with the exception of the 1% $_{L}$-leucine and 5% $_{L}$-leucine which were 54.53% and 77.56% potent, respectively. With respect to the homogeneity of the physical mixture formulations, the 0.1% $_{L}$-leucine obtained the best content homogeneity with a %CV of 5.44%.

**Table 9.7.** Potency and Homogeneity of Physical Mixtures of Mannitol-Leucine. Percent potency and content homogeneity of the Spray Dried Mannitol-Leucine physical mixture formulations (SD Mannitol, 0.1% Leu, 0.5% Leu, 1% Leu, 5% Leu, and 10% Leu), expressed as the percent coefficient of variation (%CV).

| Formulation | Potency (%) | % CV |
|---|---|---|
| **SD Mannitol** | 91.95 | 20.90 |
| **0.1% Leu** | 93.34 | 5.44 |
| **0.5% Leu** | 98.21 | 25.02 |
| **1% Leu** | 54.53 | 15.55 |
| **5% Leu** | 77.56 | 9.82 |
| **10% Leu** | 93.34 | 20.70 |

*However, has not been taken into account for *in vivo* inhalation studies.

### §§ 9.3.2.3 Spray Dried Mannitol-Lactose-Leucine

Table 9.8 presents the percent potency and the coefficient of variation (%CV), which was the

indicator used to assess the homogeneity of the formulations, for the spray dried mannitol-lactose-leucine physical mixture formulations. All of the physical mixture formulations adhered to the 75-125% potency range. Moreover, the physical mixture formulation that was the most uniform was the 1:3 [Mannitol:Lactose] formulation with a %CV of 3.15%.

**Table 9.8.** Potency and Homogeneity of Physical Mixtures of Mann.-Lac.-Leucine. Percent potency and content homogeneity of the Spray Dried Mannitol-Lactose-Leucine physical mixture formulations (SD Mannitol, SD Lactose, 1:1 [Mannitol:Lactose], 1:3 [Mannitol:Lactose], and 3:1 [Mannitol:Lactose]), expressed as the percent coefficient of variation (%CV).

| Formulation | Potency (%) | % CV |
|---|---|---|
| **SD Mannitol** | 110.07 | 11.90 |
| **SD Lactose** | 89.71 | 13.23 |
| **1:1 [Mannitol:Lactose]** | 115.07 | 8.02 |
| **1:3 [Mannitol:Lactose]** | 110.01 | 3.15 |
| **3:1 [Mannitol:Lactose]** | 84.15 | 8.88 |

*However, has not been taken into account for *in vivo* inhalation studies.

### §§ 9.3.2.4 Xylitol-Leucine Crystals

Table 9.9 presents the percent potency and the coefficient of variation (%CV), which was the indicator used to assess the homogeneity of the formulations, for the xylitol-leucine physical mixture formulations. The Xylitol with 1% Leu, Xylitol with 5% Leu, and the Xylitol with 10% Leu adhered to the 75-125% potency specification with 90.97%, 94.20%, and 94.61% (respectively) while the Commercial Xylitol and Xylitol with 0% Leu failed the specification with potencies of

51.55% and 73.42% (respectively). With respect to the uniformity of the physical mixture formulations, the Xylitol with 10% Leu was the most homogeneous amongst all of the physical mixture formulations with a %CV of 4.67%.

**Table 9.9.** Potency and Homogeneity of Physical Mixtures of Xylitol-Leu. Crystals. Percent potency and content homogeneity of the Xylitol-Leucine physical mixture formulations (Commercial Xylitol, Xylitol with 0% Leu, Xylitol with 1% Leu, Xylitol with 5% Leu, and Xylitol with 10% Leu), expressed as the percent coefficient of variation (%CV).

| Formulation | Potency (%) | % CV |
|---|---|---|
| **Commercial Xylitol** | 113.03 | 13.35 |
| **Xylitol with 0% Leu** | 73.42 | 15.95 |
| **Xylitol with 1% Leu** | 90.97 | 13.38 |
| **Xylitol with 5% Leu** | 94.20 | 5.38 |
| **Xylitol with 10% Leu** | 94.61 | 4.67 |

*However, has not been taken into account for *in vivo* inhalation studies.

**§§ 9.3.2.5 Mannitol-Lactose Crystals**

Table 9.10 presents the percent potency and the coefficient of variation (%CV), which was the indicator used to assess the homogeneity of the formulations, for the Mannitol-Lactose physical mixture formulations. The only physical mixture formulation that did not adhere to the potency specification was the 1:2 (Mannitol:Lactose) formulation which had a percent potency of 69.50%. All the other physical mixture formulations [1:1 (Mannitol:Lactose), 1:3 (Mannitol:Lactose), 2:1 (Mannitol:Lactose), and 3:1 (Mannitol:Lactose)] adhered to the potency specification [see Table

9.10]. With respect to their homogeneity, however, the most uniform physical mixture formulation was the 1:1 (Mannitol:Lactose) formulation with a %CV of 6.48%.

**Table 9.10.** Potency and Homogeneity of Physical Mixtures of Mann.-Lac. Crystals. Percent potency and content homogeneity of the Mannitol-Lactose physical mixture formulations [1:1 (Mannitol:Lactose), 1:2 (Mannitol:Lactose), 1:3 (Mannitol:Lactose), 2:1 (Mannitol:Lactose), and 3:1 (Mannitol:Lactose)], expressed as the percent coefficient of variation (%CV).

| Formulation | Potency (%) | % CV |
|---|---|---|
| **1:1 (Mannitol:Lactose)** | 108.00 | 6.48 |
| **1:2 (Mannitol:Lactose)** | 69.50 | 19.40 |
| **1:3 (Mannitol:Lactose)** | 90.88 | 18.73 |
| **2:1 (Mannitol:Lactose)** | 95.63 | 28.28 |
| **3:1 (Mannitol:Lactose)** | 114.85 | 24.60 |

*However, has not been taken into account for *in vivo* inhalation studies.

#### §§ 9.3.2.6 Mannitol-Salbutamol Crystals

As mentioned in §§ 9.2.1.6, a physical mixture comparative study was not conducted for mannitol-salbutamol formulation since it would have consisted of mixing mannitol with salbutamol sulphate, which was something that has already been done (see §§ 9.2.1.2).

### *9.4 Conclusion*

The results presented in this chapter showed that it was better to use the engineered carriers than their respective physical mixture counterpart. More optimal aerosolization performances were

attained from the engineered carriers than from the physical mixture formulations. Parameters like FPF were higher in the engineered carriers than the physical mixture formulations; such parameter is used to determine a formulation's aerosolization performance. Moreover, based on the results presented in this chapter, it was determined that it was more cost-effective to engineer the carriers than to use the physical mixture counterpart. Looking at the physical mixture formulations on their own, the results presented in this chapter have shown that the addition of $_{L}$-leucine lowers the potency of the resultant formulations. The addition of $_{L}$-leucine causes a change in the inter- and intra- molecular interactions which affects the adhesive forces of salbutamol sulphate thus affecting the formulation's aerosolization performance.

# Chapter 10

# General Discussion and Future Work

### *10.1 General Discussion*

The previous chapters illustrated an enhanced methodological approach for the enhancement of aerosolized particulates. The goal was to engineer a carrier with optimal aerosolization properties such that an increase in the FPF was observed. It was also important to engineer the carriers following the US Food and Drug Administration's guidelines, which also follow the US Pharmacopeia, in the event that any of the carriers become used for manufacturing purposes; these guidelines also follow the European pharmacopeia.[222, 223, 235, 368]

Chapter 3 looked at spray dried lactose-leucine carriers to determine their aerosolized efficiency concluding that the optimal FPF that was reached was 47.11± 9.94% from the 0.5% L-leucine carrier. It was also determined that the addition of L-leucine improved the stability of amorphous spray dried lactose while also providing a lubrication effect.[21] Moreover, the results obtained from the physical mixture comparative study (see Chapter

9) showed that it is more efficient and effective to engineer the carriers than to mix spray dried lactose, L-leucine, and salbutamol sulphate.

Chapter 4 looked at spray dried mannitol-leucine carriers and it was concluded that the optimal FPF that was reached was from the 6% L-Leucine with a FPF of 52.96 + 5.21%. The results also confirmed that mannitol can serve as a suitable alternative carrier over lactose in DPI formulations and could be suitable for lactose intolerant patients suffering from asthma, COPD, or other lung diseases which can be treated via DPI formulations.[14] [224] [258] The physical mixture comparative study showed that it is more effective to engineer the carriers than to mix spray dried mannitol, L-leucine, and salbutamol sulphate (Albuterol sulphate). Finally, the results also supported the findings from Chapter 3 where it showed L-leucine's lubrication effect.

Chapter 5 looked at spray dried mannitol-lactose-leucine carriers and it was concluded that the optimal FPF that was reached was from the 1:3 [Mannitol:Lactose] carrier with a FPF of 61.42 $\pm$ 4.21%. Comparing this to the physical mixture comparative study, it was concluded that it is more efficient to engineer the carriers than to mix spray dried lactose, sprayed dried mannitol, L-leucine, and salbutamol sulphate. The use of 5% L-leucine (w/w) modified the physicochemical properties of the spray dried particles along with their morphology. The results also showcase the lubrication effect that L-leucine provides to the carriers upon aerosolization.

In chapter 6, the type of carrier was changed from lactose and mannitol to xylitol to see if

a more suitable carrier can be developed for DPI formulations with a high FPF. Therefore, in chapter 6 xylitol-leucine crystals as carriers were developed and it was concluded that the optimal FPF that was reached was from the Xylitol with 5% LEU with a FPF of 42.94 ± 15.21%; this was because the Commercial Xylitol (FPF = 44.13 ± 11.27) failed the uniformity assessment and, as a result, could not be used or implemented. Xylitol with 5% LEU had particles classified as tomahawk, which is known to show better aerosolized efficacy over particles with a spherical morphology. The results also showed that L-leucine altered the physicochemical properties of the carriers which affected their inter- and intra-molecular interactions. Comparing these formulations to the formulations in the physical mixture comparative study, it was concluded that it was more efficient to engineer the carriers than to simply mix xylitol, L-leucine, and salbutamol sulphate together.

In Chapter 7 the idea was to develop binary mixtures of some of there main carriers including lactose and mannitol to enhance the aerosolization performance of drugs from DPI formulations. The results concluded that the optimal FPF that was observed was from the 1:3 [Mannitol:Lactose] carrier with a FPF of 68.69 ± 4.65%. This formulation had crystals classified as rhombic in structure and out-performed the 1:3 [Mannitol:Lactose] carrier from Chapter 5 whose FPF was 61.42 ± 4.21%. The results also showed an inverse relationship between particle size and concentration of mannitol with regards to the dry system; when the concentration of mannitol increased the particle size decreased. In addition, there was a positive correlation between the concentration of mannitol and the particle size with respect to the wet system; when the concentration of mannitol

increased, the particle size of the carriers also increased. Comparing these results to the physical mixture comparative study (see Chapter 9), it was determined that it was more efficient and cost-effective to engineer the carriers rather than simply mixing mannitol, lactose, and salbutamol sulphate.

In other chapters, generally, salbutamol sulphate was physically added to the engineered carrier particles, whereas in Chapter 8 the idea was to develop an engineered carrier-API via a crystallization technology. The results proved that the optimal FPF that was observed was from the 2:1 [Salbutamol:Mannitol] carrier with a FPF of 62.53 $\pm$ 6.84%. This carrier had crystals that were classified as rhombic in structure. There was also an inverse relationship between the concentration of salbutamol and the particle size of the resultant crystals; when the concentration of salbutamol increased, the crystal size decreased. These carriers were also successfully air jet milled. Comparing these results to the physical mixture comparative study (see Chapter 9), it was concluded that it was more effective to engineer the carriers than to simply mix mannitol and salbutamol sulphate.

All in all, these results have shown that it is more efficient and cost-effective to engineer carriers for pulmonary delivery than to use commercially available products. They have also shown the impact that L-leucine, as an excipient, has on the overall aerosolization performance of any given carrier. This effect was shown via the lubrication effect that L-leucine provides when it is used as an excipient.[21] Using L-leucine also alters the physical

chemical properties of the resultant carrier in such a way as to allow for an increase in the aerosolization performance, measured via the carrier's FPF, to be seen.[342] L-Leucine also alters the carrier's morphology, creating more of an irregular shape, causing a change in the carrier's aerosolization profile.[345] Furthermore, the results also provide, and support, the notion that an irregular crystal has a better aerosolization performance than a more spherical shape crystal;[356] this was seen in a number of carriers that were used throughout this overall study. The results also show that the methodology that has been presented has the capability of altering the polymorphic form of the resultant carrier wether that be via spray drying or crystallization.

Moreover, commercially available DPI have emitted doses of approximately between 50% and 80% and FPFs between 20% and 40%, but this overall study showed that FPFs can reach almost 70%.[369, 370] Table 10.1 presents all of the carriers that were used throughout this overall study highlighting their FPF and %CV, which was used as an indicator for content homogeneity. As the table shows, the 1:3 [mannitol:lactose] crystal carrier was the most effective in reaching the highest FPF among all of the carriers. Throughout this overall study, one of the goals was to attain a high FPF and a low %CV. The carrier that was the most homogeneous (lowest %CV) was the spray dried 1:3 (mannitol:lactose) carrier with a %CV of 0.76%. On an overall case, however, the bet carrier and, thus, formulation was the 1:3 [mannitol:lactose] crystal carrier.

**Table 10.1.** Summary of all Formulations. Summary of all carriers used within this Thesis highlighting FPF and content homogeneity expressed as the percent coefficient of variation (%CV).

| Formulation | FPF (%) | % CV |
|---|---|---|
| Spray Dried Lactose | 25.51 ± 1.23 | 10.29 |
| SD Lactose w/ 0.1%$_L$-Leucine | 34.99 ± 8.89 | 7.15 |
| SD Lactose w/ 0.5% $_L$-Leucine | 47.11 ± 9.94 | 5.48 |
| SD Lactose w/ 1% $_L$-Leucine | 44.33 ± 6.53 | 17.92 |
| SD Lactose w/ 5% $_L$-Leucine | 43.08 ± 7.38 | 13.23 |
| SD Lactose w/ 10% $_L$-Leucine | 44.50 ± 17.40 | 8.65 |
| Spray Dried Mannitol | 37.06 ± 8.66 | 20.90 |
| SD Mannitol w/ 0.06% L-Leucine | 37.54 ± 2.46 | 3.88 |
| SD Mannitol w/ 0.3% L-Leucine | 38.86 ± 8.54 | 14.08 |
| SD Mannitol w/ 0.6% L-Leucine | 48.45 ± 9.44 | 11.94 |
| SD Mannitol w/ 3% L-Leucine | 47.19 ± 13.76 | 11.90 |
| SD Mannitol w/ 6% L-Leucine | 52.96 ± 5.21 | 13.38 |
| SD 1:1 (Mannitol:Lactose) | 42.58 ± 18.43 | 13.22 |
| SD 1:3 (Mannitol:Lactose) | 61.42 ± 4.21 | 23.47 |
| SD 3:1 (Mannitol:Lactose) | 42.85 ± 9.36 | 0.76 |
| Commercial Xylitol | 44.13 ± 11.27 | 13.35 |
| Xylitol with 0% LEU | 34.25 ± 16.98 | 11.72 |
| Xylitol with 1% LEU | 25.84 ± 11.05 | 19.68 |
| Xylitol with 5% LEU | 42.94 ± 15.21 | 13.83 |
| Xylitol with 10% LEU | 35.61 ± 12.58 | 2.52 |
| 1:1 (Mannitol:Lactose) | 52.34 ± 15.08 | 7.39 |
| 1:2 (Mannitol:Lactose) | 49.13 ± 5.94 | 6.27 |
| 2:1 (Mannitol:Lactose) | 56.49 ± 1.54 | 12.51 |
| 1:3 (Mannitol:Lactose) | 68.69 ± 4.65 | 5.88 |
| 3:1 (Mannitol:Lactose) | 41.18 ± 11.17 | 1.60 |
| 1:1 (Salbutamol:Mannitol) | 14.52 ± 1.94 | 2.30 |
| 1:2 (Salbutamol:Mannitol) | 49.47 ± 5.23 | 7.15 |
| 1:4 (Salbutamol:Mannitol) | 43.23 ± 5.04 | 2.16 |
| 2:1 (Salbutamol:Mannitol) | 62.53 ± 6.84 | 1.66 |

| | | |
|---|---|---|
| 4:1 (Salbutamol:Mannitol) | 57.39 ± 4.93 | 2.86 |

### *10.2 Future Work*

The research that has been presented in these chapters offer a major contribution to the field of chemistry and pharmaceutical sciences. They provide an insight into how to engineer carriers and tailor them for the usage via the pulmonary tract. Nevertheless, there are other methods and techniques that can be used which have not been discussed and/or implemented within this overall study.

One of those includes co-crystals; co-crystals represent a useful way of altering chemical properties at the atomic level, by choosing a suitable co-former that will form a specific non-covalent bond, to yield an engineered supramolecular architecture. Co-crystals are formulations of increasing interest to the pharmaceutical industry given their potential of improving the solubility and dissolution behavior, while also improving the physical stability of the active pharmaceutical ingredient compared to their pure state.

Co-crystals are defined as *crystalline single phase materials composed of two or more molecular and/or ionic compounds generally in a stoichiometric ratio which are neither solvents nor salts.* Co-crystals offer an opportunity to optimize physicochemical properties, such as solubility, stability, hydration, and melting point, mechanical properties, such as flowability and compressibility, pharmacokinetic properties,

bioavailability, and permeability. Because amorphous powders have a higher surface free energy over crystalline material, it makes crystalline material a more favorable choice for drug formulation. In addition, it has been shown that co-crystals also alter the bulk and surface properties of the active pharmaceutical ingredient (API) of interest.

Another technique that can be explored further and become implemented within this overall study is spray freeze drying. Spray freeze drying is a particle engineering technology that has been investigated in the production of inhalable powder formulations. It is a process that produces lyophilized powders with a spherical morphology and one that combines the advantages of both freeze-drying and spray-drying as the drying process is extremely mild and most powders are flowable without further processing.

Subsequently, the frozen solvents produce porous particles which affect the carrier's behavior and, consequently, affect their aerosolization performance. In addition, this technique also provides a mechanism to control the size of the particles that are produced. A parameter that has been shown, in this overall study, to have critical importance.

Furthermore, another technique that can be used to further this overall study's findings is that of 3D printing. Fused deposition modeling (FDM) is a type of extrusion 3D printing technology where a polymer filament is heated and extruded through a nozzle to create an object. These objects can have ultra-fine particles which are usually less than 100 nm

in size; these ultra-fine particles can be used, if engineered to agglomerate, as carriers or as is if made from the API of interest. The ultra-fine particles are released at rates of billions of particles per minute during operation. Moreover, these 3D printers are increasingly popular because of their low cost, low weight of filaments, processing flexibility, and ease of use.

Operating these printers is done with poly-lactic acid (PLA) which is derived from renewable sources like corn. PLA is popular because of its mechanical properties, biodegradability, and low cost. Something to consider, however, is whether or not they are safe to use for inhalation purposes.

# References


1. Ali Nokhodchi and Gary P. Martin. *Pulmonary Drug* Delivery- Advances and Challenges. Wiley. 2015. ISBN:9781118799543.
2. Byron PR, Pathon JS. Drug delivery via the respiratory tract. J Aerosol Med. 1994;7:49–75.
3. Courrier HM, Butz N, Vandamme TF. Pulmonary drug delivery systems: recent developments and prospects. *Critical Reviews in Therapeutic Dug Carrier Systems.* 2002; 19 (4-5); 425-98.
4. Massaro GD, Massaro D.Formulation of pulmonary alveoli and gas exchange surface area: quantitative and regulation. *Annual Review of Physiology.* 1996; 58: 73-92.
5. Byron PR, Patton JS. Drug delivery via the respiratory tract. *Journal of Aerosol Medicine.* 1994; 7 (1): 49-75
6. Patton JS, Byron PR. Inhaling medicines: delivering drugs to the body through the lungs. *Nature Reviews Drug Discovery.* 2007; 6 (1): 67-74
7. Byron PR, Hindle M, Lange CF, et. al. In vivo-in vitro correlations: predicting pulmonary drug deposition from pharmaceutical aerosols. *Journal of Aerosol Medicine and Pulmonary Drug Delivery.* 2010; 23 (Suppl. 2): S59-69.
8. Donovan MJ, Kim SH, Raman V, Smyth HD. Dry powder inhaler device influence on carrier particle performance. J Pharm Sci. 2012;101:1107.
9. Chow AHL, Tong HHY, Chattopadhyay P, Shekunov BY. Particle engineering for pulmonary drug delivery. Pharm Res. 2007;24: 411–37.
10. De Boer AH, Hagedoorn P, Gjaltema D, Goede J, Frijlink HW. Air classifier technology (ACT) in dry powder inhalation: part 1. Introduction of a novel force distribution concept (FDC) explaining the performance of a basic air classifier on adhesive mixtures. Int J Pharm. 2003;260:187–200.
11. De Boer AH, Chan HK, Price R. A critical view on lactose-based drug formulation and devise studies for dry powder inhalation: which are relevant and what interactions to expect? Adv Drug Del Rev. 2012;64:257–74.
12. Thalberg K, Berg E, Fransson M. Modeling dispersion of dry pow- ders for inhalation: the concepts of total fines, cohesive energy and interaction parameters. Int J Pharm. 2012;427:224–33.
13. Newman SP, Busse WW. Evolution of dry powder inhaler design, formulation, and performance. Resp Med. 2002;96:293–304.
14. Smyth HDC, Hickey AJ. Carriers in dry powder delivery: implications for inhalation system design. *American Journal of Drug Delivery*. 2005. 3 (2):117-32.
15. Newman SP. Aerosol deposition considerations in inhalation therapy. *Chest*. 1985; 88 (Suppl. 2): 152S-60S.
16. Martonen TB. Mathematical model for the selective deposition of inhaled pharmaceuticals. *Journal of Pharmaceutical Sciences.* 1993; 82 (12): 1191-9.
17. C Darquenne. Particle Deposition in the Lung. 2006 Elsevier Ltd. All rights reserved.
18. Heyder J. Alveolar deposition of inhaled particles in humans. *American Industrial Hygiene Association Journal.* 1982; 43 (11): 864-6.
19. Heyder J. Particle transport onto human airway surfaces. *European Journal of Respiratory Diseases Supplement.* 1982; 119: 29-50.
20. Schulz H, Brand P, and Heyder J. Particle deposition in the respiratory tract. In: Gehr P, ans Heyder J, eds, Particle-Lung Interactions. Marcel Dekker, Inc. New York. 2000.
21. Yeh HC, Schum GM. Models of human lung airways and their appliction to inhaled particle deposition. *Bulletin of Mathematical Biology.* 1980;42 (3): 461-80.
22. Kim CS, Hu SC. Regional deposition of inhaled particles in human lungs: comparison between men and women. *Journal of Applied Physiology (1985).* 1998; 84 (6): 1834-44.
23. Lippman M, Yeates DB, Albert RE. Deposition, retention, and clearance of inhaled particles. *British Journal of Industrial Medicine.* 1980; 37 (4): 337-62.
24. Lourenco RV, Cotromanes E. Clinical aerosols II. *Therapeutic aerosols. Archives of International Medicine.* 1982; 142 (13): 2299-308.

25. Lavorini F, Magnan A, Dubus JC, *et. al.* Effect of incorrect use of dry powder inhalers on management of patients with asthma and COPD. *Respiratory Medicine*. 2008; 102 (4): 593-604.
26. Villax P, McDermott IG, Brunce M. *Single Inhaler*. US8109267 B2, 2012.
27. De Boer AH, Gjaltema D, Hagedoorn P, Frijlink HW. Comparative *in vitro* performance evaluation of the Novopulmon 200 Novolizer and Budesonide-ratiopharm Jethaler: two novel budesonide dry powder inhalers. *Die Pharmaie*. 2004; 59 (9); 692-99.
28. Al-Showair, RAM, Tarsin WY, Assi KH, *et. al.* Can all patients with COPD use the correct inhalation flow with all inhalers and does training help? *Respiratory Medicine*. 2007; 101 (1); 2395-401.
29. S. R. Percy, Improvement in drying and concentrating liquid substances by atomizing, US Patent US125406, 1872.
30. Vehring, R., 2008. Pharmaceutical particle engineering via spray drying. Pharm. Res. 25, 999–1022.
31. C. Kemp, in: E. Tsotsas, A.S. Mujumdar (Eds.), Fundamentals of energy analysis of dryers, Modern Drying Technology: Energy Savings, vol. 4, Wiley-VCH Verlag GmbH & Co. KGaA, Weinheim, Germany 2011, pp. 1–45.
32. A.S. Mujumdar, Handbook of Industrial Drying, fourth ed. CRC Press, Florida, 2014. 33. D.M. Parikh, Handbook of Pharmaceutical Granulation Technology, third ed. CRC Press, New York, 2009.
34. Singh, Abhisek and Van den Mooter, Guy. Spray drying formulation of amorphous solid dispersions. Advanced Drug Delivery Reviews. 100; 27-50. 2016.
35. Curatolo W, Nightingale J, Herbig S. Utility of hydroxypropyl- methylcellulose acetate succinate (HPMCAS) for initiation and maintenance of drug supersaturation in the GI milieu. Pharm Res. 2009;26:1419–31.
36. Gao P. Amorphous pharmaceutical solids: characterization, stabilization, and development of marketable formulations of poorly soluble drugs with improved oral absorption. Mol Pharm. 2008;5:903–4.
37. Ré, M.-I., 2006. Formulating drug delivery systems by spray drying. Dry. Technol. 24, 433–446.
38. Chiou, W.L., Rielman, S., 1971. Pharmaceutical application of solid dispersion system. J. Pharm. Sci. 60, 1281–1302.
39. Amrit Paudel, Zelalem Ayenew Worku, Joke Meeus, Sandra Guns, Guy Van den Mooter. Manufacturing of solid dispersions of poorly water soluble drugs by spray drying: Formulation and process considerations. International Journal of Pharmaceutics 453 (2013) 253–284.
40. J.W. Lubach, D. Xu, B.E. Segmuller, E.J. Munson, Investigation of the effects of phar- maceutical processing upon solid-state NMR relaxation times and implications to solid-state formulation stability, J. Pharm. Sci. 96 (2007) 777–787.
41. M. Sugimoto, T. Okagaki, S. Narisawa, Y. Koida, K. Nakajima, Improvement of disso- lution characteristics and bioavailability of poorly water-soluble drugs by novel cogrinding method using water-soluble polymer, Int. J. Pharm. 160 (1998) 11–19.
42. R. Dontireddy, A.M. Crean, A comparative study of spray-dried and freeze-dried hydrocortisone/polyvinyl pyrrolidone solid dispersions, Drug Dev. Ind. Pharm. 37 (2011) 1141–1149.
43. S. Guns, A. Dereymaker, P. Kayaert, V. Mathot, J.A. Martens, G. Van den Mooter, Comparison between hot-melt extrusion and spray-drying for manufacturing solid dispersions of the graft copolymer of ethylene glycol and vinylalcohol, Pharm. Res. 28 (2011) 673–682.
44. O. Mahmah, R. Tabbakh, A. Kelly, A. Paradkar, A comparative study of the effect of spray drying and hot-melt extrusion on the properties of amorphous solid dispersions containing felodipine, J. Pharm. Pharmacol. 66 (2014) 275–284.
45. A.M. Agrawal, M.S. Dudhedia, A.D. Patel, M.S. Raikes, Characterization and perfor- mance assessment of solid dispersions prepared by hot melt extrusion and spray drying process, Int. J. Pharm. 457 (2013) 71–81.
46. Maltesen MJ, et al. Quality by design—spray-drying of insulin intended for inhalation. Eur J Pharm Biopharm. 2008;70:828–38.
47. Prinn K, et al. Statistical modeling of protein spray-drying at the lab scale. AAPS PharmSciTech. 2002;3(1):E4.
48. Oakley DE. Spray dryer modeling in theory and practice. Dry Technol. 2004;22:1371–402.
49. E. Dobry, D.M. Settell, J.M. Baumann, Spray drying and scale-up, Pharmaceutical Sciences Encyclopedia, John Wiley & Sons, Inc. 2015, pp. 1–26.

50. F. Gaspar, J. Vicente, F. Neves, J.-R. Authelin, Spray drying: scale-up and manufacturing, in: N. Shah, H. Sandhu, D.S. Choi, H. Chokshi, A.W. Malick (Eds.), Amorphous Solid Dispersions, Springer, New York 2014, pp. 261–302.
51. K. Masters, Spray Drying Handbook, fifth ed. Longman Scientific & Technical, New York, 1991.
52. Nonelectrolytes, in: P.J. Sinko (Ed.), Martin's Physical Pharmacy and Pharmaceuti- cal Sciences, fifth ed.Lippincott Williams & Wilkins, New Delhi 2006, pp. 119–141.
53. K. Rizi, R.J. Green, M. Donaldson, A.C. Williams, Production of pH-responsive micro- particles by spray drying: investigation of experimental parameter effects on mor- phological and release properties, J. Pharm. Sci. 100 (2011) 566–579.
54. H. Al-Obaidi, S. Brocchini, G. Buckton, Anomalous properties of spray dried solid dispersions, J. Pharm. Sci. 98 (2009) 4724–4737.
55. M. Farid, A new approach to modelling of single droplet drying, Chem. Eng. Sci. 58 (2003) 2985–2993.
56. E.H.J. Kim, X. Dong Chen, D. Pearce, On the mechanisms of surface formation and the surface compositions of industrial milk powders, Drying Technol. 21 (2003) 265–278.
57. M. Mezhericher, A. Levy, I. Borde, Spray drying modelling based on advanced drop- let drying kinetics, Chem. Eng. Process. 49 (2010) 1205–1213.
58. D. Chiou, T. Langrish, R. Braham, The effect of temperature on the crystallinity of lactose powders produced by spray drying, J. Food Eng. 86 (2008) 288–293.
59. R. Aftel, A.K. Gupta, C. Cook, C. Presser, Gas property effects on droplet atomization and combustion in an air-assist atomizer, Symposium (International) on Combus- tion, Elsevier 1996, pp. 1645–1651.
60. S. Özbilen, Influence of atomising gas on particle characteristics of Al, Al–1 wt-% Li, Mg, and Sn powders, Powder Metall. 43 (2000) 173–180.
61. T. Kudra, M. Poirier, Gaseous carbon dioxide as the heat and mass transfer medium in drying, Drying Technol. 25 (2007) 327–334.
62. M.I.U. Islam, T.A.G. Langrish, The effect of different atomizing gases and drying media on the crystallization behavior of spray-dried powders, Drying Technol. 28 (2010) 1035–1043.
63. D.W. Green, Perry's Chemical Engineers' Handbook, eighth ed. McGraw-hill, New York, 2008.
64. Lane, W. R. A microburrette for producing small liquid drops of known size. Journal of Scientific Instruments. 24. 98-101; 1949.
65. Liu, W., Chen, X. D., and Selomulya, C. On the spray drying of uniform microparticles. Particuology. 22. 1-12; 2015.
66. Anders, K., Roth,N., and Frohn, A. Operation characteristics of vibrating-orifice generators: The coherence length. Particle and Particle Systems Characterization. 9. 40-43; 1992.
67. J.T. Edward, Molecular volumes and the Stokes–Einstein equation, J. Chem. Educ. 47 (1970) 261.
68. R. Vehring, W.R. Foss, D. Lechuga-Ballesteros, Particle formation in spray drying, J. Aerosol Sci. 38 (2007) 728–746.
69. S. Wang, T. Langrish, A review of process simulations and the use of additives in spray drying, Food Res. Int. 42 (2009) 13–25.
70. Healy, A.M., McDonald, B.F., Tajber, L., Corrigan, O.I., 2008. Characterisation of excipient-free nanoporous microparticles (NPMPs) of bendroflumethiazide. Eur. J. Pharm. Biopharm. 69, 1182–1186.
71. Papelis, C., Um, W., Russel, C.E., Chapman, J.B., 2003. Measuring the specific surface area of natural and manmade glasses: effects of formation process, morphology, and particle size. Colloids Surf. A: Physicochem. Eng. Aspects 215, 221–239.
72. S. Nešić, J. Vodnik, Kinetics of droplet evaporation, Chem. Eng. Sci. 46 (1991) 527–537.
73. Vehring R. Pharmaceutical particle engineering via spray-drying. Pharm Res. 2007;25:999–1022.
74. Oakley DE. Spray dryer modeling in theory and practice. Dry Technol. 2004;22:1371–402.
75. Maltesen MJ, et al. Quality by design—spray-drying of insulin intended for inhalation. Eur J Pharm Biopharm. 2008;70:828–38.
76. Prinn K, et al. Statistical modeling of protein spray-drying at the lab scale. AAPS PharmSciTech. 2002;3(1):E4.

77. A. Billon, B. Bataille, G. Cassanas, M. Jacob, Development of spray-dried acetaminophen microparticles using experimental designs, Int. J. Pharm. 203 (2000) 159–168.
78. V. Nekkanti, T. Muniyappan, P. Karatgi, M.S. Hari, S. Marella, R. Pillai, Spray-drying process optimization for manufacture of drug–cyclodextrin complex powder using design of experiments, Drug Dev. Ind. Pharm. 35 (2009) 1219–1229.
79. T. Mihajlovic, S. Ibric, A. Mladenovic, Application of design of experiments and multilayer perceptron neural network in optimization of the spray-drying process, Drying Technol. 29 (2011) 1638–1647.
80. M.J. Maltesen, S. Bjerregaard, L. Hovgaard, S. Havelund, M. Van De Weert, Quality by design—spray drying of insulin intended for inhalation, Eur. J. Pharm. Biopharm. 70 (2008) 828–838.
81. M.J. Maltesen, M. Van de Weert, H. Grohganz, Design of experiments-based mon- itoring of critical quality attributes for the spray-drying process of insulin by NIR spectroscopy, AAPS PharmSciTech 13 (2012) 747–755.
82. Spray-drying nanocapsules in presence of colloidal silica as drying auxiliary agent: formulation and process variables optimization using experimental designs, Pharm. Res. 24 (2007) 650–661.
83.D. Ormes, D. Zhang, A.M. Chen, S. Hou, D. Krueger, T. Nelson, A. Templeton, Design of experiments utilization to map the processing capabilities of a micro-spray dryer: particle design and throughput optimization in support of drug discovery, Pharm. Dev. Technol. 18 (2013) 121–129.
84. A. Baldinger, L. Clerdent, J. Rantanen, M. Yang, H. Grohganz, Quality by design ap- proach in the optimization of the spray-drying process, Pharm. Dev. Technol. 17 (2012) 389–397.
85. I.C.H.H.T. Guideline, Pharmaceutical Development Q8 (R2), Step, 42009.
86. A.S. Rathore, H. Winkle, Quality by design for biopharmaceuticals, Nat. Biotechnol. 27 (2009) 26–34.
87. Yu, L.X., Lionberger, R.A., Raw, A.S., D'Costa, R., Wu, H., Hussain, A.S., 2004. Applications of process analytical technology to crystallization processes. Adv. Drug Deliv. Rev. 56, 349– 369.
88. Lebrun, P., Krier, F., Mantanus, J., Grohganz, H., Yang, M., Rozet, E., Boulanger, B., Evrard, B., Rantanen, J., Hubert, P., 2012. Design space approach in the optimization of the spray-drying process. Eur. J. Pharm. Biopharm. 80, 226–234.
89. Kramek-Romanowska, Katarzyna, Odziomek, Marcin, Sosnowski, Tomasz R., and Gradon, Leon. Effects of process variables on the properties of spray dried mannitol and mannitol/disodium cromoglycate powders suitable for drug delivery by inhalation. Ind. Eng. Chex. Res. 50; 13922-13931. 2011.
90. Behera, A.L., Sahoo, S.K., Patil, S.V., 2010. Enhancement of solubility: A pharmaceutical overview. Der Pharmacia Lett. 2, 310–318.
91. Buchi Technical Documents, 2015.
92. T.A.G. Langrish, Assessing the rate of solid-phase crystallization for lactose: the ef- fect of the difference between material and glass-transition temperatures, Food Res. Int. 41 (2008) 630–636.
93. D.A. Miller, M. Gill, Spray-drying technology, in: R.O. Williams III, A.B. Watts, D.A. Miller (Eds.), Formulating Poorly Water Soluble Drugs, Springer Science & Business Media, New York 2011, pp. 363–442.
94. E.M. Littringer, A. Mescher, S. Eckhard, H. Schröttner, C. Langes, M. Fries, U. Griesser, P. Walzel, N.A. Urbanetz, Spray drying of mannitol as a drug carrier—the impact of process parameters on product properties, Drying Technol. 30 (2012) 114–124.
95. K. Ståhl, M. Claesson, P. Lilliehorn, H. Lindén, K. Bäckström, The effect of process variables on the degradation and physical properties of spray dried insulin intended for inhalation, Int. J. Pharm. 233 (2002) 227–237.
96. M.G. Abiad, O.H. Campanella, M.T. Carvajal, Effect of spray drying conditions on the physicochemical properties and enthalpy relaxation of α-lactose, Int. J. Food Prop. 17 (2014) 1303–1316.
97. Van Campen, L., Amidon, G.L., Zografi, G., 1983. Moisture sorption kinetics for water- soluble substances I: Theoretical considerations of heat transport control. J. Pharm. Sci. 72, 1381–1388. doi:http://dx.doi.org/10.1002/jps.2600721204.
98. Schwartzbach H. A risk-based approach to product and process quality in spray-drying. Pharm Technol. 2008.
99. Taylor (1964)

100. Goedde and Yuen (1970)
101. Lee (2002)
102. Rattes, A.L.R., Oliveira, W.P., 2007. Spray drying conditions and encapsulating composition effects on formation and properties of sodium diclofenac microparticles. Powder Technol. 171, 7–14.
103. Bittner, B., Kissel, T., 1999. Ultrasonic atomization for spray drying: a versatile technique for the preparation of protein loaded biodegradable microspheres. J. Microencapsulation 16, 325– 341.
104. Cal, K., Sollohub, K., 2010. Spray drying technique. I: Hardware and process parameters. J. Pharm. Res. 99, 575–586.
105. Mizoe, T., Beppu, S., Ozeki, T., Okada, H., 2007. One-step preparation of drug-containing microparticles to enhance the dissolution and absorption of poorly water-soluble drugs using a 4-fluid nozzle spray drier. J. Control. Release 120, 205–210.
106. Chen, R., Okamoto, H., Danjo, K., 2008. Preparation of functional composite particles of salbutamol sulfate using a 4-fluid nozzle spray-drying technique. Chem. Pharm. Bull. 56, 254–259.
107. Samantha Keshani, Wan Ramli Wan Daud, M. M. Nourouzi, Farideh Namvar, and Mostafa Ghasemi. Spray drying: An overview on wall deposition, process and modeling. Journal of Food Engineering. 146; 152-162. 2015.
108. Masters. Spray Drying Handbook, third ed. G.Godwin, New York. 1994.
109. Oakley, D. Scale-up of spray dryers with the aid of computational fluid dynamics. Drying Technol. 12 (1–2), 217–233. 1994.
110. Huang, L., Kumar, K., Mujumdar, A., 2003b. Use of computational fluid dynamics to evaluate alternative spray dryer chamber configurations. Drying Technol. 21 (3), 385–412.
111. Huang, L., Kumar, K., Mujumdar, A.S., 2003a. A parametric study of the gas flow patterns and drying performance of co-current spray dryer: results of a computational fluid dynamics study. Drying Technol. 21 (6), 957–978.
112. Keshani, S., Montazeri, M.H., Daud, W.R.W., Nourouzi, M.M., 2014. CFD Modeling of Air Flow on Wall Deposition in Different Spray Dryer Geometries. Drying Technology (in press).
113. Huang, L.X., Kumar, K., Mujumdar, A.S., 2006. A comparative study of a spray dryer with rotary disc atomizer and pressure nozzle using computational fluid dynamic simulations. Chem. Eng. Process. 45 (6), 461–470.
114. Roos, Y., 2009. Solid and liquid states of lactose. Adv. Dairy Chem., 17–34.
115. Shrestha, A.K., Howes, T., Adhikari, B.P., Bhandari, B.R., 2008. Spray drying of skim milk mixed with milk permeate: effect on drying behavior, physicochemical properties, and storage stability of powder. Drying Technol. 26 (2), 239–247.
116. J.E. Patterson, M.B. James, A.H. Forster, T. Rades, Melt extrusion and spray drying of carbamazepine and dipyridamole with polyvinylpyrrolidone/vinyl acetate copoly- mers, Drug Dev. Ind. Pharm. 34 (2008) 95–106.
117. Roos, Y., Karel, M., 1991. Applying state diagrams to food processing and development. Food Technol. 45 (12), 66, 68.
118. M. Ameri, Y.F. Maa, Spray drying of biopharmaceuticals: stability and process considerations, Drying Technol. 24 (2006) 763–768.
119. K. Sollohub, K. Cal, Spray drying technique: II. Current applications in pharmaceutical technology, J. Pharm. Sci. 99 (2010) 587–597.
120. D.E. Dobry, D.M. Settell, J.M. Baumann, R.J. Ray, L.J. Graham, R.A. Beyerinck, A model-based methodology for spray-drying process development, J. Pharm. Innov. 4 (2009) 133–142.
121. Brennan, J., Herrera, J., Jowitt, R., 1971. A study of some of the factors affecting the spray drying of concentrated orange juice, on a laboratory scale. Int. J. Food Sci. Technol. 6 (3), 295–307.
122. Bhandari, B.R., Datta, N., Crooks, R., Howes, T., Rigby, S., 1997. A semi-empirical approach to optimise the quantity of drying aids required to spray dry sugar- rich foods. Drying Technol. 15 (10), 2509–2525.
123. Meerdink, G., van't Riet, K., 1995. Modeling segregation of solute material during drying of liquid foods. AIChE J. 41 (3), 732–736.
124. Vasconcelos, T., Sarmento, B., Costa, P., 2007. Solid dispersion as strategy to improve oral bioavailability of poor water soluble drugs. Drug Discov. Today 12, 1068–1075.

125. Mooter, G.V.D., 2011. The use of amorphous solid dispersions: a formulation strategy to overcome poor solubility and dissolution rate. Drug Discov. Today: Technol.. http://dx.doi.org/10.1016/j.ddtec.2011.10.002.
126. P. Parimaladevi, K. Srinivasan. Achievement of favorable uniform crystal size distribution of alpha-lactose monohydrate ($\alpha$-LM) through swift cooling process. Journal of Food Engineering 151 (2015) 1–6
127. D.E. Alonzo, S. Raina, D. Zhou, Y. Gao, G.G. Zhang, L.S. Taylor, Characterizing the impact of hydroxypropylmethyl cellulose on the growth and nucleation kinetics of felodipine from supersaturated solutions, Cryst. Growth Des. 12 (2012) 1538–1547.
128. Kaialy, W., Hussain, T., Alhalaweh, A., Nokhodchi, A., 2014. Towards a more desirable dry powder inhaler formulation: large spray-dried mannitol microspheres outperform small microspheres. Pharm. Res. 31, 60–76.
129. H.H.Y. Tong, A.H.L. Chow, Control of physical forms of drug particles for pul- monary delivery by spray drying and supercritical fluid processing, KONA 24 (2006) 27–40.
130. T.A.G. Langrish, Assessing the rate of solid-phase crystallization for lactose: the effect of the difference between material and glass-transition temperature, Food Research International 41 (2008) 630–636.
131. M.L. Williams, R.F. Landel, J.D. Ferry, The temperature dependence of relax- ation mechanisms in amorphous polymers and other glass-forming liquids, J. American Chemical Society 77 (1955) 3701–3707.
132. B.C. Hancock, M. Parks, What is the true solubility advantage for amorphous pharmaceuticals?, Pharm Res. 17 (2000) 397–404.
133. de Bruijn, T. J. W.; de Jong, W. A.; van den Berg, P. J. Kinetic. Parameters in in Avrami-Erofeev Type Reactions from Isothermal and Non-Isothermal Experiments Themochim. Acta. 1981, 45, 315-325.
134. Johnson, W. A. and Mehl, R. F. Reaction Kinetics in Processes of Nucleation and Growth. Trans. Am. Inst. Min. Eng. 1939, 135, 416-442
135. Avrami, M. Kinetics of phase change. I. General theory. J. Chem. Phys. 1939, 7, 1103-1112.
136. Avrami, M. Kinetics of phase change. II. Tranformation-time relations for random distribution of nuclei. J. Chem. Phys. 1940, 8, 212-224.
137. Avrami, M. Granulation, phase change, and microstructure. Kinetics of phase change. III. J. Chem. Phys. 1941, 9, 177-184.
138. ERIC A. SCHMITT,* DEVALINA LAW, AND GEOFF G. Z. ZHANG. Nucleation and Crystallization Kinetics of Hydrated Amorphous Lactose above the Glass Transition Temperature. Journal of Pharmaceutical Sciences Vol. 88, No. 3, March 1999
139. C.L.N. Vo, C. Park, B.J. Lee, Current trends and future perspectives of solid disper- sions containing poorly water-soluble drugs, Eur. J. Pharm. Biopharm. 85 (2013) 799–813.
140. Bernhard Rupp. Origin and use of crystallization phase diagrams. Acta Cryst. 2015. F71, 247–260.
141. Mansouri, M., Pouretedal, H.R., Vosoughi, V., 2011. Preparation and characterization of ibuprofen nanoparticles by using solvent/antisolvent precipitation. Open Conf. Proc. J. 2, 88–94.
142. Dirksen, J.A., Ring, T.A., 1991. Fundamentals of crystallization: kinetic effects on particle size distribution and morphology. Chem. Eng. Sci. 46, 2389–2427.
143. Jennifer Chia Wee Fern, Shuji Ohsaki, Satoru Watano, Robert Pfeffer. Continuous synthesis of nano-drug particles by antisolvent crystallization using a porous hollow-fiber membrane module. International Journal of Pharmaceutics 543 (2018) 139–150
144. Tsuge, H., Yoshizawa, S., Tsuzuki, M., 1996. Reactive crystallization of calcium phosphate. Chem. Eng. Res. Des. 74, 797–802.
145. Irem Altan, Patrick Charbonneau, and Edward H. Snell. Computational crystallization. *Arch Biochem Biophys*. 2016 July 15; 602: 12–20. doi:10.1016/j.abb.2016.01.004.
146. McPherson, A. Crystallization of Biological Macromolecules. Cold Spring Harbor Laboratory; 1999.
147. Derewenda ZS. Acta Crystallogr. D Biol. Crystallogr. 2010; 66:604–615. [PubMed: 20445236]

148. Anderson MJ, Hansen CL, Quake SR. Proc. Natl. Acad. Sci. U. S. A. 2006; 103:16746–16751.

[PubMed: 17075056]
149. Saridakis E, Chayen NE. Trends Biotechnol. 2009; 27:99–106. [PubMed: 19110330]
150. Asherie N. Methods. 2004; 34:266–272. [PubMed: 15325646]
151. Sleutel M, Lutsko JF, Maes D, Van Driessche AES. Phys. Rev. Lett. 2015; 114
152. Romero, S.; Escalera, B.; Bustamante, P. Solubility behavior of polymorphs I and II of mefenamic acid in solvent mixtures. *Int. J. Pharm.* **1999**, *178*, 193–202.
153. Givand, J.C.; Teja, A.S.; Rousseau, R.W. Effect of relative solubility on amino acid crystal purity. *AlChE J.* **2001**, *47*, 2705–2712.
154. Holmbäck, X.; Rasmuson, Å.C. Size and morphology of benzoic acid crystals produced by drowning-out crystallisation. *J. Cryst. Growth* **1999**, *198*, 780–788.
155. Charmolue, H.; Rousseau, R.W. L-serine obtained by methanol addition in batch crystallization. *AlChE J.* **1991**, *37*, 1121–1128.
156. Ålander, E.M.; Rasmuson, Å.C. Mechanisms of crystal agglomeration of paracetamol in acetone-water mixtures. *Ind. Eng. Chem. Res.* **2005**, *44*, 5788–5794.
157. Yu, Z.Q.; Tan, R.B.H.; Chow, P.S. Effects of operating conditions on agglomeration and habit of paracetamol crystals in anti-solvent crystallization. *J. Cryst. Growth* **2005**, *279*, 477–488.
158. Kitamura, M.; Sugimoto, M. Anti-solvent crystallization and transformation of thiazole-derivative polymorphs—I: Effect of addition rate and initial concentrations. *J. Cryst. Growth* **2003**, *257*, 177–184.
159. Morissette, S.L.; Almarsson, Ö.; Peterson, M.L.; Remenar, J.F.; Read, M.J.; Lemmo, A.V.; Ellis, S.; Cima, M.J.; Gardner, C.R. High-throughput crystallization: polymorphs, salts, co-crystals and solvates of pharmaceutical solids. *Adv. Drug Deliv. Rev.* **2004**, *56*, 275–300.
160. Roelands, C.M.; Jiang, S.; Kitamura, M.; ter Horst, J.H.; Kramer, H.J.; Jansens, P.J. Antisolvent crystallization of the polymorphs of L-histidine as a function of supersaturation ratio and of solvent composition. *Cryst. Growth Des.* **2006**, *6*, 955–963.
161. Granberg, R.A., Bloch, D.G., Rasmuson, A.C., 1999. Crystallization of paracetamol in acetone-water mixtures. J. Crys. Growth 198, 1287–1293.
162. Tavare, N.S., 1989. Micromixing limits in an MSMPR crystallizer. Chem. Eng. Tech. 12, 1–12.
163. Betke, A., Kickelbick, G., 2014. Bottom-up, wet chemical technique for the continuous synthesis of inorganic nanoparticles. Inorganics 2, 1–15.
164. Legg, B.A., Zhu, M., Waychunas, G., Gilbert, B., Banfield, J.F., 2016. A model for nucleation when nuclei are nonstoichiometric: understanding the precipitation of iron oxyhydroxide nanoparticles. Cryst. Growth Des. 16, 5726–5737.
165. Sun, X.Y., Ouyang, J.M., 2017. Time-dependent subcellular structure injuries induced by nano-/micron-sized calcium oxalate monohydrate and dehydrate crystals. Mater. Sci. Eng. C 79, 445–456.
166. Jennifer Chia Wee Fern, Shuji Ohsaki, Satoru Watano, Robert Pfeffer. Continuous synthesis of nano-drug particles by antisolvent crystallization using a porous hollow-fiber membrane module. International Journal of Pharmaceutics 543 (2018) 139–150
167. Zarkadas, D.M., Sirkar, K.K., 2006. Antisolvent crystallization in porous hollow fiber devices. Chem. Eng. Sci. 61, 5030–5048.
168. Kieffer, R., Mangin, D., Puel, F., Charcosset, C., 2009. Precipitation of barium sulphate in a hollow fiber membrane contactor, Part I: investigation of particulate fouling. Chem. Eng. Sci. 64, 1759–1767.
169. Chen, D., Singh, D., Sirkar, K.K., Pfeffer, R., 2015. Continuous synthesis of polymer- coated drug particles by porous hollow fiber membrane-based antisolvent crystal- lization. Langmuir 31, 432–441.
170. Genck, W.J., D'Aquino, R.L., 2000. Better growth in batch crystallizers. Chem. Eng. 107, 90–95.
171. Sohnel, O., Garside, J., 1992. Precipitation: Basic Principles and Industrial Applications. Butterworth-Heinemann, Newton, MA.
172. US Food and Drug Administration. 2018. Metered Dose Inhaler (MDI) and Dry Powder Inhaler (DPI) Products - Quality Considerations- Guidance for Industry.
173. See Tittle 21 Code of Federal Regulations 3.2(e).
174. See Tittle 21 Code of Federal Regulations part 4 available at https://www.accessdata.fda.gov/scripts/cdrh/cfdocs/cfcfr/cfrsearch.cfm?cfrpart=4
175. See Tittle 21 Code of Federal Regulations 820.30

176. See Tittle 21 Code of Federal Regulations 820
177. https://www.edqm.eu/en/european-pharmacopoeia-commission
178. https://www.edqm.eu/en/european-pharmacopoeia-background-50.html
179. Anjali Verma & Satya Vir Singh (2015) Spray Drying of Fruit and Vegetable Juices—A Review, Critical Reviews in Food Science and Nutrition, 55:5, 701-719, DOI: 10.1080/10408398.2012.672939
180. Mani, S., Jaya, S. and Das, H. (2002). Sticky Issues on Spray Drying of Fruit Juices September 27–28, Paper No: MBSK 02-201 An ASAE Meeting Pre- sentation.
181. Karel, M. and Lund, D. B. (2003). Physical principles of food preservation. *Food Sci. Technol.* **129**:360–441.
182. Adhikari, B., Howes, T., Bjandari, B. R. and Troung, V. (2004). Effect of addition of maltodextrin on drying kinetics and stickiness of sugar and acid- rich foods during convective drying experiments and modelling. *J. Food Eng.* **62**(1):53–68.
183. Adhikari, B., Howes, T. and Troung, V. (2003). Surface stickiness of drops of carbohydrates and organic acid solutions during convective drying: Experi- ments and modelling. *Drying Technol.* **21**(5):839–873.
184. Grabowski, J. A., Truong, V. D. and Daubert, C. R. (2006). Spraydrying of amylase hydrolyzed sweetpotato puree and physicochemical properties of powder. J. Food Sci. **71**:E209–E217.
185. Karatas, S. (1989). A laboratory scraped surface drying chamber for spray dry- ing of tomato paste. *Lebensmittel-Wissenschaft und Technologie* **23**(4):354– 357.
186. Karatas, S. and Esin, A. (1994). Determination of moisture diffusivity and behavior of tomato concentrate droplets during drying in air. *Drying Technol.* **12**(4):799–822.
187. Masters, K. (1994). Scale-up of Spray dryers. *Drying Technol.* **12**:235– 257.
188. Masters, K. (1985). Spray Drying Handbook. 4th ed. Longman Scientific and Technical, England.
189. Ponting, J. D., Stanley, W. L. and Copley, M. J. (1973). Fruit and vegetables juices. **In**: Food Dehydration. 2nd ed., pp. 211–215. Van Arsdel, B. S., Copley, M. J. and Morgan, A. I., Eds., AVI Publishing Company Inc., Westport, Connecticut.
190. Bhandari, S. R., Datta, N. and Howes, T. (1997). Problems associate with spray drying of sugar-rich foods. *Drying Technol.* **15**(2):671–684.
191. Tonon, R. V., Brabet, C. and Hubinger, M. D. (2008). Influence of process con- ditions on the physicochemical properties of acai (Euterpe oleraceae Mart.) powder produced by spray drying. *J. Food Eng.* **88**:411–418.
192. Tonon, R. V., Brabet, C. and Hubinger, M. D. (2010). Anthocyanin stability and antioxidant activity of spray-dried açai (Euterpe oleracea Mart.) juice produced with different carrier agents. *Food Res. Int.* **43**:907–914.
193. Khalil, M. A. and Sial, M. B. (1974). Spray drying of mango juice powder. *Mesopotamia J. Agricult.* **9**(1/2):47–56.
194. Goula, A. M., Karapantsios, T. D., Achilias, D. S. and Adamopoulos, K. G. (2008). Water sorption isotherms and glass transition temperature of spray dried tomato pulp. *J. Food Eng.* **85**:73–83.
195. Chang C, Nickerson MT. Encapsulation of omega 3-6-9 fatty acids-rich oils using protein-based emulsions with spray drying.J Food Sci Technol. 2018 Aug;55(8):2850-2861. doi: 10.1007/s13197-018-3257-0. Epub 2018 Jun 19.
196. Papillo VA, Locatelli M, Travaglia F, Bordiga M, Garino C, Arlorio M, Coïsson JD. Spray-dried polyphenolic extract from Italian black rice (Oryza sativa L., var. Artemide) as new ingredient for bakery products. Food Chem. 2018 Dec 15;269:603-609. doi: 10.1016/j.foodchem.2018.07.059. Epub 2018 Jul 10.
197. Elisa Rampacci, Maria Luisa Marenzoni, Elisabetta Chiaradia, Fabrizio Passamonti, Maurizio Ricci, Marco Pepe, Mauro Coletti, & Stefano Giovagnoli. *In vitro* performances of novel co spray-dried azithromycin/rifampicin microparticles for *Rhodococcus equi* disease treatment. Scientific Reports**.** *(2018) 8:12149.* DOI:10.1038/s41598-018-30715-z
198. Takaaki Ito, Tomoyuki Okuda, Yoshimasa Takashima, and Hirokazu Okamoto. Naked pDNA inhalation powder composed of hyaluronic acid exhibits high gene expression in the lungs. *Mol. Pharmaceutics. 09 Aug 2018.* DOI: 10.1021/acs.molpharmaceut.8b00502
199. Plamen Katsarov, Bissera Pilicheva, Yordanka Uzunova, Georgi Gergov, Margarita Kassarova.

Chemical cross-linking: A feasible approach to prolong doxylamine/pyridoxine release from spray-dried chitosan microspheres. European Journal of Pharmaceutical Sciences 123 (2018) 387–394
200. Nazareth Eliana Ceschan, Verónica Bucalá, Melina Valeria Mateos, Hugh David Charles Smyth, María Verónica Ramírez-Rigo. Carrier free indomethacin microparticles for dry powder inhalation. International Journal of Pharmaceutics 549 (2018) 169–178
201. A. Bohr, J. Boetker, T. Rades, J. Rantanen, M. Yang, Application of spray-drying and electrospraying/electrospinning for poorly water soluble drugs: a particle engi- neering approach, Curr. Pharm. Des. 20 (2014) 325–348.
202. A. Jaworek, Micro-and nanoparticle production by electrospraying, Powder Technol. 176 (2007) 18–35.
203. M. Cloupeau, B. Prunet-Foch, Electrostatic spraying of liquids: main functioning modes, J. Electrost. 25 (1990) 165–184.
204. Jaworek, A. Sobczyk, Electrospraying route to nanotechnology: an overview, J. Electrost. 66 (2008) 197–219.
205. R. Bocanegra, D. Galán, M. Márquez, I. Loscertales, A. Barrero, Multiple electrosprays emitted from an array of holes, J. Aerosol Sci. 36 (2005) 1387–1399.
206. J. Almekinders, C. Jones, Multiple jet electrohydrodynamic spraying and applications, J. Aerosol Sci. 30 (1999) 969–971.
207. Z.P. Liu, L. Cui, D.G. Yu, Z.X. Zhao, L. Chen, Electrosprayed core–shell solid dispersions of acyclovir fabricated using an epoxy-coated concentric spray head, Int. J. Nanomedicine 9 (2014) 1967.
208. C. Khalloufi, A. Almeida-Rivera, in: E. Tsotsas, A.S. Mujumdar (Eds.), Mudaliar, Modern Drying Technology, Volume 5, Process Intensification, Drying Technol., 32, Wiley-VCH Verlag GmbH & Co. KgaA, Weinheim, Germany 2014, pp. 2017–2020 (359 pp.).
209. I. Zbicinski, I. Smucerowicz, C. Strumillo, C. Crowe, Application of pulse combustion technology in spray drying process, Braz. J. Chem. Eng. 17 (2000) 441–450.
210. D.N. Bikiaris, Solid dispersions, part I: recent evolutions and future opportunities in manufacturing methods for dissolution rate enhancement of poorly water-soluble drugs, Expert Opin. Drug Deliv. 8 (2011) 1501–1519.
211. T. Kudra, Pulse-combustion drying: status and potentials, Dry. Technol. 26 (2008) 1409–1420.
212. D.J. Lee, S. Jangam, A.S. Mujumdar, Some recent advances in drying technologies to produce particulate solids, KONA Powder Part. J. 30 (2013) 69–83.
213. L. Wang, F.D. Cui, H. Sunada, Improvement of the dissolution rate of nitrendipine using a new pulse combustion drying method, Chem. Pharm. Bull. 55 (2007) 1119–1125.
214. Sharifah Nur Hidayah Syed Mazlan, Mohd Shukuri Mohamad Ali, Raja Noor Zaliha Raja Abd Rahman, Suriana Sabri, Mohd Anuar Jonet, Thean Chor Leow. Crystallization and structure elucidation of GDSL esterase of Photobacterium sp. J15. International Journal of Biological Macromolecules 119 (2018) 1188–1194
215. Ou YM, Kuo SY, Lee H, Chang HT, Wang YS. An Efficient Sample Preparation Method to Enhance Carbohydrate Ion Signals in Matrix-assisted Laser Desorption/Ionization Mass Spectrometry. J Vis Exp. 2018 Jul 29;(137). doi: 10.3791/57660.
216. Afrose, Afrina, White, Edward T., Howes, Tony, George, Graeme, Rashid, Abdur, Rintoul, Llew, Islam, Nazrul. Preparation of ibuprofen microparticles by anti-solvent precipitation crystallization (APC) technique: characterization, formulation and in-vitro performance. Journal of Pharmaceutical Sciences. 2018. https://doi.org/10.1016/j.xphs.2018.07.030.
217. Xiujuan Zhang; Xiaohui Ding; Yuanmei Zhu; Huihui Chong; Sheng Cui; Jinsheng He; Xinquan Wang; Yuxian He. Structural and functional characterization of HIV-1 cell fusion inhibitor T20. AIDS. Publish Ahead of Print():, AUG 2018. DOI: 10.1097/QAD.0000000000001979. PMID: 30096076
218. D.E. Dobry, D.M. Settell, J.M. Baumann, Spray drying and scale-up, Pharmaceutical Sciences Encyclopedia, John Wiley & Sons, Inc. 2015, pp. 1–26.
219. Waseem Kaialy. A review of factors affecting electrostatic charging of pharmaceuticals and adhesive mixtures for inhalation. International Journal of Pharmaceutics 503 (2016) 262–276.
220. V. N. P. Le, T. H. Hoang Thi, E. Robins, and M. P. Flament. Dry Powder Inhalers: Study of the Parameters Influencing Adhesion and Dispersion of Fluticasone Propionate. AAPS Pharm Sci Tech, Vol.

13, No. 2, June 2012 ( # 2012) DOI: 10.1208/s12249-012-9765-8
221. Gibson, N., 1997. Static electricity—an industrial hazard under control? J. Electrostat. 40–41, 21–30. doi:http://dx.doi.org/10.1016/S0304-3886(97) 00010-7.
222. US Pharmacopeia. {601} Aerosols, nasal sprays, metered-dose inhalers, and dry powder inhaler (general chapter). United States Pharmacopeia. 35th-NF ed.
223. FDA, 1998 See Tittle 21 Code of Federal Regulations
224. Kaialy, W., Martin, G.P., Ticehurst, M.D., Royall, P., Mohammad, M.A., Murphy, J., Nokhodchi, A., 2011. Characterisation and deposition studies of recrystallised lactose from binary mixtures of ethanol/butanol for improved drug delivery from dry powder inhalers. AAPS J. 13, 30–43. doi:http://dx.doi.org/10.1208/ s12248-010-9241-x.
225. Kaialy, W., Alhalaweh, A., Velaga, S., Nokhodchi, A., 2012. Influence of lactose carrier particle size on the aerosol performance of budesonide from a dry powder inhaler. Powder Technol. 227, 74–85.
226. Steckel, H., Bolzen, N., 2004. Alternative sugars as potential carriers for dry powder inhalations. Int. J. Pharm. 270, 297–306.
227. Carlos Molina, Waseem Kaialy, Qiao Chen, Daniel Commandeur, and Ali Nokhodchi. Agglomerated novel spray-dried lactose-leucine tailored as a carrier to enhance the aerosolization performance of salbutamol sulfate from DPI formulations. *Drug Delivery and Translational Research*. 2017. https://doi.org/10.1007/s13346-017-0462-8
228. James W. Dodd and Kenneth H. Tonge. *Thermal Methods*. Analytical Chemistry by Open Learning.1987.
229. Alois Fadini and Frank-Michael Schnepel. *Vibrational Spectroscopy- Methods and Applications*. Halsted Press. New York. 1989. 15-17.
230. A. Mukherjee, S. Tothadi, S. Chakraborty, S. Ganguly, G.R. Desiraju, Synthon identification in co-crystals and polymorphs with IR spectroscopy. Primary amides as a case study, CrystEngComm 15 (2013) 4640–4654, http://dx.doi.org/10.1039/ c3ce40286j.
231. Henck, J.O., Griesser, U.J., Burger, A., 1997. Polymorphism of drug substances-an economic challenge. Pharm. Ind. 59, 165–169.
232. Shur J, Price R. Advanced microscopy techniques to assess solid- state properties of inhalation medicines. Adv Drug Del Rev. 2012;64:369–82.
233. Adi H, Larson I, Chiou H, Young P, Traini D, Stewart P. Role of agglomeration in the dispersion of salmeterol xinafoate from mixtures for inhalation with differing drug to fine lactose ratios. J Pharm Sci. 2008;97:3140–52.
234. European Pharmacopoeia. “2.9.36. Powder flow”. 2010. p. 5107.
235. United States Pharmacopeia 38 National Formulary 33 : USP 38 NF 33 2015 Ed.
236. http://online.pheur.org/EN/entry.htm
237. Kaialy W, Alhalaweh A, Velaga SP, Nokhodchi A. Effect of carrier particle shape dry powder inhaler performance. Int J Pharm. 2011;421:12–23.
238. Rahimipour Y, Kouhsoltani M, Hamishehkar H. Alternative carriers in dry powder inhaler formulations. Drug Discov Today. 2014;19: 618–26.
239. Chew NYK, Shekunov BY, Tong HHY, Chow AHL, Savage C, Wu J, et al. Effect of amino acids on the dispersion of disodium cromoglycate powders. J Pharm Sci. 2005;94:2289–300.
240. Begat P, Price R, Harris H, Morton DAV, Staniforth JN. The influence of force control agents on the cohesive–adhesive balance in dry powder inhaler formulations. KONA Powder Part J. 2005;23: 109–21.
241. Begat P, Morton DAV, Shur J, Kippax P, Staniforth JN, Price R. The role of force control agents in high-dose dry powder inhaler formulations. J Pharm Sci. 2009;98:2770–83.
242. Ibrahim BM, Jun SW, Lee MY, Kang SH, Yeo Y. Development of inhalable dry powder formulation of basic fibroblast growth factor. Int J Pharm. 2010;385:66–72.
243. Kaialy W, Ticehurst M, Nokhodchi A. Dry powder inhalers: mechanistic evaluation of lactose formulations containing salbutamol sulfate. Int J Pharm. 2012;423:184–94.
244. Aquino RP, Prota L, Auriemma G, Santoro A, Mencherini T, Colombo G, et al. Dry powder inhalers of gentamicin and leucine: formulation parameters, aerosol performance and in vitro toxicity on CuFi1 cells. Int J Pharm. 2012;426:100–7.

245. Grzybowska K, Paluch M, Wlodarczyk P, Grzybowski A, Kaminski K, Hawelek L. Enhancement of amorphous celecoxib stability by mixing it with octaacetylmaltose: the molecular dynamics study. Mol Pharm. 2012;9:894–904.
246. Kaminska E, Adrjanowicz K, Kaminski K, Wlodarczyk P, Hawelek L, Kolodziejczyk K, et al. A new way of stabilization of furosemide upon cryogenic grinding by using acylated saccharides matrices. The role of hydrogen bonds in decomposition mechanism. Mol Pharm. 2013;10:1824–35.
247. Craye G, Löbmann K, Grohganz H, Rades T, Laitinen R. Characterization of amorphous and co-amorphous simvastatin for- mulations prepared by spray drying. Molecules. 2015;20:21532–48
248. Vora C, Paradia R, Mittal K, Mashru R. Formulation develop- ment, process optimization, and in vitro characterization of spray-dried lansoprazole enteric microparticles. Sci Pharm. 2016;84:393–408.
249. Shah B, Kakumanu VK, Bansal AK. Analytical techniques for quantification of amorphous/crystalline phases in pharmaceutical solids. J Pharm Sci. 2006;95:1641–65.
250. Nakamoto K. Infrared and Raman spectra of inorganic and coordi- nation compounds: theory and applications in inorganic chemistry. Volume A. John Wiley. 2009.
251. Silverstein RM, Webster FX, Kiemle D. Spectrometric identifica- tion of organic compounds. Edition: 7th ed., John Wiley & Sons. 2015.
252. Rotthäuser B, Kraus G, Schmidt PC. Optimization of an efferves- cent tablet formulation containing spray dried L-leucine and poly- ethylene glycol 6000 as lubricants using a central composite design. Eur J Pharm Biopharm. 1998;46:85–94.
253. Labiris NR, Dolovich MB. Pulmonary drug delivery. Part I: phys- iological factors affecting therapeutic effectiveness of aerosolized medications. Br J Clin Pharmacol. 2003;56:588–99.
254. Kaialy W, Momin MN, Ticehurst MD, Murphy J, Nokhodchi A. Engineered mannitol as an alternative carrier to enhance deep lung penetration of salbutamol sulfate from dry powder inhaler. Colloids Surf B: Biointerfaces. 2010;79:345–56.
255. Kaialy W, Nokhodchi A. Freeze-dried mannitol for superior pulmonary drug delivery via dry powder inhaler. Pharm Res. 2013;30: 458–77.
256. A..J. Hickey and H.M. Mansour, Delivery of drugs by the pulmonary route. In: AT Florence, and J Siepmann, (eds). Modern Pharmaceutics. Taylor & Francis, New York. (2009) 191–219
257. F. Decimo , C. Capristo, R. Amelio, N. Maiello, A.F. Capristo, and M. Miraglia Del Giudice, Evaluation of bronchial hyperreactivity with mannitol dry powder challenge test in a paediatric population with intermittent allergic asthma or allergic rhinitis, Int. J. Immunopathol Pharmacol. 24(4) (2011) 1069–1074
258. W. Kaialy, G.P. Martin, M.D. Ticehurst, M.N. Momin, and A. Nokhodchi, The enhanced aerosol performance of Albuterol from dry powders containing engineered mannitol as excipient, Int. J. Pharm. 392 (2010) 178–188
259. E. Daviskas and B.K. Rubin, Effect of inhaled dry powder mannitol on mucus and its clearance, Expert Rev. Respir. Med. 7 (2013) 65–75
260. E. Daviskas, S.D. Anderson, S. Eberl, H.K Chan, and I.H. Young, The 24-h effect of mannitol on the clearance of mucus in patients with bronchiectasis, Chest. 119 (2001) 414–421
261. P.J. Wills and P.J. Cole, Mucolytic and mucokinetic therapy, Pulm. Pharmacol. 9 (1996) 197–204
262. J.D. Brannan, M. Gulliksson, S.D. Anderson, N. Chew, and M. Kumlin, Evidence of mast cell activation and leukotriene release after mannitol inhalation, Eur. Respir. J. 22 (2003) 491– 496
263. M. King and B.K. Rubin, Pharmacological approaches to discovery and development of new mucolytic agents, Adv. Drug Deliv. Rev. 54 (2002)1475–1490
264. E. Daviskas and S.D. Anderson, Hyperosmolar agents and clearance of mucus in the diseased airway, J. Aerosol Med. 19 (2006) 100–109
265. A. Jaques, E. Daviskas, J.A. Turton, K. McKay, P. Cooper, R.G. Stirling, C.F. Robertson, P.T. Bye, P.N. Lesoue ¨f, B. Shadbolt, S.D. Anderson, and B. Charlton, Inhaled mannitol improves lung function in cystic fibrosis, Chest. 133 (2008) 1388–1396
266. G. Saint-Lorant, et al., Influence of carrier on the performance of dry powder inhalers. Int. J. Pharm. 334 (2007) 85–91
267. W. Kaialy, M.N. Momin, M.D. Ticehurst, J. Murphy, A. Nokhodchi, Engineered mannitol as an alternative carrier to enhance deep lung penetration of Albuterol sulfate from dry powder inhaler, Colloid

Surface B. 79 (2010) 345–56
268. R.J. Malcolmson, J.K. Embleton, Dry powder formulations for pulmonary delivery, Pharm. Sci. Technol. Today 1 (1998) 394–398.
269. S.A. Shoyele, S. Cawthorne, Particle engineering techniques for inhaled biopharmaceuticals, Adv. Drug Deliv. Rev. 58 (2006) 1009–1029.
270. Jones MD, Harris H, Hooton JC, Shur J, King GS, Mathoulin CA, Nicol K, Smith TL, Dawson ML, Ferrie AR, Price R. An investi- gation into the relationship between carrier-based dry powder inhalation performance and formulation cohesive-adhesive force balances. Eur J Pharm Biopharm. 2008;69:496–507.
271. W. Kaialy and A. Nokhodchi, Freeze-Dried Mannitol for Superior Pulmonary Drug Delivery via Dry Powder Inhaler, Pharm. Res. 30 (2013) 458–477 DOI 10.1007/s11095-012- 0892-4
272. Z. Budavari, R. Zelko, I. Racz, S. Marton, Compatibility study between folic acid, vitamin B6 and tablet excipients using differential scanning calorimetry, Pharmazie. 54 (1999) 861-862
273. H. Adia, M. Paul, Younga, H.K. Chana, H. Agusb, and D. Trainia, Co-spray-dried mannitol–ciprofloxacin dry powder inhaler formulation for cystic fibrosis and chronic obstructive pulmonary disease, European Journal of Pharmaceutical Sciences. 40 (2010) 239– 247
274. Burger, H. Jan-Olav, S. Hetz, J.M. Rollinger, A.A. Weissnicht, H. Stottner, J. Pharm. Sci. 89 (2000) 457.
275. B. Debord, C. Lefebvre, A.M. Guyot-Hermann, J. Hubert, R. Bouche, J.C. Cuyot, Drug Dev. Ind. Pharm. 13 (1987) 1533.
276. F. Jones and K. Lee, Optical and crystallographic properties of three phases of Mannitol, Microscope. 18 (1970) 279
277. T. Yoshinari, R.T. Forbes, P. York, and Y. Kawashima, Moisture induced polymorphic transition of mannitol and its morphological transformation, Int. J. Pharm. 247 (2002) 69-77
278. A.L. Feng, M.A. Boraey, M.A. Gwin, P.R. Finlay, P.J. Kuehl, and R. Vehring, Mechanistic models facilitate efficient development of leucine containing microparticles for pulmonary drug delivery, Int. J. Pharm. 409 (2011) 156–163
279. M.A. Boraey, S. Hoe, H. Sharif, D.P. Miller, D. Lechuga-Ballesteros, R. Vehring, Improvement of the dispersibility of spray–dried budesonide powders using leucine in an ethanol–water cosolvent system, Powder Technol. 236 (2013) 171– 178
280. Chan J, Tyne A, Pang A, Chan HK, Young P, Britton W, Duke C, and Traini D. A rifapentine-containing inhaled triple antibiotic formulation for rapid treatment of tubercular infection, Pharm. Res. 31 (2014) 1239–1253.
281. A.M. Healy, M.I. Amaro, K.J. Paluch, and L. Tajber, Dry powders for oral inhalation free of lactose carrier particles, Adv. Drug Deliv. Rev. 75 (2014) 1–21
282. T. Sou, L.M. Kaminskas, T. Nguyen, R. Carlberg, M.P. McIntosh, D.A.V. and Morton, The effect of amino acid excipients on morphology and solid-state properties of multi- component spray-dried formulations for pulmonary delivery of biomacromolecules, Eur. J. Pharm. Biopharm. 83 (2013) 234–243
283. M.D. Jones, H. Harris, J.C. Hooton, J. Shur, G.S. King, C.A. Mathoulin, K. Nicol, T.L. Smith, M.L. Dawson, A.R. Ferrie, and R. Price, An investigation into the relationship between carrier-based dry powder inhalation performance and formulation cohesive-adhesive force balances, Eur. J. Pharm. Biopharm. 69 (2008) 496–507
284. N.R. Labiris and M.B. Dolovich, Pulmonary drug delivery. Part I: Physiological factors affecting therapeutic effectiveness of aerosolized medications, Br J Clin Pharmacol. 56 (2003) 588–599.
285. Bai TR. Beta 2 adrenergic receptors in asthma: a current perspective. Lung. 1992; 170 (3): 125-41.
286. Bateman JR, Pavia D, Sheahan NF, et al.. Impaired tracheobronchial clearance in patients with mild stage asthma. Thorax. 1983; 38 (6): 463-7.
287. Adcock IM, Gilbey T, Gelder CM, et al. Glucocorticoid receptor localisation in normal and asthmatic lungs. American Journal of Respiratory and Critical Care Medicine. 1996; 154 (3 Pt 1): 771-82.
288. Wilson SM, Shen P, Rider CF, et al. Selective prostacyclin receptor agonism augments glucocorticoid-induced gene expression in human bronchial epithelial cells. Journal of Immunology. 2009; 183 (10): 6788-99.
289. Adi S, Adi H, Tang P, et al. Micro-particle corrugation, adhesion and inhalation aerosol efficiency. European Journal of Pharmaceutical Sciences. 2008; 35 (1-2): 12-18.

290. Hassan MS, Lau R. Inhalation performance of pollen-shape carriers in dry powder formulation with different drug mixing rations: comparison with lactose carrier. International Journal of Pharmaceuticals. 2010; 386 (1-2): 6-14.
291. Owen, M.K., Ensor, D.S., 1992. Airborne particle sizes and sources found in indoor air. Atmos. Environ. Part A. Gen. Top. 26 (12), 2149–2162.
292. Oberdörster, G., Oberdörster, E., Oberdörster, J., 2005. Nanotoxicology: an emerging discipline evolving from studies of ultrafine particles. Environ. Health Perspect. 113 (7), 823–839.
293. Guidance for Industry- Metered Dose Inhaler (MDI) and Dry Powder Inhaler (DPI) drug products-chemistry, manufacturing, and controls documentation. Food and Drug Administration. (1998) 1-61
294. Guardiola, J., Rojo, V., Ramos, G., 1996. Influence of particle size, fluidization velocity and relative humidity on fluidized bed electrostatics. J. Electrostat. 37, 1–20.
295. Rowley, G., 2001. Quantifying electrostatic interactions in pharmaceutical solid systems. Int. J. Pharm. 227, 47–55. doi:http://dx.doi.org/10.1016/S0378-5173 (01) 00784-0.
296. Kaialy, W. et al. (2010) The enhanced aerosol performance of salbutamol from dry powders containing engineered mannitol as excipient. Int. J. Pharm. 392, 178–188.
297. Kaialy W, Ticehurst M, Nokhodchi A. Dry powder inhalers: mechanistic evaluation of lactose formulations containing salbutamol sulphate. Int J Pharm. 2012 Feb 28;423(2):184-94. doi: 10.1016/j.ijpharm.2011.12.018. Epub 2011 Dec 17
298. Source: Human Metabolome Database. *Record Name: D-Xylitol URL:* http://www.hmdb.ca/metabolites/HMDB02917
299. De Faveri, D., Perego, P., Converti, A., Del Borghi, M., 2002. Xylitol recovery by crystallization from synthetic solutions and fermented hemicellulose hydro- lyzates. Chem. Eng. J. 90, 291–298.
300. Williams, L., Wilkins, 2003. In: Rowe, et al. (Eds.), Handbook of Pharmaceutical Excipients. Pharmaceutical Press, London.
301. Waseem Kaialy, Mohammad Maniruzzaman, Saeed Shojaee, Ali Nokhodchi. Antisolvent precipitation of novel xylitol-additive crystals to engineer tablets with improved pharmaceutical performance. Int J Pharm. 2014; 477 (1-2): 282-93.
302. Varshosaz J, Taymouri S, Hamishehkar H. Fabrication of polymeric nanoparticles of poly (ethylene-co-vinyl acetate) coated with chitosan for pulmonary delivery of carvedilol. J Appl Polym Sci. 2014;131(1)
303. M. Pudipeddi and A. Serajuddin, J. Pharm. Sci., 2005, 94, 929.
304. Aakeroy CB, Forbes S, Desper J. Using cocrystals to systematically modulate aqueous solubility and melting behavior of an anticancer drug. J Am Chem Soc. 2009;131(47):17048–9.
305. Remenar JF, Morissette SL, Peterson ML, Moulton B, MacPhee JM, Guzman HR, *et al*. Crystal engineering of novel cocrystals of a triazole drug with 1,4-dicarboxylic acids. J Am Chem Soc. 2003;125(28):8456–7.
306. Good DJ, Rodriguez-Hornedo N. Solubility advantage of pharmaceutical cocrystals. Cryst Growth Des. 2009;9(5):2252–64.
307. Trask AV, Motherwell WDS, Jones W. Physical stability enhancement of theophylline via cocrystallization. Int J Pharm. 2006;320(1–2):114–23.
308. Trask AV, Motherwell WDS, Jones W. Pharmaceutical cocrystallization: engineering a remedy for caffeine hydration. Cryst Growth Des. 2005;5(3):1013–21.
309. Karki S, Friscic T, Fabian L, Laity PR, Day GM, Jones W. Improving mechanical properties of crystalline solids by cocrystal formation: new compressible forms of paracetamol. Adv Mater. 2009;21(38–39):3905–9.
310. Sun CC, Hou H. Improving mechanical properties of caffeine and methyl gallate crystals by cocrystallization. Cryst Growth Des. 2008;8(5):1575–9.
311. McNamara DP, Childs SL, Giordano J, Iarriccio A, Cassidy J, Shet MS, *et al*. Use of a glutaric acid cocrystal to improve oral bioavailability of a low solubility API. Pharm Res. 2006;23(8):1888–97.
312. Geetha Bolla and Ashwini Nangia. 2016. Pharmaceutical cocrystals: walking the talk. Chem. Commun. 52, 8342-8360.

313. Kaialy W, Momin MN, Ticehurst MD, Murphy J, Nokhodchi A. Engineered mannitol as an alternative carrier to enhance deep lung penetration of salbutamol sulphate from dry powder inhaler. Colloid Surface B. 2010;79:345–56.
314. Kuno, Y., Kojima, M., Ando, S., and Nakagami, H. 2005. Evaluation of rapidly disintegrating tablets manufactured by phase transition of sugar alcohols. J Control. Release.105, 16-22.
315. Carson, J., Waisbrot, S., and Jones, F. A. 1943. New form of crystalline xylitol. J. Am. Chem. Soc. 65, 1777-1778.
316. G.R. Desiraju, J.J. Vittal, A. Ramanan, Crystal engineering, A Textbook, World Scientific, Singapore, 2011.
317. G.R. Desiraju, Crystal engineering: from molecule to crystal, J. Am. Chem. Soc. 135 (2013) 9952–9967, http://dx.doi.org/10.1021/ja403264c.
318. A. Mukherjee, Building upon supramolecular synthons: some aspects of crystal en- gineering, Cryst. Growth Des. 15 (2015) 3076–3085, http://dx.doi.org/10.1021/acs. cgd.5b00242.
319. Roy S, Mumbaraddi D, Jain A, George SJ, Peter SC. Crystal Engineering in Supramolecular Polyoxometalate Hybrids through pH Controlled in Situ Ligand Hydrolysis. Inorg Chem. 2017 Dec 22. doi: 10.1021/acs.inorgchem.7b02385.
320. Bolla, Geetha and Nangia, Ashwini. Pharmaceutical cocrystals: walking the talk. Chem Commun. 2016 Jun 28 ;52 (54): 8342-60. doi: 10.1039/c6cc02943d.
321. Basavoju S, Boström D, Velaga S. Indomethacin-saccharin cocrystal: design, synthesis and preliminary pharmaceutical characterization. Pharm Res. 2008;25:530–41.
322. Jung M, Kim J, Kim M, Alhalaweh A, Cho W, Hwang S, et al. Bioavailability of indomethacin saccharin cocrystals. J Pharm Pharmacol. 2010;62:1560–8.
323. Schultheiss N, Newman A. Pharmaceutical cocrystals and their physicochemical properties. Cryst Growth Des. 2009;9:2950–67.
324. Chiou D, Langrish T. A comparison of crystallisation approaches in spray drying. J Food Eng. 2008;88:177–85.
325. Zhang GGZ, Henry RF, Borchardt TB, Lou XC. Efficient co-crystal screening using solution-mediated phase transformation. J Pharm Sci-Us. 2007;96(5):990–5.
326. Takata N, Shiraki K, Takano R, Hayashi Y, Terada K. Cocrystal screening of stanolone and mestanolone using slurry crystallization. Cryst Growth Des. 2008;8(8):3032–7.
327. Kojima T, Tsutsumi S, Yamamoto K, Ikeda Y, Moriwaki T. High-throughput cocrystal slurry screening by use of in situ Raman microscopy and multi-well plate. Int J Pharm. 2010;399(1– 2):52–9.
328. Friscic T, Childs SL, Rizvi SAA, Jones W. The role of solvent in mechanochemical and sonochemical cocrystal formation: a solubility-based approach for predicting cocrystallisation outcome. CrystEngComm. 2009;11(3):418–26.
329. Weyna DR, Shattock T, Vishweshwar P, Zaworotko MJ. Synthesis and structural characterization of cocrystals and pharmaceutical cocrystals: mechanochemistry vs slow evaporation from solution. Cryst Growth Des. 2009;9(2):1106–23.
330. Padrela L, Rodrigues MA, Velaga SP, Fernandes AC, Matos HA, de Azevedo EG. Screening for pharmaceutical cocrystals using the supercritical fluid enhanced atomization process. J Supercrit Fluids. 2010;53(1–3):156–64.
331. Dennis Douroumis, Steven A. Ross, and Ali Nokhodchi.Advanced methodologies for cocrystal synthesis. Adv. Drug Deliv. Rev. (2017), http://dx.doi.org/ 10.1016/j.addr.2017.07.008
332. Faulhammer E, Wahl V, Zellnitz S, Khinast JG, Paudel A. Carrier-based dry powder inhalation: Impact of carrier modification on capsule filling processability and in vitro aerodynamic performance. Int J Pharm. 2015 Aug 1;491(1-2):231-42. doi: 10.1016/j.ijpharm.2015.06.044. Epub 2015 Jun 29.
333. Begat P, Morton D, Staniforth J, Price R. The cohesive-adhesive balances in dry powder inhaler formulations I: direct quantification by atomic force microscopy. Pharm Res. 2004;21:1591–7.
334. Paajanen M, Katainen J, Raula J, Kauppinen E, Lahtinen J. Direct evidence on reduced adhesion of salbutamol sulphate particles due to L-leucine coating. Powder Technol. 2009;192:6– 11.
335. Zeng X, Martin G, Tee S, Ghoush A, Marriott C. Effects of particle size and adding sequence of fine lactose on the deposition of salbutamol sulphate from a dry powder formulation. Int J Pharm. 1999;182:133–44.

336. Gutmann V. The donor–acceptor approach to molecular interactions. New York: Plenum Press; 1978.
337. Feeley J, York P, Sumby B, Dicks H. Determination of surface properties and flow characteristics of salbutamol sulphate, before and after micronisation. Int J Pharm. 1998;172:89–96.
338. Ali, F.S., Ali, M.A., Ali, R.A., Inculet, I.I., 1998. Minority charge separation in falling particles with bipolar charge. J. Electrostat. 45, 139–155.
339. Engers, D.A., Fricke, M.N., Storey, R.P., Newman, A.W., Morris, K.R., 2006. Triboelectrification of pharmaceutically relevant powders during low-shear tumble blending. J. Electrostat. 64, 826–835.
340. Glor, M., 1988. Electrostatic Hazards in Power Handling. John Wiley and Sons Inc., New York, NY.
341. Trigwell, S., Grable, N., Yurteri, C.U., Sharma, R., Mazumder, M.K., 2003. Effects of surface properties on the tribocharging characteristics of polymer powder as applied to industrial processes. Ind. Appl. IEEE Trans. 39, 79–86.
342. Kaialy, W., Martin, G.P., Larhrib, H., Ticehurst, M.D., Kolosionek, E., Nokhodchi, A., 2012d. The influence of physical properties and morphology of crystallised lactose on delivery of salbutamol sulphate from dry powder inhalers. Colloids Surf. B Biointerfaces 89, 29–39.
343. Narayan, P., Hancock, B.C., 2005. The influence of particle size on the surface roughness of pharmaceutical excipient compacts. Mater. Sci. Eng. A 407, 226– 233. doi:http://dx.doi.org/10.1016/j.msea.2005.06.060.
344. Boer, A., De Hagedoorn, P., Gjaltema, D., 2003. Air classifier technology (ACT) in dry powder inhalation: part 1: Introduction of a novel force distribution concept (FDC) explaining the performance of a basic. Int. J. Pharm. 260, 187–200.
345. Shariare, M.H., de Matas, M., York, P., 2011. Effect of crystallisation conditions and feedstock morphology on the aerosolization performance of micronised salbutamol sulphate. Int. J. Pharm. 415, 62–72. doi:http://dx.doi.org/10.1016/j. ijpharm.2011.05.043.
346. Pearce, C., Lewis, D., 1972. X-ray diffraction line broadening studies of Raney copper and nickel. J. Catal. 26, 318–325.
347. Van Campen, L., Amidon, G.L., Zografi, G., 1983. Moisture sorption kinetics for water- soluble substances I: Theoretical considerations of heat transport control. J. Pharm. Sci. 72, 1381–1388. doi:http://dx.doi.org/10.1002/jps.2600721204.
348. Gallo, C.F., Lama, W.L., 1976. Classical electrostatic description of the work function and ionization energy of insulators. IEEE Trans. Ind. Appl. IA–12, 7–11. doi: http://dx.doi.org/10.1109/TIA.1976.349379.
349. Schein, L.B., 1993. Theory of toner charging. J. imaging Sci. Technol. 37, 1–4.
350. Karner, S., Urbanetz, N.A., 2013. Triboelectric characteristics of mannitol based formulations for the application in dry powder inhalers. Powder Technol. 235, 349–358. doi:http://dx.doi.org/10.1016/j.powtec.2012.10.034.
351. Carter, P.A., Rowley, G., Fletcher, E.J., Hill, E.A., 1992. An experimental investigation of triboelectrification in cohesive and non-cohesive pharmaceutical powders. Drug Dev. Ind. Pharm. 18, 1505–1526.
352. Eilbeck, J., Rowley, G., Carter, P.A., Fletcher, E.J., 2000. Effect of contamination of pharmaceutical equipment on powder triboelectrification. Int. J. Pharm. 195, 7– 11.
353. Eilbeck, J., Rowley, G., Carter, P.A., Fletcher, E.J., 1999. Effect of materials of construction of pharmaceutical processing equipment and drug delivery devices on the triboelectrification of size-fractionated lactose. Pharm. Pharmacol. Commun. 5, 429–433.
354. Kwek, J.W., Jeyabalasingam, M., Ng, W.K., Heng, J.Y.Y., Tan, R.B.H., 2012. Comparative study of the triboelectric charging behavior of powders using a nonintrusive approach. Ind. Eng. Chem. Res. 51, 16488–16494. doi:http://dx.doi.org/10.1021/ ie3016973.
355. Harnby N. The mixing of cohesive powders. In: Mixing in the process industries. Oxford: Butterworth-Heinemann; 1997. p. 79– 98.
356. Hickey, A.J., Concessio, N.M., 1997. Descriptors of irregular particle morphology and powder properties. Adv. Drug Deliv. Rev. 26, 29–40.
357. Murtomaa, M., Mellin, V., Harjunen, P., Lankinen, T., Laine, E., Lehto, V.-P., 2004a. Effect of particle morphology on the triboelectrification in dry powder inhalers. Int. J. Pharm. 282, 107–114.

358. Basavoju S, Boström D, Velaga S. Indomethacin-saccharin cocrystal: design, synthesis and preliminary pharmaceutical characterization. Pharm Res. 2008;25:530–41.
359. Jung M, Kim J, Kim M, Alhalaweh A, Cho W, Hwang S, et al. Bioavailability of indomethacin saccharin cocrystals. J Pharm Pharmacol. 2010;62:1560–8.
360. Schultheiss N, Newman A. Pharmaceutical cocrystals and their physicochemical properties. Cryst Growth Des. 2009;9:2950–67.
361. Fowkes, F.M., 1964. Attractive forces at interfaces. Ind. Eng. Chem. 56, 40–52.
362. Lowell, S., Shields, J.E., 1991. Powder Surface Area and Porosity. Springer Science & Business Media.
363. Sethuraman, V.V., Hickey, A.J., 2002. Powder properties and their influence on dry powder inhaler delivery of an antitubercular drug. AAPS PharmSciTech 3, 7–16.
364. Vladykina Deryagin, T.N.B.V., Toporov, Y.P., 1985. The effect of surface roughness on triboelectrification of insulators. Phys. Chem. Mech. Surf. 3, 2817–2821.
365. Yurteri, C.U., Mazumder, M.K., Grable, N., Ahuja, G., Trigwell, S., Biris, A.S., Sharma, R., Sims, R.A., 2002. Electrostatic effects on dispersion, transport, and deposition of fine pharmaceutical powders: development of an experimental method for quantitative analysis. Part. Sci. Technol. 20, 59–79.
366. Taylor, M.K., Ginsburg, J., Hickey, A.J., Gheyas, F. 2000. Composite method to quantify powder flow as a screening method in early tablet or capsule formulation development. AAPS Pharm. Sci. Tech. 1, 20-30.
367. Preshita P. Desai, Sanyat S. Mapara and Vandana B. Patravale. “Crystal Engineering: Upcoming Paradigm for Efficacious Pulmonary Drug Delivery”. Current Pharmaceutical Design (2018) 24: 2438. https://doi.org/10.2174/1381612824666180518080948
368. Food & Drug Administration. “Guidance for industry metered dose inhaler (MDI) and dry powder inhaler (DPI) drug products”. 1998.
369. Berkenfeld, K., Lamprecht, A., McConville, J.T., 2015. Devices for dry powder drug delivery to the lung. AAPS PharmSciTech 16, 479–490. http://dx.doi.org/10.1208/s12249-015- 0317-x.
370. Son, Y.-J., McConville, J.T., 2008. Advancements in dry powder delivery to the lung. Drug Dev. Ind. Pharm. 34, 948–959. http://dx.doi.org/10.1080/03639040802235902.
371. Korycka P, Mirek A, Kramek-Romanowska K, Grzeczkowicz M, Lewińska D. Effect of electrospinning process variables on the size of polymer fibers and bead-on-string structures established with a $2^3$ factorial design. Beilstein J Nanotechnol. 2018 Sep 17;9:2466-2478. doi: 10.3762/bjnano.9.231. eCollection 2018.